Journal of Applied Mechanics

(Contributions of the ASME Applied Mechanics Division)

Laminar Swirling Pipe Flow . . . . . *L. Talbot* 1
Quasi-Static Variational Principles for Damped Systems . . . . . *Morris Morduchow* 8
Flexibility of Piping Systems Supported by Equally Spaced Rigid Hangers . . . . . *J. E. Brock* 11
The Stepped Thrust Bearing—A Solution by Relaxation Methods . . . . . *C. F. Kettleborough* 19
A Theory of Torsion Bending for Multicell Beams . . . . . *S. U. Benscoter* 25
Vibrations of Reinforced Shells in a Vacuum and in a Fluid . . . . . *M. C. Junger* 35
Stress Concentration Due to Elliptical Holes in Orthotropic Plates . . . . . *H. D. Conway* 42
Bending of Circular and Ring-Shaped Plates on an Elastic Foundation . . . . . *Herbert Reismann* 45
Contact of Elastic Spheres Under an Oscillating Torsional Couple . . . . . *H. Deresiewicz* 52
Stress Concentration Due to a Hemispherical Pit at a Free Surface . . . . . *R. A. Eubanks* 57
Plastic Deformation in a Steel Cylinder Striking a Rigid Target . . . . . *E. H. Lee and S. J. Tupper* 63
Coulomb Friction, Plasticity, and Limit Loads . . . . . *D. C. Drucker* 71
The Wave Method for Solving Flexural Vibration Problems . . . . . *R. P. N. Jones* 75
On the Strain Energy of Shells . . . . . *H. L. Langhaar and D. R. Carver* 81
On Small Spherical or Spheroidal Inclusion in a Twisted Cylinder . . . . . *Sisir Chandra Das* 85

Brief Notes
Note on Thermal Stresses . . . . . *J. L. Bogdanoff* 88

Discussion on previously published papers by *S. Levy and R. A. Saben; R. W. Cornell; W. N. Findley; E. D. Sweetland and E. R. Parker; G. R. Irwin; W. Prager; H. H. Bleich and F. Di Maggio; W. T. Russell and R. H. MacNeal; Henry Shapiro and D. R. Hudson; J. O. Smith and C. K. Liu* 89

Book Reviews 97

MARCH, 1954

VOL. 21, NO. 1

Transactions of The American Society of Mechanical Engineers

Journal of Applied Mechanics

Papers Contributed to the Transactions by the ASME Applied Mechanics Division

EXECUTIVE COMMITTEE OF THE APPLIED MECHANICS DIVISION

N. M. Newmark, *Chairman* — N. J. Hoff, *Secretary*

James M. Lemelle, *Technical Editor*

Published Quarterly by

The American Society of Mechanical Engineers

Publication Office, 20th and Northampton Streets, Easton, Pa.
Editorial Department at the Headquarters of the Society, 29 West Thirty-Ninth Street, New York 18, N. Y.

OFFICERS OF THE SOCIETY

Lewis K. Sillcox, *President*

Joseph L. Koerb, *Treasurer* — C. B. Davies, *Secretary*
E. J. Kates, *Assistant Treasurer*

PUBLICATIONS COMMITTEE

Paul T. Norton, Jr., *Chairman* — George A. Stetson, *Editor*
K. W. Clemondson, *Mgr. Editor*

By-Law: The Society shall not be responsible for statements or opinions advanced in papers or . . . printed in its publications (B13, Par. 4).

Published quarterly by The American Society of Mechanical Engineers. Publication office at 20th and Northampton Streets, Easton, Pa. The editorial department is located at the headquarters of the Society, 29 West Thirty-Ninth Street, New York 18, N. Y. Cable address, "Dynamic, New York." Price $1.25 a copy; $5.00 a year to members $2.50 a year; single copy price to members, $1.00. Changes of address must be received at Society headquarters not later than the date when they are to be effective on the mailing list. Please send old as well as new address. . . . By-Law: The Society shall not be responsible for statements or opinions advanced in papers or . . . printed in its publications (B13, Par. 4). . . . Entered as second-class matter March 14, 1955, at the Post Office at Easton, Pa., under the act of August 24, 1912. . . . Copyrighted, 1954, by The American Society of Mechanical Engineers. Reprints from this publication may be made on condition that full credit be given the JOURNAL OF APPLIED MECHANICS and the author, and that date of publication be stated.

Laminar Swirling Pipe Flow[1]

By L. TALBOT,[2] BERKELEY, CALIF.

The problem of the decay of a rotationally symmetric steady swirl superimposed on Poiseuille flow in a round pipe was investigated theoretically and experimentally. The object was to determine the degree to which the rate of decay of the swirl as predicted by a linearized theory agreed with measured rates of decay at flow conditions near the critical conditions for swirl instability. The solution to the linearized equation of motion for the swirl was obtained. Swirling flow was produced experimentally by rotating a section of the test pipe. Swirl velocities were determined from motion-picture studies of colored oil droplets introduced in the flow. The stability of the swirl was investigated through visualization of a dye filament, and a critical curve for swirl instability was determined experimentally relating the angular velocity of the rotating section to the Reynolds number. The theoretical and experimental values for the decay parameter were found to agree closely, even at conditions of flow near the critical conditions for instability. It was concluded that in the problem under consideration the nonlinear effects are not appreciable for stable decay of the swirl.

THE problem treated here is that of determining the resulting fluid motion obtained when a swirl is superimposed upon Poiseuille flow in a straight round pipe. (The term "swirl" in the sense used here denotes motion in concentric circles about the pipe axis.) In particular, interest is centered upon determination of the space rate of decay of the swirl as it is convected down the pipe, the stability of the swirl, and the interaction between the superimposed swirl and the main Poiseuille flow.

Swirling flows such as the one described, or flows similar to it, do at times occur in practice. A few examples of engineering interest are the flows which occur in pipe bends and in certain types of heat exchangers and spray nozzles. Also, some of the results obtained here have bearing on the general problems of laminar instability and transition. However, no attempt will be made to connect this work with any particular problem.

Basic Equations

The mathematical model under consideration is as follows:

(*a*) A steady-state, rotationally symmetric swirl is superimposed on Poiseuille flow in a straight round pipe.

(*b*) The swirl is of prescribed magnitude at $z = 0$ in the coordinate system in Fig. 1.

The exact Navier-Stokes equations for the rotationally symmetric steady motion of an incompressible fluid, neglecting body forces, are

$$u\frac{\partial u}{\partial r} + w\frac{\partial u}{\partial z} - \frac{v^2}{r} = -\frac{\partial p}{\partial r} + \frac{1}{\mathrm{Re}}\left(\nabla^2 u - \frac{u}{r^2}\right) \quad [1]$$

$$u\frac{\partial v}{\partial r} + w\frac{\partial v}{\partial z} + \frac{uv}{r} = \frac{1}{\mathrm{Re}}\left(\nabla^2 v - \frac{v}{r^2}\right) \quad [2]$$

$$u\frac{\partial w}{\partial r} + w\frac{\partial w}{\partial z} = -\frac{\partial p}{\partial z} + \frac{1}{\mathrm{Re}}\nabla^2 w \quad [3]$$

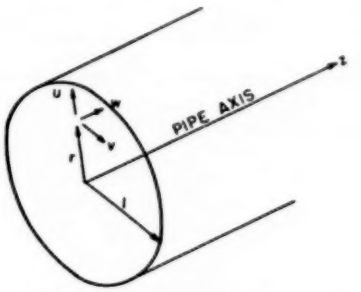

Fig. 1 Co-Ordinate System and Velocity Notation
(Wall of pipe is at $r = 1$ in nondimensional scheme of variables employed.)

where Re is the Reynolds number, u, v, w are velocities as indicated in Fig. 1, and ∇^2 is the Laplacian operator

$$\nabla^2 = \frac{\partial^2}{\partial r^2} + \frac{1}{r}\frac{\partial}{\partial r} + \frac{\partial^2}{\partial z^2} \quad [4]$$

In the foregoing equations all velocities have been made nondimensional by referring them to the characteristic velocity W_m, here taken to be the maximum velocity of the Poiseuille flow. The pressure p has been made nondimensional by referring it to the characteristic pressure ρW_m^2, where ρ is the density of the fluid. The independent variables r and z have been referred to the characteristic length a, here taken to be the radius of the pipe. With this system of nondimensional variables, the Reynolds number is then given by $\mathrm{Re} = W_m a/\nu$, where ν is the kinematical viscosity.

The second equation of motion, Equation [2], may be linearized by replacing the axial velocity w by $W + w'$, where w' is a perturbation and W is the main Poiseuille flow, given by $W = 1 - r^2$. With neglect of the terms involving u and w', the resulting linear partial differential equation, hereafter designated as the "swirl equation," is

$$W\frac{\partial v}{\partial z} = \frac{1}{\mathrm{Re}}\left(\nabla^2 v - \frac{v}{r^2}\right) \quad [5]$$

Solution to Swirl Equation

A separation of variables in Equation [5] is effected by putting

$$v = \varphi(\mathrm{Re}, \beta, r)e^{-\beta z} \quad [6]$$

The resulting ordinary linear differential equation is

$$\frac{d^2\varphi}{dr^2} + \frac{1}{r}\frac{d\varphi}{dr} + \left[\beta^2 + \mathrm{Re}\beta(1 - r^2) - \frac{1}{r^2}\right]\varphi = 0 \quad [7]$$

---

[1] Part of PhD thesis presented to University of Michigan, Ann Arbor, Mich., 1952.

[2] Assistant Professor of Mechanical Engineering, University of California.

Presented at the National Conference of the Applied Mechanics Division, Minneapolis, Minn., June 18–20, 1953, of The American Society of Mechanical Engineers.

Discussion of this paper should be addressed to the Secretary, ASME, 29 West 39th Street, New York, N. Y., and will be accepted until one month after final publication of the paper itself in the Journal of Applied Mechanics.

Note: Statements and opinions advanced in papers are to be understood as individual expressions of their authors and not those of the Society. Manuscript received by ASME Applied Mechanics Division, July 30, 1952. Paper No. 53—APM-24.

Two boundary conditions on v are necessary for the solution of Equation [7]. The swirl velocity v must be zero at $r = 1$ (the wall of the pipe) and must vanish as well at $r = 0$ (the center line of the pipe). Since these conditions must be true for all z, it follows that the boundary conditions on Equation [7] are

$$\varphi(\mathrm{Re}, \beta, 0) = \varphi(\mathrm{Re}, \beta, 1) = 0 \quad [8]$$

Equation [7] may be reduced to a standard form of the confluent hypergeometric equation[3] by putting

$$\varphi(\mathrm{Re}, \beta, r) = \xi^{1/2} e^{-\xi/2} g(\mathrm{Re}, \beta, \xi) \quad [9]$$

where

$$\xi = \sqrt{\mathrm{Re}\beta}\, r^2 \quad [10]$$

With these transformations, the resulting equation is the confluent hypergeometric equation

$$\xi \frac{d^2g}{d\xi^2} + (2 - \xi)\frac{dg}{d\xi} - \left(1 - \frac{\beta^2 + \mathrm{Re}\beta}{4\sqrt{\mathrm{Re}\beta}}\right) g = 0 \quad [11]$$

The solution of Equation [11] which is regular at $r = 0$ is

$$g = M(\alpha, \gamma; \xi) = 1 + \frac{\alpha}{\gamma}\xi + \frac{\alpha(\alpha+1)}{\gamma(\gamma+1)}\frac{\xi^2}{2!} + \cdots \quad [12]$$

where

$$\left.\begin{aligned} \alpha &= 1 - \frac{\beta^2 + \mathrm{Re}\beta}{4\sqrt{\mathrm{Re}\beta}} \\ \gamma &= 2 \end{aligned}\right\} \quad [13]$$

Then from Equations [9], [10], and [12]

$$\varphi(\mathrm{Re}, \beta, r) = \left(\sqrt{\mathrm{Re}\beta}\, r^2\right)^{1/2} \exp\left(-\frac{1}{2}\sqrt{\mathrm{Re}\beta}\, r^2\right) \times M\left(1 - \frac{\beta^2 + \mathrm{Re}\beta}{4\sqrt{\mathrm{Re}\beta}},\ 2;\ \sqrt{\mathrm{Re}\beta}\, r^2\right) \quad [14]$$

and from Equation [6]

$$v = A\varphi(\mathrm{Re}, \beta, r) e^{-\beta z} \quad [15]$$

where A is arbitrary.

The boundary condition at $r = 0$ is automatically satisfied by the function given in Equation [14]. The remaining boundary condition $(\mathrm{Re}, \beta, 1) = 0$ is used to determine the eigenvalues β_n, which are functions of the Reynolds number. The equation for the determination of the β_n is

$$M\left(1 - \frac{\beta_n^2 + \mathrm{Re}\beta_n}{4\sqrt{\mathrm{Re}\beta_n}},\ 2;\ \sqrt{\mathrm{Re}\beta_n}\, r^2\right)_{r=1} = 0 \quad [16]$$

The eigenvalues may be calculated in several ways. Some values may be obtained directly from existing tables for the function $M(\alpha, \gamma; x)$.[6,7] However, these tables are not extensive enough to yield all the desired values.

The complex integral representation of $M(\alpha, \gamma; x)$ provides a useful method for obtaining the eigenvalues β_n for large values of Re. Lauwerier[8] has shown that the function $M(\alpha, \gamma; x)$, which in his notation is ${}_1F_1(\alpha, \gamma; x)$, may be represented by the integral

$${}_1F_1\left(\frac{1}{2} - k + m,\ 2m + 1;\ x\right) = e^{\frac{x}{2}} 2^{2m}(2m!)\frac{x}{2\pi i}^{-2m} \int e^{\frac{\lambda x}{2}} \left(\frac{\lambda - 1}{\lambda + 1}\right)^k \times \frac{d\lambda}{(\lambda^2 - 1)^{m + 1/2}} \quad [17]$$

the path of integration starting at negative infinity, circling both -1 and $+1$ once in the positive direction, and going back to infinity.

If one makes the asymptotic approximation $\beta^2 \to 0$ as $\mathrm{Re} \to \infty$, $\mathrm{Re}\beta$ remaining finite, then the quantities k, m, and x may be identified, by virtue of Equations [13], [14], as

$$\left.\begin{aligned} m &= \frac{1}{2} \\ k &= \frac{\sqrt{\mathrm{Re}\beta}}{4} \\ x &= \sqrt{\mathrm{Re}\beta}\, r^2 \end{aligned}\right\} \quad [18]$$

The determination of the eigenvalues is then reduced to the problem of finding the values of $\sqrt{\mathrm{Re}\beta}$ for which the integral of Equation [17] vanishes when evaluated at $r = 1$. Thus, with the notation $2\omega = \sqrt{\mathrm{Re}\beta}$, one has as the integral analog of Equation [16]

$$\text{Imag. part of } \int e^{\lambda\omega}\left(\frac{\lambda - 1}{\lambda + 1}\right)^{\omega} \frac{d\lambda}{\lambda^2 - 1} = 0 \quad [19]$$

The calculations required to evaluate this integral are somewhat detailed, and since they have been exhibited and discussed elsewhere[8] they will not be reproduced here. The final result is

$$\mathrm{Re}\beta_n = 16\left(n + \frac{1}{6}\right)^2 \qquad n = 1, 2, 3, \ldots \quad [20]$$

which is an asymptotic formula from which the eigenvalues β_n may be calculated for any large value of the Reynolds number, say, $\mathrm{Re} > 100$.

The eigenvalues and eigenfunctions[9] also were calculated directly from Equation [7] on a differential analyzer Values for β_1, β_2, and β_3 obtained from the analyzer are plotted in Fig. 2, and the first two eigenfunctions $\varphi(\mathrm{Re}, \beta_1, r)$ and $\varphi(\mathrm{Re}, \beta_2, r)$ can be seen in Fig. 3. The asymptotic values for the products $\mathrm{Re}\beta_n$ obtained from the differential analyzer are compared in Table 1 with values computed from Equation [20]. The analyzer values for $\mathrm{Re}\beta_1$ and $\mathrm{Re}\beta_2$ are probably more reliable than those computed from the formula, but for $n \geq 3$ the formula values are likely to be better.

In Table 2 are given values for β_1, β_2, and β_3 obtained by direct calculation from existing tables for the confluent hypergeometric function.[6,7] Where it was possible to compare results it was found that values for β_n obtained from the differential analyzer agreed

[3] A considerable literature exists on the properties and solutions of this equation, and for this reason no details will be given here. See, for example, Bateman[4] and Whittaker and Watson.[5]

[4] "Partial Differential Equations of Mathematical Physics," by H. Bateman, Dover Publications, New York, N. Y., 1944, p. 457.

[5] "Modern Analysis," by E. T. Whittaker and G. N. Watson, Cambridge University Press, Cambridge, England, fourth edition, 1950, p. 337.

[6] "British Association for Advancement of Science Reports," 45th Meeting, Leeds, England, 1927, p. 220.

[7] "Tables of the Function $e^{-\omega z/\gamma} M(\alpha, \gamma; z)$," by A. D. MacDonald, Technical Report No. 130, Massachusetts Institute of Technology Research Laboratory of Electronics, July, 1944.

[8] "The Use of Confluent Hypergeometric Functions in Mathematical Physics and the Solution of an Eigenvalue Problem," by H. A. Lauwerier, Applied Scientific Research, vol. A2, 1950, p. 184.

[9] In what follows, it will be convenient to refer to these eigenfunctions $\varphi(\mathrm{Re}, \beta_n, r)$ corresponding to the different values of β_n, as the "harmonics" of the swirl.

TABLE 1 ASYMPTOTIC VALUES FOR $\mathrm{Re}\beta_n$

n	$\mathrm{Re}\beta_n = 16\left(n + \frac{1}{6}\right)^2$	$\mathrm{Re}\beta_n$ from analyzer
1	21.78	22.2
2	75.11	74.3
3	160.4	159.5
4	277.8	277
5	427.1	427
6	608.4	607

TABLE 2 VALUES OF β_n AND Re FOR FIRST THREE SWIRL HARMONICS[a]

First harmonic		Second harmonic		Third harmonic	
Re	β_1	Re	β_2	Re	β_3
0.146	3.780	2.394	6.262	3.626	9.040
0.436	3.690	3.833	5.867	4.966	8.663
1.155	3.464	8.057	4.842	7.598	7.997
2.811	2.998				
11.800	1.530				

[a] Calculated from tables in references 6, 7.

within 1 per cent of those computed from the tables as is seen in Fig. 2.

Several observations can be made concerning the asymptotic behavior of the eigenvalues for both large and small Reynolds numbers. From Fig. 2 it can be seen that the β_n approach finite values as Re tends to zero. These asymptotes are, in fact, located

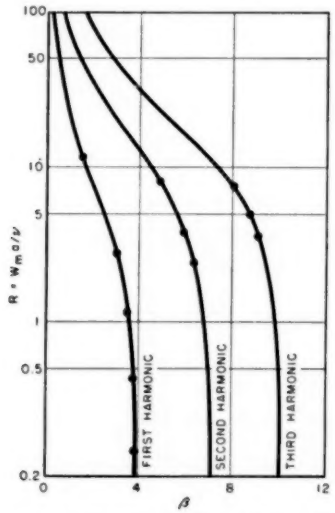

FIG. 2 CALCULATED VALUES FOR FIRST THREE EIGENVALUES (For Reynolds numbers greater than 100, see Equation [20]. Solid circles denote values of β from Table 2.)

at the zeros of the Bessel function of first order, $J_1(\beta r)_{r=1}$. This may be verified immediately by examination of Equation [7] which reduces to Bessel's equation when Re = 0. This limiting case corresponds to the physical situation of a pipe closed at one end, with a swirl of prescribed magnitude maintained at the other. The solution to Equation [5] is then a Fourier-Bessel expansion of the form

$$v = \sum_{n=1}^{\infty} b_n J_1(\beta_n r) e^{-\beta_n z}$$

which gives the intensity of the swirl for all z, with the constants b_n determined in the usual way to satisfy the prescribed initial conditions on $v(r, z)$ at $z = 0$.

The behavior of the quantities β_n and $\mathrm{Re}\beta_n$ as Re tends to infinity suggests that it is permissible, in obtaining solutions for large Re, to drop the term β^2 in the generating Equation [7], equivalent to the neglect of $\partial^2 v/\partial z^2$ in the Laplacian operator in Equation [2]. This results in an important simplification. Whereas with the term β^2 retained, it appears that the eigenfunctions are not orthogonal (note that the eigenvalue cannot be factored out), with the neglect of β^2 the resulting generating equation is of Sturm-Liouville type and, in principle at least, it is then possible to obtain orthogonal expansions.

An asymptotic representation for the eigenfunctions themselves also may be obtained. If in Equation [7] the following form for $\varphi(\mathrm{Re}, \beta, r)$ is assumed

$$\varphi(\mathrm{Re}, \beta, r) = \varphi_0(\mathrm{Re}, \beta, r) + \frac{1}{\mathrm{Re}^{1/4}}\varphi_1(\mathrm{Re}, \beta, r) + \frac{1}{\mathrm{Re}}\varphi_2(\mathrm{Re}, \beta, r) + \ldots\ldots [21]$$

one finds

$$\varphi(\mathrm{Re}, \beta, r) \sim J_1(\sqrt{\mathrm{Re}\beta}\, r) \ldots\ldots\ldots\ldots [22]$$

correct to terms of order $1/\mathrm{Re}$, where $J_1(\sqrt{\mathrm{Re}\beta}\, r)$ is the Bessel function of first order with argument $\sqrt{\mathrm{Re}\beta}\, r$. The eigenvalues obtained from this approximation by applying the boundary condition $\varphi(\mathrm{Re}, \beta, 1) = 0$ do not at all agree with those obtained from the differential analyzer. Using $\bar{\beta}_n$ to denote the values of β for which $J_1(\sqrt{\mathrm{Re}\beta}\ 1) = 0$

$$\mathrm{Re}\bar{\beta}_1 = 14.68$$
$$\mathrm{Re}\bar{\beta}_2 = 49.22$$
$$\mathrm{Re}\bar{\beta}_3 = 103.5$$

which may be compared with the values given in Table 1.

Although the eigenvalues obtained from the Bessel-function approximation are different from the analyzer values, the eigenfunctions themselves, apart from amplitude, are not far different, as may be seen in Fig. 3. The amplitude of the exact solution is uncertain, however, since it is not possible to obtain an absolute value for the maximum amplitude from the differential analyzer. It was assumed that the maximum amplitude of $\varphi(\mathrm{Re}, \beta, r)$ as $\mathrm{Re} \to \infty$ was the same as for very small Re where the confluent hypergeometric function

$$M\left(1 - \frac{\beta^2 + \mathrm{Re}\beta}{4\sqrt{\mathrm{Re}\beta}}, 2;\ \sqrt{\mathrm{Re}\beta}\, r^2\right)$$

has been computed. This assumption is certainly not rigorously correct.

As a final remark it is suggested that for engineering calculations the exact solution (Equations [14] and [15]) might be replaced by the approximation

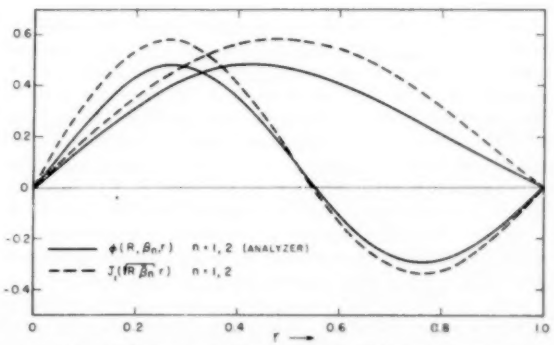

FIG. 3 FIRST AND SECOND SWIRL EIGENFUNCTIONS

$$v(r, z) \approx \sum_{n=1}^{\infty} b_n J_1 \left(\sqrt{\mathrm{Re}\bar{\beta}_n}\, r\right) e^{-\beta_n z} \quad [23]$$

where the $\bar{\beta}_n$ are obtained from the zeros of the Bessel function and the β_n are given by $\mathrm{Re}\beta_n = 16(n + 1/6)^2$. The coefficients b_n would be determined by a Fourier-Bessel expansion of the initial conditions on $v(r, z)$ at $z = 0$.

Determination of Perturbations u and w'

The swirl produces a pressure gradient in the radial direction, and since the swirl velocity decays in the z-direction, this radial pressure gradient is also a function of z. It follows that the total pressure gradient in the z-direction is no longer a constant, as for Poiseuille flow alone, and hence the axial-velocity distribution must depart from the parabolic Poiseuille shape.

This interaction between swirl and axial velocities is essentially nonlinear in character, and it does not appear possible to obtain an analytical solution to the exact equations. However, some estimate of the orders of magnitude of u and w' may be obtained by a momentum-integral method analogous to those commonly employed in boundary-layer problems.

Referring to Equation [1], it may be seen that if the radial velocity u and its derivatives are small compared to the swirl velocity v, this equation may be satisfied approximately by setting

$$\frac{v^2}{r} \approx \frac{\partial p}{\partial r} \quad [24]$$

then

$$\frac{\partial p}{\partial z} \approx \frac{\partial}{\partial z} \int_0^r \frac{v^2}{r}\, dr + K \quad [25]$$

where the constant of integration K is the pressure gradient produced by Poiseuille flow, which is $K = -4/\mathrm{Re}$ in the nondimensional scheme of variables employed. It will be recalled that in linearizing the exact equation of motion, Equation [2], it was necessary to discard terms involving w' and u. No assumption was made concerning the magnitude of the swirl velocity v; it may be of the same order of magnitude as the velocity of Poiseuille flow, W. Thus it seems likely, in the case where u and w' are in fact small compared to W and v, that the radial-pressure gradient can be given with good approximation by $v^2/r \approx \partial p/\partial r$.

The initial conditions to be imposed on u and w' in the momentum integral analysis require some attention. It can be shown by direct substitution into Equations [1, 2, 3] that solutions for $v(r)$ which are independent of z do not exist, so that in a fixed pipe the only swirl velocity distribution which is independent of z is $v \equiv 0$. In a rotating pipe, however, one can find the solution $v(r) = Cr$ which leaves the Poiseuille axial velocity distribution unchanged.

Now the theoretical model for the problem under consideration is that of a swirl of prescribed magnitude at $z = 0$ superimposed on Poiseuille flow in a stationary pipe, and it is evident from the foregoing discussion that about as close as one could come to achieving the conditions of the theoretical model is to change discontinuously from the rotating-pipe boundary condition to the fixed-pipe boundary condition. Under such circumstances the initial values of the perturbations u and w' at $z = 0+$ cannot be prescribed, and in fact it might be suspected they will come out to be infinite. Therefore, in order to calculate the magnitudes of u and w' for any finite z one must use as "initial" conditions the conditions at $z = \infty$, where the swirl has decayed to zero and $u = w' = 0$.

The starting point of the momentum integral analysis is the integration of Equation [3] over the pipe cross section

$$\int_0^1 ru \frac{\partial w}{\partial r}\, dr + \int_0^1 rw \frac{\partial w}{\partial z}\, dr = -\int_0^1 r \frac{\partial p}{\partial z}\, dr + \frac{1}{\mathrm{Re}} \left(\frac{\partial w}{\partial r}\right)_{r=1} \quad [26]$$

where the term $\partial^2 w/\partial z^2$ in $\nabla^2 w$ has been neglected, since in the integrated form of the equation this term does not contribute to the momentum-force balance. The continuity equation

$$\frac{\partial u}{\partial r} + \frac{u}{r} = -\frac{\partial w}{\partial z} \quad [27]$$

is used to eliminate u from Equation [26]; after some manipulations and integrations by parts, the resulting equation is

$$\frac{d}{dz} \int_0^1 rw^2\, dr = -\int_0^1 r \frac{\partial p}{\partial z}\, dr + \frac{1}{\mathrm{Re}} \left(\frac{\partial w}{\partial r}\right)_{r=1} \quad [28]$$

Besides satisfying the momentum relation Equation [28], w must satisfy certain initial, boundary, and continuity conditions; namely

$$\left.\begin{aligned} &w = 1 - r^2 \text{ at } z = \infty \\ &(w)_{r=1} = \left(\frac{\partial w}{\partial r}\right)_{r=0} = 0 \text{ for all } z \\ &\frac{d}{dz} \int_0^1 rw\, dr = 0 \text{ for all } z \end{aligned}\right\} \quad [29]$$

Assuming an expansion of the form $w = W + w'$, as follows

$$w = 1 - r^2 + a_0 + a_1 r + a_2 r^2 + a_3 r^3 \quad [30]$$

where the a's are functions of z, it may be easily verified that the conditions of Equations [29] are satisfied if

$$\left.\begin{aligned} a_1 &= 0 \\ a_2 &= -6a_0 \\ a_3 &= 5a_0 \end{aligned}\right\}$$

so that

$$w = 1 - r^2 + a_0(z) \times (1 - 6r^2 + 5r^3) \quad [31]$$

Using Equations [25] and [31], the momentum Equation [28] reduces to

$$\left(1 + \frac{3a_0}{2}\right) \frac{da_0}{dz} - \frac{42a_0}{\mathrm{Re}} = -14 \int_0^1 r\, dr \left\{\frac{\partial}{\partial z} \int_0^r \frac{[v(x, z)]^2}{x}\, dx\right\} \quad [32]$$

The solution to Equation [32] will be discussed for the particular case of a one-term approximation to $v(r, z)$

$$v(r, z) \approx 0.8 J_1\left(\sqrt{\mathrm{Re}\bar{\beta}_1}\, r\right) e^{-\beta_1 z} \quad [33]$$

with

$$\mathrm{Re} = 1000, \quad \beta_1 = 0.0222, \quad \bar{\beta}_1 = 0.01468$$

(The coefficient 0.8 was chosen arbitrarily. For comparison, the coefficient of the first term in a Fourier-Bessel expansion of $v(r, 0) = r/2$ comes out to be $b_1 = 0.648$.) With the swirl velocity $v(r, z)$ prescribed, the integral on the right of Equation [32] was evaluated by graphical integration. The resulting first-order nonlinear equation is

$$\left(1 + \frac{3}{2}a_0\right)\frac{da_0}{dz} = K_1 a_0 + K_2 e^{-2\beta_1 z} \quad \ldots\ldots [34]$$

$$K_1 = 0.0420, \quad K_2 = 0.0435$$

with the variable a_0 subject to the condition $a_0 = 0$ at $z = \infty$.

In order to investigate the properties of Equation [34] it is convenient to make the transformation, $t = e^{-2\beta_1 z}$, giving

$$\frac{da_0}{dt} = -\frac{K_1 a_0 + K_2 t}{2\beta_1 t + 3\beta_1 a_0 t} \quad \ldots\ldots [35]$$

the initial condition now being $a_0 = 0$ at $t = 0$. This equation is of the type studied by Poincaré,[10] who showed that any equation of the form $dy/dx = P(x, y)/Q(x, y)$ where both $P(x, y)$ and $Q(x, y)$ simultaneously vanish at $x = y = 0$ had a singularity at the origin identical to the singularity of the equation

$$\frac{dy}{dx} = \frac{ax + by}{cx + dy} \quad \ldots\ldots [36]$$

formed by keeping only the linear terms in $P(x, y)$ and $Q(x, y)$. The singularity at the origin may be a spiral, node, center, or saddle depending on the values of the coefficients a, b, c, d; in particular a saddle point singularity is characterized by the conditions $ad - bc > 0$, $(b - c)^2 + 4ad > 0$.

Returning to Equation [35], the coefficients a, b, c, d are identified as

$$\left.\begin{aligned} a &= -K_2 \\ b &= -K_1 \\ c &= 2\beta_1 \\ d &= 0 \end{aligned}\right\} \quad \ldots\ldots [37]$$

and it is seen that the conditions for a saddle point singularity are satisfied. The solution to Equation [36], with $d = 0$, is

$$ax + (b - c)y = \text{const}\left(\frac{c}{b - c}x\right)^{b/c} \quad \ldots\ldots [38]$$

so that the solution for Equation [35] in the vicinity of $t = 0$ is

$$K_2 t + \left((K_1 + 2\beta_1)a_0\right)\left(\frac{-2\beta_1 t}{K_1 + 2\beta_1}\right)^{\frac{K_1}{2\beta_1}} = \text{const} = D \quad \ldots\ldots [39]$$

The integral curves of Equation [39] passing through $t = a_0 = 0$ (the particular case of $D = 0$) are the asymptotes

$$K_2 t + (K_1 + 2\beta_1)a_0 = 0$$
$$t = 0$$

and of these two, the first is the proper choice to start the integration of Equation [34]. The integral curve which starts out from the origin along this asymptote has the slope

$$\frac{da_0}{dt} = -\frac{K_2}{K_1 + 2\beta_1}$$

which transforms back to the original variable z as

$$\frac{da_0}{dz} = \frac{2\beta_1 K_2}{K_1 + 2\beta_1} e^{-2\beta_1 z} \quad \ldots\ldots [40]$$

and therefore

$$a_0 = -\frac{K_2}{K_1 + 2\beta_1} e^{-2\beta_1 z} \quad \ldots\ldots [41]$$

Equation [41] is the asymptotic solution to Equation [34] valid in the vicinity of $z = \infty$, and the numerical integration is begun with this expression for a_0 and is carried forward toward $z = 0$. This asymptotic approximation could have been deduced directly from Equation [34] by noting that for $z \to \infty$ the term $3a_0/2$ may be neglected as small compared to unity. With this simplification Equation [41] follows immediately. There is no assurance however that this is the *only* integral curve which starts from $z = \infty$ with $a_0 = 0$, and the foregoing examination of the singular point is necessary to establish uniqueness of the solution.

The results of the numerical integration are presented in Figs. 4, 5, and 6. Fig. 4 shows a comparison between the Poiseuille velocity distribution and the perturbed axial velocity distribution, calculated for an intermediate value of a_0. For larger values of a_0 the maximum of $W + w'$ is at a finite value of r and not at the center line of the pipe. Fig. 5 exhibits the variation with r of the radial velocity u. The equation for u is obtained by integrating the continuity Equation [27] with w given by Equation [31].

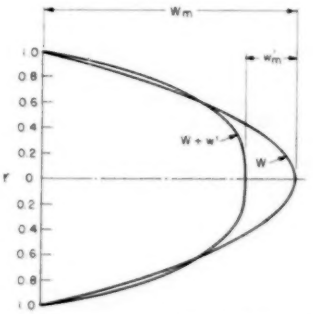

FIG. 4 DISTRIBUTIONS OF AXIAL VELOCITY WITH AND WITHOUT SWIRL

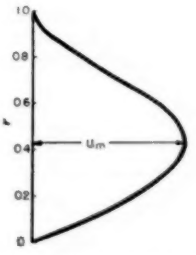

FIG. 5 DISTRIBUTION OF RADIAL VELOCITY INDUCED BY SWIRL

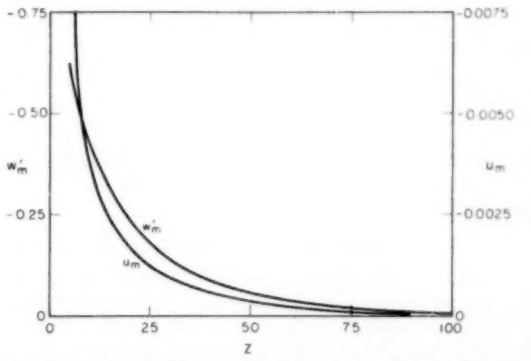

FIG. 6 CALCULATED MAXIMA OF AXIAL AND RADIAL-VELOCITY PERTURBATIONS AS A FUNCTION OF AXIAL DISTANCE DOWNSTREAM FROM SWIRL SECTION

(Term z is measured in number of pipe radii, and u_m and w'_m are measured in fraction of maximum velocity of undisturbed Poiseuille flow. Positive values of w'_m and u_m indicate, respectively, an increase in axial velocity and a radial velocity directed outward from pipe axis.)

The variations with z of the perturbation maxima u_m and w'_m are shown in Fig. 6. Both u_m and w'_m become infinite at $z = 0$, indicating that the entire analysis is not valid in this vicinity. The magnitude of w'_m at any given z can be used as an indication of the error introduced by the linearization of the swirl equation.

[10] See, for example, "Nonlinear Vibrations" by J. J. Stoker, Interscience Publishers, Inc., New York, N. Y., 1950, p. 36. Also see "Ordinary Differential Equations," by E. L. Ince, Dover Publications, New York, N. Y., p. 303.

Simple formulas for w'_m and u_m which are valid for large z may be written out explicitly. For large values of z the swirl always may be approximated by its first harmonic, $v(r, z) \approx b_1 J_1(\sqrt{14.68}\ r)e^{-\beta_1 z}$, and the term $3a_0/2$ dropped from Equation [32]. Now it was found by graphical integration that

$$\int_0^1 r\,dr \int^r \frac{[J_1(\sqrt{14.68}\ x)]^2}{x}\,dx = 0.109$$

so that by substitution in the linearized form of Equation [32]

$$w_m' = a_0 \approx -\frac{0.109 \times 14 \times b_1^2}{2\beta_1 + \frac{42}{\mathrm{Re}}} 2\beta_1 e^{-2\beta_1 z} \quad \ldots\ldots [42]$$

for large z. With this expression for a_0, Equation [31] is substituted into the continuity equation and the latter is integrated with the final result

$$u_m \approx 0.133 \times 2\beta_1 w'_m \quad \ldots\ldots [43]$$

Equations [42] and [43] can be used to estimate the magnitudes of u_m and w'_m at large z. The value of β_1 is known once the Reynolds number Re is known, and it is only necessary to choose b_1, which is the coefficient of $J_1(\sqrt{14.68}\ r)$ in the expansion of $v(r, 0)$.

As a concluding remark on the calculation of the perturbations u and w', it is possible as an alternative to numerical integration of Equation [34] to obtain a Diriclet's series expansion for $a_0(z)$

$$a_0(z) = \sum_{n=1}^{\infty} c_n e^{-2n\beta_1 z} \quad \ldots\ldots [44]$$

The recursion formula for the c_n comes out to be

$$c_n = -\frac{3\beta_1}{K_1 + 2n\beta_1} \sum_{k=1}^{n-1} k c_k c_{n-k} \quad \ldots\ldots [45]$$

with

$$c_1 = -\frac{K_2}{2\beta_1 + K_1}$$

The series

$$a_0(0) = \sum_{n=1}^{\infty} c_n$$

diverges, and the complicated nature of the recursion formula for the c_n makes it difficult to demonstrate convergence[11] of Equation [44] for all $z > 0$.

Experimental Investigation

Apparatus. The apparatus is shown schematically in Fig. 7. The test pipe was constructed of sections of Plexiglas tubing of nominal dimensions 1.25 in. ID × 1.50 in. OD. The water passed from a constant-head tank into a fixed section of pipe about 175 diam long, which was followed by a rotating section of about 25 diam in length. Following this "swirl section," the flow entered another fixed section, the test section, which was enclosed by a rectangular water-filled Plexiglas box, the purpose of which was to reduce optical distortion. The length of entrance section of pipe was sufficiently long to insure established Poiseuille flow for all Re < 2700; however, it can be estimated from the preceding analysis that at Re = 2700 the swirl section would have to be greater than 200 diam in length in order to obtain an approximately linear swirl-velocity distribution. Hence, in the tests, the actual swirl-velocity distribution at the entrance to the test section was not well defined. This, however, did not prove to be a serious problem since, as will be seen later, the values for the decay rate β can be determined without the knowledge of the initial swirl distribution.

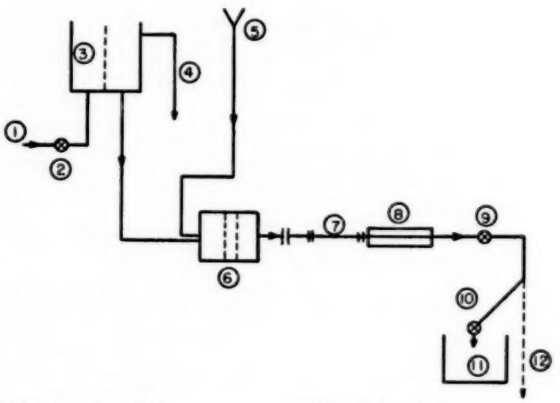

1 City water supply
2 Inlet control valve
3 Constant-head tank
4 Overflow to sump
5 Dye or oil-drop reservoir
6 Entrance chamber
7 Rotating section
8 Test section
9 Discharge valve
10 Fine control valve
11 Weighing tank
12 Discharge to sump

Fig. 7 Schematic of Flow System

Description of Tests. The first series of tests were made to determine the laminar flow stability limits in the form of a limiting curve of angular velocity of swirl section versus Reynolds number. Instability of the flow was determined through observation of a filament of dye introduced at the pipe entrance. At fixed Reynolds number the angular velocity of the swirl section was increased slowly until a definite breakup of the dye filament was observed, as illustrated in Fig. 8.

Two markedly different types of instability were observed. For Reynolds numbers less than about 1800 the instability of the swirl was characterized by seemingly nonperiodic sinuous motions

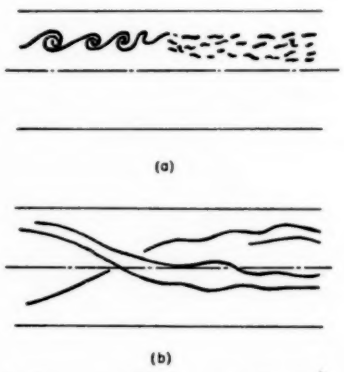

Fig. 8 Schematics of Observed Instabilities

(*a*, Initial periodic eddy structure obtained at high Reynolds numbers. Eddies broke up into turbulent flow. *b*, Sinuous oscillations obtained at low Reynolds numbers. These oscillations destroyed swirl but flow remained laminar throughout, returning to Poiseuille flow far downstream of instability.)

[11] Convergence theorems for Diriclet's series may be found in "The General Theory of Diriclet's Series," by G. H. Hardy and M. Riesz, Cambridge Tracts in Mathematics and Mathematical Physics, No. 18, University Press, Cambridge, England, 1915.

of the dye filament. These disturbances grew until there was no longer any detectable swirl; thereafter the disturbances decayed and some distance downstream from the unstable region the flow became laminar again.

For Reynolds numbers in excess of about 2500 the instability of the swirl appeared to begin as a series of eddies of definite spatial frequency, somewhat like the Taylor-type instability found under certain conditions in the annulus between two concentric rotating cylinders.[12] These eddies grew rapidly into bursts of turbulence; the flow downstream from the instability was a turbulent flow with no detectable mean velocity of rotation. In the intermediate range $1800 < \mathrm{Re} < 2500$ the instability was of mixed type.

The location of the first unstable oscillations or eddies was found to move downstream with increased Reynolds number. It was interesting to note that from the end of the rotating section, up to the onset of the instability, the flow in the pipe was a decaying swirling laminar flow. Evidently the disturbances responsible for the ultimate instability are of high frequency and initially infinitesimal. Under suitable conditions these disturbances will grow even though the main motion decays.

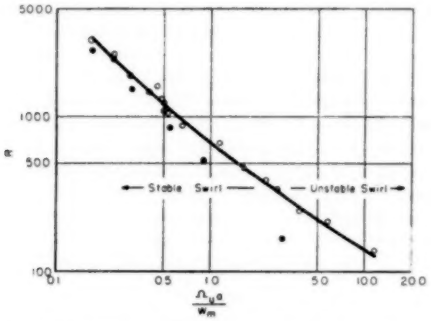

FIG. 9 CRITICAL CURVE FOR SWIRL INSTABILITY

(Ω_u denotes angular velocity of swirl section at onset of instability, a radius of pipe, and W_m maximum velocity of undisturbed Poiseuille flow. Solid circles denote points at which measurements of stable decay were made.)

The dimensionless parameter $\Omega_u a/W_m$ is plotted against Re in Fig. 9 where Ω_u denotes that angular velocity of the swirl section at which instability occurred. It should be remarked that these instability data are strictly applicable only for the case at hand, and that other values of Ω_u in all likelihood would have been obtained if the swirl section had been of different length.

Measurement of Swirl-Decay Rate. Velocity measurements were made through motion-picture studies of oil droplets introduced in the flow at the pipe entrance. The oil used was a mixture of mineral oil and α-chloronaphthalene, dyed red. While this velocity-measurement technique was adequate for measurement of the decay rate β, it was found to be not sufficiently precise for measurement of the perturbations u and w', and hence no experimental data were obtained for these latter quantities.

Swirl velocities were measured at successive stations downstream from the rotating sections. If the solutions to the swirl equation are of the form

$$v(r, z) = v(r, 0)e^{-\beta z}$$

then

$$\beta = -\frac{1}{v(r, z)} \frac{\partial v(r, z)}{\partial z}$$

The value for β may be thus obtained from measured values of v and $\partial v/\partial z$; no knowledge of the initial distribution $v(r, 0)$ is required.

Measurements of swirl decay were made at Reynolds numbers Re = 177, 530, 860, 1515, 2700, and at successive distances downstream from the swirl section. The angular velocity of the swirl section was kept constant at $\Omega = 1.95$ radians per sec, for all tests. This value for the angular velocity was chosen so that test conditions would be near critical conditions for swirl instability, as can be seen in Fig. 9. Tests were made at near critical conditions because it is here that the greatest departure from results predicted by a linear theory should be expected.

The experimental results are plotted in Fig. 10. It may be seen that measured values for β lie between the theoretical values for β_1 and β_2 and more closely coincide with the value of β_1 with increasing distance downstream. This constitutes a confirmation of the theory. One expects to find an over-all decay rate higher than that of the first harmonic, since the swirl is composed of all harmonics. However, sufficiently far downstream the decay rate

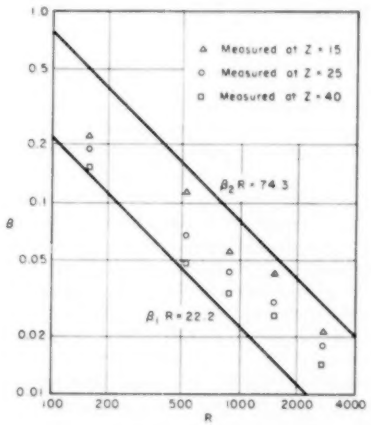

FIG. 10 COMPARISON OF THEORETICAL AND EXPERIMENTAL VALUES FOR DECAY PARAMETER

(Axial distance z given in number of pipe radii downstream from swirl section. Estimated error in measurement less than approximately ±10 per cent.)

should approach that of the first harmonic, since contributions from the higher harmonics decay faster than the first.

CONCLUSIONS

1 The decay of a rotationally symmetric swirl superimposed on Poiseuille flow may be predicted successfully by linearized theory, even at conditions near the critical conditions for instability of the swirl.

2 At least two different types of swirl instability occur. For $\mathrm{Re} < 1800$ the instability is aperiodic and sinuous; whereas at higher Reynolds numbers the instability begins initially as a series of periodic eddies.

ACKNOWLEDGMENT

The author wishes to thank Prof. W. W. Hagerty for his assistance and encouragement during the course of this investigation. The author is grateful to Prof. R. A. Dodge and Prof. P. F. Chenea for many helpful criticisms and suggestions. Appreciation is expressed to Messrs. M. A. Brull, J. R. Sellars, and J. E. Cline for aid in computations and data reduction, and to Mr. M. W. Kaufman for his help in the construction of the equipment.

[12] "Stability of a Viscous Fluid Contained Between Two Rotating Cylinders," by G. I. Taylor, *Philosophical Transactions*, vol. 223, 1923, p. 289.

On Application of a Quasi-Static Variational Principle to a System With Damping

By MORRIS MORDUCHOW,[1] BROOKLYN, N. Y.

The principal bending modes of vibration of a beam with a damping force proportional to the velocity are considered. It is shown that, in an important class of cases, the damping has exactly no effect on the mode shapes. It is further shown that the linear differential equation for the vibrating beam with damping can be transformed mathematically into a stationary condition after eliminating the time as a variable. Application of the Rayleigh method to this condition then leads to general approximate results for the logarithmic decrement, and for the effect of damping on the natural frequency, not only in the fundamental mode, but also in any higher principal mode.

Introduction

The aim of this paper is to show how a stationary condition, leading to fruitful results, can sometimes be derived rigorously for a nonconservative system by first eliminating the time as a variable. Let, for example, a system be characterized by a linear homogeneous partial differential equation containing, in addition to inertia terms, damping terms proportional to first-time derivatives of displacement. Moreover, let the coefficients of the equation be independent of time. Then, by writing the solution as an exponential function of the time, the time can be eliminated completely, and the damping (nonconservative) terms will now appear similar to the other terms in the resulting equation. A stationary condition may now be obtainable from this latter equation, and the fact that some terms are present which originally represented damping effects will in itself have no bearing on whether such a condition can now actually be derived.

In the present analysis, the existence and use of such a quasi-static variational principle for a nonconservative system will be illustrated by the relatively simple case of a vibrating beam with a damping force proportional to the velocity. This force is of the familiar dashpot type. Such a force may arise, for example, in the slow oscillations of a moving wing in air, where it represents a (restoring) lift force due to the change of angle of attack caused by a small (vibrational) velocity normal to the direction of flight. In addition to the theoretical significance of a variational principle for such a case, such a principle also has considerable practical value here, since by a simple application of the Rayleigh method, useful general approximate results can be obtained.

A secondary result of the present analysis is the theorem that under certain conditions (which are physically quite possible) a dashpot type of damping force has exactly no effect on the shapes of the principal modes of vibration. This helps justify the assumption, which otherwise might have to be made on a possibly less concrete basis, that, in general, the damping forces have only little effect on the mode shapes. As will be seen in the analysis, an assumption of this sort must be made in applying the Rayleigh method here, and it is only through this assumption that the final results to be obtained are approximate.

It is, perhaps, worth while to remark that in dynamics the existence, per se, of variational principles for certain types of nonconservative systems is well known. Thus Hamilton's principle in the form valid for a conservative system is known also to be valid for systems representable by a generalized velocity-dependent potential, for example, reference (1).[2] The quasi-static type of stationary condition derived here, however, is of a different nature. The simple type of damping force treated here is, in fact, not representable by a velocity-dependent potential,[3] and the partial differential equation for the vibrating beam with such a damping force could not be transformed into a stationary condition by standard procedures (a good account of which can be found in reference 3) without first eliminating the time.

It also may be remarked that although work-energy methods have been applied for the analysis of damped systems (4, 5), the relatively direct quasi-static variational approach given in the present analysis appears not to have been thus far expounded, although a specific application of this approach has been made in reference (6).

Analysis

The linear equation for the free bending vibrations of an elastic beam, neglecting shearing effects, with a damping force $f(x)\dot{Y}$ per unit length proportional to the bending velocity, can be written as

$$(EIY'')'' + f(x)\dot{Y} + m\ddot{Y} = 0 \quad \ldots\ldots [1]$$

where $EI(x)$ is the cross-sectional bending stiffness of the beam, $m(x)$ is the mass per unit length of the beam, $Y(x,t)$ is the bending displacement, x is distance along the beam measured from one end, and a prime and dot denote, respectively, (partial) differentiation with respect to x and to the time t. The terms in Equation [1] represent, respectively, the elastic resistance, external damping forces, and inertia forces.

The time can be eliminated from Equation [1] by writing the solution as

$$Y(x,t) = y(x)e^{pt} \quad \ldots\ldots [2]$$

where p is a (complex) constant. Equation [1] then leads to the following ordinary differential equation for $y(x)$

$$(EIy'')'' + [f(x)p + m(x)p^2]y = 0 \quad \ldots\ldots [3]$$

Equation [3] shows that the damping term now appears mathematically like the inertia term, except that it is proportional to p instead of p^2.

The nontrivial solutions for the eigenvalues p_n and the corresponding modes of deflection $y_n(x)$ determine the properties of the principal modes of vibration. Methods of obtaining these solu-

[1] Associate Professor of Mathematics, Polytechnic Institute of Brooklyn.

Contributed by the Applied Mechanics Division and presented at the Annual Meeting, New York, N. Y., November 29–December 4, 1953, of The American Society of Mechanical Engineers.

Discussion of this paper should be addressed to the Secretary, ASME, 29 West 39th Street, New York, N. Y., and will be accepted until April 12, 1954, for publication at a later date. Discussion received after the closing date will be returned.

Note: Statements and opinions advanced in papers are to be understood as individual expressions of their authors and not those of the Society. Manuscript received by ASME Applied Mechanics Division, December 18, 1952. Paper No. 53—A-3.

[2] Numbers in parentheses refer to the Bibliography at the end of the paper.

[3] This is not the same as Rayleigh's dissipation function, which can be used to represent such a force, references (1) and (2).

tions without damping are well known (2, 7). In this analysis, emphasis will be placed on determination of the effect of damping on the modes.

By multiplying Equation [3] by $(\delta y)dx$, where δy denotes a variation in y (essentially a virtual displacement) satisfying the boundary conditions, integrating Equation [3] over the length l of the beam, and using the technique of integration by parts together with the well-known relation $d(\delta y) = \delta(dy)$ (reference 3), one obtains the following stationary condition under a wide variety of boundary conditions[4]

$$\delta\left\{\int_0^l \frac{1}{2} EIy''^2 dx + \int_0^l \frac{1}{2} [f(x)p + m(x)p^2]y^2 dx\right\} = 0 \quad [4]$$

Thus the nonconservative system treated here, and characterized by the partial differential Equation [1], is also characterized by a quasi-static variational condition, namely, Equation [4].

Equation [4] can be interpreted physically. The first integral there is the familiar quantity representing the strain energy of the entire beam in bending for a static deflection $y(x)$. The second integral represents the sum of the work done against the damping forces and the inertia forces, which now appear like a combined static unit loading of $w(x) = [f(x)p + m(x)p^2]y(x)$, proportional to the deflection $y(x)$.

By applying Rayleigh's method (8), Equation [4] can be used to advantage in obtaining approximately the effect of the damping on the principal modes. As an approximation in obtaining the eigenvalues p_n it may be assumed that in any principal mode the deflection shape $y_n(x)$ is affected negligibly by the damping. Although this assumption may appear reasonable physically, it should be noted further that it will be exactly valid when the ratio $f(x)/m(x)$ is a constant[5] (even if the damping coefficient $f(x)$ is large). A proof is given in the Appendix.

For any principal mode with damping, let

$$y_n(x) = a_n y_{n0}(x) \quad [5]$$

where a_n is a constant considered as unknown, and $y_{n0}(x)$ is the mode of deflection without damping, considered to be known. Then, setting the derivative of the braced quantity in Equation [4] with respect to a_n equal to zero, and requiring $a_n \neq 0$, leads to the following value of p_n for the nth mode

$$p_n = -D_n \pm if_n \quad [6a]$$

where

$$D_n = \frac{1}{2}\frac{\int_0^l f(x)y_{n0}^2(x)\,dx}{\int_0^l m(x)y_{n0}^2(x)\,dx}, \quad f_n = P_{n0}\left[1 - \left(\frac{D_n}{P_{n0}}\right)^2\right]^{1/2} \quad [6b]$$

$$p_{n0} = \pm iP_{n0} \quad (P_{n0} \text{ real})$$

and p_{n0} is the value of p_n without damping $[f(x) = 0]$. In deriving Equations [6a] and [6b] use has been made of the relation

$$\int_0^l EIy''_{n0}{}^2\,dx = -p_{n0}^2 \int_0^l m y_{n0}^2\,dx$$

Equations [6a] and [6b] are particularly simple, since they have a form which is quite familiar in the theory of a system of one degree of freedom with constant damping and elastic coefficients per unit mass. In any principal mode, the natural frequency will be proportional to f_n, while the logarithmic decrement will be proportional to D_n/f_n. If D_n is negative, the vibrations are dynamically unstable.

It should be observed that in this type of application, giving the effect of the (positive or negative) damping on the decay or growth, as well as on the frequencies, of the principal modes of oscillation once the natural frequencies (P_{n0}) of the undamped system are determined, Rayleigh's method can be applied with accuracy not only to the fundamental mode (as is ordinarily done), but also to the higher modes. This is not to be confused with Ritz's extension—Rayleigh-Ritz method—of Rayleigh's method to higher modes, which consists of assuming, contrary to Equation [5], more than one unknown coefficient in the expression for the deflected shape (7).

From Equation [6b] for D_n, it is seen that the value of D_n is not expected to be very sensitive to the function $y_{n0}(x)$. The value of D_n can, in fact, be interpreted as one half of the ratio of the weighted average value of $f(x)$ to the weighted average value of $m(x)$ over the length of the beam, the weights being proportional to the square of the deflection shape $y_{n0}^2(x)$. Consequently D_n will be approximately independent of the mode of vibration. Hence the logarithmic decrement will be approximately inversely proportional to the natural frequency f_n. The expression in Equation [6b] for f_n, which gives the effect of the damping on the natural frequencies,[6] indicates that the type of damping assumed here, in general, will decrease the natural frequency in any mode, and that this decrease becomes relatively smaller and smaller in the higher modes (where P_{n0} assumes higher and higher values). Equations [6a] and [6b] are convenient to apply in practice.[7] Equations essentially of the form of the variational condition, Equation [4], and of the results, Equations [6a] and [6b], have been applied specifically to vibrations of rotating helicopter blades in quasi-steady flow (6).

BIBLIOGRAPHY

1 "Classical Mechanics," by H. Goldstein, Addison-Wesley Press, Inc., Cambridge, Mass., 1951, pp. 19–22, 38–40.

2 "Mathematical Methods in Engineering," by Th. von Kármán and M. A. Biot, McGraw-Hill Book Company, Inc., New York, N. Y., 1940, pp. 216–220, 286–294, 352–358.

3 "Methods of Applied Mathematics," by F. B. Hildebrand, Prentice-Hall, Inc., New York, N. Y., 1952, chapter 2.

4 "Mechanical Vibrations," by J. P. Den Hartog, McGraw-Hill Book Company, Inc., New York, N. Y., third edition, 1947, pp. 168–170.

5 "Dynamic Effects in Rotor Blade Bending," by A. H. Flax and L. Goland, *Journal of Aeronautical Sciences*, vol. 18, 1951, pp. 813–829.

6 "A Theoretical Analysis of Elastic Vibrations of Fixed-Ended and Hinged Helicopter Blades in Hovering and Vertical Flight," by M. Morduchow, NACA Technical Note, No. 1999, January, 1950.

7 "Vibration Problems in Engineering," by S. Timoshenko, McGraw-Hill Book Company, second edition, 1937, pp. 83–93, 307–348, 370–382.

8 "Theory of Sound," by Lord Rayleigh, Dover Publications, New York, N. Y., 1945, pp. 112–113, 287–289.

Appendix

It is desired to prove that if (and only if) the ratio $f(x)/m(x)$ is a constant, then the shapes of the modes of deflection determined by the differential Equation [1] are unaffected by the damping term $f(x)\dot{Y}$.

Let p_{n0} and $y_{n0}(x)$ be, respectively, the value of p and the mode-

[4] Namely, $[(\delta y')(EIy'') - (\delta y)(EIy'')']_0^l = 0$

[5] It may be observed, at least in the present case, that if this condition holds, then there will be no damping coupling, since then $\int_0^l f(x)\varphi_n(x)\varphi_m(x)dx = 0$, where φ_n and φ_m are two different principal mode shapes of vibration.

[6] This is in contrast to the analysis, for example, in reference (4) where it is assumed that the damping will have a negligible effect on the natural frequencies as well as on the mode shapes.

[7] In actual calculations, an approximate value of D_n for all modes can be calculated rapidly by inserting in Equations [6b] a simple function, such as a polynomial, satisfying the boundary conditions.

shape $y_n(x)$ for the nth mode without damping. Then Equation [3] without damping implies

$$(EIy_{n0}'')'' = -mp_{n0}^2 y_{n0} \quad [7]$$

Substituting $y = y_{n0}(x)$ into Equation [3], and using Equation [7], it follows that Equation [3] with the damping term will be satisfied by the solution $y = y_{n0}(x)$ if and only if

$$y_{n0}(x)[f(x)p_n + m(x)p_n^2 - p_{n0}^2 m(x)] = 0 \quad [8]$$

Since $y_{n0}(x) \not\equiv 0$, the bracketed quantity in Equation [8] must vanish. This condition can be written as

$$\frac{p_n^2 - p_{n0}^2}{p_n} = -\frac{f(x)}{m(x)} \quad [9]$$

Since the left side of Equation [9] is a constant for any particular mode, the right side also must be a constant. This proves the theorem.

It may be noted that by solving Equation [9] for p_n in case $f(x)/m(x)$ is a constant, one obtains exactly the same results as Equations [6a] and [6b] for that case.

Flexibility of Piping Systems Supported by Equally Spaced Rigid Hangers

By J. E. BROCK,[1] ST. LOUIS, MO.

Exact methods are developed for the analysis of single-plane piping configurations in which there occur long horizontal runs supported on equally spaced hangers of rigid type. Two important cases are treated in detail and are illustrated by examples.

Nomenclature

The following nomenclature is used in the paper:

a = spacing between supports, in.
b = overhang (see Figs. 5, 6, 10, and 12), in.
$c = b + 2aq \approx b + 0.2887\ a$, in.
$d = b(b/2 + 2aq) \approx b(b/2 + 0.2887a)$, in.[2]
$e = b^2(b/3 + 2aq) \approx b^2(b/3 + 0.2887a)$, in.[3]
$f = b^2(b/6 + aq) - qa^3/6 \approx b^2(b/6 + 0.1443a) - 0.0241a^3$, in.[3]
$g = b^3(b/8 + aq) - qa^3b/6 \approx b^3(b/8 + 0.1443a) - 0.0241a^3b$, in.[4]
h = height of riser (see Table 2 and Figs. 8 and 12), in.
k = number identifying support point
k = bend flexibility factor $= 0.4125\ (D - t)^2/Rt$ (but not less than 1.0)
l = semi-width of expansion "U" bend (see Table 2), in.
m, n = number of bays
$p_m = (1 - \beta_1{}^m)/(1 + \beta_1{}^m)$; $p_m \approx 1.0$ for $m > 4$
$q_m = p_m/4\sqrt{3}$; $q_m \approx 0.1443$ for $m > 4$
r_1, r_2, r_3; s_1, s_2, s_3 = coefficients in Equations [22] and [23] (see Table 2)
t = wall thickness of pipe, in.
$t = Ka^3/24\ EI$ (parameter used in Appendix)
w = unit weight of pipe, covering, and contents, lb per in.
x = horizontal co-ordinate (see text after Equation [27]), in.
y = vertical co-ordinate (see Appendix), in.
$A_{1, 2, 3, 4}$ = constants of summation in Equations [4] and [66], lb-in.
D = outside diameter of pipe, in.
E = modulus of elasticity, psi
F = supporting force acting on riser (see Fig. 12), lb
I = moment of inertia of pipe cross section, in.[4]
K = spring constant (see Appendix), lb per in.
M, N = moment, lb-in.
P = horizontal thrust, lb
$Q, \bar{Q}$ = vertical force (see Figs. 8, 12, 14, 15), lb
R = vertical reaction at support, lb
R = (center line) radius of pipe bend or elbow, in.
$\bar{R}$ = "preset" force (see Appendix), lb
α = angle of double offset expansion bend (see Table 2)
$\beta_1 = -2 + \sqrt{3} = -0.26795$
$\beta_2 = -2 - \sqrt{3} = -3.73205$
δ = vertical deflection, in.
ϵ = thermal expansion in vertical leg, in.
ζ, η, λ; μ, ν, ξ; ρ, σ, τ = coefficients (see Equations [42] through [50])
θ = slope
$\lambda_{1, 2, 3, 4}$ = roots of indicial equation (see Appendix)
Δ = horizontal expansion, in.

While some symbols serve double duty (e.g., the symbol R), this should cause no confusion.

Introduction

It is customary when analyzing the flexibility of piping systems to assume that the system of supports and hangers is such as to provide vertical upward forces exactly equal and opposite to the downward forces exerted by gravity, and indeed such that this equilibrium is maintained as the piping system suffers deformations due to thermal expansion. While it is evident that the discrete upward forces provided by the supporting system cannot locally equilibrate the weight of the structure, in certain cases the assumption is warranted that support and gravity forces can be neglected during the flexibility analysis. This is true, for example, if constant-support-type spring hangers are employed and vertical deflections are small.

However, if rigid hangers or ordinary spring hangers are used, it is necessary to consider critically the possibility that an analysis based on neglecting hanger and gravity forces is totally invalid. This also may be true even if constant-support hangers are used. For example, in the case of a 500-ft line containing a square U-bend 20 ft long and 20 ft high somewhere near its center, 1 ft of thermal expansion (corresponding to saturated steam at about 150 psig) would call for a lateral deflection of about 42 in. at the legs of the U-bend and in its plane. If this deflection were vertical, no reasonable combination of ordinary hangers could accommodate it; if it were horizontal, an unusual arrangement of rollers or the use of inordinately long hanger rods would be called for. Otherwise, an analysis based on the aforementioned assumption would be invalid.

In the following we will consider systems lying in one plane and supported by "rigid" hangers having the following properties: At the point of support they (*a*) exert no axial force on the pipe, (*b*) completely prevent deflection perpendicular to the pipe and in the plane of the configuration, and (*c*) exert no moment on the pipe in the plane of the configuration. Inasmuch as attention will be confined to cases where there is no load or deflection perpendicular to the plane of the configuration, it is not necessary to define the behavior of the supports with respect to forces perpendicular to this plane or moments whose representative vectors lie in this plane.

Such supports are widely used in practice. If the configu-

---

[1] Director of Research, Midwest Piping Company, Inc. Mem. ASME.

Contributed by the Applied Mechanics Division and presented at the Annual Meeting, New York, N. Y., November 29–December 4, 1953, of The American Society of Mechanical Engineers.

Discussion of this paper should be addressed to the Secretary, ASME, 29 West 39th Street, New York, N. Y., and will be accepted until April 12, 1954, for publication at a later date. Discussion received after the closing date will be returned.

Note: Statements and opinions advanced in papers are to be understood as individual expressions of their authors and not those of the Society. Manuscript received by ASME Applied Mechanics Division, December 24, 1952. Paper No. 53—A-6.

ration is vertical, rigid hangers, Fig. 1(*a*), or roller supports, Fig. 1(*b*), exert constraints of this nature. If the configuration is horizontal, roller supports behave in this manner. In the case of the rigid hangers, it is presumed that the axial deflection is small compared to the length of the hanger rod, say not over one-fifth its length, so that the "lift" as the point of support swings in the arc of a circle does not exceed one-tenth the axial deflection. If the hanger rods are set so that they are vertical at a temperature half way between the hot and cold extremes, the lift will not exceed one-fortieth of the axial motion.

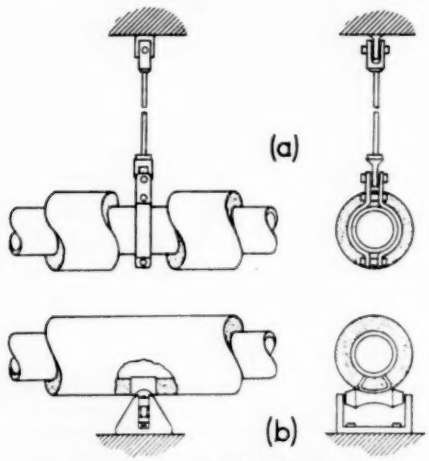

FIG. 1 TYPICAL PIPE-HANGER DETAILS

In what follows, attention is confined to configurations which lie in a vertical plane.

END RIGIDITY OF CONTINUOUS BEAMS

In this section we will obtain some relations between end moments applied to uniformly loaded equispan continuous beams and the angular rotations observed at the ends.

Fig. 2 represents a typical span. From elementary considerations, we have

$$-EI\theta_k = wa^3/24 + M_k a/3 + M_{k+1}a/6 \quad [1]$$

$$EI\theta_{k+1} = wa^3/24 + M_k a/6 + M_{k+1}a/3 \quad [2]$$

(Here and later, the index k assumes only integer values.) From these equations, we easily obtain the "three-moment equation"

$$M_k + 4M_{k+1} + M_{k+2} = -wa^2/2 \quad [3]$$

This is a nonhomogeneous linear difference equation of second order. The solution of the corresponding homogeneous equation is given by von Kármán and Biot[1] and to it we add the obvious complementary function, $-wa^2/12$, to obtain

$$M_k = -wa^2/12 + A_1\beta_1^k + A_2\beta_2^k \quad [4]$$

where

$$\beta_1 = -2 + \sqrt{3} = -0.26795 \quad [5]$$

$$\beta_2 = -2 - \sqrt{3} = -3.73205 \quad [6]$$

For future use, we note that

$$\beta_1\beta_2 = 1 \quad [7]$$

[1] "Mathematical Methods in Engineering," by Th. von Kármán and M. A. Biot, McGraw-Hill Book Company, Inc., New York, N. Y., 1940, p. 443.

Substituting the solution into Equation [1], we find

$$\theta_k = a(A_2\beta_2^k - A_1\beta_1^k)/2\sqrt{3}\ EI \quad [8]$$

It is also of interest to note in passing that θ_k satisfies the homogeneous difference equation

$$\theta_k + 4\theta_{k+1} + \theta_{k+2} = 0 \quad [9]$$

The first application we shall make of the foregoing is to the situation illustrated in Fig. 3, where moments of equal magnitude and sense are applied at the ends of a uniformly loaded beam having n equal spans and it is desired to find the relation between these moments and the end rotations which are produced. If we number the support points starting with zero on the left and ending with n on the right, symmetry requires that

$$M_k = M_{n-k} \quad [10]$$

From this relation, it easily may be determined that

$$A_2 = A_1\beta_1^n \quad [11]$$

so that

$$M_k = -wa^2/12 + A\,(\beta_1^{n-k} + \beta_1^k) \quad [12]$$

and

$$\theta_k = aA\,(\beta_1^{n-k} - \beta_1^k)/2\sqrt{3}\ EI \quad [13]$$

We thus have

$$\theta_k = \frac{a}{2\sqrt{3}\,EI}(M_k + wa^2/12)\frac{(\beta_1^{n-k} - \beta_1^k)}{(\beta_1^{n-k} + \beta_1^k)} \quad [14]$$

For the ends, we may take $k = 0$, and we get

$$\theta_0 = \frac{-a}{2\sqrt{3}\,EI}(M_0 + wa^2/12)\,p_n = \frac{-2a}{EI}(M_0 + wa^2/12)q_n \quad [15]$$

where

$$p_n = (1 - \beta_1^n)/(1 + \beta_1^n) \quad [16]$$

and

$$q_n = p_n/4\sqrt{3} \quad [17]$$

Now, comparing Figs. 2 and 3, we see that M_0 corresponds to the end moment M whereas θ_0 corresponds to the negative of the end slope θ. Thus, the desired relationship is

$$\theta = \frac{2aq_n}{EI}(M + wa^2/12) \quad [18]$$

The second application we shall make is derivable directly from the first. Let a uniformly loaded beam having m spans be built in horizontally at one end and loaded by a moment M at the other. We seek the relationship between this end moment and the corresponding rotation at this point. The situation is illustrated in Fig. 4.

This case is easily seen to derive from the preceding upon taking $n = 2m$. Thus, the desired relation is

$$\theta = \frac{2aq_{2m}}{EI}(M + wa^2/12) \quad [19]$$

The values of p_n and q_n are easily calculated and the results are given in Table 1.

For simplicity in application, we next incorporate the effect of overhanging "ears" of length b. With the use of Equations [18] and [19] we find

$$EI\theta = Mc - Qd - wf \quad [20]$$

$$EI\delta = Md - Qe - wg \quad [21]$$

where in the formulas for c, d, e, f, and g (see nomenclature) we use q_n for q in the case illustrated in Fig. 5, and we use q_{2n} for q in the case illustrated in Fig. 6.

TABLE 1 VALUES OF p_n AND q_n

n	p_n	q_n
0	0.000000	0.000000
1	1.732051	0.250000
2	0.866025	0.125000
3	1.039230	0.150000
4	0.989743	0.142857
5	1.002766	0.144737
6	0.999260	0.144231
7	1.000197	0.144366
8	0.999947	0.144330
9	1.000014	0.144340
10	0.999996	0.144337
11	1.000001	0.144338
12 or more	1.000000	0.144338

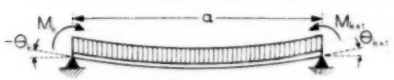

FIG. 2 TYPICAL SPAN

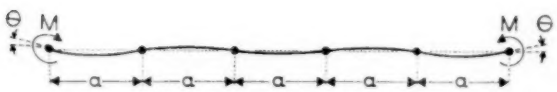

FIG. 3 UNIFORMLY LOADED BEAM WITH n EQUAL SPANS

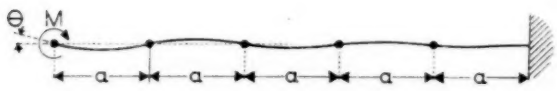

FIG. 4 UNIFORMLY LOADED BUILT-IN BEAM WITH m EQUAL SPANS

FIG. 5 SYMMETRICAL BEAM WITH OVERHANGING "EARS"

FIG. 6 BUILT-IN BEAM WITH OVERHANGING "EARS"

APPLICATIONS

Fig. 7 shows several typical configurations which may be analyzed by the use of the preceding developments. Specific examples illustrating the cases shown in Fig. 7 (a) and (b) will be given in what follows but a few general remarks are in order before doing so.

In case (a), one may use Equations [20] and [21] with the appropriate values of n even though the spans adjacent to the walls are shorter than the other spans; actually one may as well take n as being indefinitely large since the values of q are so insensitive to values of n as long as $n > 3$. Thus, in case (b), we may assume that the U-bend is acted upon by a symmetrically disposed set of forces and moments; this obviously will simplify the analysis. In effect, as "seen" from the vantage point of the U-bend, the straight run to the right is just as flexible as the straight run to the left. Case (c) may be regarded as a combination of two of the cases shown in Fig. 6 and one of the cases shown in Fig. 5. Actually, of course, the symmetry assumed in Fig. 5 does not quite hold true, but the difference is very slight as long as the corresponding overhanging ears are equal in length. For case (d), the difference in length of the risers does not permit the assumption of symmetry so that the case shown in Fig. 5 cannot be used. However, this case can be considered as two examples of case (a), placed "back to back"; or in other words, considering all horizontal runs as infinitely long, all changes in height can be handled in precisely the same fashion. These remarks hold true also in case (c) and provide an approach in the event that the corresponding overhanging ears are not equal in length.

The first and simplest specific application we will consider is that shown in Fig. 7(b), where the two horizontal legs are long enough that the assumption of symmetry is valid. The expansion bend may be characterized by the relations

$$EI\theta = -r_1M + r_2P - r_3w \quad [22]$$

$$EI\Delta = -s_1M + s_2P - s_3w \quad [23]$$

Formulas for $r_{1,\,2,\,3}$ and $s_{1,\,2,\,3}$ are given in Table 2 for square corner, round corner, and double offset expansion bends. The bend flexibility factor k which occurs in some of the coefficients accounts for the increased flexibility due to flattening the cross section in bending a curved pipe. A uniformly distributed weight of w lb per in. of actual length has been assumed and the sign conventions, which are indicated in Fig. 8, agree with those used previously. Note that the symbol Δ denotes the total horizontal movement which is accommodated by the expansion bend.

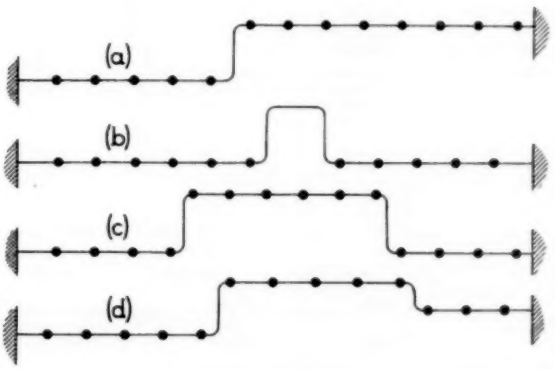

FIG. 7 TYPICAL CONFIGURATIONS FREQUENTLY ENCOUNTERED

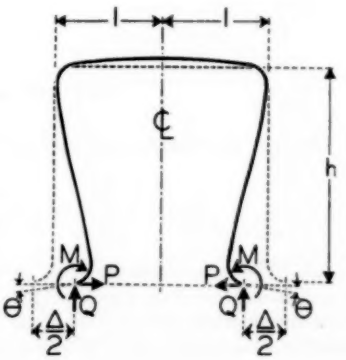

FIG. 8 DIMENSIONS AND NOTATION FOR EXPANSION U-BEND

TABLE 2 FORMULAS FOR COEFFICIENTS IN EQUATIONS [22] AND [23]

		r_1	r_2	r_3	s_1	s_2	s_3
SQUARE CORNER $Q=w(l+h)$	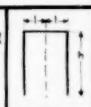	$l+h$	$h(l+h/2)$	$l^3/3$	$h(2l+h)$	$2l^2(l+h/3)$	$2l^3h/3$
ROUND CORNER $Q=w(l+h+\pi R-3R)$		$k\pi R+l+h-3R$	$\frac{1}{2}h(k\pi R+h+2l-4R)$	$kR^2[\pi(l+h/2)+h-R(6-\pi^2/2)]$ $+R(h-2R)[l+h-R(2-\pi/2)]+$ $\frac{1}{3}(l-R)[l^2+4lR+3hR-(11-3\pi)R^2]$	$\frac{1}{2}k(k\pi R+h+2l-4R)$	$kR[\pi(h^2-2hR+3R^2)$ $+4R(h-2R)]$ $+(2/3)[(h-R)^3-R^3]$ $+2k^2(l-R)$	$kR^2[\pi h^2-hR(4\pi-\pi^2-1)$ $-lR(2\pi-6)+lh(2\pi-2)$ $+R^2(7\pi-\pi^2-12)]+$ $R(h-2R)[h^2+lh-hR(2-\frac{\pi}{2})$ $+(2h/3)(l-R)\times$ $[l^2+3hR+4lR-R^2(11-3\pi)]$
DOUBLE OFFSET $Q=2wR\alpha$		$2kR\alpha$	$2kR^2\alpha(1-\cos\alpha)$	$kR^3[4(\alpha-\sin\alpha)+2\alpha^2\sin\alpha]$	$4kR^2\alpha(1-\cos\alpha)$	$kR^3[6(\alpha-\sin\alpha\cos\alpha)$ $-8\alpha\cos\alpha(1-\cos\alpha)]$	$kR^4[4\alpha^2\sin\alpha(1-2\cos\alpha)+$ $2\alpha(5+3\cos\alpha)(1-\cos\alpha)$ $-8\sin\alpha(1-\cos\alpha)]$

$6-\pi^2/2=1.06520$; $2-\pi/2=0.42920$; $11-3\pi=1.57522$; $4\pi-\pi^2-1=1.69677$; $7\pi-\pi^2-12=0.12154$

TABLE 3 COMPARISON OF SOLUTIONS OF EXAMPLE 1

CASE	ANALYSIS NEW	ANALYSIS OLD	CORNERS RND	CORNERS SQ	WEIGHT YES	WEIGHT NO	HORIZ FORCE P	MOMENT AT POINT INDICATED IN FIG. 10 (THOUSANDS OF INCH-POUNDS) A	B	C	D	E	F	G	H
1	X		X		X		2250	-244.9	-254.5	—	-177.0	183.0	—	231.5	208.8
2	X		X			X	2087	-254.3	-254.3	—	-170.8	163.1	—	246.6	246.6
3	X			X	X		2796	-311.3	-321.0	-333.1	-221.2	226.2	338.0	292.1	267.3
4	X			X		X	2601	-318.0	-318.0	-318.0	-214.0	202.1	306.2	306.2	306.2
5		X	X			X	962	-209.9	-209.9	—	-171.4	-17.6	—	20.9	20.9
6		X		X		X	1176	-261.0	-261.0	-261.0	-214.0	-25.7	21.3	21.3	21.3
7		X	X			X	2561	-273.0	-273.0	—	-170.6	239.2	—	341.6	341.6
8		X		X		X	3404	-350.1	-350.1	350.1	-214.0	330.7	466.9	466.9	466.9

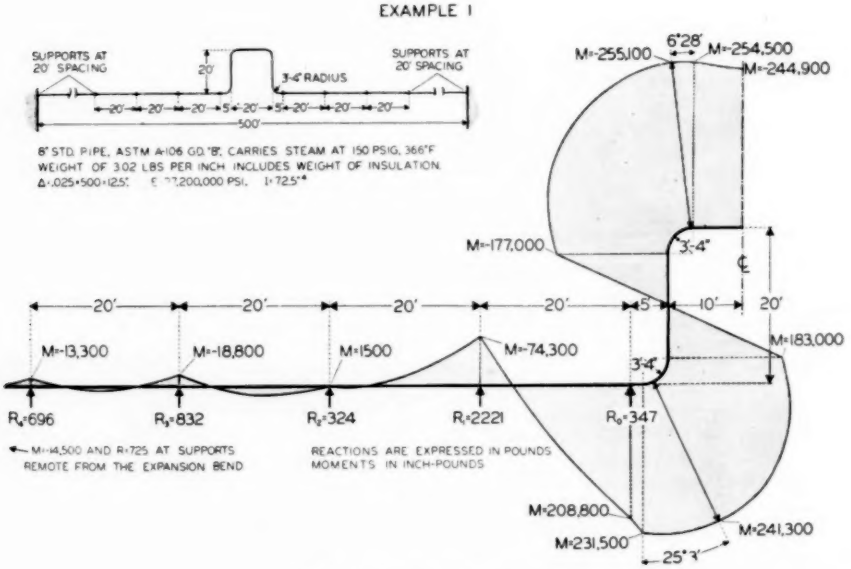

FIG. 9 DETAILS OF EXAMPLE 1

Solving Equations [20], [22], and [23] together yields the result

$$M = \frac{EI\Delta r_2/s_2 + w\,(f - r_3 + r_2 s_3/s_2) + Qd}{(c - s_1 r_2/s_2 + r_1)} \quad \ldots\ldots [24]$$

Appropriate values of Q also are given in Table 2. When M has been determined, $EI\theta$ can be obtained from Equation [20], and finally P can be obtained from Equation [22] or from Equation [23]. Once these quantities are known, it is not difficult to obtain all other shears, moments, reactions, slopes, and deflections in the system.

The value

$$M_0 = M - Qb - wb^2/2 \quad \ldots\ldots [25]$$

is the value of the moment applied at the end in Fig. 4. From Equation [12] we have

$$M_k = -wa^2/12 + (M_0 + wa^2/12)\,\frac{(\beta_1^{n-k} + \beta_1^k)}{(\beta_1^n + 1)} \quad \ldots [26]$$

for the value of the moment at the kth support. Little error is involved by taking $\beta_1^n = \beta_1^{n-k} = 0$. Thus, we have

$$M_k = -wa^2/12 + (-0.26795)^k (M_0 + wa^2/12) \ldots [27]$$

as an approximation for the moment at the kth support. Between supports the moment follows a parabolic law with a quadratic term given by $-wx^2/2$.

For the reactions, we obtain the following values

$$R_0 = (M_1 - M_0)/a + Q + w(b + a/2) \ldots [28]$$

$$R_k = wa + (M_{k+1} - 2M_k + M_{k-1})/a \ldots [29]$$

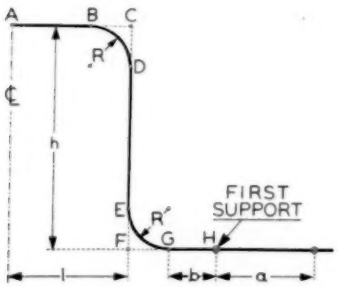

FIG. 10 POINTS AT WHICH MOMENT IS COMPUTED FOR TABLE 3

shown in cases 2 and 4 of Table 3. In the present example, at any rate, case 2 affords a good approximation to the more accurate results of case 1 and might lead to the assumption that results sufficiently accurate for most purposes may be obtained by analyzing an "equivalent" guided expansion bend in which the guides are located at a distance $0.2887a$ from the first actual support measured toward the fixed ends. However, such a procedure might lead to quite incorrect results unless certain implicit assumptions are satisfied.

In the present example, if the run were 633 ft or longer, rather than 500 ft, the additional expansion would cause the pipe to rise off the first support on each side of the expansion bend

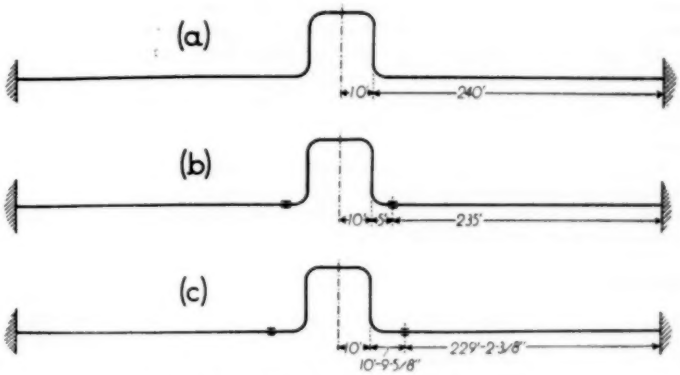

FIG. 11 IDEALIZED CASES ANALYZED FOR TABLE 3

Example 1, the details of which are shown in Fig. 9, illustrates the use of the formulas. In this example, it is presumed that the U-bend is not located within a distance of about 80 ft from either end of the 500-ft line. As regards the sign of the bending moment, throughout we have taken as positive a moment tending to cause a beam to be concave upward; however, for convenience in constructing Fig. 9, these positive bending moments are plotted downward from the reference axis. The bending stress is 15,200 psi, and no matter how one calculates and combines the hoop stress and the longitudinal pressure stress, the resulting "equivalent" stress will not exceed the value 22,500 psi permitted by Section 1 of the ASA Code for Pressure Piping (B 31.1–1951).

Table 3 gives a comparison of the results obtained by various methods of solution. The horizontal thrust is given as well as the bending moment at the several points indicated in Fig. 10. The exact solution shown in Fig. 9 is included as case 1. Cases 2, 3, and 4 also are based upon the present analysis but with the simplifying assumption indicated. Cases 5, 6, 7, and 8 are based upon the customary analysis which neglects the weight and idealizes the supporting system. In cases 5 and 6, the dimensions are as shown in Fig. 11(a), the entire line being presumed free to deflect. In cases 7 and 8 the dimensions are as shown in Fig. 11(b), it being presumed that the first support on either side of the expansion bend actually constitutes a guide which prevents rotation and lateral deflection but which permits axial motion. It is evident that the assumption illustrated in Fig. 11(a) results in underestimating moments and thrust while that illustrated in Fig. 11(b) results in an overestimate. The implicit assumption of symmetry in cases 5, 6, 7, and 8 does not have a large influence upon the results so long as the expansion bend actually is located fairly well in the middle of the run.

It should be evident from Equation [20], and indeed may be confirmed by calculation, that customary analysis applied to the configuration illustrated in Fig. 11(c) yields exactly the results

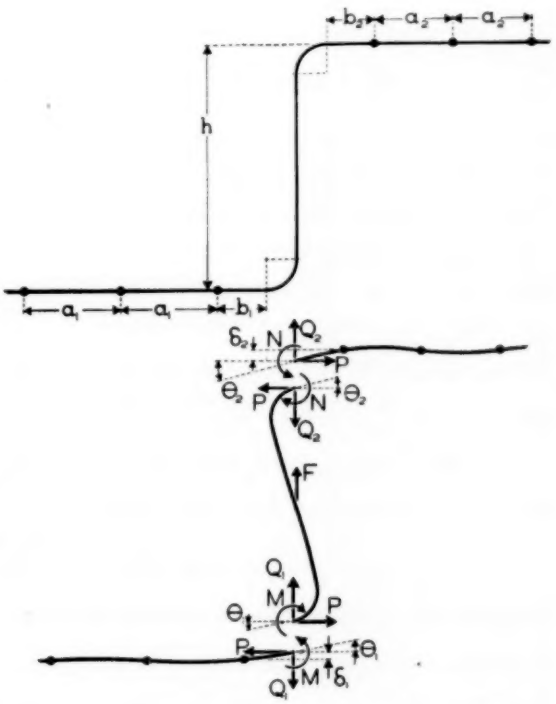

FIG. 12 DIMENSIONS AND NOTATION FOR ZEE-BEND

($R_0 = 0$) and the situation would be altered appreciably. In this case, moreover, it would not be reasonable to neglect the weight of the pipe since the maximum unsupported (horizontal) length would be 70 ft rather than 30 ft. Only an analysis such as is given here is capable of predicting such behavior and the formulas are not at all difficult to apply in any case.

As a second application, we consider the analysis of the offset shown in Fig. 7(*a*). As mentioned previously, such an analysis also is applicable to cases such as shown in Fig. 7(*c*) or (*d*). Dimensions and sign conventions are shown in Fig. 12. Subscripts 1 and 2 are used to distinguish between the lower and upper levels, respectively. However, inasmuch as subscripts have been used and will be used to distinguish between values of bending moment at the various support points, here we use the symbol M for the moment at the lower level and the symbol N for the moment at the upper level. Furthermore, while the straight lower run of pipe looks like Fig. 6, the upper run is inverted by comparison; this will involve some appropriate interpretations of the algebraic signs of the bending moment and of the reactions for the upper run.

For the sake of generality, a vertical upward force F is assumed to be applied at some point of the riser. This force actually may be zero or, by means of suitably adjusting a spring hanger, an advantageous upward force may be applied.

From the foregoing and from elementary analysis, we find the following equations

$$EI\theta_1 = c_1M - d_1Q_1 - f_1w \quad [30]$$

$$EI\delta_1 = d_1M - e_1Q_1 - g_1w \quad [31]$$

$$EI\theta_2 = c_2N - d_2Q_2 + f_2w \quad [32]$$

$$EI\delta_2 = d_2N - e_2Q_2 + g_2w \quad [33]$$

$$Q_2 = Q_1 + F \quad [34]$$

$$Ph = R(Q_1 + Q_2) + M + N \quad [35]$$

$$EI[\epsilon + \delta_1 + \delta_2 + R(\theta_1 + \theta_2)] + R\mu P = R\lambda(M + N) + R\zeta(Q_1 + Q_2) \quad [36]$$

$$2EI\Delta = hEI(\theta_1 + \theta_2) + \xi P - R\mu(Q_1 + Q_2) - h\lambda(M + N) \quad [37]$$

$$EI(\theta_1 - \theta_2) + R\lambda(Q_1 - Q_2) + \lambda(M - N) + \nu F = \eta w \quad [38]$$

This system may be simplified to

$$M(Rc_1 + d_1 + \rho - R\lambda) + N(Rc_2 + d_2 + \rho - R\lambda) - P(h\rho - R\mu) = w[(g_1 - g_2) + R(f_1 - f_2)] - \frac{1}{2}F[(e_1 - e_2) + R(d_1 - d_2)] - EI\epsilon \quad [39]$$

$$M(hc_1 + \sigma - h\lambda) + N(hc_2 + \sigma - h\lambda) - P(h\sigma - \xi) = 2EI\Delta + wh(f_1 - f_2) - \frac{1}{2}Fh(d_1 - d_2) \quad [40]$$

$$M(\tau + \lambda + c_1) + N(\tau - \lambda - c_2) - Ph\tau = w(f_1 + f_2 + \eta) - \frac{1}{2}F(d_1 + d_2 - 2R\lambda + 2\nu) \quad [41]$$

In Equations [36] through [41], the following symbols are used

$$\zeta = \frac{1}{4}kR^2(5\pi - 8) - \frac{1}{2}R(h - 2R) = 1.9270kR^2 - \frac{1}{2}R(h - 2R) \quad [42]$$

$$\eta = kR^2\left[R\left(6 - 3\pi + \frac{\pi^2}{2}\right) + h\left(\frac{\pi}{2} - 1\right)\right] + \left(\frac{\pi}{2} - 1\right)(h - 2R)R^2 = kR^2(1.5100R - 0.5708h) + 0.5708(h - 2R)R^2 \quad [43]$$

$$\lambda = \frac{1}{2}(k\pi R + h - 2R) \quad [44]$$

$$\mu = kR[3R - h + \pi(h - R)] + \frac{1}{2}h(h - 2R) \quad [45]$$

$$\nu = kR^2\left(\frac{\pi}{2} - 1\right) = 0.5708kR^2 \quad [46]$$

$$\xi = k[\pi(h^2 - 2hR + 3R^2) + 4R(h - 2R)] + \frac{2}{3}[(h - R)^3 - R^3] \quad [47]$$

$$\rho = \frac{1}{2}(d_1 + d_2) + (e_1 + e_2)/2R + \zeta \quad [48]$$

$$\sigma = h(d_1 + d_2)/2R + \mu \quad [49]$$

$$\tau = (d_1 - d_2)/2R \quad [50]$$

It is more convenient to obtain the numerical values of the coefficients in Equations [39], [40], and [41] and solve this simultaneous system of three equations than it is to carry the solution farther in literal terms. Having values of M, N, and P, we find

$$Q_1 = -\frac{F}{2} + (Ph - M - N)/2R \quad [51]$$

$$Q_2 = \frac{F}{2} + (Ph - M - N)/2R \quad [52]$$

$$M_0 = M - Q_1b_1 - wb_1^2/2 \text{ . . . . (lower level)} \quad [53]$$

$$M_0 = -N + Q_2b_2 - wb_2^2/2 \text{ . . . . (upper level)} \quad [54]$$

$$M_k = -wa^2/12 + (-0.26795)^k(M_0 + wa^2/12) \text{ . . . . (either level)} \quad [55]$$

$$R_0 = Q_1 + wb_1 + wa_1/2 + (M_1 - M_0)/a_1 \text{ . . . . (lower level)} \quad [56]$$

$$R_0 = -Q_2 + wb_2 + wa_2/2 + (M_1 - M_0)/a_2 \text{ . . . . (upper level)} \quad [57]$$

$$R_k = wa + (M_{k+1} - 2M_k + M_{k-1})/a \text{ . . . . (either level)} \quad [58]$$

In these equations, the algebraic signs for R and M on the upper level have been manipulated suitably so that R is indeed positive upward and M is positive for a beam bent concave upward. In determining values of R, values of M calculated for the corresponding level are used.

For a given choice of dimensions, a value for F may be selected so as to minimize the maximum moment. This may be done most readily by obtaining the matrix inverse to the coefficient matrix of Equations [39], [40], and [41] and postmultiplying by a column matrix composed of the right-hand sides of Equation [44]. A few trial values for F will suffice to indicate an optimum choice which, in practice, can be applied (in the hot condition) by a calibrated spring hanger.

It also should be noted that a negative value for any of the reactions implies that the pipe lifts off the corresponding support and requires a repetition of the analysis using appropriately

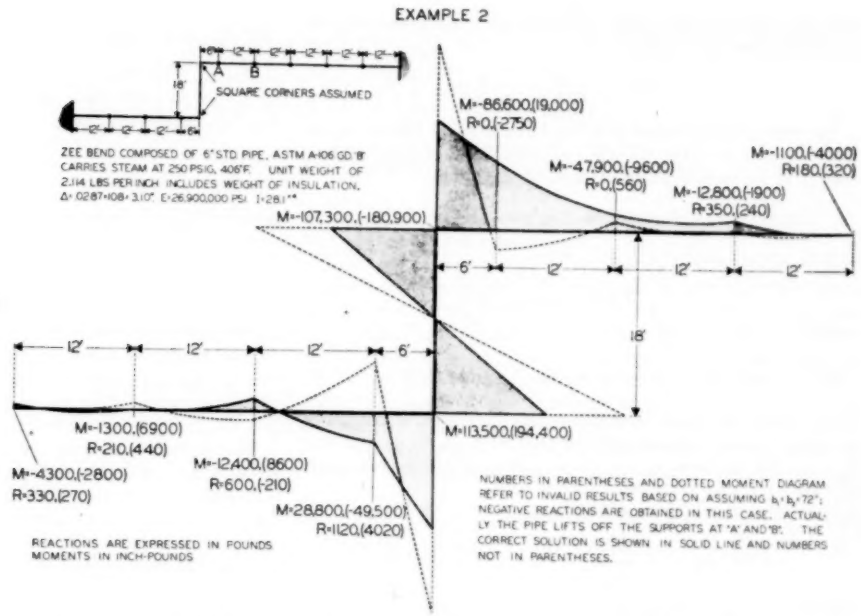

FIG. 13 DETAILS OF EXAMPLE 2

modified dimensions. This is most apt to occur at the first one or more support points on the upper level.

An illustration of this analysis is provided by Example 2, the details of which are shown in Fig. 13. For the sake of simplicity, the corners were assumed to be square ($R = 0$) although, of course, the practical validity of the solution is thereby compromised. Presuming all supports are active (i.e., taking $b_1 = b_2 = 72$ in.) leads to the results shown by dotted line in the drawing and by the figures enclosed in parentheses. Negative values for some of the reactions indicate that this solution is invalid. A second trial assuming $b_1 = 72$ in., $b_2 = 216$ in. (i.e., assuming that the pipe lifts off the support marked A) leads to similar invalid results. A third trial with $b_1 = 72$ in., $b_2 = 360$ in. (i.e., presuming that the pipe lifts off both supports A and B) leads to a solution in which all active supports exert positive reactions.

The mechanical labor of evaluating the coefficients and solving the system of Equations [39], [40], and [41] is not inconsiderable. However, it does not appear that any approximate analysis is capable of predicting the actual behavior of such a structure as the one under discussion.

Appendix

In this Appendix, we will obtain some relations holding for equispan uniformly loaded beams with elastic support points. The procedure is basically the same as for the case of simple support points as treated in the body of the paper, but here we must deal with a fourth-order rather than a second-order linear difference equation. The added complexity in this case does not permit the results to be given in as useful or as complete a form as those of the body of the paper.

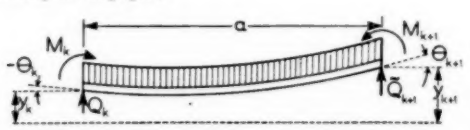

FIG. 14 TYPICAL SPAN ON SPRING SUPPORTS

Fig. 14 represents a typical span. From elementary considerations, we have the relations

$$Q_k + \bar{Q}_{k+1} = wa \quad \ldots [59]$$

$$Q_k = wa/2 + (M_{k+1} - M_k)/a \quad \ldots [60]$$

$$EI\theta_{k+1} = EI\theta_k + aM_k + a^2Q_k/2 - wa^3/6 \quad \ldots [61]$$

$$EIy_{k+1} = EIy_k + EIa\theta_k + a^2M/2 + a^3Q_k/6 - wa^4/24 \quad \ldots [62]$$

Also, the nature of the spring support at point k is such that the total force on the spring is related to the deflection by the equation

$$Ky_k = \bar{R}_k - Q_k - \bar{Q}_k \quad \ldots [63]$$

Here K is the spring constant, assumed to be the same for all supports and $\bar{R}$ is the "preset" force. From these equations may be obtained the following difference equation for moments

$$M_{k+4} - (4 - 4t)M_{k+3} + (6 + 16t)M_{k+2} - (4 - 4t)M_{k+1} + M_k = a(\bar{R}_{k+2} - 2\bar{R}_{k+1} + \bar{R}_k) - 2wa^2t \quad \ldots [64]$$

where

$$t = Ka^3/24\,EI \quad \ldots [65]$$

If we presume that the preset forces $\bar{R}_k$ are all the same, the solution to Equation [63] may be written as

$$M_k = A_1\lambda_1^k + A_2\lambda_2^k + A_3\lambda_3^k + A_4\lambda_4^k - wa^2/12 \quad \ldots [66]$$

where the λ_i are roots of the indicial equation

$$\lambda^4 - (4 - 4t)\lambda^3 + (6 + 16t)\lambda^2 - (4 - 4t)\lambda + 1 = 0 \quad \ldots [67]$$

These roots are

$$\left.\begin{aligned}
\lambda_1 &= 1 - t + \sqrt{t^2 - 6t} + \sqrt{2t^2 - 8t + (2 - 2t)\sqrt{t^2 - 6t}} \\
\lambda_2 &= 1 - t - \sqrt{t^2 - 6t} + \sqrt{2t^2 - 8t - (2 - 2t)\sqrt{t^2 - 6t}} \\
\lambda_3 &= 1 - t + \sqrt{t^2 - 6t} - \sqrt{2t^2 - 8t + (2 - 2t)\sqrt{t^2 - 6t}} \\
\lambda_4 &= 1 - t - \sqrt{t^2 - 6t} - \sqrt{2t^2 - 8t - (2 - 2t)\sqrt{t^2 - 6t}}
\end{aligned}\right\} \quad \ldots [68]$$

From Equation [67] it should be observed that these roots are pairwise reciprocals; indeed

$$\lambda_1\lambda_3 = \lambda_2\lambda_4 = 1 \quad \ldots\ldots\ldots\ldots\ldots\ldots [69]$$

The principal application is to the symmetrically loaded n-span beam illustrated in Fig. 15. We wish to find θ_0 and y_0 as functions of w, Q_0, and M_0. The symmetry condition

$$M_k = M_{n-k} \quad \ldots\ldots\ldots\ldots\ldots\ldots [70]$$

leads to the relations

$$A_3 = A_1\lambda_1^n; \quad A_4 = A_2\lambda_2^n \quad \ldots\ldots\ldots\ldots [71]$$

so that

$$M_k = -wa^2/12 + A_1(\lambda_1^{n-k} + \lambda_1^k) + A_2(\lambda_2^{n-k} + \lambda_2^k) \ldots [72]$$

It may easily be shown that this symmetrical form also satisfies all other ways of expressing the symmetry such as $\bar{Q}_{n-k} = Q_k$; $\theta_{n-k} = -\theta_k$; $y_{n-k} = y_k$, and so on. It is, of course, presumed that $Q_0 = \bar{Q}_n$ and $M_0 = M_n$.

From Equations [60] and [72] we have

$$A_1(\lambda_1^n + 1) + A_2(\lambda_2^n + 1) = M_0 + wa^2/12 \ldots\ldots [73]$$

$$A_1\lambda_1(\lambda_1^{n-2} + 1) + A_2\lambda_2(\lambda_2^{n-2} + 1) = M_0 + aQ_0 - 5wa^2/12 \quad \ldots\ldots\ldots [74]$$

so that

$$A_1 = \frac{(M_0 + aQ_0 - 5wa^2/12)(\lambda_2^n + 1) - (M_0 + wa^2/12)\lambda_2(\lambda_2^{n-2} + 1)}{\lambda_1(\lambda_1^{n-2} + 1)(\lambda_2^n + 1) - \lambda_2(\lambda_2^{n-2} + 1)(\lambda_1^n + 1)} \ldots\ldots [75]$$

$$A_2 = \frac{(M_0 + wa^2/12)\lambda_1(\lambda_1^{n-2} + 1) - (M_0 + aQ_0 - 5wa^2/12)(\lambda_1^n + 1)}{\lambda_1(\lambda_1^{n-2} + 1)(\lambda_2^n + 1) - \lambda_2(\lambda_2^{n-2} + 1)(\lambda_1^n + 1)} \ldots\ldots [76]$$

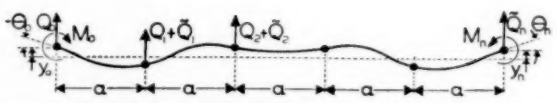

FIG. 15 UNIFORMLY LOADED SYMMETRICAL BEAM OF n SPANS SUPPORTED BY SPRINGS

We also can show that

$$\theta_k = -[M_{k+3} + (4t - 3)M_{k+2} + (20t + 3)M_{k+1} + (12t - 1)M_k + 3wa^2t]/Ka^2 \ldots\ldots [77]$$

so that

$$\theta_0 = -\{A_1[(\lambda_1^{n-3} + \lambda_1^3) + (4t - 3)(\lambda_1^{n-2} + \lambda_1^2) + (20t + 3)(\lambda_1^{n-1} + \lambda_1) + (12t - 1)(\lambda_1^n + 1)] + A_2[(\lambda_2^{n-3} + \lambda_2^3) + (4t - 3)(\lambda_2^{n-2} + \lambda_2^2) + (20t + 3)(\lambda_2^{n-1} + \lambda_2) + (12t - 1)(\lambda_2^n + 1)]\}/Ka^2 \quad \ldots\ldots\ldots [78]$$

The analysis is actually somewhat more general than it might first appear. Equation [66] is the solution to Equation [64] not only if the $\bar{R}$'s have a common value but more generally if the term $(\bar{R}_{k+2} - 2\bar{R}_{k+1} + \bar{R}_k)$ vanishes, and if this term has a constant value B, independent of k, a corresponding term $Ba/24t$ should be added to the right side of Equation [66]. This term will show up again in Equation [72] and subsequently, but will not seriously complicate the analysis. However, a serious complication results from the fact that the roots λ_i are generally complex for reasonable values of the parameter t. This imposes obvious computational difficulties.

The Stepped Thrust Bearing—A Solution by Relaxation Methods

By C. F. KETTLEBOROUGH,[1] MELBOURNE, AUSTRALIA

Analytical investigation into the stepped thrust bearing was first carried out by Lord Rayleigh, whose solution neglected side leakage. More recently Archibald has presented a solution with side leakage not neglected but limited by the step being straight across the bearing surface perpendicular to the direction of motion. This paper gives an alternative solution, using relaxation methods, which is applicable to any shape of the step. Results show that the load capacity of the completely internal step is much greater than that for the simple tilting slider.

Nomenclature

The following nomenclature is used in the paper:

μ = viscosity of lubricant
U = linear velocity of moving boundary
u = velocity of oil within oil film
ω = angular velocity
L = length of pad in direction of motion
B = width of pad
p = pressure
h = film thickness
h_1 = outlet film thickness
h_2 = inlet film thickness
k = ratio h_2/h_1
W = total load

Other notations are introduced as required.

Introduction

The maximum load per unit width perpendicular to the direction of motion which can be supported by a tilting pad when side leakage is neglected is given by

$$(W)_{max} = 0.160 \frac{\mu U L^2}{h_1^2} \quad \ldots\ldots\ldots\ldots\ldots [1]$$

This presupposes the optimum condition that the ratio of inlet to outlet film thickness is 2.2.

Lord Rayleigh (1)[2] analyzed in detail the simple slider, neglecting side leakage, and found the maximum load capacity per unit width was produced when there was a stepped convergence to the oil film. For this case Rayleigh showed that

$$(W)_{max} = 0.206 \frac{\mu U L^2}{h_1^2} \quad \ldots\ldots\ldots\ldots\ldots [2]$$

This constitutes an increase in load-carrying capacity of 29 per cent as compared with Equation [1].

More recently Archibald (2) analyzed the stepped slider with side leakage considered. This solution is based on expressing the pressure as the summation of a trigonometrical series and applies only when the step extends across the bearing perpendicular to the direction of motion. In this case the maximum oil pressure occurs at the step where the oil-film thickness is a maximum. To reduce this side leakage Archibald suggested the use of a completely internal step.

It is proposed here to give an alternative solution using relaxation techniques applicable to any shape of the step.

Analysis

Reynolds equation with side leakage considered is

$$\frac{\partial}{\partial x}\left[\frac{h^3}{\mu}\frac{\partial p}{\partial x}\right] + \frac{\partial}{\partial z}\left[\frac{h^3}{\mu}\frac{\partial p}{\partial z}\right] = 6U\frac{\partial h}{\partial x} \quad \ldots\ldots\ldots [3]$$

The stepped slider, Fig. 1, consists of two regions, i.e., region 1, where the oil-film thickness is h_1 over a length c_1; region 2, where the oil-film thickness is h_2 over a length c_2. The co-ordinate axes for the slider also are shown.

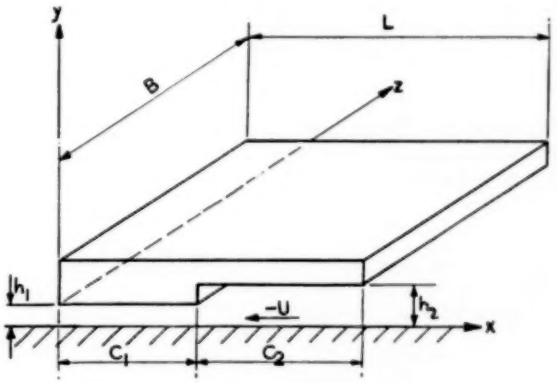

Fig. 1 The Simple Hydrodynamic Slider

For both regions, the film thickness is a constant and, assuming the viscosity remains constant, Equation [3] reduces to

$$\frac{\partial^2 p}{\partial x^2} + \frac{\partial^2 p}{\partial z^2} = 0 \quad \ldots\ldots\ldots\ldots\ldots [4]$$

This is Laplace's partial differential equation. The pressure on the exterior boundaries are all zero and normally the only solution to Equation [4] is that $p = 0$ everywhere.

However, in this case, for each region the pressures on the exterior boundaries are all zero but there is a common pressure on the interior boundary, which is not equal to zero but determined by the magnitude of the step.

The rate of flow across any point in the x-direction is given by

---

[1] Senior Lecturer, School of Engineering, University of Melbourne.

[2] Numbers in parentheses refer to the Bibliography at the end of the paper.

Contributed by the Applied Mechanics Division and presented at the Annual Meeting, New York, N. Y., November 29–December 4, 1953, of The American Society of Mechanical Engineers.

Discussion of this paper should be addressed to the Secretary, ASME, 29 West 39th Street, New York, N. Y., and will be accepted until April 12, 1954, for publication at a later date. Discussion received after the closing date will be returned.

Note: Statements and opinions advanced in papers are to be understood as individual expressions of their authors and not those of the Society. Manuscript received by ASME Applied Mechanics Division, September 2, 1952. Paper No. 53—A-9.

$$q_x = -\frac{h^3}{12\mu}\frac{\partial p}{\partial x} - \frac{Uh}{2}$$

At any point on the common boundary the rate of flow out of region 2 is equal to the rate of flow into region 1. Hence

$$\left[-\frac{h^3}{12\mu}\frac{\partial p}{\partial x} - \frac{Uh}{2}\right]_{①} = \left[-\frac{h^3}{12\mu}\frac{\partial p}{\partial x} - \frac{Uh}{2}\right]_{②}$$

Subscripts ① and ② refer to region 1 and 2, respectively, i.e.

$$\frac{h_1^3}{12\mu}\left(\frac{\partial p}{\partial x}\right)_{①} + \frac{Uh_1}{2} = \frac{h_2^3}{12\mu}\left(\frac{\partial p}{\partial x}\right)_{②} + \frac{Uh_2}{2} \quad \ldots\ldots [5]$$

where

$$\left(\frac{\partial p}{\partial x}\right)_{①} \quad \text{and} \quad \left(\frac{\partial p}{\partial x}\right)_{②}$$

are the slopes of the pressure curves for region 1 and 2, respectively, at the common boundary.

Substituting $h_2 = kh_1$, and simplifying Equation [5]

$$\left(\frac{\partial p}{\partial x}\right)_{①} - k^3\left(\frac{\partial p}{\partial x}\right)_{②} = \frac{6\mu U}{h_1^2}(k-1) \quad \ldots\ldots [6]$$

Equations [4] and [6] uniquely solve the distribution of pressure over the bearing surface for any given values of k, μ, U, and h_1. Having determined the pressure distribution, the other operating characteristics such as the load-carrying capacity and friction can be determined easily.

Relaxation Procedure

Before proceeding further it is usually convenient to arrange equations such as Equations [4] and [6] to be nondimensional. This can be done by expressing

$$p = \frac{6\mu UL}{h_1^2}P \quad \ldots\ldots [7]$$

The dimensions of $(6\mu UL/h_1^2)$ are those of pressure and hence P is nondimensional.

Substituting also

$$\left.\begin{aligned} z &= Z_1 L \\ x &= X_1 L \end{aligned}\right\} \quad \ldots\ldots [8]$$

this makes the length co-ordinates nondimensional; Z_1 and X_1 are the new nondimensional variables.

Equations [4] and [6] reduce to

$$\frac{\partial^2 P}{\partial X_1^2} + \frac{\partial^2 P}{\partial Z_1^2} = 0, \text{ i.e., } \nabla^2 P = 0 \quad \ldots\ldots [9]$$

$$\left(\frac{\partial P}{\partial X_1}\right)_{①} - k^3\left(\frac{\partial P}{\partial X_1}\right)_{②} = (k-1) \quad \ldots\ldots [10]$$

Equation [9] expressed in terms of finite-difference approximations is given by

$$\nabla^2 P = \frac{2}{h_1(h_3+h_1)}P_1 + \frac{2}{h_3(h_1+h_3)}P_3 + \frac{2}{h_2(h_4+h_2)}P_2 + \frac{2}{h_4(h_2+h_4)}P_4 - \left[\frac{2}{h_1h_3} + \frac{2}{h_2h_4}\right]P_0 = 0$$

where P_1, P_2, P_3, and P_4 are the values of the function P at distances h_1, h_2, h_3, and h_4 from the mesh point at which $P = P_0$ as in Fig. 2(*b*). When $h_1 = h_2 = h_3 = h_4$, Equation [9] reduces to

$$\nabla^2 P = P_1 + P_2 + P_3 + P_4 - 4P_0 = 0$$

It is also necessary to express the derivative $(\partial P/\partial X_1)$ in terms of finite differences

$$\left(\frac{\partial P}{\partial X_1}\right)_0 = -\left[\frac{(P_2 - P_0)h_1^2 - (P_1 - P_0)(h+h_1)^2}{hh_1(h+h_1)}\right] = -\left(\frac{3P_0 - 4P_1 + P_2}{2h}\right) \text{ when } h = h_1$$

P_0, P_1, and P_2 are defined as in Fig. 2(*a*).

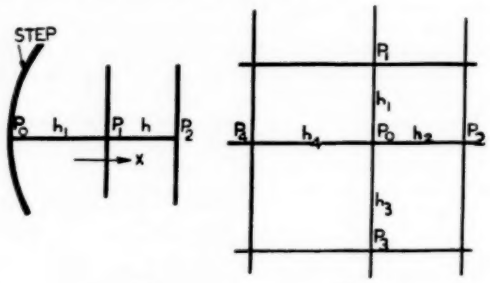

Fig. 2 Finite-Difference Systems

Application of Equations [9] and [10]

Step Perpendicular to Direction of Motion. Case 1. Archibald determined that the optimum values for a square slider for maximum load-carrying capacity are $k = 1.7$, and $c_2/c_1 = 54/45$. To ease the computational work this ratio was made equal to 55:45, a negligible difference; hence a convenient length of the mesh in the x-direction is 1/10 and at the boundary 1/20. Some even irregular stars are introduced but add no difficulty.

The slope Equation [10] becomes

$$\left(\frac{3P_0 - 4P_1 + P_2}{2h}\right)_{①} - k^3\left(\frac{4P_1 - 3P_0 - P_2}{2h}\right)_{②} = (k-1) \quad \ldots\ldots [10a]$$

with $h = 0.05$ and $k = 1.7$

$$P_0 = 0.003946 + 0.2255(P_1)_1 - 0.0564(P_2)_1 + 1.10784(P_1)_2 - 0.27696(P_2)_2$$

where P_0, $(P_1)_1$, $(P_2)_1$, $(P_1)_2$, and $(P_2)_2$ are defined in Fig. 3. P_0 is the value at the boundary. The values of P elsewhere are defined according to Equation [9]. There is an axis of symmetry in the direction of motion and hence only one half needs to be relaxed.

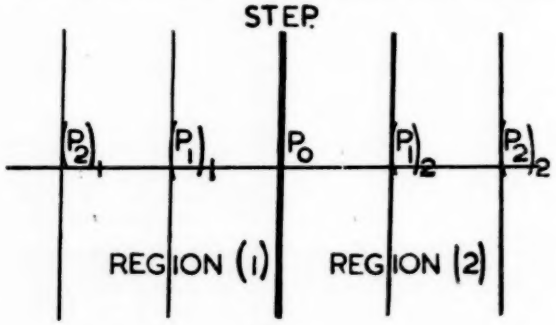

Fig. 3

In the relaxation procedure a change in the value of $(P_1)_1$, $(P_2)_1$, $(P_1)_2$, $(P_2)_2$, at the points adjacent to the boundary not only causes a change in the residual at the point itself and the surrounding mesh points controlled by $\nabla^2 P = 0$ but also in the value of P_0 at the step according to Equation [10a]. It must be noted that any change in the value of P_0 automatically will alter the residuals at points $(P_1)_1$ and $(P_1)_2$. Fig. 4 shows the final relaxed distribution.

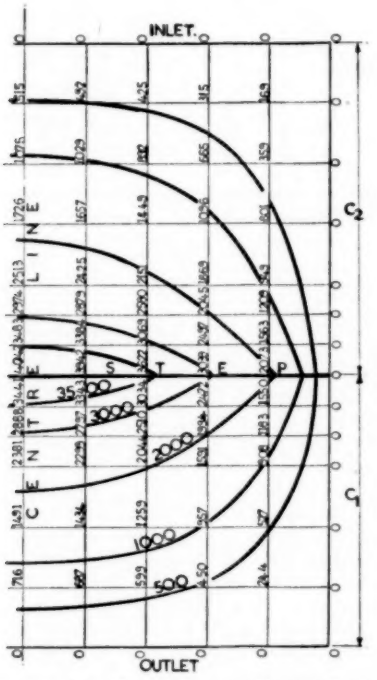

FIG. 4 VALUES OF $P \times 10^3$ FOR OPTIMUM STEPPED SLIDER—CASE 1

Case 1A. A square slider was then considered with the step on the center line of the pad, i.e., on the axis of symmetry perpendicular to the direction of motion. In this case the pressure distribution over region 1 is identical to that over region 2. Hence $(P_1)_1 = (P_1)_2$ and $(P_2)_1 = (P_2)_2$.

The slope equation corresponding to Equation [10] with $k = 1.7$ and $h = h_1 = 0.125$ simplifies to

$$P_0 = 0.00987 + \frac{4}{3} P_1 - \frac{1}{3} P_2$$

Several systems were relaxed as follows: Mesh lengths $^1/_{16}$, $^1/_8$, and $^1/_{10}$, and to five figures as in Case 1 and to four figures. The integrated load indicated that a mesh length of $^1/_{10}$ with relaxation carried out to four figures gave sufficiently accurate results without undue computational work.

The Complete Internal Step. For this case it is necessary to consider the flow of oil across an elemental width of step ds as in Fig. 5(a), in which the components of flow in the x and z directions across co-ordinate elemental widths dx and dz are shown. To satisfy the continuity equation the oil flow out of region 2 is equal to the flow into region 1, hence the continuity equation becomes

$$Fx_2 dz + Fy_2 dx = Fx_1 dz + Fy_1 dx \ldots\ldots\ldots [11]$$

Substituting for the components of flow, Equation [11] becomes

$$\left[\left(\frac{\partial P}{\partial X_1}\right)_① - k^3\left(\frac{\partial P}{\partial X_1}\right)_②\right] + \left[\left(\frac{\partial P}{\partial Z_1}\right)_① - k^3\left(\frac{\partial P}{\partial Z_1}\right)_②\right]\frac{\partial X_1}{\partial Z_1}$$

$$= (k-1)\ldots\ldots [12]$$

Replacing the derivatives by finite difference expressions, and evaluating for the case where $k = 2$ and $h = 0.1$, the equation for P_0 becomes

$$81P_0 = 32(P_1)_2 - 8(P_2)_2 + 64(P_3)_2 - 16(P_4)_2 + 4(P_1)_1 - (P_2)_1 + 8(P_3)_1 - 2(P_4)_1 + 0.20$$

where $(P_1)_2$, $(P_2)_2$, $(P_3)_2$, $(P_4)_2$, $(P_1)_1$, $(P_2)_1$, $(P_3)_1$, $(P_4)_1$, are as shown in Fig. 5(b) and $\cot\theta = \dfrac{dx}{dz} = 2$ (as for case 2 to follow).

For $k = 2$ and $\cot\theta = 2$ but $h = 0.1$ in the x direction and $h = 0.05$ in the z direction the equation for P_0 becomes

$$135P_0 = 32(P_1)_2 - 8(P_2)_2 + 128(P_3)_2 - 32(P_4)_2 + 4(P_1)_1 - (P_2)_1 + 16(P_3)_1 - 4(P_4)_1 + 0.20$$

Case 2. This deals with the complete internal step for the rectangular slider. For simplification in the relaxation process the step shown in Fig. 6 was taken. The part AB was chosen so that the step passed through existing grid points. The value of P at the step was found by using the equation of continuity, as given by Equation [11], whenever the stepped boundary crossed a grid line perpendicular to the direction of motion. This required further subdivision of the grid as indicated. The reason for this step was to simplify the initial setting up—all the finite-difference formulas for the equation of continuity where the same and the formulas for $\nabla^2 P = 0$ for mesh points adjacent to the step had mesh lengths of h and $h/2$ only.

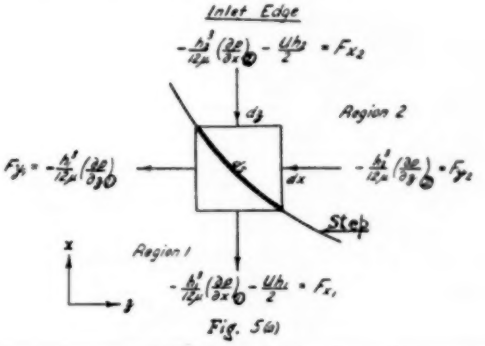

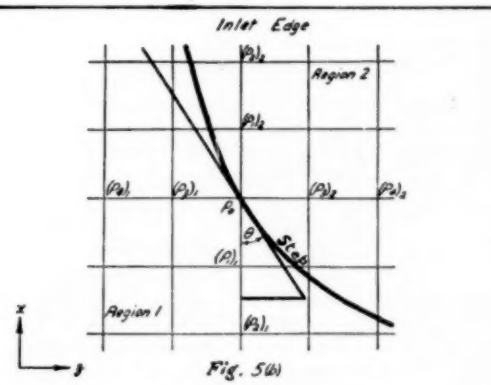

FIG. 5 INTERNAL STEP

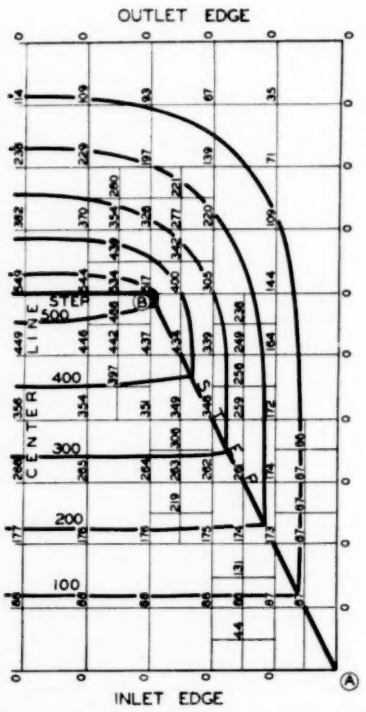

FIG. 6 VALUES OF $P \times 10^4$ FOR SIMPLE INTERNAL STEP—CASE 2

CALCULATION OF OPERATING CHARACTERISTICS

Total Load

$$W_1 = \frac{6\mu UL^3}{h_1^2} \int_0^{C_1} \int_0^{B/L} P \, dX_1 \, dZ_1 \text{ for region 1}$$

Similarly

$$W_2 = \frac{6\mu UL^3}{h_1^2} \int_{C_1}^{C_1+C_2} \int_0^{B/L} P \, dX_1 \, dZ_1 \text{ for region 2}$$

Total load $W = W_1 + W_2$ for the complete slider.

Friction

$$u = \frac{y(y-h)}{2\mu} \frac{\partial p}{\partial x} - \frac{U(h-y)}{h}$$

The shear stress in the oil $= s = \mu \partial u / \partial y$.

Total friction force acting on moving surface $= F$

$$= [\int \int s \, dx \, dz]_{y=0}$$

For region 1

$$F_1 = -\frac{3\mu UL^2}{h_1} \int_0^{B/L} P_e dZ_1 + \frac{\mu UL^2}{h_1} \int_0^{C_1} \int_0^{B/L} dX_1 \, dZ_1$$

For region 2

$$F_2 = k \frac{3\mu UL^2}{h_1} \int_0^{B/L} P_e dZ_1 + \frac{\mu UL^2}{kh_1} \int_{C_1}^{C_1+C_2} \int_0^{B/L} dX_1 dZ_1$$

Total friction $F = F_1 + F_2$.

Flow of Lubricant

$$\text{Inlet flow} = \frac{ULh_1}{2} k \int_0^{B/L} \left[1 + k^2 \left(\frac{\partial P}{\partial X_1} \right)_{\text{inlet}} \right] dZ_1$$

$$\text{Outlet flow} = \frac{ULh_1}{2} \int_0^{B/L} \left[1 + \left(\frac{\partial P}{\partial X_1} \right)_{\text{outlet}} \right] dZ_1$$

$$\text{Side flow} = \frac{ULh_1}{2} \int_0^{C_1} \frac{\partial P}{\partial Z_1} dX_1 + k^2 \frac{ULh_1}{2} \int_{C_1}^{C_1+C_2} \frac{\partial P}{\partial Z_1} dX_1$$

Full details of numerical integration and differentiation are available in references (3) and (4), respectively.

CALCULATED RESULTS

Table 1 gives the principal operating factors for the case specified.

Case 1 illustrates that there is good agreement between the mathematical and relaxation method. Case 2 clearly indicates the increased load capacity available; the load supported by the completely internal step is 1.58 times the maximum load which can be supported by the tilting pad. At the same time the friction force increases but not in the same proportion.

The numerical values of the operating factors for the simple slider have been evaluated using Norton's (5) figs. 34, 38, and 76, involving the use of side-leakage correction factors.

The diagrams of the pressure-function distribution clearly show the marked effect of the stepped convergence of the oil film. There is a sudden change in the direction of lines of equal pressure at the step. Examination of the pressure in region 2 in the transverse direction in Fig. 6 clearly indicates the very small pressure gradient causing oil to flow outward to the edges. Owing to the increased pressure gradient at the entrance to the pad opposing the inward flow of the oil, the inlet oil flow decreases considerably as the load capacity increases. Together with the increased friction, the temperature rise would be greater than for the simple slider. On the other hand, the dissipation of heat is considerably improved because of the large mass of metal behind the bearing faces.

With the simple stepped boundary, as in Case 2, preliminary investigations indicate that the load capacity is not altered greatly as k varies from about 1.5 to about 3.0. With k constant and equal to 2, the load capacity is further increased as the width of the step increases. No attempt has been made to determine the optimum shape of the step.

PRACTICAL CONSIDERATIONS

The step of Case 2 was chosen only to simplify the relaxation. From the point of view of production the best shape would be semicircular. Fig. 7 shows a suggested arrangement. Each pad subtends an angle of 60 deg and the step is made by grinding

TABLE 1 OPERATING FACTORS

	Load capacity		Friction force				
	By relaxation $\times \left(\frac{\mu UL^2}{h_1^2}\right)$	After Archibald $\times \left(\frac{\mu UL^2}{h_1^2}\right)$	By relaxation $\times \left(\frac{\mu UL^2}{h_1}\right)$	After Archibald $\times \left(\frac{\mu UL^2}{h_1}\right)$	Relative load capacity	Relative friction force	Inlet oil flow $\times (ULh_1)$
Case 1	0.0725	0.07254	0.837	0.8369	1.01	1.184	0.584
			(Film ratio $k = 1.7$)				
Case 2	0.114	.....	0.902	....	1.58	1.28	0.675
			(Film ratio $k = 2$)				
Simple slider	0.072	.....	0.707	....	1.00	1.00	0.90
			(Optimum slider film ratio $k = 2.2$)				

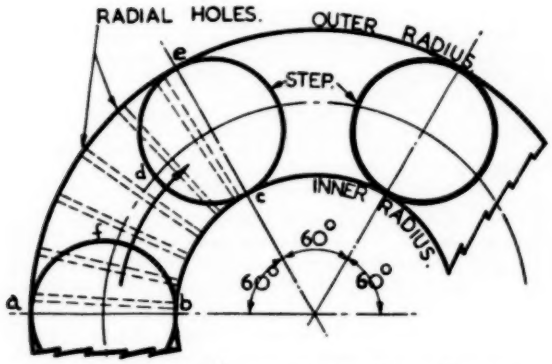

FIG. 7 SUGGESTED PRACTICAL STEPPED THRUST BEARING

a complete circle to the required depth which may be of the order of 0.002 to 0.003 in. With the direction of rotation of the moving member as shown, the operating bearing area would be *a-b-c-d-e*, the step occurring along *a-f-b*. For reverse running the operating bearing area would now be *a-f-b-c-e*, the step now occurring across *c-d-e*. Hence per 60-deg arc the bearing area not in use would be that of one semicircle. To insure adequate oil for lubrication, oil can be fed through holes along diameters such as *a-b* and *c-e;* this also would prevent any tendency for the oil pressure to fall below the supply pressure when leaving the previous pad. Additional holes drilled radially through the bearing ring and close to the bearing surface improve the heat dissipation.

In the case of vertical water-wheel turbines, high-pressure oil can be fed to some point between the semicircular recesses to facilitate initial starting.

The tilting-pad bearing accommodates itself easily to variation in load—for a given pivot position an increase in load causes a decrease in the minimum film thickness, but the slope of the pad decreases so that the film ratio remains constant (neglecting viscosity effects). With a Rayleigh-type bearing, an increase in load also decreases the film thickness but the film ratio increases. Hence it would seem that the stepped thrust bearing is only advisable when operating conditions are constant, particularly the load, as, for example, the water-turbine thrust bearing.

Another method of producing the depression is to press a tool of the required shape to just greater than the depth required into the bearing material, the upper face then being ground to remove burrs and bring the recess to the correct depth.

SECTOR-SHAPED PAD

Reynolds equation in polar co-ordinates with the origin at the center of the circular arcs forming the boundaries of the pad in the direction of the circular motion is

$$\frac{\partial}{\partial\theta}\left(\frac{h^3}{\mu}\frac{\partial p}{\partial\theta}\right) + r\frac{\partial}{\partial r}\left(r\frac{h^3}{\mu}\frac{\partial p}{\partial r}\right) = 6\omega r\frac{\partial h}{\partial\theta}$$

Substituting

$$\theta = \alpha\Theta;\quad r = r_0\,e^{\alpha R};\quad p = \frac{6\mu\omega\alpha r_0^2}{h_1^2}P$$

assuming the viscosity has a constant (mean) value; then for each region 1 and 2, where the film thickness is constant, Reynolds equation becomes

$$\frac{\partial^2 P}{\partial\Theta^2} + \frac{\partial^2 P}{\partial R^2} = 0$$

The continuity equation is now

$$q_\theta = -\frac{h^3}{12\mu r}\frac{\partial p}{\partial\theta} - \frac{Uh}{2}$$

Following the same procedure as for the rectangular slider

$$\frac{\partial\theta}{\partial R}\left[\left(\frac{\partial P}{\partial R}\right)_1 - k^3\left(\frac{\partial P}{\partial R}\right)_2\right] + \left[\left(\frac{\partial P}{\partial\Theta}\right)_1 - k^3\left(\frac{\partial P}{\partial\Theta}\right)_2\right] = e^{2\alpha R}(k-1)$$

The boundaries are now defined by $\Theta = 0$ to $\Theta = c_1$ and $(c_1 + c_2)$ and

$$R = 0 \text{ to } R = \frac{1}{\alpha}\log_e\frac{r_1}{r_0}$$

and in these new co-ordinates the pad can be considered to be rectangular.

The formulas for the total load, inlet and outlet oil flow, and the friction are identical to those derived by Christopherson (6), e.g.

$$\text{Total load} = \frac{6\mu\omega\alpha^3 r_0^4}{h_1^2}\int\int Pe^{2\alpha R}\,dR\,d\Theta$$

In order to evaluate the characteristics of a sector pad it is convenient to fix leading dimensions. A convenient number of pads is six and, assuming these to be machined from one piece, each pad will subtend an angle of 60 deg. The circumferential interval was taken as 0.1. The outer diameter was fixed at 10 in. and an inner diameter of 4.327 in. chosen so that the circumferential boundaries were defined by $R = 0$ to $R = 0.8$. Semicircular steps were chosen, being the most convenient to machine.

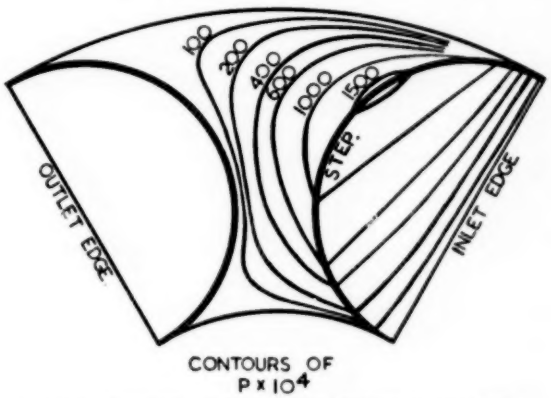

FIG. 8 CONTOURS OF $P \times 10^4$ FOR STEPPED SECTOR PAD

Fig. 8 shows the final nondimensional pressure parameter distribution. The pressure has been assumed to be zero over the outlet step. Irregular finite-difference equations exist along both curved steps. The system shown is reversible.

Graphical integration gave the load supported to be

$$0.946\frac{\mu\omega r_0^4}{h_1^2}$$

As a basis for comparison, a tilting-sector pad was taken with the same inner and outer radius, but the angle subtended was reduced so that the working area of both pads was the same. In both cases the inlet oil-film thickness was twice the outlet film thickness.

For the equivalent sector pad the load capacity is given by

$$0.236 \frac{\mu \omega r_0^4}{h_1^2}$$

For this particular case only the load capacity of the stepped pad is 4 times that of an equivalent conventional pad.

Conclusion

The stepped slider has much to commend it on the grounds of its simplicity and greatly increased load capacity as compared with the tilting pad.

A full experimental program is being carried out on this bearing to evaluate its practical performance characteristics.

Acknowledgment

Acknowledgment is made to Mr. B. J. Curtis, third-year electrical-engineering student of the University of Melbourne, for assistance in some of the relaxation.

BIBLIOGRAPHY

1 "Notes on the Theory of Lubrication," by Lord Rayleigh, *Philosophical Magazine and Journal of Science*, vol. 35, 1918, pp. 1–12.

2 "A Simple Hydrodynamic Thrust Bearing," by F. R. Archibald, Trans. ASME, vol. 72, 1950, pp. 393–400.

3 "Formulae for Numerical Integration," by W. G. Bickley, *Mathematical Gazette*, vol. 23, 1939, pp. 352–359.

4 "Formulae for Numerical Differentiation," by W. G. Bickley, *Mathematical Gazette*, vol. 25, 1941, pp. 19–27.

5 "Lubrication," by A. E. Norton, McGraw-Hill Book Company, Inc., New York, N. Y., 1942.

6 "A New Mathematical Method for the Solution of Film Lubrication Problems," by D. G. Christopherson, Proceedings of The Institution of Mechanical Engineers, vol. 146, 1941, pp. 126–135.

7 "The Theory of Lubrication," by R. O. Boswall, Longmans, Green and Company, Ltd., London, England, 1928.

8 "Relaxation Methods Applied to Engineering Problems—III. Problems Involving Two Independent Variables," by D. G. Christopherson and R. V. Southwell, Proceedings of the Royal Society of London, series A, vol. 168, 1938, pp. 317–350.

For fuller details of the mathematical theory of lubrication see references (5) and (7); for fuller details of the relaxation method see reference (8)

A Theory of Torsion Bending for Multicell Beams

By S. U. BENSCOTER,[1] PASADENA, CALIF.

Differential equations and boundary conditions, relating warping displacements and rotations to the applied torsional load, are developed for nonuniform beams with thin-walled multicell cross sections. The loading distribution and end conditions are arbitrary. A formula resembling the flexure formula is given for the normal stress in terms of a warping moment. The torsion-bending theory is of approximately the same accuracy as engineering bending theory and is exactly analogous to the case of bending with axial tension when shearing strains are taken into account.

Nomenclature

The following nomenclature is used in the paper:

A_n = area of nth cell
C = torsion-bending constant
E = Young's modulus
E' = $E/(1 - \mu^2)$
f = spanwise variation of axial displacements
G = shearing modulus of elasticity
I_c = central moment of inertia
I_w = warping moment of inertia
j = number of a junction
J = torsion constant
M_w = warping moment
n = number of a cell
p = normal stress flow
q = shear flow
q' = primary shear flow in torsion bending
q'' = secondary shear flow in torsion bending
r = radius to a tangent
r_t = radius from center of twist
s = tangential co-ordinate
t = applied torsional load
t_w = thickness of a web
T = section torque
w = axial displacement
x = horizontal co-ordinate
y = vertical co-ordinate
z = axial co-ordinate
γ = shearing strain
ϵ = normal strain
θ = rate of twist
η = a section constant defined by Equation [43]
μ = Poisson's ratio
ϕ = rotation (angle-of-twist)
ξ = tangential displacement
σ = normal stress
τ = shearing stress

A bar over a geometric quantity indicates that it is measured from the centroidal axes.

A bar over a stress or displacement indicates that the quantity is a basic transverse distribution.

An asterisk indicates that the quantity is to be computed from Saint Venant torsion theory.

Introduction

The action of torsional loads in producing normal stresses in the axial direction of a beam has been commonly referred to as torsion bending. During the past 25 years many authors have attempted to formulate a satisfactory torsion-bending theory for thin-walled beams with closed cross sections. In the present paper an approximate solution is given which is believed to have sufficient accuracy for engineering design use and yet not requiring an excessive amount of calculation effort.

The loading, end conditions, and cross-sectional shape of the beam are considered to be arbitrary. The beam is assumed to be nonuniform and of multicell design. The theory is applicable to stiffened or unstiffened sections. However, in the interest of brevity, the development of the theory is given only for monocoque, or unstiffened, sections. The theory rests on the basic assumption that the axial displacements leading to normal stresses have the same transverse distribution at a section of an arbitrary beam as would occur in Saint Venant torsion of a uniform beam with that section. Differential equations are developed which relate the spanwise variation of warping displacements to the applied torsional load and also which relate the rotation (angle of twist) to the load. Methods for calculating the various stress distributions are given.

Historical Note

No attempt will be made to review all of the many papers which have been written on the subject of torsion bending of beams. Instead the author wishes to mention those papers which have made significant contributions to the development of an approximate engineering theory for beams with closed cross sections. One must distinguish between "accurate" and "approximate" solutions. After the assumption of closely spaced rigid ribs has been introduced the mathematical problem may be solved in an exact manner. Such accurate solutions are contained in references (1, 2, 3, 4)[2] for beams of arbitrary cross sections. Approximate solutions also may be developed and may prove to be more useful from a practical standpoint.

The first approximate solution of a thin-walled beam with closed cross section was given in 1926 by Reissner (5). The cross section of the beam was of doubly symmetrical rectangular shape without stiffeners. The axial displacements, and hence axial normal stresses, were assumed to have linear variation over each wall in agreement with the axial displacements of Saint

[1] Research Associate, California Institute of Technology; also Structures Engineer for Aerophysics Development Corporation.

Contributed by the Applied Mechanics Division and presented at the Annual Meeting, New York, N. Y., November 29–December 4, 1953, of The American Society of Mechanical Engineers.

Discussion of this paper should be addressed to the Secretary, ASME, 29 West 39th Street, New York, N. Y., and will be accepted until April 12, 1954, for publication at a later date. Discussion received after the closing date will be returned.

Note: Statements and opinions advanced in papers are to be understood as individual expressions of their authors and not those of the Society. Manuscript received by ASME Applied Mechanics Division, October 3, 1952. Paper No. 53—A-27.

[2] Numbers in parentheses refer to the Bibliography at the end of the paper.

Venant torsion. This linear variation of axial stress led to the adoption of the expression "torsion-bending stresses." It is found in more general cases that the variation of axial displacements in Saint Venant torsion is linear along all straight wall segments of any cross section.

It was noted in 1933 by Ebner (6) and in 1934 by Grzedzielski (7) that the solution for a rectangular section could be obtained by analyzing an idealized section having four corner flanges assumed to carry all of the normal stress and to have areas equal to one sixth of the adjacent webs. The concept of idealization permitted the theory to be applied to a rectangular section with four built-in corner flanges.

The next generalization of the cross section was given by Kirste (8) in 1937. In a paper which has received little notice this author gave a remarkable advancement over previous work. He considered a four-flange section with unequal flange areas in arbitrary spatial positions. The webs, or shear-carrying areas, were of arbitrary shape. Kirste introduced the principal shear axes and the associated section properties of the shear-carrying area. He also located the zero warping axis and showed that the warping displacements are due to torque about this axis. Although Kirste's formulas were derived for a single-cell section they also are applicable to a multicell section.

In 1944 von Kármán and Christensen (9) gave an analysis for an unstiffened beam with arbitrary multicell cross section. By mathematical argument these authors arrived at a transverse distribution of axial displacements and normal stresses proportional to the axial displacements of Saint Venant torsion. These authors also obtained correct basic transverse distributions of primary and secondary shear flows. The spanwise variation of stresses and rotations obtained by these authors was incorrect owing to their failure to consider, with sufficient accuracy, the effect of shearing strains upon deflections. Von Kármán and Christensen gave practical methods for computing the basic stress distributions by introducing the use of a beam analogy.

In 1945 an analysis was published by Fine and Williams (10) for the special case of a cantilever of infinite length with a torque applied at the tip. These authors considered a single-cell cross section of arbitrary shape with, or without, stiffeners. They assumed the transverse distribution of axial stress to be proportional to the axial displacements of Saint Venant torsion. They assumed the spanwise variation to be given by an exponential function with an unknown rate of decay determined by the theory of least work. The method is very similar to one used earlier by Timoshenko (11) for solid sections and thin-walled open sections. Fine and Williams gave correct formulas for computing the axial displacements of Saint Venant torsion and showed that such computations yield, as a by-product, the coordinates of the center of twist. They also showed, for a single-cell section, that this center of twist coincides with the shear center as computed from Saint Venant bending theory. The spanwise variation of stress obtained by these authors does not agree with that contained in the present paper except, perhaps, for the rectangular four-flange section. The special case solved by these authors does not offer any suggestion as to how one might formulate a differential equation relating the stresses or rotations to the applied loads.

In 1948 a paper by Beskin (12) presented an analysis for a single-cell unstiffened section. Using a method of argument somewhat similar to that of von Kármán and Christensen, this author derived an equation relating the spanwise variation of normal stress to the applied load. No direct relation was given between the rotations and the applied load. The spanwise distribution of stress given by Beskin does not agree with that given by Fine and Williams or that given in the present paper. Beskin gave the location of the center of twist and also proved, for a single-cell unstiffened section, that the center of twist coincides with the shear center.

In the method of solution given by Beskin, and also that given by Fine and Williams, the designer is required to calculate an additional section property which is not required in the theory of the present paper. This additional section property is computed as the integral over the shear-carrying area of the square of the secondary shear-flow distribution. By analogy with ordinary engineering bending theory such a section property should not be required in an ordinary engineering torsion-bending theory. It can be shown that the method of analysis used by von Kármán and Christensen will lead to a solution in complete agreement with that contained in the present paper if appropriate modifications are introduced to correct their spanwise variations of stresses and rotations.

Fundamental Equations of Elasticity

The type of beam to be considered is one in which the skin and shear webs are very thin and are assumed to act essentially as membranes. The shape of the cross section is preserved by closely spaced rigid ribs which are infinitely stiff in their own plane but completely free to warp out of their plane. A number of assumptions must be introduced as approximations in order to obtain an engineering theory of torsion bending. Each approximation has its analogous approximation in engineering bending theory.

The reference axes and co-ordinates are shown in Fig. 1. A point on the cross section may be located by giving the spanwise co-ordinate z, and the tangential co-ordinate s. The exact posi-

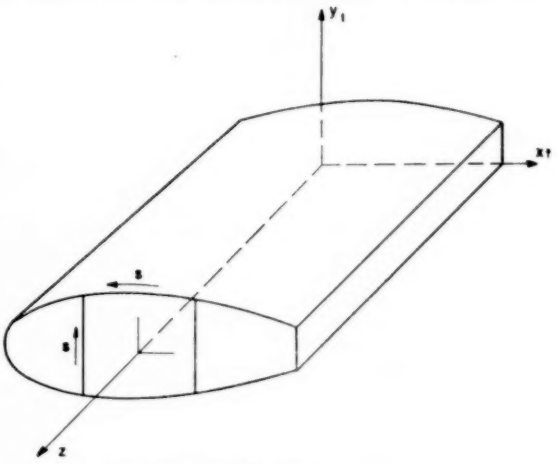

(a) RECTANGULAR AXES

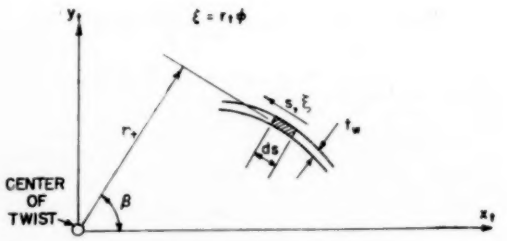

(b) COORDINATES IN A CROSS-SECTION

Fig. 1 Reference Axes and Co-Ordinates

tion of the z-axis in the cross section will be determined later. The tangential co-ordinate is measured positive in the counterclockwise direction in the exterior webs and positive in the positive direction of the y-axis in the interior webs. (All thin-wall segments will be referred to as webs.) The forces acting on a differential element of a web are shown in Fig. 2.

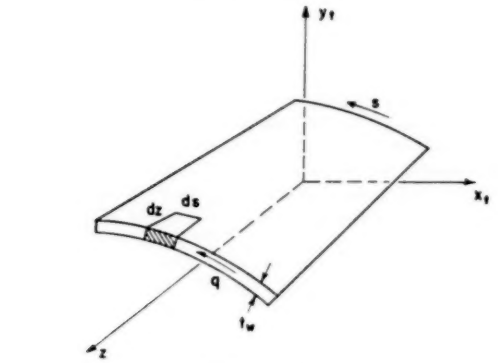

(a) DIFFERENTIAL ELEMENT

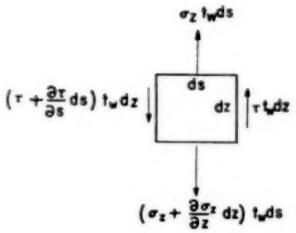

(b) AXIAL FORCES

FIG. 2 FORCES ACTING ON A WALL ELEMENT

The basic equations which govern the problem will be stated briefly since they are well known. The shearing stress is related to the shearing strain by the formula

$$\tau = G\gamma \quad [1]$$

Since the rigid ribs prevent transverse strain, the relation between axial normal stress and strain is given by

$$\sigma = E'\epsilon \quad [2]$$

where

$$E' = \frac{E}{1 - \mu^2} \quad [3]$$

The strains are expressed in terms of the displacements by the following equations

$$\gamma = \frac{\partial w}{\partial s} + \frac{\partial \xi}{\partial z} \quad [4]$$

$$\epsilon = \frac{\partial w}{\partial z} \quad [5]$$

Normal stress flows and shear flows may be introduced by the following definitions

$$q = \tau t_w \quad [6]$$

$$p = \sigma t_w \quad [7]$$

The equation of equilibrium of a differential element of a web is given by

$$\frac{\partial p}{\partial z} + \frac{\partial q}{\partial s} = 0 \quad [8]$$

The equation of equilibrium relating internal shear flows to the section torque computed from external loads is given by

$$\int_a qr ds = T \quad [9]$$

The subscript a on the integral indicates that the integration is carried over the complete cross-sectional area. The condition of continuity of axial displacements is expressed by the following equation

$$\oint_n \frac{\partial w}{\partial s} ds = 0 \quad [10]$$

The subscript n indicates that the line integration is carried around the nth cell. This equation must be satisfied for each cell.

A second-order equation governing the displacements may be derived easily. The stresses may first be expressed in terms of the displacements. The stress flows may then be expressed in terms of the displacements. These stress flows may then be substituted into the differential equation of equilibrium to obtain

$$E' \frac{\partial}{\partial z}\left(t_w \frac{\partial w}{\partial z}\right) + G \frac{\partial}{\partial s}\left(t_w \frac{\partial w}{\partial s}\right) + G \frac{\partial}{\partial s}\left(t_w \frac{\partial \xi}{\partial z}\right) = 0 \quad [11]$$

AXIAL DISPLACEMENTS FROM SAINT VENANT TORSION THEORY

In forming an engineering theory for the bending of nonuniform beams with arbitrary loading and end conditions, it is assumed that the tranverse distribution of axial displacements will be the same as would occur in a uniform beam, with that cross section acted upon by a bending moment at either end (the Saint Venant bending problem). Consequently, it seems reasonable to make the same identical assumption in forming an engineering torsion-bending theory. The axial displacements at a section of a beam will be assumed to have the same basic transverse distribution as would occur in Saint Venant torsion for a uniform beam with that section. This means that the designer must be able to compute the axial displacements in Saint Venant torsion. A practical method for making this calculation will be described.

Quantities which occur in Saint Venant torsion will be indicated with an asterisk. The warping displacement may be expressed as the product of a basic transverse distribution (the unit warping function) and the rate of twist

$$w^* = \bar{w}^*\theta^* \quad [12]$$

The shearing stress is related to the displacements by

$$\tau^* = G \frac{\partial w^*}{\partial s} + G \frac{\partial \xi^*}{\partial z} \quad [13]$$

The spanwise derivative of the tangential displacement is given by the product $r_i\theta^*$ and Equation [13] becomes

$$\tau^* = G \frac{\partial w^*}{\partial s} + Gr_i\theta^* \quad [14]$$

The shearing stress also may be expressed as the product of a basic transverse distribution and $G\theta^*$

$$\tau^* = \bar{\tau}^* G\theta^* \quad [15]$$

Equations [12] and [15] may be substituted into Equation [14]. After canceling out the common factor $G\theta^*$ the result becomes

$$\frac{\partial \bar{w}^*}{\partial s} = \bar{\tau}^* - r_t \quad [16]$$

Convenient numerical methods for computing the basic shearing stress distribution for multicell sections are given in reference (13). The integration for $\bar{w}^*$ may be indicated by

$$\bar{w}^* = \int_{s_0}^{s} (\bar{\tau}^* - r_t)\, ds + C_1 \quad [17]$$

The integration is begun at an arbitrary point s_0 where the warping is assumed to be zero. The warping distribution may then be calculated over the complete cross section since $\bar{w}^*$ is continuous. The constant C_1 remains to be determined. The integration which is indicated in Equation [17] may be considered to be a computation in which a loading distribution is being integrated to obtain a shear diagram. This beam analogy was introduced by von Kármán and Christensen (9).

In the subsequent analysis the unit warping function $\bar{w}^*$ arises as a basic distribution of normal stress with warping restraint.

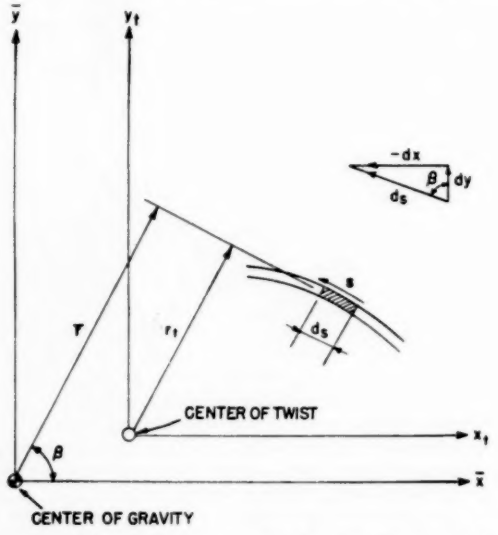

FIG. 3 CO-ORDINATES RELATIVE TO PRINCIPAL BENDING AXES

It then becomes necessary to require that $\bar{w}^*$ shall satisfy the following three conditions (see Fig. 3 for centroidal axes)

$$\int_a \bar{w}^* t_w\, ds = 0 \quad [18a]$$

$$\int_a \bar{w}^* \bar{x}\, t_w\, ds = 0 \quad [18b]$$

$$\int_a \bar{w}^* \bar{y}\, t_w\, ds = 0 \quad [18c]$$

Equation [18*a*] must be used to determine the constant of integration which appears in Equation [17]. Equations [18*b*] and [18*c*] determine the location of the center of twist. It was shown by Fine and Williams (10), and also by Beskin (12), that Equations [18*b*] and [18*c*] will be satisfied automatically if the center of twist is assumed to coincide with the shear center as obtained from the engineering theory of bending of beams. The proof, as given by these authors for single-cell sections, can be extended to multicell sections.

SPANWISE VARIATION OF WARPING DISPLACEMENTS AND ROTATIONS

As previously stated, the warping displacements will be assumed to have the same basic transverse distribution as in Saint Venant torsion. Thus the warping displacements may be expressed as follows

$$w = \bar{w}^* f(z) \quad [19]$$

In the case of a thin-walled rectangular section it is found that $\bar{w}^*$ is proportional to the product $\bar{x}\bar{y}$ and hence is independent of the spanwise co-ordinate even for nonuniform beams. For other cross sections, which vary in shape arbitrarily along the span, the function $\bar{w}^*$ usually will have some dependence upon z. However, this dependence will be neglected wherever it becomes convenient in the analysis.

Equation [11] will be solved by using Galerkin's method. Multiplying through Equation [11] by $\bar{w}^*$ and integrating over the cross section gives

$$E' \int_a \bar{w}^* \frac{\partial}{\partial z}\left(t_w \frac{\partial w}{\partial z}\right) ds + G \int_a \bar{w}^* \frac{\partial}{\partial s}\left(t_w \frac{\partial w}{\partial s}\right) ds + G \int_a \bar{w}^* \frac{\partial}{\partial s}\left(t_w \frac{\partial \xi}{\partial z}\right) ds = 0 \quad [20]$$

It is necessary to perform an integration by parts on the second and third integrals in this equation. If this is done for a single-cell section without corners the bracketed term will vanish. Since the functions $\partial w/\partial s$ and ξ are discontinuous at junctions (including corners) the bracketed term for a single-cell section with corners or a multicell section will make a finite contribution at each junction or corner. The contribution of the bracketed terms may be indicated as summations over the junctions. For this purpose it is necessary to introduce the generalized differencing operator Δ_j which indicates the difference between outflow and inflow at the jth junction of any "flow-type" of quantity. This operator was introduced in reference (4).

Performing an integration by parts on the second and third integrals of Equation [20] gives

$$\int_a \bar{w}^* \frac{\partial}{\partial s}\left(t_w \frac{\partial w}{\partial s}\right) ds = \sum_j \bar{w}_j^* \Delta_j \left(t_w \frac{\partial w}{\partial s}\right) - \int_a t_w \frac{\partial \bar{w}^*}{\partial s} \frac{\partial w}{\partial s}\, ds \quad [21]$$

$$\int_a \bar{w}^* \frac{\partial}{\partial s}\left(t_w \frac{\partial \xi}{\partial z}\right) ds = \sum_j \bar{w}_j^* \Delta_j \left(t_w \frac{\partial \xi}{\partial z}\right) - \int_a t_w \frac{\partial \bar{w}^*}{\partial s} \frac{\partial \xi}{\partial z}\, ds \quad [22]$$

It will now be shown that the summations in Equations [21] and [22] vanish when added. Multiplying through Equation [4] by t_w, and using Equations [1] and [6] gives

$$q = G t_w \frac{\partial w}{\partial s} + G t_w \frac{\partial \xi}{\partial z} \quad [23]$$

Applying the operator Δ_j to this equation gives

$$\Delta_j q = G \Delta_j \left(t_w \frac{\partial w}{\partial s}\right) + G \Delta_j \left(t_w \frac{\partial \xi}{\partial z}\right) \quad [24]$$

Since there are no flanges at the junctions, the equation of equilibrium of a junction becomes

$$\Delta_j q = 0 \quad [25]$$

Substituting Equation [25] into Equation [24] and dividing by G gives

$$0 = \Delta_j \left(t_w \frac{\partial w}{\partial s} \right) + \Delta_j \left(t_w \frac{\partial \xi}{\partial z} \right) \quad [26]$$

Equation [26] must be valid at each junction. Consequently it is evident that each term of the summation of Equation [21] will be canceled by a corresponding term of the summation of Equation [22] when these two summations are added. Thus when Equations [21] and [22] are substituted back into Equation [20] the summations may be disregarded. Substituting Equations [21] and [22] into Equation [20] gives

$$E' \int_a \bar{w}^* \frac{\partial}{\partial z} \left(t_w \frac{\partial w}{\partial z} \right) ds - G \int_a t_w \frac{\partial \bar{w}^*}{\partial s} \frac{\partial w}{\partial s} ds - G \int_a t_w \frac{\partial \bar{w}^*}{\partial s} \frac{\partial \xi}{\partial z} ds = 0 \quad [27]$$

An evaluation of the first integral in Equation [27] requires the use of two approximations. The variation of $\bar{w}^*$ with z must be neglected and the order of integration and differentiation must be interchanged. Using Equation [19] the integral becomes

$$\int_a \bar{w}^* \frac{\partial}{\partial z} \left(t_w \frac{\partial w}{\partial z} \right) ds = \frac{d}{dz} \int_a (\bar{w}^*)^2 t_w \frac{\partial f}{\partial z} ds = \frac{d}{dz} \left(I_w \frac{df}{dz} \right) \quad [28]$$

where

$$I_w = \int_a (\bar{w}^*)^2 t_w ds \quad [29]$$

Equation [29] defines a section constant which will be called the warping moment of inertia. Substituting Equations [16] and [28] into Equation [27] gives

$$\frac{d}{dz} \left(E' I_w \frac{df}{dz} \right) - G \int_a t_w (\bar{\tau}^* - r_t) \frac{\partial w}{\partial s} ds - G \int_a t_w (\bar{\tau}^* - r_t) \frac{\partial \xi}{\partial z} ds = 0 \quad [30]$$

This equation contains both axial and tangential displacements. A second equation is obtained from the equilibrium between internal shear flows and section torque as expressed by Equation [9]. The radius r in Equation [9] may be measured from any point in the cross section and will be assumed to be measured from the center of twist. Substituting Equation [23] into Equation [9] gives

$$G \int_a t_w r_t \frac{\partial w}{\partial s} + G \int_a t_w r_t \frac{\partial \xi}{\partial z} ds = T \quad [31]$$

Some simplification of Equation [30] can be obtained by subtracting Equation [31] from it. The result is as follows

$$\frac{d}{dz} \left(E' I_w \frac{df}{dz} \right) - G \int_a t_w \bar{\tau}^* \frac{\partial w}{\partial s} ds - G \int_a t_w \bar{\tau}^* \frac{\partial \xi}{\partial z} ds = T \quad [32]$$

The second term in Equation [32] may be shown to vanish. The basic Saint Venant shear flow may be defined by

$$\bar{q}^* = t_w \bar{\tau}^* \quad [33]$$

The integral becomes

$$\int_a t_w \bar{\tau}^* \frac{\partial w}{\partial s} ds = \int_a \bar{q}^* \frac{\partial w}{\partial s} ds = \sum_n \bar{q}_n^* \oint_n \frac{\partial w}{\partial s} ds \quad [34]$$

The right-hand side of Equation [34] vanishes because of the continuity condition on w as expressed by Equation [10]. Consequently Equation [34] becomes

$$\int_a t_w \bar{\tau}^* \frac{\partial w}{\partial s} ds = 0 \quad [35]$$

Substituting Equation [35] into Equation [32] gives

$$\frac{d}{dz} \left(E' I_w \frac{df}{dz} \right) - G \int_a q^* \frac{\partial \xi}{\partial z} ds = -T \quad [36]$$

Equations [31] and [36] must now be solved simultaneously. It is necessary to introduce the relation between tangential displacements and rotations which is expressed as follows

$$\xi = r_t \phi \quad [37]$$

This formula does not represent a true separation of the variables for a nonuniform beam since r_t varies along the span. If Equations [19] and [37] are substituted into Equation [31] the following is obtained

$$Gf \int_a t_w r_t \frac{\partial \bar{w}^*}{\partial s} ds + G \int_a t_w r_t \frac{\partial}{\partial z} (r_t \phi) ds = T \quad [38]$$

In order to evaluate the second integral it is necessary to assume that the variation of r_t along the span is negligible. This is a rather severe limitation upon the taper of the beam. Introducing this assumption and substituting Equation [16] into the first integral gives

$$Gf \int_a t_w r_t (\bar{\tau}^* - r_t) ds + G\theta \int_a t_w r_t^2 ds = T \quad [39]$$

The second integral is the central moment of inertia as introduced by Kirste (8)

$$I_c = \int_a t_w r_t^2 ds \quad [40]$$

This value of the central moment of inertia is almost equal to the principal value which would be obtained by measuring the radius from the origin of the principal shear axes. Introducing Equation [40] into Equation [39] gives

$$Gf \int_a t_w \bar{\tau}^* r_t ds - GI_c f + GI_c \theta = T \quad [41]$$

The integral in Equation [41] is the torque of the basic Saint

Venant shear flows. This was shown in reference (13) to be equal to the torsion constant. This may be seen to be true by multiplying through Equation [15] by $r_t t_w\, ds$ and integrating over the cross section. Equation [41] becomes

$$Gf\,(J - I_e) + GI_e\theta = T \quad [42]$$

It is convenient to introduce a dimensionless section constant defined as follows

$$\eta^2 = 1 - \frac{J}{I_e} \quad [43]$$

This constant was defined originally for a rectangular cross section by Ebner (6). It indicates the slenderness of the cross section or the amount by which the section is nonregular. For a regular polygon it has a value of zero. For a very thin supersonic wing it approaches unity. For a subsonic airplane with a fairly thick wing the value of η^2 will be in the neighborhood of one half. Substituting Equation [43] into Equation [42] gives

$$GI_e\theta - GI_e\,\eta^2 f = T \quad [44]$$

This equation may be solved for θ to obtain

$$\theta = \frac{T}{GI_e} + \eta^2 f \quad [45]$$

The first term gives the rate of twist due to shearing strains and the second term gives the rate of twist due to axial warping displacements.

Substituting Equation [37] into Equation [36] gives

$$\frac{d}{dz}\left(E'I_w \frac{df}{dz}\right) - GJ\theta = -T \quad [46]$$

It is possible to combine Equations [45] and [46] to obtain equations relating f or θ to the applied load. If θ is eliminated the equation governing the spanwise variation of the warping displacements is as follows

$$\frac{d}{dz}\left(E'I_w \frac{df}{dz}\right) - GJ\,\eta^2 f = -\eta^2 T \quad [47]$$

If f is eliminated the equation governing the rate of twist is

$$\frac{d}{dz}\left[E'I_w \frac{d}{dz}\left(\frac{\theta}{\eta^2}\right)\right] - GJ\theta = -T + \frac{d}{dz}\left[E'I_w \frac{d}{dz}\left(\frac{\theta_0}{\eta^2}\right)\right] \quad [48]$$

where

$$\theta_0 = \frac{T}{GI_e} \quad [49]$$

In solving Equation [48] one may regard θ/η^2 as the unknown. However, Equation [43] suggests that η will have only a small variation along the span if the general shape of the cross section does not change rapidly. The section properties J and I_e are both properties of the shear-carrying area. If the variation of η with z is neglected, Equation [48] takes the form

$$\frac{d}{dz}\left(E'C \frac{d\theta}{dz}\right) - GJ\theta = -T + \frac{d}{dz}\left(E'C \frac{d\theta_0}{dz}\right) \quad [50]$$

where

$$C = \frac{I_w}{\eta^2} \quad [51]$$

The torsion-bending constant C has been introduced and defined by Equation [51]. Equation [50] reduces to the form given by von Kármán and Christensen (9) if η is set equal to unity and θ_0 is set equal to zero.

It is necessary to state the boundary conditions which govern the functions f and θ. At a fixed end such as the root of a cantilever the warping displacements must be zero. Assuming the fixed end to be at $z = 0$ gives the end condition

$$f(0) = 0 \quad [52]$$

The corresponding end condition for the rate of twist is obtained by substituting Equation [52] into Equation [45]

$$\theta(0) = \theta_0(0) = \frac{T(0)}{GI_e} \quad [53]$$

At the free end of a cantilever (or at a simple support) the end condition is that the normal stress is zero. Equation [19] may be substituted into Equation [5] to obtain a formula for the normal strain. This result may then be substituted into Equation [2] to obtain the following formula for normal stress

$$\sigma = E' \frac{\partial}{\partial z}(\bar{w}^* f) \quad [54]$$

As has been done previously it will be assumed that the variation of $\bar{w}^*$ along the span may be neglected as an engineering approximation. With this assumption Equation [54] becomes

$$\sigma = E'\bar{w}^* \frac{df}{dz} \quad [55]$$

Considering a cantilever beam of length L, the boundary condition at the tip where $z = L$ becomes

$$\left(\frac{df}{dz}\right)_{z=L} = 0 \quad [56]$$

From Equations [45] and [56] it is seen that the boundary condition for θ is

$$\left(\frac{d\theta}{dz}\right)_{z=L} = \left[\frac{d}{dz}\left(\frac{T}{GI_e}\right)\right]_{z=L} \quad [57]$$

An inspection of the differential equations and boundary conditions indicates that it will be more convenient to solve for the spanwise variation of the warping displacements and then to use Equation [45] to determine the rotations. Equation [47] may be solved by a series method or it may be replaced by difference equations. Since the equation is of second order the matrix of coefficients of the difference equations will be a continuant matrix and the distribution procedure used in reference (13) may be employed. Such a procedure may be used for static loading. However, for vibrations or dynamic loading it is necessary to develop an equation relating the rotations to the applied torsional loading. The rotation ϕ and the rotation with zero-warping ϕ_0 must be introduced according to the following formulas

$$\theta = \frac{d\phi}{dz} \quad [58a]$$

$$\theta_0 = \frac{d\phi_0}{dz} \quad [58b]$$

Substituting Equations [58] into Equation [50] and differentiating with respect to z gives

$$\frac{d^2}{dz^2}\left(E'C \frac{d^2\phi}{dz^2}\right) - \frac{d}{dz}\left(GJ \frac{d\phi}{dz}\right) = \frac{d^2}{dz^2}\left(E'C \frac{d^2\phi_0}{dz^2}\right) \quad [59]$$

For a uniform beam Equation [59] may be written in the following form

$$E'C\frac{d^4\phi}{dz^4} - GJ\frac{d^2\phi}{dz^2} = t - \frac{E'C}{GI_s}\frac{d^2t}{dz^2} \quad [60]$$

The problem of torsion bending is exactly mathematically analogous to the problem of bending with axial tension when the effect of shearing strains are taken into account.

Calculation of Normal Stresses

Equation [55] appears to offer a satisfactory formula for the calculation of the normal stress. However, for nonuniform beams the differential equation for f must be solved by approximate numerical methods. In such cases the derivative cannot be determined accurately without an excessive amount of calculation effort. An alternate method of solution, which seems to be preferable, can be developed.

It is convenient to introduce the concept of a warping moment (corresponding to bending moment) by the following definition

$$M_w = \int_a \bar{w}^*\sigma t_w\, ds \quad [61]$$

This formula defines the warping moment in terms of the internal normal stresses. The warping moment may be related to the spanwise variation of the warping displacements by multiplying through Equation [55] by $\bar{w}^*$ and integrating over the cross section

$$M_w = E'I_w\frac{df}{dz} \quad [62]$$

Equation [29] has been introduced. By combining Equations [55] and [62] it is possible to obtain a stress formula corresponding to the flexure formula as follows

$$\sigma = \frac{M_w\bar{\sigma}}{I_w} \quad [63]$$

where

$$\bar{\sigma} \equiv \bar{w}^* \quad [64]$$

The symbol $\bar{\sigma}$ has been introduced to represent the basic transverse stress distribution for better consistency of notation.

A method for computing the warping moment is obtained by substituting Equation [62] into Equation [47] to obtain

$$\frac{dM_w}{dz} = GJ\,\eta^2 f - \eta^2 T \quad [65]$$

This equation may be integrated in the same manner that a shear diagram is integrated to obtain bending moments. In the case of a cantilever beam the integration may begin at the tip to give

$$M_w = \int_L^z \eta^2\,(GJf - T)\,dz \quad [66]$$

If the designer is interested only in stresses it is possible to combine Equations [62] and [65] to eliminate f. The resulting equation is

$$\frac{d}{dz}\left(\frac{1}{GJ\eta^2}\frac{dM_w}{dz}\right) - \frac{M_w}{E'I_w} = -\frac{d}{dz}\left(\frac{T}{GJ}\right) \quad [67]$$

This equation may be solved by a series method or may be replaced by difference equations and solved by a distribution procedure.

Shear Flows Determined by Condition of Continuity

The distribution of shear flows consists of two parts. One part (the primary distribution) has the same transverse distribution as in Saint Venant torsion. The other part (the secondary distribution) is in equilibrium with the normal stresses. Two methods of analysis may be used. One method may be called the method of displacements, while the other may be called the method of forces. The method of displacements, which requires the use of the condition of continuity of axial displacements, will be explained first. This method was used by von Kármán and Christensen (9) and hence will be stated briefly without detailed development.

The total shear-flow distribution is assumed to consist of a primary part and a secondary part as follows

$$q = q' + q'' \quad [68]$$

The primary shear flows at a given section are assumed to have the same values as would occur in Saint Venant torsion with the same rate of twist. Thus the primary shear flow is given by

$$q' = \bar{q}^*\,G\theta \quad [69]$$

The formula for the secondary shear flow, as given by von Kármán and Christensen (9), must be modified slightly to allow for the fact that the normal stresses are directly related to the warping displacements rather than the rate of twist. If the formula also is modified to become applicable to a nonuniform beam, it may be written as follows

$$q'' = E'\frac{\partial}{\partial z}\left(\bar{q}''\frac{df}{dz}\right) \quad [70]$$

Equation [70] corresponds to Equation [22] of reference (9).

It is necessary to define the basic distribution $\bar{q}''$ of the secondary shear flow. Owing to the requirement of continuity of axial displacements the shear flow must satisfy the following well-known equation

$$\int_n q\frac{ds}{t_w} = 2A_n\,G\theta \quad [71]$$

Owing to the assumed definition of the primary shear flow as given in Equation [69] the secondary shear flow must satisfy the following equation

$$\oint_n q''\frac{ds}{t_w} = 0 \quad [72]$$

This equation is the same as that which is used in engineering bending theory. The actual shear flow due to load can satisfy Equation [72] only if the basic distribution $\bar{q}''$ satisfies Equation [72]. As in bending theory the secondary shear flow consists of a statically determinate part which is obtained by integrating the normal stresses and an indeterminate part which is obtained by solving a set of simultaneous algebraic equations.

The two parts of the basic distribution of the secondary shear flow may be indicated as follows

$$\bar{q}'' = \bar{q}_s'' - \bar{q}_i'' \quad [73]$$

The statically determinate part is obtained by integrating the basic distribution of the normal stress flow from an arbitrary point in each cell as follows

$$\bar{q}_s'' = -\int_{s_0}^{s} t_w\,\bar{w}^*\,ds \quad [74]$$

The indeterminate part is obtained by solving a system of equations of which the nth equation appears as follows

$$\oint_n \bar{q}_i^* \frac{ds}{t_w} = K_n \quad \ldots\ldots [75]$$

where

$$K_n = \oint_n \bar{q}_n^* \frac{ds}{t_w} \quad \ldots\ldots [76]$$

A constant K_n must be computed for each cell by integrating the known statically determinate part of the stress. The system of equations to be solved has the same matrix of coefficients as in Saint Venant torsion and hence the numerical procedure of reference (13) may be used with the same distribution factors.

The final formula for the shear flow may be written as

$$q = \bar{q}^* G\theta + E' \frac{\partial}{\partial z}\left(\bar{q}^* \frac{df}{dz}\right) \quad \ldots\ldots [77]$$

This formula may be modified in various ways by substituting for θ or f from various formulas which are given in preceding sections of the paper.

It may be shown that if f and θ are determined to satisfy Equation [46], the formula for shear flow as given by Equation [77] will satisfy over-all equilibrium as expressed by Equation [9]. In fact, Equation [77] may be substituted into Equation [9] to give a second method of deriving Equation [46]. This was the method used by von Kármán and Christensen (9). The use of Galerkin's method of solving a differential equation, as in this paper, emphasizes the point that in the present torsion-bending theory the differential equation relating rotation to applied load is not dependent upon the actual distribution of the shearing stresses on the cross section. This is in analogous agreement with engineering bending theory of thin-walled beams.

Shear Flows Determined by Condition of Equilibrium

An alternate method for computing shear flows will be stated briefly. This method may be called the method of forces. The shear flow will be expressed in terms of section forces rather than displacements. The formula for q is obtained by using again the equation of differential equilibrium and the equation of over-all equilibrium in place of the equation expressing continuity.

While the method of forces may be developed independently, it is much more convenient to use formulas from the preceding section. Equation [46] may be solved for $G\theta$ and the result substituted into Equation [77] to obtain

$$q = \frac{T\bar{q}^*}{J} + \frac{\bar{q}^*}{J}\frac{d}{dz}\left(E' I_w \frac{df}{dz}\right) + E' \frac{\partial}{\partial z}\left(\bar{q}^* \frac{df}{dz}\right) \quad \ldots\ldots [78]$$

Substituting Equation [62] into Equation [78] gives

$$q = \frac{T\bar{q}^*}{J} + \frac{\bar{q}^*}{J}\frac{dM_w}{dz} + \frac{\partial}{\partial z}\left(\frac{M_w \bar{q}^*}{I_w}\right) \quad \ldots\ldots [79]$$

This formula can be shown to satisfy the equation of differential equilibrium when the normal stress is given by Equation [63]. It is easily seen that over-all equilibrium is satisfied by recalling a few known relations. It has been noted previously that the torque of the basic Saint Venant shear flow is equal to the torsion constant

$$\int_a \bar{q}^* r_t \, ds = J \quad \ldots\ldots [80]$$

It was shown by von Kármán and Christensen (9) that the torque of the basic secondary shear flow is equal to the warping moment of inertia with a negative sign

$$\int_a \bar{q}^* r_t \, ds = -I_w \quad \ldots\ldots [81]$$

From Equation [80] it is seen that the first term in the formula for q, as given in Equation [79], contributes the total torque. Hence the remaining terms must be self-equilibrating. In view of Equations [80] and [81] it is seen that the torque from the second term will cancel the torque from the third term if approximations, such as have been used previously, are employed in the calculation of the torque of the third term.

It can also be shown that Equation [79] satisfies the condition of continuity if M_w is defined by Equation [62] and f is determined from Equation [46]. In fact, the condition of continuity could be used to derive Equation [46]. This provides a third possible method whereby the equations governing the warping displacements and the rotations could be derived. Energy methods also may be used.

A short discussion of the terms in Equation [79] is desirable in order that they can be associated by analogy with the shear flows in ordinary bending theory. The first term gives the Saint Venant torsion solution. The remaining terms occur because of the existence of normal stresses. The third term, which has a Kármán-Christensen distribution, provides equilibrium with the normal stresses. The second term, with a Saint Venant distribution, is then added to cancel the torque of the Kármán-Christensen distribution.

Analysis of Stiffened Sections

In practice, design calculations usually are carried out on equivalent idealized stiffened sections. It is possible to develop the torsion-bending theory for idealized stiffened sections in a manner corresponding to that which has been given for unstiffened sections. For this purpose it is convenient to use generalized difference equations in place of differential equations as has been illustrated in reference (4). In order to keep the paper down to a reasonable length it is necessary to omit the development of the theory for stiffened sections.

It is worth noting, for practical purposes, that the central moment of inertia is computed for an idealized stiffened section by integrating over the shear-carrying area only. The warping moment of inertia is computed by integrating only over the normal stress-carrying area. If greater accuracy is desired in the shear-flow calculation it is possible to use the "unit method" as given by Shanley and Cozzone (14) for the bending case.

For uniform beams with doubly symmetrical four-flange cross sections the present theory will give the same solution as the exact methods of references (1 to 4). If, in the methods of references (1 to 4), an approximate solution is obtained for a beam with a doubly symmetrical cross section by retaining only one term in the series for warping displacements, formulas and equations may be obtained which have the same form as those contained in this paper.

Numerical Example

A simple illustration will be given for the basic stress distributions on a cross section having three square cells and constant wall thickness as shown in Fig. 4(a). The basic Saint Venant shear flows may be computed to be

$$\bar{q}_1^* = 5ct/7 \quad \ldots\ldots [82a]$$

$$\bar{q}_2^* = 6ct/7 \quad \ldots\ldots [82b]$$

$$\bar{q}_3^* = 5ct/7 \quad \ldots\ldots [82c]$$

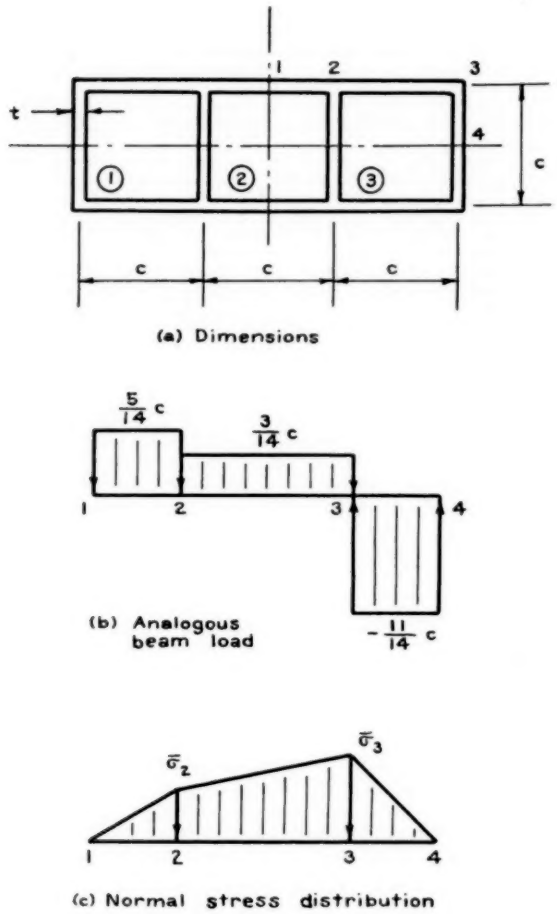

FIG. 4 THREE-CELL MEMBER

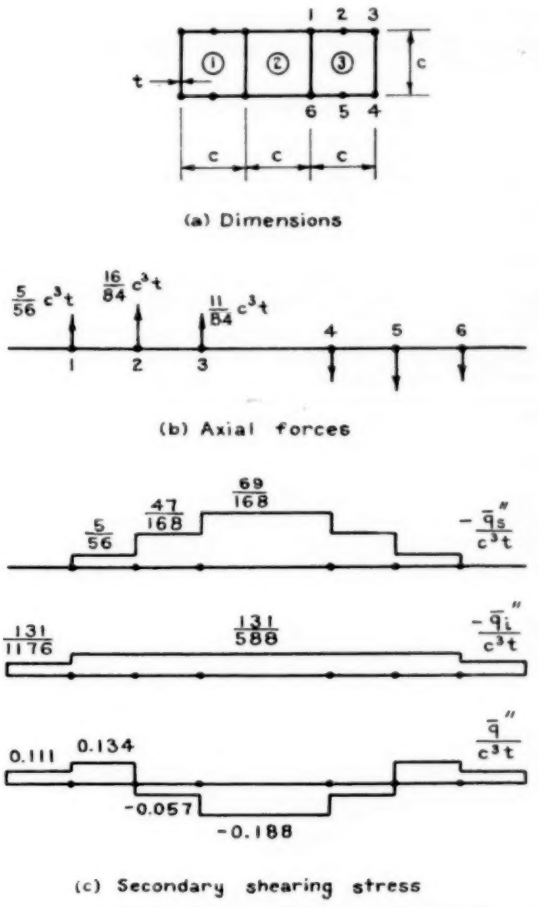

FIG. 5 IDEALIZED SEMIMONOCOQUE THREE-CELL MEMBER

For this section the geometric center is the center of twist. The quantity $(\bar{\tau}^* - r_i)$ may be computed to be as shown in Fig. 4(*b*), as an analogous beam load. An integration of the beam load gives the basic normal stress distribution which is shown in Fig. 4(*c*). The distribution of the normal stress must be antisymmetric about both axes of symmetry of the cross section and have a value of zero along each axis. Consequently, it is only necessary to compute the stress in one quadrant. Since the normal stress varies linearly over each wall segment between junctions, the distribution is completely defined by giving the values of $\bar{\sigma}$ at points 2 and 3 which are as follows

$$\bar{\sigma}_2 = 5c^2/28 \quad [83a]$$

$$\bar{\sigma}_3 = 11c^2/28 \quad [83b]$$

The basic normal stress may be integrated to obtain the secondary shear-flow distribution which will have parabolic variations over the wall segments. In order to simplify this problem for illustrative purposes the cross section will be idealized as shown in Fig. 5(*a*). The quantity which is preserved in the idealization is the normal stress at each point where a stiffener is located. Since the normal stress varies linearly over each wall segment it is necessary to preserve the area and moment of inertia of each segment. This is accomplished by placing one sixth of the web area in a stiffener at either end of the web and two thirds of the area in a stiffener at the center of the web. From the basic normal stresses in Fig. 4(*c*) the flange forces are computed to be as shown in Fig. 5(*b*). These may be integrated to obtain the statically determinate part of the secondary shear flow. The indeterminate part is obtained by solving three algebraic equations for which the constant terms are

$$K_1 = -131c^4/168 \quad [84a]$$

$$K_2 = 0 \quad [84b]$$

$$K_3 = -131c^4/168 \quad [84c]$$

Superposition gives the final values of the Kármán-Christensen distribution of shear flows as shown in Fig. 5(*c*).

CONCLUSION

An engineering theory of torsion bending has been developed for nonuniform beams with multicell cross sections. The accuracy of the theory is approximately the same as engineering bending theory although the approximations appear to place a more severe limitation upon the taper ratio in the torsion case. In a straight wing under normal flight conditions approximately 10 per cent of the maximum normal stress at the root is due to torsion. In such cases (except for very low aspect ratios) the accu-

racy of the present theory should be adequate. The present theory cannot be applied to swept wings until it is modified to allow for rib distortion.

BIBLIOGRAPHY

1 "The General Theory of Cylindrical and Conical Tubes Under Torsion and Bending Loads," by J. Hadji-Argyris and P. C. Dunne, *Journal of the Royal Aeronautical Society*, vol. 51, 1947, pp. 199–269, 757–784, and 884–930; vol. 53, 1949, pp. 461–483, 558–620.

2 "Torsion With Variable Twist," by Th. von Kármán and W. Z. Chien, *Journal of the Aeronautical Sciences*, vol. 13, October, 1946, pp. 503–510.

3 "A Numerical Procedure for the Stress Analysis of Stiffened Shells," by J. E. Duberg, *Journal of the Aeronautical Sciences*, vol. 16, August, 1949, pp. 451–462.

4 "Secondary Stresses in Thin-Walled Beams With Closed Cross-Sections," by S. U. Benscoter, TN 2529, NACA, October, 1951.

5 "Neuere Probleme aus der Flugzeugstatik," by H. Reissner, *Zeitschrift für Flugtechnic und Motorluftshiffart*, vol. 17, September, 1926, pp. 384–393; vol. 18, April, 1927, pp. 153–158.

6 "Torsional Stresses in Box Beams With Cross-Sections Partially Restrained Against Warping," by H. Ebner, (*Zeitschrift für Mathematik*, vol. 24, December, 1933); translated as TM NACA 744, 1934.

7 "Sur un Cas Particulier de Coopération des Longerons d'Ailes," by A. Grzedzielski, Sprawozdania Institute Rech. de l'Aero, Warsaw, Poland, vol. 13, 1934, pp. 5–19.

8 "Sur le Calcul des Poutres en Caisson," by L. Kirste, *L'Aeronautique*, vol. 19 (*L'Aerotechnique*), January, 1937, pp. 1–6; May, 1937, pp. 57–58.

9 "Methods of Analysis for Torsion With Variable Twist," by Th. von Kármán and N. B. Christensen, *Journal of the Aeronautical Sciences*, vol. 11, April, 1944, pp. 110–124.

10 "Effect of End Constraint on Thin-Walled Cylinders Subject to Torque," by M. Fine and D. Williams, R and M, 2223, Aeronautical Research Council, May, 1945.

11 "Theory of Elasticity," by S. Timoshenko, first edition, McGraw-Hill Book Company, Inc., New York, N. Y., 1934, p. 273.

12 "Warping and Shear Lag in Closed Cylindrical Shells," by L. Beskin, *Journal of the Aeronautical Sciences*, vol. 15, April, 1948, pp. 221–231.

13 "Numerical Transformation Procedures for Shear-Flow Calculation," by S. U. Benscoter, *Journal of the Aeronautical Sciences*, vol. 13, August, 1946, pp. 438–443.

14 "Unit Method of Beam Analysis," by F. R. Shanley and F. P. Cozzone, *Journal of the Aeronautical Sciences*, vol. 8, April, 1941, pp. 246–255.

Dynamic Behavior of Reinforced Cylindrical Shells in a Vacuum and in a Fluid[1]

By MIGUEL C. JUNGER,[2] CAMBRIDGE, MASS.

The vibrations of an infinite cylindrical shell reinforced with periodically spaced septa and stiffening rings are studied in a vacuum and in a fluid medium. Lagrange equations are used to derive the dynamic equations; the fluid reaction is obtained from the solution of the wave equation. The solution gives the dynamic characteristics of the shell, the amplitude of forced vibration, and the sound field generated thereby. The theory can be extended to shells embodying complex stiffening structures and load distributions. Certain features of the fluid reaction suggest interesting applications: Its inertial component becomes extremely large under certain conditions, thus tending to eliminate some modes of vibration; also, the resistive, i.e., damping, component may vanish for certain modes, which therefore do not radiate any sound.

Nomenclature

The following nomenclature is used in the paper:

a = mean radius of shell
A = cross-sectional area of stiffening rings
c = velocity of sound in fluid medium
E = Young's modulus
h = half-thickness of shell
I_p, I_r = polar moment of inertia of ring cross section and moment about radial direction, respectively
$j = -\sqrt{-1}$
L = distance between adjoining septa
∇_r^2 = Laplacian operator in cylindrical co-ordinates
ϵ_n = Neumann factor; $\epsilon_0 = 1$; $\epsilon_n = 2$ for $n \neq 0$
$\epsilon_\phi, \epsilon_x, \gamma_{x\phi}$ = strains in cylindrical co-ordinates, in Timoshenko's notation
$\lambda = 2\pi c/\omega$, wave length in fluid medium
ν = Poisson's ratio
ρ, ρ_s = density of fluid medium and of shell material, respectively
$\chi_\phi, \chi_x, \chi_{\phi x}$ = changes of curvature in cylindrical co-ordinates, in Timoshenko's notation
ω = circular frequency

Bessel and related functions:
$J_n(x)$ = Bessel function of first kind
$N_n(x)$ = Neumann function
$H_n^{(2)}(x) = J_n(x) - jN_n(x)$, Hankel function of second kind
$K_n^{(2)}(x) = (-j)^{n+1}(\pi/2)H_n^{(2)}(-jx)$
$J_n'(x) = dJ_n(x)/dx$, etc.

[1] This research has been aided by funds made available under a contract with the ONR.

[2] Research Fellow in Acoustics, Acoustics Research Laboratory, Harvard University. Assoc. Mem. ASME.

Contributed by the Applied Mechanics Division and presented at the Annual Meeting, New York, N. Y., November 29–December 4, 1953, of The American Society of Mechanical Engineers.

Discussion of this paper should be addressed to the Secretary, ASME, 29 West 39th Street, New York, N. Y., and will be accepted until April 12, 1954, for publication at a later date. Discussion received after the closing date will be returned.

Note: Statements and opinions advanced in papers are to be understood as individual expressions of their authors and not those of the Society. Manuscript received by ASME Applied Mechanics Division, January 26, 1953. Paper No. 53—A-1.

Introduction

A submerged cylindrical shell, reinforced by periodically spaced stiffeners, displays certain unusual dynamics, determined by the fluid reaction, different both from the uniform submerged shell and from the reinforced shell vibrating in vacuo. The associated acoustical phenomena also are characterized by certain particular features. The mathematical complexity of this type of problem arises from the fact that the fluid reaction, which affects the vibration of the shell, is itself determined by the amplitude of the modes of vibration.

This problem is analyzed here for conditions corresponding to an idealized form of a system of practical importance: A cylindrical shell, freely suspended in a fluid medium, is reinforced by regularly spaced septa, or partitions, attached to the inner shell surface, Fig. 1. The septa are considered to be perfectly rigid

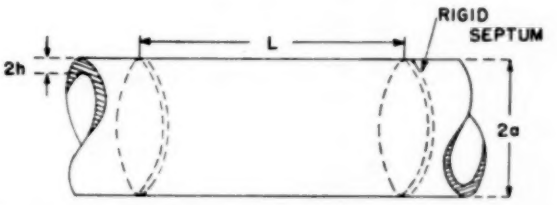

Fig. 1 Cylindrical Shell Reinforced With Periodically Spaced Septa

when used in conjunction with the relatively flexible shell. (Expressions also are given for shells having additional stiffeners in the form of elastic rings, i.e., rings embodying a flexibility of the same order as that of the shell.) The shell material is assumed to be isotropic, devoid of friction, and to obey Hooke's law. The shell thickness and deflections are sufficiently small to insure linearity of the equations. The shell is of infinite length. The surrounding fluid medium obeys the simplified wave equation. The dynamic effect of hydrostatic pressure is neglected.

Elastic and stability problems connected with reinforced cylindrical shells have been investigated extensively; however, the study of vibrations of these shells is incomplete, and none apparently has been made public in the technical literature. Previous work on the dynamics of submerged elastic systems and of the associated fluid reaction has dealt mostly with plates and membranes (1),[3] (2).[4] Great attention has been paid to ship-hull vibrations,[5] but the approach has, in general, been empirical. Exact analyses, using the solution of the wave equation, have been published recently for uniform cylindrical and spherical shells for steady (4, 5, 6) and transient (7) conditions.

The approach to the present problem is the one used in an analysis of the uniform cylinder (4, 6); it consists of constructing the Lagrange equations of the system and introducing the fluid

[3] Numbers in parentheses refer to the Bibliography at the end of the paper.

[4] Sections V. 19–21.

[5] See the complete bibliography in reference (3).

reaction as generalized forces expressed in terms of acoustic impedances, i.e., of damping forces and accessional inertia forces.

Dynamic Equations of Shell

The components δ, τ, and ζ of dynamic deflection of a shell element, Fig. 2, may be expressed as Fourier series in ϕ and z.

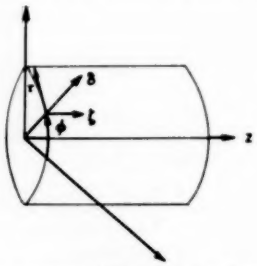

Fig. 2 Displacement Components of Shell Surface

ϕ and z-axes are chosen so as to correspond to planes of symmetry of the system; noting that the presence of the rigid septa causes the shell configuration to be periodic in z, these series are of the form

$$\left.\begin{aligned}\delta &= \sum_{n=0}^{\infty}\sum_{m=0}^{\infty} a_{nm}\cos(2\pi mz/L)\cos n\phi \\ \tau &= \sum_{n=1}^{\infty}\sum_{m=0}^{\infty} b_{nm}\cos(2\pi mz/L)\sin n\phi \\ \zeta &= \sum_{n=0}^{\infty}\sum_{m=1}^{\infty} f_{nm}\sin(2\pi mz/L)\cos n\phi\end{aligned}\right\} \quad \ldots\ldots [1]$$

The Fourier coefficients are proportional to $e^{j\omega t}$. From the requirement that no deformation of the shell occur at the septa, it follows that

$$\left.\begin{aligned}a_{n0} &= -\sum_{m=1}^{\infty} a_{nm} \\ b_{n0} &= -\sum_{m=1}^{\infty} b_{nm}\end{aligned}\right\} \quad \ldots\ldots [2]$$

With these relations substituted, the Fourier Series [1] for δ and τ becomes, Fig. 3

$$\left.\begin{aligned}\delta &= \sum_{n=0}^{\infty}\sum_{m=1}^{\infty} a_{nm}[\cos(2\pi mz/L) - 1]\cos n\phi \\ \tau &= \sum_{n=1}^{\infty}\sum_{m=1}^{\infty} b_{nm}[\cos(2\pi mz/L) - 1]\sin n\phi\end{aligned}\right\} \quad \ldots [3]$$

The energies associated with this dynamic configuration can now be evaluated in terms of the generalized co-ordinates a_{nm} b_{nm}, and f_{nm}. The kinetic energy is given by the integral

$$T = ha\rho_s \int_0^L \int_0^{2\pi} \left[\left(\frac{d\delta}{dt}\right)^2 + \left(\frac{d\tau}{dt}\right)^2 + \left(\frac{d\zeta}{dt}\right)^2\right] d\phi\, dz \quad \ldots\ldots [4]$$

The potential energy connected with extension of the shell middle surface is (8)[6]

$$V_e = \frac{haE}{1-\nu^2}\int_0^L \int_0^{2\pi} \left[(\epsilon_\phi + \epsilon_z)^2 - 2(1-\nu)\left(\epsilon_\phi\epsilon_z - \frac{1}{4}\gamma_{z\phi}^2\right)\right] d\phi\, dz \ldots\ldots [5]$$

When the strains are written in terms of components of shell deflections,[7] expressed as Fourier series, this integral can be evaluated in terms of the generalized co-ordinates.

Since two adjoining septa and the length of shell between them form a closed surface, any deformation of the shell involves considerable extension of its middle surface (9). In such a case it is customary to use the membrane theory of shells, i.e., to neglect the potential energy V_b connected with curvature changes of the shell, since this energy is proportional to $(h/a)^3$, and therefore much smaller than V_e, which varies as h/a. In the present case, however, if the elastic forces connected with V_b are omitted from the Lagrange equations below, amplitudes a_{nm} having the same n are of approximately the same magnitude, regardless of the order m of the mode, particularly when $n = 0$. Significantly, no term of the form $\partial\delta/\partial z$ occurs in the Integral [5]. The physical significance of this degenerate solution is illustrated by the fact that the extensional energy of a shell undergoing essentially radial vibrations is equivalent to the sum of potential energies of a number of rings vibrating primarily in their plane, which is evidently not a function of m. It is therefore necessary to calculate the flexural energy (8), which is evaluated from the integral[7]

$$V_b = \frac{Eh^3a}{3(1-\nu^2)}\int_0^L \int_0^{2\pi} [(\chi_\phi + \chi_z)^2 - 2(1-\nu)(\chi_\phi\chi_z - \chi_{\phi z}^2)]\, d\phi\, dz \ldots\ldots [6]$$

The quantity χ_z^2 will give rise to terms proportional to m^4. However, if the quantity h/a is small, their effect may not become noticeable till fairly large values of m are reached; in other words, the convergence of the Fourier series for δ may be slow at first, the amplitudes of the first modes being all of the same order of magnitude. The lowest natural frequencies will similarly be clustered together.

The dynamic behavior of the shell obeys the Lagrange equations

$$\frac{d}{dt}\frac{\partial T}{\partial \dot{q}_{nm}} - \frac{\partial T}{\partial q_{nm}} + \frac{\partial}{\partial q_{nm}}(V_e + V_b) = Q_{nm} \ldots\ldots [7]$$

[6] See p. 530.

[7] Expressions for the strains and curvature changes in cylindrical co-ordinates are given in reference (8), p. 543.

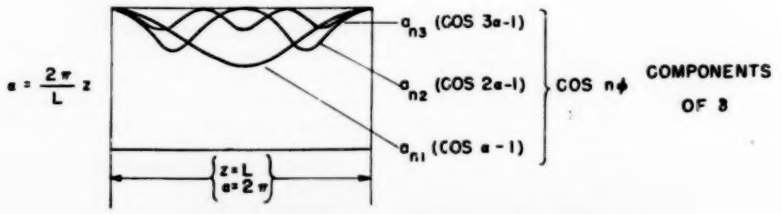

Fig. 3 Effect of Rigid Septa on Dynamic Configuration

where q_{nm} is a_{nm}, b_{nm}, or f_{nm}. The generalized forces Q_{nm} are zero for the latter two generalized co-ordinates, provided only radial loads are applied to the shell, and if the surrounding fluid medium is nonviscous, i.e., unable to exert shear stress.

For a concentrated force $Fe^{j\omega t}$ applied at the point (ϕ, z), and for a distributed force of intensity $w(\phi,z)e^{j\omega t}$ per unit area, the generalized forces are, respectively

$$\left.\begin{aligned} Q_{nm} &= e^{j\omega t} F\,[\cos(2\pi mz/L) - 1]\cos n\phi \\ Q_{nm} &= e^{j\omega t} a \int_0^L \int_0^{2\pi} w(\phi,z)\,[\cos(2\pi mz/L) - 1]\cos n\phi\, d\phi\, dz \end{aligned}\right\} \quad \ldots [8]$$

When the Integrals [4], [5], and [6] are substituted in Equation [7], the following three sets of Lagrange equations are obtained

$$\left.\begin{aligned} &\left\{-\frac{\alpha}{\epsilon_n}\omega^2 + \frac{\gamma}{\epsilon_n} + \frac{\Gamma}{2}\left[\frac{3}{a^4}n^4 + \left(\frac{2\pi}{L}\right)^4 \frac{2}{\epsilon_n} m^4 + 2\left(\frac{2\pi}{La}\right)^2 n^2m^2\right]\right\} a_{nm} \\ &+ \left(-\frac{2\alpha\omega^2}{3\epsilon_n} + \frac{2\gamma}{3\epsilon_n} + \frac{\Gamma n^4}{a^4}\right) \sum_{\mu=1}^{\infty}{}' a_{n\mu} + \frac{n}{2}\left\{\gamma + \frac{\Gamma}{a^2}\left[\frac{3}{a^2}n^2 + (2-\nu)\left(\frac{2\pi}{L}\right)^2 m^2\right]\right\} b_{nm} \\ &+ n\left(\frac{\gamma}{3} + \frac{\Gamma n^2}{a^4}\right) \sum_{\mu=1}^{\infty}{}' b_{n\mu} + \theta\frac{m}{\epsilon_n} f_{nm} = A_{nm}, \quad \text{for } n \geq 0,\ m > 0 \\ &\frac{n}{2}\left\{\gamma + \frac{\Gamma}{a^2}\left[\frac{3n^2}{a^2} + (2-\nu)\left(\frac{2\pi}{L}\right)^2 m^2\right]\right\} a_{nm} + n\left(\frac{\gamma}{3} + \frac{\Gamma}{a^4}n^2\right) \sum_{\mu=1}^{\infty}{}' a_{n\mu} \\ &+ \left\{-\frac{\alpha\omega^2}{2} + \frac{\gamma}{2}n^2 + \eta m^2 + \frac{\Gamma}{2a^2}\left[\frac{3}{a^2}n^2 + 2(1-\nu)\left(\frac{2\pi}{L}\right)^2 m^2\right]\right\} b_{nm} \\ &+ \left(-\frac{\alpha\omega^2}{3} + \frac{\gamma}{3}n^2 + \frac{\Gamma}{a^4}n^2\right) \sum_{\mu=1}^{\infty}{}' b_{n\mu} + \kappa nm\, f_{nm} = 0, \quad \text{for } n > 0,\ m > 0 \\ &\theta\frac{m}{\epsilon_n} a_{nm} + \kappa nm\, b_{nm} + \left(-\frac{\alpha\omega^2}{3\epsilon_n} + \upsilon n^2 + \frac{\psi m^2}{\epsilon_n}\right) f_{nm} = 0, \quad \text{for } n \geq 0,\ m > 0 \end{aligned}\right\} \quad \ldots [9]$$

The symbol $\sum_{\mu=1}^{\infty}{}'$ indicates a summation over all positive integers μ, with the exception of $\mu = m$. The parameters α, etc., which were obtained from the derivatives of T and V, are defined as

$$\left.\begin{aligned} \alpha &= 6aL\pi h\rho_s & \upsilon &= \frac{\pi hLE}{2(1+\nu)a} \\ \gamma &= \frac{6\pi hLE}{(1-\nu^2)a} & \psi &= \frac{8\pi^3 haE}{L(1-\nu^2)} \\ \eta &= \frac{2\pi^3 ahE}{L(1+\nu)} & \theta &= \frac{4\pi^2 hE\nu}{1-\nu^2} \\ \kappa &= \frac{hE\pi^2}{1-\nu} & \Gamma &= \frac{2Eh^3La\pi}{3(1-\nu^2)} \end{aligned}\right\} \quad \ldots [10]$$

The coupling between m-modes arises from the presence of the rigid septa.

The natural frequencies of the shell are obtained by solving the characteristic equation $\Delta(j\omega) = 0$, where $\Delta(j\omega)$ is the determinant of the homogeneous Lagrange equations. Reinforcing a typical "thin" cylindrical shell with septa raises its fundamental frequency by one or two orders of magnitude because of the extensional character of the vibrations.

Fluid Reaction and Sound Radiation

The fluid reaction on the shell is determined by the pressure in the sound field generated by the shell vibrations. This pressure satisfies the wave equation

$$\nabla_r^2 p = \frac{1}{c^2}\frac{\partial^2 p}{\partial t^2} \quad \ldots [11]$$

The general solution of this equation, for outgoing waves, is of the form of a double series, in n and m, of products of Hankel functions in r, and trigonometric functions in ϕ and z (2),[8] (10),[9] and (11). The particular solution giving the sound pressure in terms of the radial deformation of the cylindrical surface and of acoustic impedance ratios (defined later) is obtained by imposing boundary conditions on the foregoing general solution. This procedure has been presented elsewhere in detail (11).

Imposing Condition [2], the sound pressure is finally found to be

$$p(r,\phi,z) = \rho c \sum_{n=0}^{\infty}\sum_{m=1}^{\infty}{}^{*} \dot{a}_{nm}\left\{[\theta_{nm}(\kappa_m r) + j\chi_{nm}(\kappa_m r)]\right. \\ \left.\cos(2\pi mz/L) - [\theta_{n0}(\kappa_0 r) + j\chi_{n0}(\kappa_0 r)]\right\}\cos n\phi \quad \ldots [12]$$

where

$$\kappa_m = \frac{\omega}{c}\left[1 - \left(\frac{\lambda m}{L}\right)^2\right]^{1/2} \quad \ldots [13]$$

The acoustic reactance ratio χ_{nm}, which represents an accession to the inertia of the shell caused by acceleration of the fluid mass, is given by the expressions (11)

$$\left.\begin{aligned} \chi_{nm}(\kappa_m r) &= -\frac{J_n(\kappa_m r)J_n'(\kappa_m a) + N_n(\kappa_m r)N_n'(\kappa_m a)}{\left[1-\left(\frac{\lambda m}{L}\right)^2\right]^{1/2}\left|H_n^{(2)'}(\kappa_m a)\right|^2}, \\ &\qquad \text{for } \lambda < L/m \\ \chi_{nm}(\kappa_m r) &= -\frac{K_n(|\kappa_m| r)}{\left[\left(\frac{\lambda m}{L}\right)^2 - 1\right]^{1/2} K_n'(|\kappa_m| a)}, \\ &\qquad \text{for } \lambda > L/m \end{aligned}\right\} \quad [14]$$

Extensive graphs of this function, as well as of the function θ_{nm}, defined later, have been published.[10] The acoustic resistance

[8] Chapter VII.

[9] See p. 396.

[10] See reference (5) for $m = 0$, (i.e., the z-independent case), and reference (11) for $m > 0$.

ratio θ_{nm}, which represents a damping force embodying the sound energy radiated to the fluid, is defined as follows (11)

$$\left.\begin{aligned}
\theta_{nm}(\kappa_m r) &= \frac{J_n(\kappa_m r)\,N_n'(\kappa_m a) - N_n(\kappa_m r)\,J_n'(\kappa_m a)}{\left[1-\left(\frac{\lambda m}{L}\right)^2\right]^{1/2}\,|\,H_n^{(2)\prime}(\kappa_m a)\,|^2}, \text{ for } \lambda < L/m \\
\theta_{nm}(\kappa_m a) &= \frac{2}{\pi(\omega a/c)\,[1-(\lambda m/L)^2]\,|\,H_n^{(2)\prime}(\kappa_m a)\,|^2}, \text{ for } \lambda < L/m \\
\theta_{nm}(\kappa_m r) &= 0, \text{ for } \lambda > L/m
\end{aligned}\right\} \quad \ldots [15]$$

Hence no sound is radiated by modes nm such that $m > L/\lambda$. For $L = 1000$ cm, in water, the lowest cut-off frequency (which corresponds to $m = 1$) is 144 cycles per sec (cps). A peculiarity of the graphs of $\chi_{nm}(\kappa_m r)$ is that these functions have a pronounced maximum for certain values of $\kappa_m r$. In the case of $\chi_{0m}(\kappa_m r)$, corresponding to axially symmetrical modes, this maximum value, which occurs at $\kappa_m = 0$, i.e., $\lambda = L/m$, is ∞, Fig. 4. The physical significance of these two phenomena has been discussed elsewhere (11). A numerical illustration will be given. With $p(a, \phi, z)$ considered as a distributed load, the corresponding generalized forces P_{nm}, obtained by integration as indicated in Equation [8], can be expressed as the sum of a damping and an inertia force which represent the reaction of the fluid on the shell vibrating in the mode nm

$$P_{nm} = -\frac{\pi a L \rho c}{\epsilon_n}\left\{\theta_{nm}(\kappa_m a)\,\dot{a}_{nm} + \frac{\chi_{nm}(\kappa_m a)}{\omega}\,\ddot{a}_{nm} + 2\sum_{\mu=1}^{\infty}\left[\theta_{n0}(\kappa_0 a)\,\dot{a}_{n\mu} + \frac{\chi_{n0}(\kappa_0 a)}{\omega}\,\ddot{a}_{n\mu}\right]\right\} \quad \ldots [16]$$

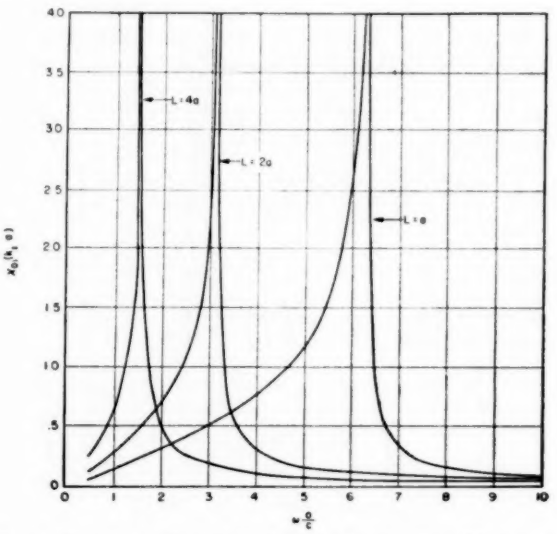

FIG. 4 REACTANCE RATIO FOR AXIALLY SYMMETRICAL MODES OF VIBRATION

(These curves were taken from families of curves published in an acoustical paper, reference 11.)

VIBRATIONS OF A SUBMERGED SHELL

The Lagrange equations must now include the generalized forces representing the fluid Reaction [16]. They differ from the usual generalized forces in that they are functions of $\dot{a}_{nm}$ and $\ddot{a}_{nm}$. It is therefore expedient to combine them with terms on the left side of the equation containing these quantities; hence

$$\left.\begin{aligned}
&\left\{-(\alpha+\bar{\alpha})\frac{\omega^2}{\epsilon_n} + j\frac{\bar{\beta}\omega}{\epsilon_n} + \frac{\gamma}{\epsilon_n} + \frac{\Gamma}{2}\left[\frac{3}{a^4}n^4 + \left(\frac{2\pi m}{L}\right)^4\frac{2}{\epsilon_n} + 2\left(\frac{2\pi n m}{La}\right)^2\right]\right\} a_{nm} \\
&+\left[-\left(\frac{2}{3}\alpha+\bar{\epsilon}\right)\frac{\omega^2}{\epsilon_n} + j\frac{\bar{\zeta}\omega}{\epsilon_n} + \frac{2\gamma}{3\epsilon_n} + \Gamma\frac{n^4}{a^4}\right]\sum_{\mu=1}^{\infty}{}' a_{n\mu} + \frac{n}{2}\left\{\gamma + \frac{\Gamma}{a^2}\left[3\frac{n^2}{a^2}\right.\right. \\
&\left.\left.+(2-\nu)\left(\frac{2\pi m}{L}\right)^2\right]\right\} b_{nm} + n\left(\frac{\gamma}{3} + \frac{\Gamma}{a^4}n^2\right)\sum_{\mu=1}^{\infty}{}' b_{n\mu} + \frac{\theta m}{\epsilon_n} f_{nm} = A_{nm}, \text{ for } n \geq 0,\ m > 0
\end{aligned}\right\} \quad \ldots [17]$$

where

$$\left.\begin{aligned}
\bar{\alpha} &= (\pi a L \rho c/\omega)\,[\chi_{nm}(\kappa_m a) + 2\chi_{n0}(\kappa_0 a)] \\
\bar{\beta} &= \pi a L \rho c\,[\theta_{nm}(\kappa_m a) + 2\theta_{n0}(\kappa_0 a)] \\
\bar{\epsilon} &= (2\pi a L \rho c/\omega)\,\chi_{n0}(\kappa_0 a) \\
\bar{\zeta} &= 2\pi a L \rho c\,\theta_{n0}(\kappa_0 a) \\
A_{nm} &= \text{generalized forces not caused by fluid reaction}
\end{aligned}\right\} \quad \ldots [18]$$

The Lagrange equations in b_{nm} and f_{nm} are not changed from Equations [9].

These equations can be solved simultaneously to obtain the amplitude of vibration of the submerged shell. It is notable that certain modes nm will be greatly reduced if ω corresponds to a maximum value of χ_{nm}. Symmetrical, i.e., $0m$-modes, can even be suppressed completely if $\omega = 2\pi cm/L$. This condition is highly frequency selective when it occurs at low frequencies, i.e., when L is large.

The natural frequencies of the submerged shell are obtained, as in the foregoing, by solving the characteristic equation, $\Delta(j\omega) = 0$, where $\Delta(j\omega)$ is the determinant of the homogeneous Lagrange equations including fluid reaction. Natural frequencies now obtained will be complex, since they contain an exponential factor indicating the damping caused by the dissipation of energy connected with θ_{nm}.

EFFECT OF ELASTIC STIFFENERS AND OF A DEAD LOAD

This analysis can be broadened to account for various complications introduced in the shell structure. One case of practical importance is that of a shell which is stiffened by elastic rings, Fig. 5, in addition to rigid septa. The subject of ring vibrations was studied by Hoppe (12), who gave an approximate solution for a ring undergoing inextensional, flexural vibrations in its own plane; by Michell (13), who proved the existence of coupling

between torsional and flexural vibrations at right angles to the plane of the ring; and by Bassett (14), who presented a general analysis of the problem, including extensional and high-frequency torsional vibrations. The whole subject is presented by Love (8).[11]

The object of this analysis is not primarily the ring vibrations, but their effect on the dynamics of the composite shell. The approach will be entirely heuristic and practical, and consists in evaluating approximately the kinetic and potential energies of the rings (in contradistinction to the methods used by the authors cited who derive their differential equations from equilibrium considerations). These energies then can be added to those of the shell, and the Lagrange equations of the composite structure constructed.

Since the shell of whose motion the rings partake undergoes extensional deformations (for reasons mentioned earlier), an approximate evaluation of the effect of the rings can be obtained by calculating only those energies which are connected with the two types of modes of vibration characterized by high energies, namely, the extensional and the high-frequency torsional modes. The ring radius is assumed to differ little from that of the shell, and the ring width is considered negligible in comparison to L. The dynamic configuration of the shell, as given by the Fourier series [1], taken at $z = l$, must necessarily be that of the boundary of the ring which is in contact with the shell surface in Fig. 5, i.e., the inner boundary of the ring; the outer boundary, however, will tend to be less deformed. In selecting an average deformation representative of the ring as a whole, this effect must be taken into account. For typical stiffeners the average radial and tangential displacements differ little from the corresponding δ and τ for the shell, but the axial displacement may vary considerably from one ring boundary to the other since such a variation entails only relatively small elastic forces. This is particularly true when the stiffener cross section is that of an I-beam, the load being applied to one flange, and transmitted to the other flange by the web deflected in its direction of least stiffness. The axial displacement of the ring elements therefore will be taken equal to

$$\zeta = \sum_{n=0}^{\infty} \sum_{m=1}^{\infty} \pi_n f_{nm} \sin (2\pi ml/L) \cos n\phi \quad \ldots\ldots [19]$$

where π_n is an empirical factor which is unity for $n = 0$, and tends toward zero with increasing n. It may be determined experimentally, or by a detailed elastic analysis of the ring, for the proper boundary conditions. If found necessary, similar factors can, of course, be applied to the other two displacement components.

Having thus determined their dynamic configuration, the energies of the rings can be computed. The kinetic energy connected with extensional displacements is

$$\left.\begin{aligned} T_e &= \frac{Aa\rho_s}{2} \int_0^{2\pi} \left[\left(\frac{d\delta}{dt}\right)^2 + \left(\frac{d\tau}{dt}\right)^2 + \left(\frac{d\zeta}{dt}\right)^2\right] d\phi, \text{ at } z = l \\ &= \pi Aa\rho_s \sum_{n=0}^{\infty} \frac{1}{\epsilon_n} \left\{\left[\sum_{m=1}^{\infty} \dot{a}_{nm} \left(\cos \frac{2\pi ml}{L} - 1\right)\right]^2 + \left[\sum_{m=1}^{\infty} \dot{b}_{nm} \left(\cos \frac{2\pi ml}{L} - 1\right)\right]^2 \right. \\ &\quad \left. + \pi_n^2 \left[\sum_{m=1}^{\infty} \dot{f}_{nm} \sin \frac{2\pi ml}{L}\right]^2\right\} \end{aligned}\right\} \quad \ldots\ldots [20]$$

Using the expression for the extensional potential energy of a deformed shell, but allowing for lateral contraction, the potential

[11] See p. 451.

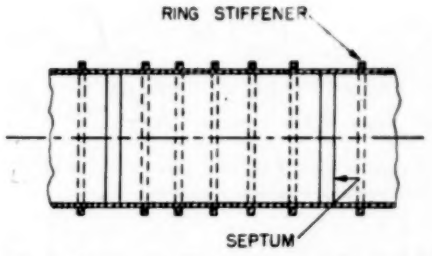

FIG. 5 SHELL REINFORCED WITH SEPTA AND STIFFENING RINGS

energy connected with the extensional vibrations is

$$\left.\begin{aligned} V_e &= \frac{AaE}{2} \int_0^{2\pi} \left[(\epsilon_\phi + \epsilon_z)^2 - 2(1-\nu)\right. \\ &\qquad \left.(\epsilon_\phi \epsilon_z - \frac{1}{4}\gamma_{z\phi}^2)\right] d\phi, \text{ at } z = l \\ &= AaE\left[\frac{I_1}{2} - (1-\nu) I_2 + (1-\nu)\frac{I_3}{4}\right] \end{aligned}\right\} \quad \ldots [21]$$

where

$$I_1 = 2\pi \sum_{n=0}^{\infty} \frac{1}{\epsilon_n} \left\{\sum_{m=1}^{\infty} \left[\frac{1}{a}(a_{nm} + nb_{nm})\left(\cos \frac{2\pi ml}{L} - 1\right) + \frac{2\pi}{L} m\pi_n f_{nm} \cos \frac{2\pi ml}{L}\right]\right\}^2$$

$$I_2 = \frac{4\pi^2}{La} \sum_{n=0}^{\infty} \frac{1}{\epsilon_n} \left[\sum_{m=1}^{\infty} (a_{nm} + nb_{nm})\left(\cos \frac{2\pi ml}{L} - 1\right)\right] \left[\sum_{m=1}^{\infty} m\pi_n f_{nm} \cos \frac{2\pi ml}{L}\right]$$

$$I_3 = \pi \sum_{n=1}^{\infty} \left[\sum_{m=1}^{\infty} \left(\frac{2\pi}{L} m b_{nm} + \frac{\pi_n}{a} n f_{nm}\right) \sin \frac{2\pi ml}{L}\right]^2$$

The kinetic energy connected with high-frequency torsional vibrations about the center line of the ring cross section is

$$\left.\begin{aligned} T_t &= \frac{\rho_s a I_p}{2} \int_0^{2\pi} \dot{\beta}^2 \, d\phi, \text{ at } z = l \\ &= \rho_s a I_p \frac{4\pi^2}{L^2} \sum_{n=0}^{\infty} \frac{1}{\epsilon_n} \left(\sum_{m=1}^{\infty} m\dot{a}_{nm} \sin 2\pi ml/L\right)^2 \end{aligned}\right\} \quad \ldots\ldots [22]$$

The potential energy connected with torsional vibrations consists of two quantities, one representing shearing effects, and the other the energy required to twist the ring out of its plane

$$V_t = \frac{EI_p}{4(1+\nu)a}\int_0^{2\pi}\left(\frac{\partial\beta}{\partial\phi}\right)^2 d\phi + \frac{EI_r}{2a}\int_0^{2\pi}\beta^2\,d\phi, \text{ at } z = l$$
$$= \frac{4\pi^3}{aL^2}\sum_{n=0}^{\infty}\frac{E}{\epsilon_n}\left[\frac{I_p n^2}{2(1+\nu)} + I_r\right]\left(\sum_{m=1}^{\infty} ma_{nm}\sin\frac{2\pi ml}{L}\right)^2 \quad \ldots\ldots [23]$$

where the angle of twist β has been taken equal to $\partial\delta/\partial z$.

The corresponding Lagrange equations

$$\sum_{l=l_1}^{lN}\left[\frac{d}{dt}\frac{\partial}{\partial\dot{q}_{nm}}(T_e + T_t) + \frac{\partial}{\partial q_{nm}}(V_e + V_t)\right] = 0 \quad \ldots [24]$$

(where $q_{nm} = a_{nm}$, b_{nm}, and f_{nm}, and N is the number of rings between two septa) are then added to Equations [9] or [17] to obtain the equations of motion of the composite reinforced shell. Equations [24] which, for brevity sake, are not presented explicitly, display a slight asymmetry which is due to the fact that strains are assumed to exist in the z-direction, even though the integrations are not performed in that direction. The usual symmetry can be restored if V_e is evaluated either by integration with respect to both ϕ and z (instead of setting $z = l$), or by setting $\pi_n = 0$, the latter procedure implying that the load applied by the shell to the ring boundary cannot strain the ring as a whole in the axial direction to any appreciable amount.

The Lagrange equations for longitudinal stiffeners, i.e., beams attached to the shell surface and oriented in the direction of the cylindrical axis, also were derived, but will not be presented here.

Another case of practical interest is that of a shell carrying a dead load having a mass $m(\phi, z)$ per unit area. No potential energy is connected with such a load; the corresponding kinetic energy is

$$T = \frac{a}{2}\int_0^L\int_0^{2\pi} m(\phi,z)\left[\left(\frac{d\delta}{dt}\right)^2 + \left(\frac{d\tau}{dt}\right)^2 + \left(\frac{d\zeta}{dt}\right)^2\right] dz\,d\phi \quad \ldots\ldots [25]$$

Practical Applications

The practical significance of these results depends on the importance of end effects in an actual, "finite-length" shell. The present analysis should hold for phenomena determined by effects occurring in regions closer to the shell surface than to its ends, i.e., for forced vibrations and natural frequencies of the submerged shell, fluid reaction, and near zone sound field. The far zone field may be expected to be altered completely by end effects.

The general features of the vibrations of submerged shells have been discussed elsewhere (4). Two features are peculiar to reinforced cylindrical shells. From the vibrational point of view, the most remarkable one is that for every mode of vibration, the accession to inertia owing to fluid reaction becomes very large at a certain frequency; for axially symmetrical modes, this maximum accession to inertia occurs when the wave length in the fluid is equal to the period of this mode along the z-axis, and is, in theory, infinite. As a result, the amplitude-frequency curve for each mode displays a pronounced antiresonance which is highly frequency sensitive. This is illustrated in Fig. 6 where this antiresonant region is displayed for the 01-mode. The curves were calculated for a steel shell, reinforced by septa only; the physical parameters in CGS units are as follows: $E = 19 \times 10^{11}$, $\rho_s = 7.7$, $\nu = 0.27$, $c = 14.41 \times 10^4$, $\rho = 1$, $a = 250$, $L = 576.4$, and $h/a = 1/30$. The shell is excited by a uniform pressure of the form $P_0 e^{i\omega t}$. In order to accelerate convergence[12] of the series for δ, by emphasizing the effect of change of curvature, a relatively thick shell with closely spaced bulkheads was selected. An extensive numerical investigation of a practical case is under way.

The practical application of this phenomenon is quite obvious.

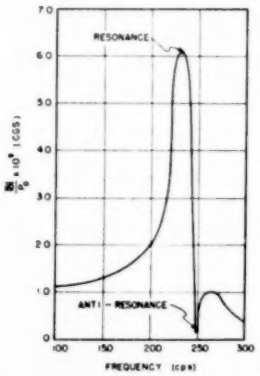

Fig. 6 Amplitude of Radial Dynamic Deflection of Surface of Submerged Shell Midway Between Septa for an Axially Symmetrical Exciting Force in a Frequency Range Displaying the Antiresonant Zone of the Fundamental Mode

It might be attempted to run rotating machinery mounted in a submerged shell at a speed such that the frequency of the resulting disturbance coincides with the antiresonant frequency of a particularly objectionable mode of shell vibration; the same result of course could be achieved by selecting the proper distance between septa. The surrounding fluid might then be considered as a dynamic vibration absorber tuned to that mode.

Another result of practical importance is that machinery may be mounted in a shell so as to excite mostly modes whose cutoff frequency is above the frequency of the exciting force, i.e., to achieve the condition $\omega < 2\pi c/Lm$. Then, even though a mode is excited, it would radiate almost no sound, if the shell were infinitely long.[13]

The analytical method here used can of course be extended, without any theoretical difficulty, to shells carrying a complicated load and embodying complex stiffening structures. However, it seems that the next step in this investigation should be the study of shells of finite length. The main difficulty in such a case does not lie in the analysis of the vibrations of the shell, but in the solution of the wave equation in the fluid medium. Such an investigation is under way.

Acknowledgment

The author wishes to express his grateful appreciation to Prof. F. V. Hunt[14] who suggested this study, and to Mrs. E. Bockelman[14] who did the numerical work and checked some of the algebra.

BIBLIOGRAPHY

1 "The Effect of Radiation on the Vibration of a Circular Diaphragm," by M. Lax, *Journal of the Acoustical Society of America*, vol. 16, 1944, p. 5.

[12] As explained previously, the convergence is slow at first, and then rapid. Since only a manual calculating machine was available, the series was truncated at $m = 3$. The graph in Fig. 6, even though only approximate, does illustrate adequately the point being made.

[13] These applications were suggested in an acoustical paper (11).

[14] Acoustics Research Laboratory, Harvard University.

2 "Vibration and Sound," by P. M. Morse, McGraw-Hill Book Company, Inc., New York, N. Y., 1948.

3 "Recent Developments in the Theory of Ship Vibration," by R. T. McGoldrick, A. N. Gleyzal, R. L. Hess, and G. K. Hess, Jr., Taylor Model Basin Report 739, 1951.

4 "Vibrations of Elastic Shells in a Fluid Medium and the Associated Radiation of Sound," by M. C. Junger, JOURNAL OF APPLIED MECHANICS, Trans. ASME, vol. 74, 1952, pp. 439–445.

5 "Radiation Loading of Cylindrical and Spherical Surfaces," by M. C. Junger, *Journal of the Acoustical Society of America*, vol. 24, 1952, p. 288.

6 "Sound Scattering by Thin Elastic Shells," by M. C. Junger, *Journal of the Acoustical Society of America*, vol. 24, 1952, p. 366.

7 "Response of an Elastic Cylindrical Shell to a Transverse, Step Shock Wave," by R. D. Mindlin and H. H. Bleich, JOURNAL OF APPLIED MECHANICS, Trans. ASME, vol. 75, 1953, pp. 189–195.

8 "A Treatise on the Mathematical Theory of Elasticity," by A. E. M. Love, Dover Publications, New York, N. Y., 1944.

9 "On the Properties of Inextensible Surfaces," by J. M. Jellett, *Royal Irish Academy Transactions*, vol. 22, 1855, p. 377.

10 "Methods of Theoretical Physics," by P. M. Morse and H. Feshbach, Technology Press, Massachusetts Institute of Technology, Cambridge, Mass., 1946.

11 "The Physical Interpretation of the Expression for an Outgoing Wave in Cylindrical Coordinates," by M. C. Junger, *Journal of the Acoustical Society of America*, vol. 25, 1952, pp. 40–47.

12 "Vibrationen eines Ringes in seiner Ebene," by R. Hoppe, *Journal für Mathematik, Crelle*, vol. 73, 1871, p. 158.

13 "The Small Deformation of Curves and Surfaces With Application to the Vibrations of a Helix and of a Circular Ring," by J. H. Michell, *Messenger of Mathematics*, vol. 19, 1889, p. 68.

14 "On the Theory of Elastic Wires," by A. B. Bassett, Proceedings of the London Mathematical Society, London, England, vol. 23, 1891, p. 105.

Stress Concentration Due to Elliptical Holes in Orthotropic Plates

By H. D. CONWAY,[1] ITHACA, N. Y.

Two plane stress problems of elliptical holes in infinite orthotropic sheets are treated: (*a*) Hole loaded by a pair of concentrated forces acting at the ends of the major or minor axis, and (*b*) hole in plate which is subjected to uniform tension. The solutions are obtained in a simple manner by transformation from corresponding problems in which the holes are circular. Closed-form expressions are obtained for the stress-concentration factors.

Introduction

PROBLEMS in orthotropic plane stress involve the solution of the equation

$$\left(\frac{\partial^2}{\partial x^2} + \alpha_1^2 \frac{\partial^2}{\partial y^2}\right)\left(\frac{\partial^2}{\partial x^2} + \alpha_2^2 \frac{\partial^2}{\partial y^2}\right) \chi = 0 \quad \ldots\ldots [1]$$

subject to the boundary conditions, the stresses being given in terms of the stress function χ by the equations

$$\sigma_x = \partial^2\chi/\partial y^2, \qquad \sigma_y = \partial^2\chi/\partial x^2, \qquad \tau_{xy} = -\partial^2\chi/\partial x \partial y \quad [2]$$

The constants α_1^2 and α_2^2 are functions of the elastic constants and are given by

$$\alpha_1^2\alpha_2^2 = S_{11}/S_{22}, \quad \alpha_1^2 + \alpha_2^2 = (S_{66} + 2S)_{12}/S_{22} \quad \ldots [3]$$

where the moduli are defined by the stress-strain equations

$$\left.\begin{aligned} \epsilon_x &= S_{11}\,\sigma_x + S_{12}\,\sigma_y \\ \epsilon_y &= S_{12}\,\sigma_x + S_{22}\,\sigma_y \\ \gamma_{xy} &= S_{66}\,\tau_{xy} \end{aligned}\right\} \quad \ldots\ldots [4]$$

it being assumed that the x, y-directions correspond to the principal axes of orthotropy. Consider first the problem of an orthotropic plate containing a circular hole,[2] the plate being subjected either to tractions at infinity or to tractions around the edge of the hole.

Now consider a linear transformation of the y-co-ordinates by means of the equation $y^* = yb/a$ $(a > b)$. Equation [1] becomes

$$\left(\frac{\partial^2}{\partial x^2} + \frac{\alpha_1^2 b^2}{a^2}\frac{\partial^2}{\partial y^{*2}}\right)\left(\frac{\partial^2}{\partial x^2} + \frac{\alpha_2^2 b^2}{a^2}\frac{\partial^2}{\partial y^{*2}}\right) \chi^* = 0 \quad \ldots [5]$$

and Equations [2] are

$$\sigma_x = \frac{b^2}{a^2}\frac{\partial^2\chi^*}{\partial y^{*2}}, \qquad \sigma_y = \frac{\partial^2\chi^*}{\partial x^2}, \qquad \tau_{xy} = -\frac{b}{a}\frac{\partial^2\chi^*}{\partial x \partial y^*} \quad \ldots [6a]$$

A property of the circle is that, by means of this transformation, it becomes an ellipse the ratio of the lengths of the semi-major and semi-minor axes of which is a/b. If the problem of a circular hole in an infinite orthotropic sheet can be solved, a solution to a corresponding problem of an elliptical hole in a sheet having different elastic constants ($\alpha_1\, b/a$ replacing α_1 and $\alpha_2\, b/a$ replacing α_2) can be obtained. If the values of α_1 and α_2 in the case of the circle are replaced by $\alpha_1\, a/b$ and $\alpha_2\, a/b$, respectively, the values of the constants for the ellipse will be α_1 and α_2 as defined by Equations [3].

The stresses in the corresponding problem of the ellipse are given by

$$\sigma_x^* = \frac{\partial^2\chi^*}{\partial y^{*2}}, \qquad \sigma_y^* = \frac{\partial^2\chi^*}{\partial x^2}, \qquad \tau_{xy}^* = -\frac{\partial^2\chi^*}{\partial x \partial y^*} \quad \ldots [6b]$$

Hence, by comparing Equations [6a] and [6b]

$$\sigma_x^* = \frac{a^2}{b^2}\,\sigma_x, \qquad \sigma_y^* = \sigma_y, \qquad \tau_{xy}^* = \frac{a}{b}\,\tau_{xy} \quad \ldots [6c]$$

The boundary conditions are generally modified by the transformation, and the connection is required between the tractions on an elementary arc length of the circle and the corresponding tractions on the image arc of the ellipse.

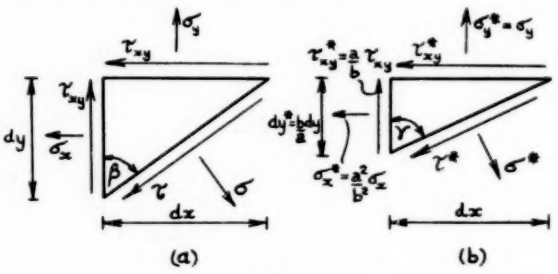

FIG. 1

Fig. 1(*a*) shows an element bounded on the hypothenuse by an arc of the circle, and Fig. 1(*b*) shows the transformed element bounded on the hypothenuse by an arc of the ellipse. The normal and shearing stresses on the arc of the circle are denoted σ and τ, respectively, and these transform so that the normal and shearing stresses on the arc of the ellipse are σ^* and τ^*, respectively.

From the equilibrium of Fig. 1(*a*), it follows that

$$\sigma = \sigma_x \cos^2\beta + \sigma_y \sin^2\beta + 2\tau_{xy} \sin\beta\cos\beta. \quad \ldots [7a]$$

$$\tau = \tau_{xy}(\cos^2\beta - \sin^2\beta) + (\sigma_y - \sigma_x)\sin\beta\cos\beta \quad \ldots [7b]$$

and, from Fig. 1(*b*)

$$\sigma^* = \frac{a^2}{b^2}\,\sigma_x \cos^2\gamma + \sigma_y \sin^2\gamma + \frac{2a}{b}\,\tau_{xy} \sin\gamma\cos\gamma \quad \ldots [8a]$$

$$\tau^* = \frac{a}{b}\,\tau_{xy}(\cos^2\gamma - \sin^2\gamma) + \left(\sigma_y - \frac{a^2}{b^2}\,\sigma_x\right)\sin\gamma\cos\gamma \quad \ldots [8b]$$

Noting that $\tan\gamma = (a/b)\tan\beta$, we obtain after some reduction

---

[1] Professor of Mechanics, Cornell University. John Simon Guggenheim Fellow, Imperial College of Science, London University, London, England. Assoc. Mem. ASME.

[2] Such a plate is the simplest form of multiply-connected body, and an additional investigation of the displacements is necessary for the solution of certain problems.

Contributed by the Applied Mechanics Division and presented at the Annual Meeting, New York, N. Y., November 29–December 4, 1953, of THE AMERICAN SOCIETY OF MECHANICAL ENGINEERS.

Discussion of this paper should be addressed to the Secretary, ASME, 29 West 39th Street, New York, N. Y., and will be accepted until April 12, 1954, for publication at a later date. Discussion received after the closing date will be returned.

NOTE: Statements and opinions advanced in papers are to be understood as individual expressions of their authors and not those of the Society. Manuscript received by ASME Applied Mechanics Division, January 22, 1953. Paper No. 53—A-30.

$$\sigma^* = \frac{\sigma a^2}{a^2 \sin^2 \beta + b^2 \cos^2 \beta} = \frac{\sigma a^4}{b^2 x^2 + a^2 y^2} \quad \ldots\ldots [9a]$$

$$\tau^* = \frac{a}{b}\left[\tau + \sigma \frac{(b^2 - a^2) \sin \beta \cos \beta}{a^2 \sin^2 \beta + b^2 \cos^2 \beta}\right]$$

$$= \frac{a}{b}\left[\tau + \sigma \frac{xy(b^2 - a^2)}{b^2 x^2 + a^2 y^2}\right] \quad \ldots\ldots [9b]$$

where the origin is taken at the center of the hole. In particular it will be observed that traction-free arcs of the circle transform into traction-free arcs of the ellipse.

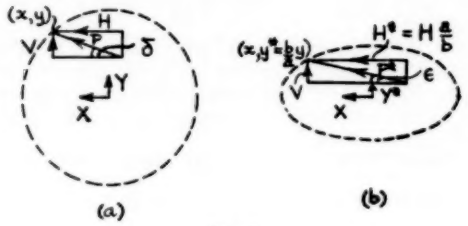

FIG. 2

The case of concentrated forces acting on the boundary of the hole is now considered. Fig. 2(*a*) shows a force P acting at a point (x, y) on the boundary of a circular hole, the horizontal and vertical components being H and V, respectively. Transforming the circle into the ellipse shown in Fig. 2(*b*), the vertical stresses and horizontal dimensions of the plate remain unchanged and it follows that the vertical component V at (x, y) on the circle transforms to V at $(x, y^* = yb/a)$ on the ellipse. However, from Equations [6c], the horizontal stresses are increased by the factor a^2/b^2 on transforming, while the vertical dimensions of the plate are decreased by the factor b/a. It follows that the horizontal component H of the force at (x, y) on the circle transforms to

$$H^* = \frac{Ha^2}{b^2} \frac{b}{a} = \frac{Ha}{b}$$

at $(x, y^* = yb/a)$ on the ellipse. The force $P = \sqrt{H^2 + V^2}$ inclined at $\delta = \arctan V/H$ to the horizontal and at (x, y) on the circle therefore transforms to

$$P^* = \sqrt{\frac{a^2 H^2}{b^2} + V^2}$$

inclined at $\epsilon = \arctan (Vb)/(Ha)$ to the horizontal and at $(x, y^* = yb/a)$ on the ellipse.

The solution to an infinite orthotropic plate having a circular hole, the edge of which is subjected to any system of tractions, is easily obtained by the use of a method due to Green (1).[1] By means of this method and the foregoing linear transformation, several important problems of elliptical holes in orthotropic sheets can be solved. It is further important to note that Green's method gives the circumferential stresses around the edge of the circular hole in closed form and hence the stresses around the edge of the corresponding elliptical hole are also obtained in closed form.

The foregoing method is applied here to two problems: (*a*) Elliptical hole loaded by a pair of concentrated forces acting at the ends of the major or minor axis; (*b*) elliptical hole in a plate which is subjected to uniform tension. The isotropic version of the first problem has been discussed by Symonds (2) and the results were obtained later in closed form by Green (3). However, they considered only the case of loads acting at the ends of the minor axis. The second problem has been treated by Green (4) as a special case of his theory of perforated plates.

It is interesting to note that Okubo (5) has attempted to solve the problem of a circular orthotropic disk compressed by diametrically opposite forces using a similar transformation from a compressed isotropic elliptical disk. His solution is of limited value since the degree of orthotropy has to be assumed to be very slight, whereas the following solutions are exact and applicable to any degree of orthotropy.

Elliptical Hole Loaded by Concentrated Forces

Consider an infinite orthotropic plate containing a circular hole of radius a, the edge of the hole being subjected to equal and opposite compressive forces P per unit plate thickness. Assume that the direction of the forces corresponds to the direction in which the modulus S_{11} is measured.

Expanding the loading in a Fourier series, we have

$$-\sigma_{r(r=a)} = \frac{P}{\pi a} + \frac{2P}{\pi a} \sum_{n=2,4}^{\infty} \cos n\theta \quad \ldots\ldots [10]$$

where θ is measured from one of the loads. Using Green's method for the circular hole, the resultant circumferential stress, except at the loads, around the hole is

$$\sigma_{\theta(r=a)} = \frac{2P}{\pi a} \frac{(1 - \gamma_1\gamma_2)(1 + \gamma_1\gamma_2 + \gamma_1 + \gamma_2)}{(1 + \gamma_1^2 - 2\gamma_1 \cos 2\theta)(1 + \gamma_2^2 - 2\gamma_2 \cos 2\theta)}$$

$$= \frac{P}{\pi a} \frac{(\alpha_1 + \alpha_2)(\alpha_1\alpha_2)}{(\alpha_1^2 \sin^2 \theta + \cos^2 \theta)(\alpha_2^2 \sin^2 \theta + \cos^2 \theta)} \quad \ldots\ldots [11]$$

where $\gamma_1 = (\alpha_1 - 1)/(\alpha_1 + 1)$ and $\gamma_2 = (\alpha_2 - 1)/(\alpha_2 + 1)$.

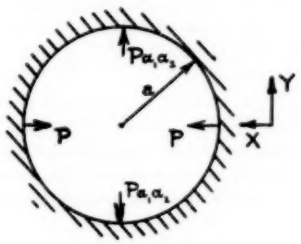

FIG. 3

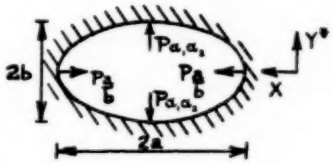

FIG. 4

If the direction of the forces corresponds to the S_{22} direction and θ is measured from S_{11} direction, the values of S_{11} and S_{22} are interchanged, thus causing a changing in the signs of γ_1 and γ_2 or replacing α_1 and α_2 by their reciprocals. In addition, θ is replaced by its complement. If this is done, the circumferential stress is $1/\alpha_1\alpha_2$ times Equation [11]. Considering now the problem shown in Fig. 3, by the superposition of the two previous cases, it is interesting to note that the periphery of the hole is completely free from stress except of course at the loads.

[1] Numbers in parentheses refer to the Bibliography at the end of the paper.

The foregoing is true whether the material is orthotropic or isotropic. In the latter case, α_1 and α_2 are both unity and Equation [11] degenerates to

$$\sigma_\theta = \frac{2P}{\pi a} \quad [12]$$

Since this stress is independent of θ, any two pairs of equal and diametrically opposite forces P—one set compressive and the other set tensile—induce no stress on the boundary of the hole, whether or not pairs of forces be at right angles to one another. As before, this excepts the load points. Equation [12] was first obtained by Filon (6).

We next consider the corresponding problem of an elliptical hole subjected at the ends of its major axis to concentrated forces P per unit plate thickness. Assuming that the direction of the forces corresponds to the direction in which S_{11} is measured, we obtain from Equation [11]

$$\sigma_{\theta(r=a,\ \theta=\pi/2)} = \frac{P}{\pi a}\,\frac{\alpha_1 + \alpha_2}{\alpha_1\alpha_2}$$

Now this stress is in the x-direction and, from Equations [6c], is increased by the factor a^2/b^2 by the transformation $y^* = yb/a$, while the load P transforms to Pa/b. Hence, for concentrated forces P acting at the ends of the major axis, the stresses at the ends of the minor axis are

$$\sigma = \frac{P}{\pi a}\left(\frac{\alpha_1 + \alpha_2}{\alpha_1\alpha_2}\right)\left(\frac{a^2}{b^2}\right)\left(\frac{b}{a}\right) = \frac{P}{\pi b}\left(\frac{\alpha_1 + \alpha_2}{\alpha_1\alpha_2}\right)$$

However, this is for a material having elastic constants $\alpha_1\ b/a$ and $\alpha_2\ b/a$ and, for elastic constants α_1 and α_2, we finally obtain

$$\sigma = \frac{P}{\pi b}\,\frac{(\alpha_1\ a/b) + (\alpha_2\ a/b)}{(\alpha_1\ a/b)\,(\alpha_2\ a/b)} = \frac{P}{\pi a}\,\frac{\alpha_1 + \alpha_2}{\alpha_1\ \alpha_2} \quad [13]$$

Considering now the case when the forces P act at the ends of the minor axis of the ellipse and that this corresponds to the direction in which S_{22} is measured, the stress obtained in a similar manner at the ends of the major axis is

$$\sigma = \frac{P}{\pi b}\,(\alpha_1 + \alpha_2) \quad [14]$$

The isotropic version of this result has been obtained by Green (3) by another method. To reverse the directions of the moduli in Equations [13] and [14], all that is necessary is to replace α_1 and α_2 by their reciprocals.

To extend the result of Fig. 3 to the case of an elliptical hole, we transform as before. Thus, referring to Fig. 4, we note that the boundary of the elliptical hole is free from stress, except at the loads, whether the material is orthotropic or isotropic.

Elliptical Hole in Plate Subjected to Tension at Infinity

When discussing this problem, use is made of a solution due to Green (1) for a circular hole. If the tension T per unit area is in the direction in which the modulus S_{11} is measured, the circumferential stress around the circular hole is

$$\sigma_{\theta(r=a)} = \frac{T(1+\gamma_1)\,(1+\gamma_2)\,(1+\gamma_1+\gamma_2-\gamma_1\gamma_2-2\cos 2\theta)}{(1+\gamma_1^2-2\gamma_1\cos 2\theta)\,(1+\gamma_2^2-2\gamma_2\cos 2\theta)}$$

$$= \frac{T\alpha_1\alpha_2\,[(\alpha_1+\alpha_2+\alpha_1\alpha_2)\sin^2\theta-\cos^2\theta]}{(\alpha_1^2\sin^2\theta+\cos^2\theta)\,(\alpha_2^2\sin^2\theta+\cos^2\theta)} \quad [15]$$

where θ is measured from the S_{11}-direction. As before, tension in the direction of S_{22} can be obtained by replacing α_1 and α_2 by their reciprocals.

To treat the case of an elliptical hole, the foregoing transformation is made and, since the circular hole is free from tractions, so also is the elliptical hole. The general expressions for the stresses around the hole are relatively complex and only the more important results are given.

(a) Tension T in S_{11}-direction, major axis in S_{11}-direction

$$\text{Stress at ends of major axis} = -\alpha_1\alpha_2\,T \quad [16]$$

$$\text{Stress at ends of minor axis} = \left(1 + \frac{\alpha_1+\alpha_2}{\alpha_1\alpha_2}\,\frac{b}{a}\right)T \quad [17]$$

(b) Tension T in S_{11}-direction, major axis in S_{22}-direction

$$\text{Stress at ends of major axis} = \left(1 + \frac{\alpha_1+\alpha_2}{\alpha_1\alpha_2}\,\frac{a}{b}\right)T \quad [18]$$

$$\text{Stress at ends of minor axis} = -\alpha_1\alpha_2\,T \quad [19]$$

To reverse the S_{11} and S_{22}-directions in the foregoing, α_1 and α_2 are replaced by their reciprocals. To obtain the well-known isotropic results, write $\alpha_1 = \alpha_2 = 1$. This can be obtained from a solution by Green (4) by another method.

BIBLIOGRAPHY

1 "Stress Systems in Aelotropic Plates, IV," by A. E. Green, Proceedings of the Royal Society of London, London, England, series A, vol. 180, 1942, p. 173.

2 "Concentrated-Force Problems in Plane Strain, Plane Stress and Transverse Bending of Plates," by P. S. Symonds, Journal of Applied Mechanics, Trans. ASME, vol. 68, 1946, p. A-183.

3 "A Concentrated Force Problem of Plane Strain or Plane Stress," by A. E. Green, Journal of Applied Mechanics, Trans. ASME, vol. 69, 1947, p. A-246.

4 "Stress Systems in Isotropic and Aelotropic Plates," by A. E. Green, Proceedings of the Royal Society of London, London, England, series A, vol. 184, 1945, p. 231.

5 "The Stress Distribution in an Aelotropic Circular Disk," by H. Ōkubo, *Philosophical Magazine*, vol. 27, 1939, p. 508.

6 "The Stresses in a Circular Ring," by L. N. G. Filon, The Institution of Civil Engineers, Selected Papers, 1924, No. 12.

Bending of Circular and Ring-Shaped Plates on an Elastic Foundation

By HERBERT REISMANN,[1] FORT WORTH, TEXAS

This paper develops a method for the evaluation of deflections, moments, shears, and stresses of a circular or ring-shaped plate on an elastic foundation under transverse loads. A series solution is derived for plates subjected to edge and/or concentrated loads and is given in terms of tabulated functions. It is exact within the assumptions underlying the classical theory of plates and includes, as a particular case, the known solution of the corresponding radially symmetric problem. Two examples displaying radial asymmetry are worked. A solution is given for (*a*) a circular plate resting on an elastic foundation, clamped at the boundary and subjected to an arbitrarily placed concentrated load, and (*b*) a plate of infinite extent, resting on an elastic foundation and clamped to the boundary of a rigid circular disk to which a pure moment is applied.

Nomenclature

The following nomenclature is used in the paper:

ω = deflection of median surface
r = radial co-ordinate
θ = angular co-ordinate
k = modulus of elastic foundation
D = flexural rigidity of plate = $\dfrac{Eh^3}{12(1-\nu^2)}$
E = Young's modulus
h = plate thickness
ν = Poisson's ratio
q = load intensity
$M_r, M_\theta, M_{r\theta}$ = radial, tangential, and twisting moments
Q_r, Q_θ = radial and tangential shearing forces
$\sigma_r, \sigma_\theta, \tau_{r\theta}$ = radial, tangential, and shearing stresses
F = magnitude of concentrated load
λ = stiffness parameter = $\sqrt[4]{k/D}$
W = load parameter = $\dfrac{F}{2\pi\lambda^2 D}$
ξ = dimensionless radius of inner ring boundary = λa
δ = dimensionless radius of load circle = λb
ϕ = angular co-ordinate of load point
η = dimensionless radius of outer ring boundary = λc
ρ = dimensionless radial co-ordinate = λr
α = angular displacement of rigid disk
L = magnitude of moment applied to rigid disk
$i = \sqrt{-1}$
Re = "real part of"
Im = "imaginary part of"

$$\nabla^2 = \frac{\partial^2}{\partial r^2} + \frac{1}{r}\frac{\partial}{\partial r} + \frac{1}{r^2}\frac{\partial^2}{\partial \theta^2}$$

Introduction

Circular plates on an elastic foundation subjected to transverse loading have been discussed in references (1, 2, 3, 4, 5).[2] In their treatment of circular plates, these authors have restricted their discussion to "full" circular plates as distinguished from "ring-shaped" plates bounded by two concentric circles. The only exception to this limitation is given by F. Schleicher (3) who discusses a number of cases pertaining to ring-shaped plates. In all instances, however, the treatment has been limited to the special case of radial symmetry, and, therefore, it is not applicable to cases where the loads are distributed arbitrarily over the surfaces and edges of a circular or ring-shaped plate. It is the object of this paper to find a general solution under very general boundary conditions for the deflection, moments, shears, and stresses of a circular or ring-shaped plate resting on an elastic foundation and subjected to arbitrarily specified transverse loads acting on the edges and surfaces of the plate.

The theory of circular plates on an elastic foundation has direct application to the analysis and design of footings and foundations of buildings where platelike elements are surrounded by soil such that their behavior under applied loads is approximated by the basic assumptions of the underlying theory. In addition, it has been shown that the following problems are closely related to special cases of the theory developed in this paper:

1 Bending of beams on an elastic foundation where (*a*) the flexural rigidity of the beam is variable along its length (4), and (*b*) the modulus of the foundation varies along the length of the beam (4).

2 Stresses and deflections of a cylindrical tank with variable wall thickness (4, 5, 6, 7).

3 Stresses and deflections of a conical shell (4).

4 Temperature distributions and thermal stresses in plane stress and strain under periodically varying temperature effects (8).

Formulation of Problem

According to the classical small-deflection theory, the transverse deflection of the median plane of the plate is characterized by

$$D\nabla^4\omega = q_1(r, \theta) \qquad [1]$$

where q_1 and D are the load intensity and flexural rigidity, respectively. The bending moments, shears, and stresses are related to the deflections ω by means of the following equations which, for our purposes, we refer to polar co-ordinates (5)

[1] Project Structures Engineer, Consolidated Vultee Aircraft Corporation; and Graduate Lecturer, Southern Methodist University.

Contributed by the Applied Mechanics Division and presented at the Annual Meeting, New York, N. Y., November 29–December 4, 1953, of The American Society of Mechanical Engineers.

Discussion of this paper should be addressed to the Secretary, ASME, 29 West 39th Street, New York, N. Y., and will be accepted until April 12, 1954, for publication at a later date. Discussion received after the closing date will be returned.

Note: Statements and opinions advanced in papers are to be understood as individual expressions of their authors and not those of the Society. Manuscript received by ASME Applied Mechanics Division, December 13, 1952. Paper No. 53—A-7.

[2] Numbers in parentheses refer to the Bibliography at the end of the paper.

$$\left.\begin{aligned} M_r &= -D\left[\frac{\partial^2\omega}{\partial r^2} + \nu\left(\frac{1}{r^2}\frac{\partial^2\omega}{\partial\theta^2} + \frac{1}{r}\frac{\partial\omega}{\partial r}\right)\right] \\ M_\theta &= -D\left[\nu\frac{\partial^2\omega}{\partial r^2} + \frac{1}{r^2}\frac{\partial^2\omega}{\partial\theta^2} + \frac{1}{r}\frac{\partial\omega}{\partial r}\right] \\ M_{r\theta} &= M_{\theta r} = -(1-\nu)\,D\,\frac{\partial}{\partial r}\left(\frac{1}{r}\frac{\partial\omega}{\partial\theta}\right) \end{aligned}\right\} \quad [2]$$

$$\left.\begin{aligned} Q_r &= -D\frac{\partial}{\partial r}(\nabla^2\omega) \\ Q_\theta &= -D\frac{1}{r}\frac{\partial}{\partial\theta}(\nabla^2\omega) \end{aligned}\right\} \quad [3]$$

$$\left.\begin{aligned} \sigma_r &= \frac{12zM_r}{h^3} \\ \sigma_\theta &= \frac{12zM_\theta}{h^3} \\ \tau_{r\theta} &= \frac{12zM_{r\theta}}{h^3} \end{aligned}\right\} \quad [4]$$

With particular reference to the problem at hand, we shall assume that the load intensity q_1 consists of two distinct parts

$$q_1 = q + q_2 \quad [5]$$

where $q = q(r,\theta)$ is a given external load acting on the plate and q_2 is the reaction of the subgrade to the deflection of the plate. We shall assume that

$$q_2 = -k\omega \quad [6]$$

i.e., the deflection of the plate will produce a continuously distributed transverse reaction the magnitude of which is linearly proportional to the deflection and the sense of which is such as to oppose this deflection, whether it be in the up or down direction. The constant of proportionality k is called the modulus of the foundation.

Substituting Equations [5] and [6] into Equation [1], we obtain the differential equation characterizing the deflection of a plate on an elastic foundation

$$D\nabla^4\omega + k\omega = q(r,\theta) \quad [7]$$

In the subsequent development it will be convenient to introduce the change of variable $\lambda r = \rho$, where

$$\lambda^4 = \frac{k}{D} \quad [8]$$

Then Equation [7] may be written

$$\nabla_\rho^4\omega + \omega = \frac{q}{\lambda^4 D} \quad [9]$$

where

$$\nabla_\rho^2 = \frac{\partial^2}{\partial\rho^2} + \frac{1}{\rho}\frac{\partial}{\partial\rho} + \frac{1}{\rho^2}\frac{\partial^2}{\partial\theta^2}$$

Plates Subjected to Edge Loading Only

If the plate is subjected to loads applied at the boundary only, the load intensity $q(r,\theta) = 0$ and the equation characterizing its deflection becomes

$$\nabla_\rho^4\omega + \omega = 0 \quad [10]$$

To find the general solution of Equation [10] we assume

$$\omega_G = \omega_1 + \omega_2 \quad [11]$$

If ω_1 and ω_2 satisfy, respectively, the relations

$$\left.\begin{aligned} \nabla_\rho^2\omega_1 &= i\omega_1 \\ \nabla_\rho^2\omega_2 &= -i\omega_2 \end{aligned}\right\} \quad [12]$$

then it can be verified readily that both ω_1 and ω_2 individually satisfy Equation [10], because

$$\nabla_\rho^4\omega_1 = \nabla_\rho^2(\nabla_\rho^2\omega_1) = \nabla_\rho^2(i\omega_1) = i\nabla_\rho^2\omega_1 = -\omega_1$$

and

$$\nabla_\rho^4\omega_2 = \nabla_\rho^2(\nabla_\rho^2\omega_2) = \nabla_\rho^2(-i\omega_2) = -i\nabla_\rho^2\omega_2 = -\omega_2$$

Consequently, the general solution of Equation [10] can be reduced to finding the solution of the following equations

$$\frac{\partial^2\omega_1}{\partial\rho^2} + \frac{1}{\rho}\frac{\partial\omega_1}{\partial\rho} + \frac{1}{\rho^2}\frac{\partial^2\omega_1}{\partial\theta^2} = i\omega_1 \quad [13]$$

$$\frac{\partial^2\omega_2}{\partial\rho^2} + \frac{1}{\rho}\frac{\partial\omega_2}{\partial\rho} + \frac{1}{\rho^2}\frac{\partial^2\omega_2}{\partial\theta^2} = -i\omega_2 \quad [14]$$

To solve Equations [13] and [14] we assume solutions in the form

$$\omega_1 = \sum_{n=0}^{\infty} P_n^{(1)}\cos n\theta + \sum_{n=0}^{\infty} S_n^{(1)}\sin n\theta \quad [15]$$

$$\omega_2 = \sum_{n=0}^{\infty} P_n^{(2)}\cos n\theta + \sum_{n=0}^{\infty} S_n^{(2)}\sin n\theta \quad [16]$$

where $P_n^{(1)}$, $S_n^{(1)}$, $P_n^{(2)}$, and $S_n^{(2)}$ are functions of the radial co-ordinate ρ only, and, because of the requirement that $\omega_G(\rho,\theta)$ be single valued, $n = 0, 1, 2, 3, \ldots$.

Substitution of the assumed solution, Equation [15], into the differential Equation [13] results in

$$\frac{d^2P_n^{(1)}}{d\rho^2} + \frac{1}{\rho}\frac{dP_n^{(1)}}{d\rho} - \left(i + \frac{n^2}{\rho^2}\right)P_n^{(1)} = 0 \quad [17]$$

$$\frac{d^2S_n^{(1)}}{d\rho^2} + \frac{1}{\rho}\frac{dS_n^{(1)}}{d\rho} - \left(i + \frac{n^2}{\rho^2}\right)S_n^{(1)} = 0 \quad [18]$$

Similarly, substitution of Equation [16] into Equation [14] results in

$$\frac{d^2P_n^{(2)}}{d\rho^2} + \frac{1}{\rho}\frac{dP_n^{(2)}}{d\rho} + \left(i - \frac{n^2}{\rho^2}\right)P_n^{(2)} = 0 \quad [19]$$

$$\frac{d^2S_n^{(2)}}{d\rho^2} + \frac{1}{\rho}\frac{dS_n^{(2)}}{d\rho} + \left(i - \frac{n^2}{\rho^2}\right)S_n^{(2)} = 0 \quad [20]$$

Equations [17], [18], [19], and [20] are the well-known Bessel differential equations of order n and their solutions are given, respectively, by

$$\left.\begin{aligned} P_n^{(1)} &= \bar{A}_n I_n(\rho i^{1/2}) + \bar{B}_n K_n(\rho i^{1/2}) \\ S_n^{(1)} &= \bar{A}_n' I_n(\rho i^{1/2}) + \bar{B}_n' K_n(\rho i^{1/2}) \\ P_n^{(2)} &= \bar{C}_n I_n(\rho i^{-1/2}) + \bar{D}_n K_n(\rho i^{-1/2}) \\ S_n^{(2)} &= \bar{C}_n' I_n(\rho i^{-1/2}) + \bar{D}_n' K_n(\rho i^{-1/2}) \end{aligned}\right\} \quad [21]$$

where $\bar{A}_n$, $\bar{B}_n$, $\bar{C}_n$, $\bar{D}_n$, $\bar{A}_n'$, $\bar{B}_n'$, $\bar{C}_n'$, and $\bar{D}_n'$ are arbitrary constants of integration and I_n and K_n are known as the modified Bessel functions of the first and second kind, respectively, of order n.[3] Since it is awkward to manipulate Bessel functions with

[3] Reference (9), chapter vii.

complex arguments, we note the following definitions

$$\left.\begin{aligned} i^n I_n(\rho i^{1/2}) &= \mathrm{ber}_n\rho + i\,\mathrm{bei}_n\rho \\ i^{-n} K_n(\rho i^{1/2}) &= \mathrm{ker}_n\rho + i\,\mathrm{kei}_n\rho \end{aligned}\right\} \quad [22]$$

$$\left.\begin{aligned} i^{-n} I_n(\rho i^{-1/2}) &= \mathrm{ber}_n\rho - i\,\mathrm{bei}_n\rho \\ i^n K_n(\rho i^{-1/2}) &= \mathrm{ker}_n\rho - i\,\mathrm{kei}_n\rho \end{aligned}\right\} \quad [23]$$

The defining series expansions for the functions ber_n, bei_n, ker_n, and kei_n are given in the Appendix.

If we now let

$$\left.\begin{aligned} R_n &= P_n^{(1)} + P_n^{(2)} \\ R_n' &= S_n^{(1)} + S_n^{(2)} \end{aligned}\right\} \quad [24]$$

then by virtue of Equations [11], [15], and [16] we have the general solution of Equation [10]

$$\omega_G(\rho, \theta) = \sum_{n=0}^{\infty} R_n \cos n\theta + \sum_{n=0}^{\infty} R_n' \sin n\theta \quad [25]$$

with

$$R_n = A_n\,\mathrm{ber}_n\rho + B_n\,\mathrm{bei}_n\rho + C_n\,\mathrm{ker}_n\rho + D_n\,\mathrm{kei}_n\rho \quad [26]$$

$$R_n' = A_n'\,\mathrm{ber}_n\rho + B_n'\,\mathrm{bei}_n\rho + C_n'\,\mathrm{ker}_n\rho + D_n'\,\mathrm{kei}_n\rho \quad [27]$$

where we have used the identities, Equations [22] and [23] and redefined the constants of integration appearing in Equations [21]. The functions ber_n, bei_n, ker_n, and kei_n play an important role in the theory of alternating electric currents and are discussed from that point of view in reference (10). They have been tabulated, and some of their properties relevant to this investigation are given in references (9) and (11).

Reduction to Radial Symmetry

If the load intensity q is independent of the angular co-ordinate θ and the boundary condition (or edge loading) is radially symmetric, then the deflection also will be radially symmetric. In this case the solution, Equation [25] of the differential equation of equilibrium, Equation [10], reduces to

$$\omega(\rho) = R_0 = A_0\,\mathrm{ber}_0\rho + B_0\,\mathrm{bei}_0\rho + C_0\,\mathrm{ker}_0\rho + D_0\,\mathrm{kei}_0\rho \quad [28]$$

In reference (3) the solution of the radially symmetric problem is presented in the form

$$\omega(\rho) = C_1Z_1(\rho) + C_2Z_2(\rho) + C_3Z_3(\rho) + C_4Z_4(\rho) \quad [29]$$

where

$$\left.\begin{aligned} Z_1(\rho) &= \mathrm{Re}\,J_0(\rho i^{1/2}) \\ Z_2(\rho) &= \mathrm{Im}\,J_0(\rho i^{1/2}) \\ Z_3(\rho) &= \mathrm{Re}\,H_0^{(1)}(\rho i^{1/2}) \\ Z_4(\rho) &= \mathrm{Im}\,H_0^{(1)}(\rho i^{1/2}) \end{aligned}\right\} \quad [30]$$

and where J_0 and $H_0^{(1)}$ are the Bessel functions of the first and third kind, respectively, of zero order. We have the following identities (10)

$$\left.\begin{aligned} I_0(\rho i^{-1/2}) &= J_0(\rho i^{1/2}) = \mathrm{ber}_0\rho - i\,\mathrm{bei}_0\rho \\ K_0(\rho i^{-1/2}) &= \frac{\pi}{2}\,i\,H_0^{(1)}(\rho i^{1/2}) = \mathrm{ker}_0\rho - i\,\mathrm{kei}_0\rho \end{aligned}\right\} \quad [31]$$

Thus, comparing Equations [30] and [31], we obtain

$$Z_1(\rho) = \mathrm{ber}_0\rho$$

$$Z_2(\rho) = -\mathrm{bei}_0\rho$$

$$Z_3(\rho) = -\frac{2}{\pi}\,\mathrm{kei}_0\rho$$

$$Z_4(\rho) = -\frac{2}{\pi}\,\mathrm{ker}_0\rho$$

and with a redefinition of the arbitrary constants of integration the equivalence of the results as given by Equations [28] and [29] is established.

Plates Subjected to Concentrated Loads

We shall now assume that the plate is subjected to a concentrated load of magnitude F located at the point (δ, ϕ) of the polar co-ordinates system as shown in Fig. 1. Thus a point P on the plate is determined uniquely by its dimensionless polar co-ordinates ρ and θ where $\xi \leq \rho \leq \eta$ and $0 \leq \theta \leq 2\pi$. The boundary conditions will be prescribed on the edges of the plate characterized by $\rho = \xi$ and $\rho = \eta$. The problem, then, consists of determining a function $\omega(\rho, \theta)$ which satisfies Equation [10] throughout the region $\xi \leq \rho \leq \eta$ with the exception of the point of application of the concentrated load where it must possess the appropriate singularity. This function, moreover, must conform to the boundary conditions of the particular case under consideration.

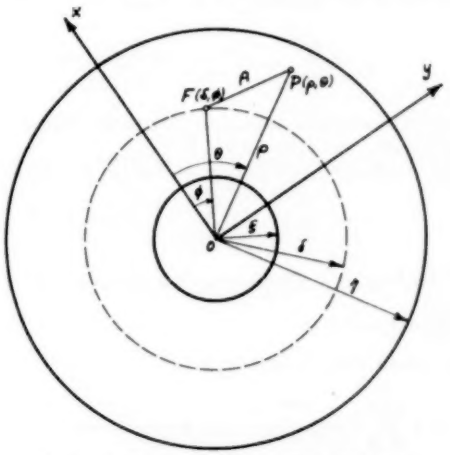

Fig. 1 Eccentrically Loaded Ring Plate

We shall assume that the solution of Equation [9] may be written

$$\omega(\rho, \theta) = \omega_G + \omega_P \quad [32]$$

where ω_P is a particular solution of Equation [9] and ω_G is the general solution of the homogeneous Equation [10]. A particular solution of Equation [9] is

$$\frac{\omega_P}{W} = \mathrm{kei}\rho_1 \quad [33]$$

where

$$W = -\frac{F}{2\pi\lambda^2 D}$$

and where ω_P is the deflection at P due to a load F at a distance ρ_1 from P as shown in Fig. 1. It is the deflection function of a plate of infinite extent on an elastic foundation under a concentrated load (1, 4).

The function ω_P may be expanded into an infinite trigonometric series. With the notation indicated in Fig. 1

$$\rho_1^2 = \rho^2 + \delta^2 - 2\,\delta\rho\cos(\theta - \phi) \quad [34]$$

We shall now apply Neumann's addition theorem for modified Bessel functions of the second kind (12) which states that for $\rho < \delta$

$$K_0(\rho_1 i^{1/2}) = K_0(\delta i^{1/2}) I_0(\rho i^{1/2}) + 2 \sum_{n=1}^{\infty} K_n(\delta i^{1/2}) I_n(\rho i^{1/2}) \cos n(\theta - \phi) \quad [35a]$$

and for $\rho > \delta$

$$K_0(\rho_1 i^{1/2}) = I_0(\delta i^{1/2}) K_0(\rho i^{1/2}) + 2 \sum_{n=1}^{\infty} I_n(\delta i^{1/2}) K_n(\rho i^{1/2}) \cos n(\theta - \phi) \quad [35b]$$

Applying the identities, Equations [22], to the series expansions Equations [35], we obtain for $\rho < \delta$

$$\ker \rho_1 + i \operatorname{kei} \rho_1 = (\ker \delta \operatorname{ber} \rho - \operatorname{kei} \delta \operatorname{bei} \rho) + i(\operatorname{kei} \delta \operatorname{ber} \rho + \ker \delta \operatorname{bei} \rho) + 2 \sum_{n=1}^{\infty} [(\ker_n \delta \operatorname{ber}_n \rho - \operatorname{kei}_n \delta \operatorname{bei}_n \rho) + i(\operatorname{kei}_n \delta \operatorname{ber}_n \rho + \ker_n \delta \operatorname{bei}_n \rho)] \cos n(\theta - \phi)$$

Taking imaginary parts

$$\operatorname{kei} \rho_1 = \operatorname{kei} \delta \operatorname{ber} \rho + \ker \delta \operatorname{bei} \rho + 2 \sum_{n=1}^{\infty} (\operatorname{kei}_n \delta \operatorname{ber}_n \rho + \ker_n \delta \operatorname{bei}_n \rho) \cos n(\theta - \phi) \quad [36a]$$

and similarly, for $\rho > \delta$

$$\operatorname{kei} \rho_1 = \operatorname{bei} \delta \ker \rho + \operatorname{ber} \delta \operatorname{kei} \rho + 2 \sum_{n=1}^{\infty} (\operatorname{bei}_n \delta \ker_n \rho + \operatorname{ber}_n \delta \operatorname{kei}_n \rho) \cos n(\theta - \phi) \quad [36b]$$

The general solution of Equation [10] is given by Equation [25]. It represents the deflection of a circular or ring-shaped plate on an elastic foundation subjected to loads at the boundary only. This solution contains an infinity of initially arbitrary constants.

The ordinary boundary conditions of the classical, small deflection theory of thin plates impose, in general, two separate conditions upon any particular edge of the plate. For instance, in the case of a ring plate we shall have four boundary-condition equations, two for each edge. Substitution of the solution, Equation [32] into the boundary conditions will result in identities in θ giving rise to a system of eight equations in eight unknowns, thus yielding the constants of integration of the problem. A similar argument may be presented for a solid circular plate and an infinite plate with an internal circular cutout, since these represent limiting cases of the ring plate. The number of equations to be solved in each case can be reduced substantially by the proper positioning of the load with respect to the co-ordinate system, and this convenience is used in the examples which follow.

Applications

We shall now apply the method developed in this paper to the solution of the problem of a clamped circular plate of radius c resting on an elastic foundation of modulus k. The plate is subjected to a concentrated transverse load of magnitude F, the point of application of the load being at $(\delta, 0)$, i.e., $\phi = 0$, and the load lies on the x-axis. Since the deflection and slope remain finite at the center, $C_n = D_n = 0$ in Equation [26], while $R_n' = 0$, because the deflection function must be symmetrical with respect to the x-axis. In addition, we must satisfy the following boundary conditions

$$\left.\begin{aligned} \omega(\eta, \theta) &= 0 \\ \left[\frac{\partial \omega}{\partial \rho}\right]_{(\eta, \theta)} &= 0 \end{aligned}\right\} \quad [37]$$

In the light of the foregoing discussion we may express the general solution of Equation [9] in the following form to suit our present purpose

$$\frac{\omega_G(\rho, \theta)}{W} = R_0 + 2 \sum_{n=1}^{\infty} R_n \cos n\theta \quad [38a]$$

where

$$\left.\begin{aligned} R_n &= A_n \operatorname{ber}_n \rho + B_n \operatorname{bei}_n \rho \\ n &= 0, 1, 2, 3, \ldots . \end{aligned}\right\} \quad [38b]$$

Upon application of the boundary condition Equations [37] to the solution as given by the superposition of Equations [38] and [33], and making use of Equation [36b], we obtain identities in θ giving rise to a system of two equations in two unknowns

$$\left.\begin{aligned} A_n \operatorname{ber}_n \eta + B_n \operatorname{bei}_n \eta &= -(\operatorname{bei}_n \delta \ker_n \eta + \operatorname{ber}_n \delta \operatorname{kei}_n \eta) \\ A_n \operatorname{ber}_n' \eta + B_n \operatorname{bei}_n' \eta &= -(\operatorname{bei}_n \delta \ker_n' \eta + \operatorname{ber}_n \delta \operatorname{kei}_n' \eta) \end{aligned}\right\} \quad [39]$$

Solving

$$\left.\begin{aligned} A_n &= \operatorname{bei}_n \delta \frac{\operatorname{bei}_n \eta \ker_n' \eta - \operatorname{bei}_n' \eta \ker_n \eta}{\operatorname{ber}_n \eta \operatorname{bei}_n' \eta - \operatorname{ber}_n' \eta \operatorname{bei}_n \eta} + \operatorname{ber}_n \delta \frac{\operatorname{bei}_n \eta \operatorname{kei}_n' \eta - \operatorname{bei}_n' \eta \operatorname{kei}_n \eta}{\operatorname{ber}_n \eta \operatorname{bei}_n' \eta - \operatorname{ber}_n' \eta \operatorname{bei}_n \eta} \end{aligned}\right\} \quad [40a]$$

$$\left.\begin{aligned} B_n &= \operatorname{ber}_n \delta \frac{\operatorname{kei}_n \eta \operatorname{ber}_n' \eta - \operatorname{kei}_n' \eta \operatorname{ber}_n \eta}{\operatorname{ber}_n \eta \operatorname{bei}_n' \eta - \operatorname{ber}_n' \eta \operatorname{bei}_n \eta} + \operatorname{bei}_n \delta \frac{\ker_n \eta \operatorname{ber}_n' \eta - \ker_n' \eta \operatorname{ber}_n \eta}{\operatorname{ber}_n \eta \operatorname{bei}_n' \eta - \operatorname{ber}_n' \eta \operatorname{bei}_n \eta} \end{aligned}\right\} \quad [40b]$$

Substituting Equations [40] into Equation [38b] we obtain, after some simplification

$$\left.\begin{aligned} R_n &= \frac{(\operatorname{ber}_n \delta \operatorname{kei}_n \eta + \operatorname{bei}_n \delta \ker_n \eta)(\operatorname{ber}_n' \eta \operatorname{bei}_n \rho - \operatorname{bei}_n' \eta \operatorname{ber}_n \rho)}{(\operatorname{ber}_n \eta \operatorname{bei}_n' \eta - \operatorname{ber}_n' \eta \operatorname{bei}_n \eta)} \\ &+ \frac{(\operatorname{ber}_n \delta \operatorname{kei}_n' \eta + \operatorname{bei}_n \delta \ker_n' \eta)(\operatorname{ber}_n \eta \operatorname{bei}_n \rho - \operatorname{bei}_n \eta \operatorname{ber}_n \rho)}{(\operatorname{ber}_n \eta \operatorname{bei}_n' \eta - \operatorname{ber}_n' \eta \operatorname{bei}_n \eta)} \\ n &= 0, 1, 2, 3, \ldots . \end{aligned}\right\} \quad [41]$$

By superposition of Equations [38] and [33], and in conjunction with Equation [34], we obtain the following series expression for

the deflection function valid for $0 \leq \rho \leq \eta$ and $0 \leq \theta \leq 2\pi$

$$\frac{\omega}{W} = \text{kei}\,(\rho^2 + \delta^2 - 2\delta\rho\cos\theta)^{1/2} + R_0 + 2\sum_{n=1}^{\infty} R_n \cos n\theta \quad \ldots\ldots [42]$$

where R_n is defined by Equation [41]. A dimensionless plot of the deflection profile along a diameter passing through the load point is shown in Fig. 2 for the special case of $\eta/\delta = 2$.

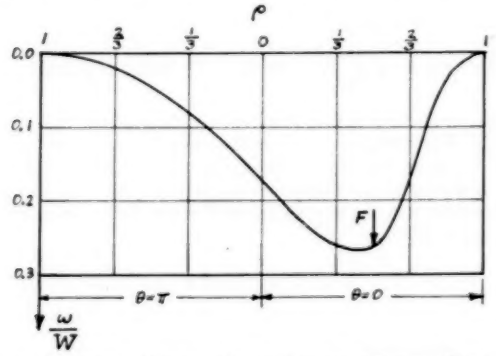

FIG. 2 DEFLECTION PROFILE ALONG DIAMETER PASSING THROUGH LOAD POINT

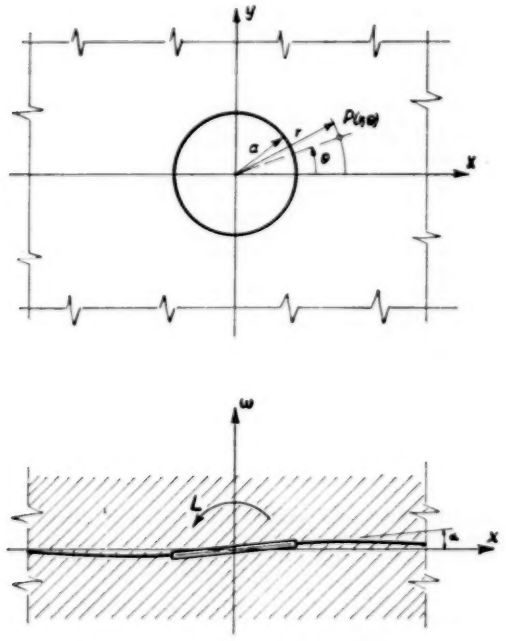

FIG. 3 RADIALLY ASYMMETRICAL CASE OF BENDING OF PLATE ON ELASTIC FOUNDATION

Another problem which does not display radial symmetry is now considered. An infinite plate on an elastic foundation is clamped at the circular boundary of a rigid disk with radius of length a as shown in Fig. 3. A pure moment of magnitude L is applied to the disk, causing it to rotate through an angle α about a diameter which lies on the y-axis. With notations $\lambda r = \rho$ and $\lambda a = \xi$, the boundary conditions may be stated as follows

$$\lim_{\rho\to\infty} \omega(\rho, \theta) = 0 \quad \ldots\ldots [43]$$

$$\lim_{\rho\to\infty} \left(\frac{\partial\omega}{\partial\rho}\right)_{(\rho,\,\theta)} = 0 \quad \ldots\ldots [44]$$

$$\frac{1}{a\alpha}\,\omega(\xi, \theta) = \cos\theta \quad \ldots\ldots [45]$$

$$\frac{1}{a\alpha}\left(\frac{\partial\omega}{\partial\rho}\right)_{(\xi,\,\theta)} = \frac{1}{\xi}\cos\theta \quad \ldots\ldots [46]$$

With reference to Equations [25] and [26], we have a solution of the form

$$\frac{1}{a\alpha}\,\omega(\rho, \theta) = (A\,\text{ker}_1\rho + B\,\text{kei}_1\rho + C\,\text{ber}_1\rho + D\,\text{bei}_1\rho)\cos\theta \quad \ldots\ldots [47]$$

Satisfaction of boundary condition Equations [43] and [44] requires that $C = D = 0$. Application of boundary condition Equations [45] and [46] results in

$$\left.\begin{aligned} A\,\text{ker}_1\xi + B\,\text{kei}_1\xi &= 1 \\ A\,\text{ker}_1'\xi + B\,\text{kei}_1'\xi &= \frac{1}{\xi} \end{aligned}\right\} \quad \ldots\ldots [48]$$

Solving

$$\left.\begin{aligned} A &= \frac{\text{kei}_1'\xi - \frac{1}{\xi}\,\text{kei}_1\xi}{\text{ker}_1\xi\,\text{kei}_1'\xi - \text{ker}_1'\xi\,\text{kei}_1\xi} \\ B &= \frac{\frac{1}{\xi}\,\text{ker}_1\xi - \text{ker}_1'\xi}{\text{ker}_1\xi\,\text{kei}_1'\xi - \text{ker}_1'\xi\,\text{kei}_1\xi} \end{aligned}\right\} \quad \ldots\ldots [49]$$

Substituting the solution, Equation [47] into Equations [2] and [3], respectively, we obtain the moments and shears

$$\frac{M_r(\rho, \theta)}{a\alpha\lambda^2 D\cos\theta} = A\left[\text{kei}_1\rho + \frac{(1-\nu)}{\rho}\left(\text{ker}_1'\rho - \frac{1}{\rho}\,\text{ker}_1\rho\right)\right] + B\left[-\text{ker}_1\rho + \frac{(1-\nu)}{\rho}\left(\text{kei}_1'\rho - \frac{1}{\rho}\,\text{kei}_1\rho\right)\right] \quad \ldots\ldots [50]$$

$$\frac{M_\theta(\rho, \theta)}{a\alpha\lambda^2 D\cos\theta} = A\left[\nu\,\text{kei}_1\rho - \frac{(1-\nu)}{\rho}\left(\text{ker}_1'\rho - \frac{1}{\rho}\,\text{ker}_1\rho\right)\right] + B\left[-\nu\,\text{ker}_1\rho - \frac{(1-\nu)}{\rho}\left(\text{kei}_1'\rho - \frac{1}{\rho}\,\text{kei}_1\rho\right)\right] \quad \ldots\ldots [51]$$

$$\frac{M_{r\theta}(\rho, \theta)}{a\alpha\lambda^2 D(1-\nu)\sin\theta} = \frac{A}{\rho}\left(\frac{1}{\rho}\,\text{ker}_1\rho - \text{ker}_1'\rho\right) + \frac{B}{\rho}\left(\frac{1}{\rho}\,\text{kei}_1\rho - \text{kei}_1'\rho\right) \quad \ldots\ldots [52]$$

$$\frac{Q_r(\rho, \theta)}{a\alpha\lambda^3 D\cos\theta} = A\,\text{kei}_1'\rho - B\,\text{ker}_1'\rho \quad \ldots\ldots [53]$$

$$\frac{Q_\theta(\rho, \theta)}{a\alpha\lambda^3 D\cos\theta} = \frac{1}{\rho}(-A\,\text{kei}_1\rho + B\,\text{ker}_1\rho) \quad \ldots\ldots [54]$$

Considerations of static equilibrium of the rigid disk under the applied moment L, the reactive moments and shears at the edge of the disk, and the reaction of the elastic foundation require that

$$L = \int_0^{2\pi} [aM_r(a, \theta) \cos \theta + aM_{r\theta}(a, \theta) \sin \theta - a^2 Q_r(a, \theta) \cos \theta] \, d\theta + \int_0^{2\pi} \int_0^a k\alpha r^3 \cos^2 \theta \, dr \, d\theta \ldots [55]$$

Carrying out the indicated integrations, we obtain

$$\frac{L}{\pi D\alpha} = \frac{\xi^4}{4} - \frac{\xi^3 \left[\left(\mathrm{kei}_1'\xi - \frac{1}{\xi} \mathrm{kei}_1\xi \right)^2 + \left(\frac{1}{\xi} \mathrm{ker}_1\xi - \mathrm{ker}_1'\xi \right)^2 \right]}{\mathrm{ker}_1\xi \, \mathrm{kei}_1'\xi - \mathrm{ker}_1'\xi \, \mathrm{kei}_1\xi} \ldots [56]$$

A dimensionless plot of applied moment versus disk radius is shown in Fig. 4.

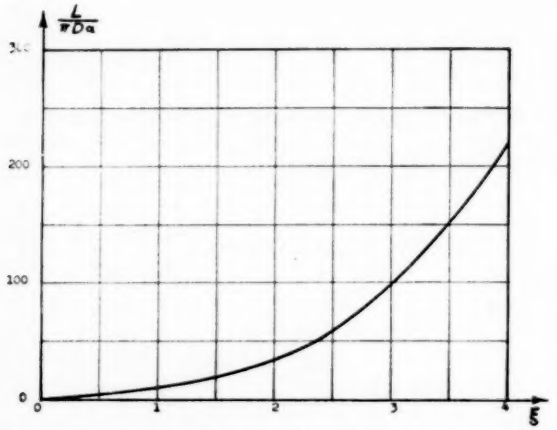

FIG. 4 DIMENSIONLESS PLOT OF APPLIED MOMENT VERSUS DISK RADIUS

CONCLUSIONS

The method developed in this paper leads to exact solutions for circular or ring-shaped plates on an elastic foundation. The solution is given in terms of tabulated functions which permit rapid and convenient numerical evaluation of results.

The solution to any given problem of the type considered here must satisfy Equation [9] as well as the appropriate boundary conditions. In general, this may be accomplished in two ways. For a given applied load, a particular solution of Equation [9] must be found. This particular solution added to the general solution of the homogeneous Equation [10] constitutes a complete solution of the problem, provided the constants of integration are adjusted in such a manner that the complete solution also satisfies the boundary conditions. However, the specific form of the particular solution depends on the load intensity $q(\rho, \theta)$, and with reference to practical computation it may be difficult to find a suitable function to satisfy the complete Equation [9].

Because of this possible inherent difficulty, the following approach is suggested: As shown in detail, concentrated force problems are readily solvable and because of the nature of the solution, very general boundary conditions can be satisfied. It is, then, possible to find the "influence function" of the particular problem under consideration, and this function can then be utilized together with the given load distribution to yield the solution of the problem by an integration over the region of the plate.

For instance, let $\omega_I = \omega_I(\rho, \theta; \delta, \phi)$ be the deflection function of a circular plate resting on an elastic foundation under the influence of a unit concentrated load located at the point whose co-ordinates are (δ, ϕ). Then the deflection of the same plate subjected to the distributed load characterized by the load intensity $q(\rho, \theta)$ is given by

$$\omega(\rho, \theta) = \int_0^{\eta} \int_0^{2\pi} q(\delta, \phi) \, \omega_I(\rho, \theta; \delta, \phi) \, \delta \, d\delta \, d\phi \ldots [57]$$

where ω_I is the influence function. Having shown that concentrated force problems can be solved readily, it may be inferred that arbitrary loading conditions can be treated as well, since the indicated integration shown by Equation [57] always can be performed, if not analytically, then certainly by standard numerical methods.

BIBLIOGRAPHY

1 "Über das Gleichgewicht Schwimmender Elastischer Platten," by H. Hertz, Wiedemann's *Annalen der Physik und Chemie*, vol. 22, 1884, p. 255.

2 "Vorlesungen über Technische Mechanik," by A. Föppl, Teuber, Leipzig, Germany, vol. 5, 1922, p. 103.

3 "Kreisplatten auf Elastischer Unterlage," by F. Schleicher, Julius Springer, Berlin, Germany, 1926.

4 "Beams on Elastic Foundation," by M. Hetenyi, The University of Michigan Press, Ann Arbor, Mich., 1946.

5 "Theory of Plates and Shells," by S. Timoshenko, McGraw-Hill Book Company, Inc., New York, N. Y., 1940.

6 "Über die Spannungsverteilung in Zylindrischen Behaelterwaenden," by H. Reissner, *Beton und Eisen*, vol. 7, 1908, p. 150.

7 "Statik und Dynamik der Schalen," by W. Flügge, Julius Springer, Berlin, Germany, 1934.

8 "The Two-Dimensional Problem in the Case of Periodically Altering Temperature Effects," by P. Lardy, Publications of the International Association for Bridge and Structural Engineering, Zurich, Switzerland, vol. 12, 1952, pp. 201–220.

9 "Bessel Functions for Engineers," by N. W. McLachlan, Oxford University Press, London, England, 1934.

10 "Bessel Functions for Alternating Current Problems," by H. B. Dwight, Transactions of the American Institute of Electrical Engineers, vol. 48, July, 1929, pp. 812–820.

11 "Tables of Integrals and Other Mathematical Data," by H. B. Dwight, The Macmillan Company, New York, N. Y., 1947 (revised edition).

12 "Bessel Functions," by A. Gray, G. B. Mathews, and T. M. McRobert, Macmillan and Company, Ltd., London, England, 1931.

Appendix

The Bessel functions employed in this paper are defined by the following series expansions

$$\mathrm{ber}_n x = \sum_{p=0}^{\infty} \frac{(-1)^{n+p} \left(\frac{1}{2} x \right)^{n+2p}}{p! \, (n+p)!} \cos \frac{(n+2p)\pi}{4} \ldots [58]$$

$$\mathrm{bei}_n x = \sum_{p=0}^{\infty} \frac{(-1)^{n+p+1} \left(\frac{1}{2} x \right)^{n+2p}}{p! \, (n+p)!} \sin \frac{(n+2p)\pi}{4} \ldots [59]$$

$$\left.\begin{aligned}\ker_n x &= \left(\log\frac{2}{x}-\gamma\right)\operatorname{ber}_n x+\frac{\pi}{4}\operatorname{bei}_n x\\ &\quad+\frac{1}{2}\sum_{p=0}^{n-1}\frac{(-1)^{n+p}(n-p-1)!}{p!}\left(\frac{x}{2}\right)^{2p-n}\cos\frac{(n+2p)\pi}{4}\\ &\quad+\frac{1}{2}\sum_{p=0}^{\infty}\left(1+\frac{1}{2}+\frac{1}{3}+\ldots+\frac{1}{p}+1+\frac{1}{2}+\frac{1}{3}+\ldots+\frac{1}{n+p}\right)\\ &\qquad\qquad\frac{(-1)^{n+p}\left(\frac{1}{2}x\right)^{n+2p}}{p!\,(n+p)!}\cos\frac{(n+2p)\pi}{4}\end{aligned}\right\}\ldots[60]$$

$$\left.\begin{aligned}\operatorname{kei}_n x &= \left(\log\frac{2}{x}-\gamma\right)\operatorname{bei}_n x-\frac{\pi}{4}\operatorname{ber}_n x\\ &\quad+\frac{1}{2}\sum_{p=0}^{n-1}\frac{(-1)^{n+p}(n-p-1)!}{p!}\left(\frac{x}{2}\right)^{2p-n}\sin\frac{(n+2p)\pi}{4}\\ &\quad-\frac{1}{2}\sum_{p=0}^{\infty}\left(1+\frac{1}{2}+\frac{1}{3}+\ldots+\frac{1}{p}+1+\frac{1}{2}+\frac{1}{3}+\ldots+\frac{1}{n+p}\right)\\ &\qquad\qquad\frac{(-1)^{n+p}\left(\frac{1}{2}x\right)^{n+2p}}{p!\,(n+p)!}\sin\frac{(n+2p)\pi}{4}\end{aligned}\right\}\ldots[61]$$

The following asymptotic series are valid for large values of x

$$\operatorname{ber}_n x \backsimeq \frac{e^{x/\sqrt{2}}}{\sqrt{2\pi x}}\left[L_n(x)\cos\left(\frac{x}{\sqrt{2}}-\frac{\pi}{8}+\frac{n\pi}{2}\right)-M_n(x)\sin\left(\frac{x}{\sqrt{2}}-\frac{\pi}{8}+\frac{n\pi}{2}\right)\right]\ldots[62]$$

$$\operatorname{bei}_n x \backsimeq \frac{e^{x/\sqrt{2}}}{\sqrt{2\pi x}}\left[M_n(x)\cos\left(\frac{x}{\sqrt{2}}-\frac{\pi}{8}+\frac{n\pi}{2}\right)+L_n(x)\sin\left(\frac{x}{\sqrt{2}}-\frac{\pi}{8}+\frac{n\pi}{2}\right)\right]\ldots[63]$$

$$\ker_n x \backsimeq \left(\frac{\pi}{2x}\right)^{1/2}e^{-x/\sqrt{2}}\left[L_n(-x)\cos\left(\frac{x}{\sqrt{2}}+\frac{\pi}{8}+\frac{n\pi}{2}\right)+M_n(-x)\sin\left(\frac{x}{\sqrt{2}}+\frac{\pi}{8}+\frac{n\pi}{2}\right)\right]\ldots[64]$$

$$\operatorname{kei}_n x \backsimeq \left(\frac{\pi}{2x}\right)^{1/2}e^{-x/\sqrt{2}}\left[M_n(-x)\cos\left(\frac{x}{\sqrt{2}}+\frac{\pi}{8}+\frac{n\pi}{2}\right)-L_n(-x)\sin\left(\frac{x}{\sqrt{2}}+\frac{\pi}{8}+\frac{n\pi}{2}\right)\right]\ldots[65]$$

where

$$L_n(x)=1-\frac{4n^2-1^2}{1!\,(8x)}\cos\frac{\pi}{4}+\frac{(4n^2-1^2)(4n^2-3^2)}{2!\,(8x)^2}\cos\frac{2\pi}{4}-\ldots\ldots[66]$$

$$M_n(x)=\frac{4n^2-1^2}{1!\,(8x)}\sin\frac{\pi}{4}-\frac{(4n^2-1^2)(4n^2-3^2)}{2!\,(8x)^2}\sin\frac{2\pi}{4}+\ldots\ldots[67]$$

In Equations [58] to [67] n is a positive integer or zero, $p = 0, 1, 2, 3, \ldots$, and γ is Euler's constant 0.5772157.

Contact of Elastic Spheres Under an Oscillating Torsional Couple[1]

By H. DERESIEWICZ,[2] NEW YORK, N. Y.

The traction, moment-twist relation, torsional compliances, and frictional energy loss per cycle are computed for two like, elastic spheres in Hertz contact acted upon by a small oscillating torsional couple.

Introduction

THE problem of two elastic bodies in Hertz contact subjected to a monotonically increasing torsional couple applied about the axis of symmetry of the system was first considered by Mindlin (1)[3] who found that, in the absence of slip on the interface, the tangential traction rises to infinity on the elliptic boundary of contact. The torsional contact of two like spheres was re-examined by Lubkin (2) who made allowance for the occurrence of slip.

The present paper extends the Lubkin solution to the case in which the normal force is held constant while the torsional couple, after having reached a certain value, decreases, and to the case in which the torsional couple oscillates between fixed amplitudes. In the latter, the curve relating twisting moment to angle of twist forms a closed loop, the area of which represents the frictional energy dissipation per cycle. For small amplitudes, this energy loss is found to vary as the cube of the twisting moment. The solution is, strictly speaking, valid only for small amplitudes of the applied moment, because of an approximation made at the start. Practically, however, it is good over a large portion of the permissible range of moment-normal force ratios.

An approximate expression is obtained for the torsional compliance which depends upon the past history of loading. The initial value of the compliance during the first loading process is found to be the same as given in reference (1).

Summary of Previous Work

The Hertz problem for two like spheres (3) predicts a plane, circular contact surface of radius

$$a = (QNR)^{1/3} \quad [1]$$

where N is the normal force, R the radius of the spheres, and $Q = 3(1 - \nu^2)/4E$, in which ν and E are Poisson's ratio and Young's modulus, respectively, of the material.

The distribution of normal traction on the contact surface is given by

$$\sigma = \frac{3N}{2\pi a^3}(a^2 - \rho^2)^{1/2} \quad [2]$$

where ρ is the radial distance from the center of the contact surface.

If, now, an additional moment M is applied about the axis of normal contact, and if it is assumed that no slip occurs, symmetry considerations lead to the conclusion that no normal component of traction is induced and that the entire contact surface rotates as a rigid body with respect to a distant point of one of the spheres. The situation is thus reduced to a mixed-boundary-value problem in elasticity. With a system of cylindrical coordinates whose origin is at the center of the circle of contact and the z-axis along the axis of symmetry of the two spheres, the boundary conditions are: On the contact surface, the normal component of traction σ_z (zero) and the tangential component of displacement u_θ (proportional to the distance from the origin) are given. On the remainder of the surface of the sphere, approximated as plane, the three components of traction τ_{zr}, $\tau_{z\theta}$, σ_z (all zero) are given. Solution of this problem (1) gives the shearing stress $\tau_{z\theta}$ on the contact surface

$$\tau \equiv \tau_{z\theta})_{z=0} = \frac{3M}{4\pi a^3}\rho(a^2 - \rho^2)^{-1/2} \quad [3]$$

and the torsional compliance of a single body

$$c_\tau = \frac{d\beta}{dM} = \frac{3}{16\mu a^3} \quad [4]$$

where β is the angle of rotation of the contact surface with respect to a distant point in the body $z \geqslant 0$, and μ is the shear modulus of the material.

Since τ becomes infinite on the boundary of the contact circle, slip must result from an applied twisting moment, no matter how small. It may be expected to start at the edge of the contact surface where the singularity occurs and, because of the radial symmetry of τ, to progress radially inward on an annulus. Further, it is assumed that, on the annulus of slip, $\tau = f\sigma$, where f is a constant coefficient of friction, and that it does not exceed this value elsewhere. On account of symmetry, the rigid rotation remains unaffected for the region over which no slip has occurred (the "adhered" portion). This gives rise to another mixed-boundary-value problem in elasticity. The normal component of traction σ_z (zero) and the tangential component of displacement u_θ (proportional to the distance from the origin) are given on the adhered portion and the traction is given over the remainder of the boundary ($\tau = f\sigma$, $\tau_{zr} = \sigma_z = 0$ on the annulus of slip and all components of traction zero outside). Solution of this problem (2) yields the shear stress

$$\tau = \frac{3fN}{2\pi a^3}(a^2 - \rho^2)^{1/2}, \quad c \leqslant \rho \leqslant a$$

$$\tau = \frac{3fN}{2\pi a^3}(a^2 - \rho^2)^{1/2}\left\{1 + \frac{2}{\pi}\left[k^2 \boldsymbol{D}(k)F(k', \varphi) - \boldsymbol{K}(k)E(k', \varphi)\right]\right\}, \quad \rho \leqslant c \quad [5]$$

[1] This investigation was supported by the Office of Naval Research under Contract Nonr-266(09) with Columbia University.

[2] Assistant Professor of Civil Engineering, Columbia University. Assoc. Mem. ASME.

[3] Numbers in parentheses refer to the Bibliography at the end of the paper.

Contributed by the Applied Mechanics Division and presented at the Annual Meeting, New York, N. Y., November 29–December 4, 1953, of The American Society of Mechanical Engineers.

Discussion of this paper should be addressed to the Secretary, ASME, 29 West 39th Street, New York, N. Y., and will be accepted until April 12, 1954, for publication at a later date. Discussion received after the closing date will be returned.

Note: Statements and opinions advanced in papers are to be understood as individual expressions of their authors and not those of the Society. Manuscript received by ASME Applied Mechanics Division, February 13, 1953. Paper No. 53—A-31.

where c is the inner radius of the annulus, $k' = c/a$, $k = (1 - k'^2)^{1/2}$, $F(k', \varphi)$ and $E(k', \varphi)$ are incomplete elliptic integrals of the first and second kind, respectively, of modulus k' and amplitude

$$\varphi = \arcsin \frac{1}{k'} \sqrt{\frac{k'^2 - \rho^2/a^2}{1 - \rho^2/a^2}}$$

and $\boldsymbol{D}(k)$ is a tabulated (4) complete elliptic integral, of modulus k

$$\boldsymbol{D} = (\boldsymbol{K} - \boldsymbol{E})/k^2 \quad [6]$$

Here, $\boldsymbol{K}$ and $\boldsymbol{E}$ are, respectively, the complete elliptic integrals of the first and second kind, of modulus k. A cross section of the distribution of τ is illustrated by curve a-A-O in Fig. 1.

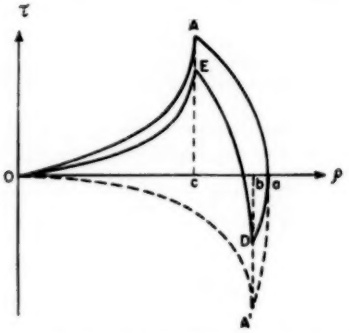

FIG. 1 PROFILE OF DISTRIBUTION OF $\tau_{z\theta}$ ON CONTACT SURFACE (a-A-O represents stress during initial loading; a-D-E-O, during initial unloading.)

The relation between the applied moment and the inner radius of slip is given by the condition of equilibrium

$$M = 2\pi \int_0^a \tau \rho^2 \, d\rho \quad [7]$$

Hence[4]

$$M = \frac{fNa}{4\pi} \left\{ \frac{3\pi^2}{4} + k'k^2[6\,\boldsymbol{K} + (4k'^2 - 3)\boldsymbol{D}] - 3k\,\boldsymbol{K} \sin^{-1} k' - 3k^2 \left[\boldsymbol{K} \int_0^{\pi/2} \frac{\sin^{-1}(k' \sin \alpha) d\alpha}{(1 - k'^2 \sin^2 \alpha)^{1/2}} - \boldsymbol{D} \int_0^{\pi/2} \frac{\sin^{-1}(k' \sin \alpha) d\alpha}{(1 - k'^2 \sin^2 \alpha)^{1/2}} \right] \right\} \quad [8]$$

Further, the relation between the angle of twist and the inner radius of slip is

$$\beta = \frac{3fN}{4\pi\mu a^3} k^3 \boldsymbol{D} \quad [9]$$

Equations [8] and [9] express, implicitly, the relation between the applied twisting moment and the resulting angle of twist. This is represented graphically by curve O-P-F in Fig. 2. The value of the moment at which slip occurs over the entire contact surface, i.e., sliding is initiated, is $M/fNa = 3\pi/16$. This corresponds to an infinite value of the angle of twist.

APPROXIMATE FORMULAS FOR $M/fNa \ll 1$

In what follows it will be necessary to have explicit and reversible relations between each pair of the three quantities: Inner radius of the slip annulus, twisting moment, and angle of twist. This is manifestly impossible for the exact solution (Equations [8] and [9]). Let us, therefore, confine our efforts to the range of small M/fNa, i.e., $k' = c/a \approx 1$.

First, however, it is desirable to obtain a different form of M. Starting with the following expression for τ[5]

$$\tau = \frac{3fN}{2\pi a^3} (a^2 - \rho^2)^{1/2}, \quad c \leqslant \rho \leqslant a$$

$$\tau = \frac{3fN}{\pi^2 a^4} \rho (c^2 - \rho^2)^{1/2} \int_0^{\pi/2} \frac{a^2 k^2 \sin^2 \alpha/(a^2 - \rho^2)}{[1 - a^2 k^2 \sin^2 \alpha/(a^2 - \rho^2)] \sqrt{1 - k^2 \sin^2 \alpha}} d\alpha, \quad \rho \leqslant c \quad [10]$$

inserting it into the condition of equilibrium, Equation [7], reversing the order of integration, and noting that (5)

$$\int_0^{\pi/2} \frac{\sin^2 \alpha}{\sqrt{1 - k^2 \sin^2 \alpha}} d\alpha = \boldsymbol{D}$$

$$\int_0^{\pi/2} \sin^2 \alpha \sqrt{1 - k^2 \sin^2 \alpha} \, d\alpha = \frac{2k^2 - 1}{3k^2} \boldsymbol{E} + \frac{k'^2}{3k^2} \boldsymbol{K}$$

we find

$$\frac{M}{fNa} = \frac{2}{\pi} k'k^2 \boldsymbol{E} + \frac{6}{\pi} k^3 \int_0^{\pi/2} \sin^2 \alpha \cos \alpha \sqrt{1 - k^2 \sin^2 \alpha} \tan^{-1} \left(\frac{k}{k'} \cos \alpha \right) d\alpha \quad [11]$$

This expression is easily expanded in a power series in k with the result

$$\frac{M}{fNa} \simeq k^2 \left(1 - \frac{3}{8} k^2 - \frac{1}{64} k^4 - \ldots \right) \quad [12]$$

Table 1 compares the values of M/fNa, calculated by retaining two and three terms in the expansion, Equation [12], with the exact values tabulated in reference (2).

[4] This is equation [49] of reference (2), with a typographical error corrected.

[5] In reference (2), insert Equation [47] into Equation [36]. The a' is here replaced by c.

TABLE 1 COMPARISON OF VALUES OF M/fNa

		M/fNa				
$k' = c/a$	$k^2 = 1 - k'^2$	Exact	Three-term approx	Per cent error	Two-term approx	Per cent error
1	0	0	0	0	0	0
0.95	0.0975	0.0938	0.09392	0.1	0.09393	0.1
0.9	0.19	0.1764	0.17636	0	0.17646	0
0.85	0.2775	0.2482	0.24829	0	0.24862	0.2
0.8	0.36	0.3105	0.31067	0.1	0.31140	0.3
0.7	0.51	0.4082	0.41039	0.5	0.41246	1.0
0.6	0.64	0.4805	0.48230	0.4	0.48640	1.2
0.5	0.75	0.5286	0.53247	0.7	0.53906	2.0
0.4	0.84	0.5592	0.56613	1.2	0.57540	2.9
0.3	0.91	0.5769	0.58768	1.9	0.59946	3.9
0.2	0.96	0.5855	0.60058	2.6	0.61440	4.9
0	1	0.5890	0.60937	3.4	0.62500	6.1

A similar expansion of β in Equation [9] yields

$$\frac{\mu a^2\beta}{fN} \simeq \frac{3}{16}k^3\left(1+\frac{3}{8}k^2+\frac{15}{64}k^4+\ldots\right) \quad [13]$$

but its use must be confined to small k, since the expression in Equation [9] diverges for $k = 1$. Exact and approximate values of $\mu a^2\beta/fN$ are compared in Table 2.

$$\left.\begin{aligned}\tau_c &= -\frac{3fN}{\pi a^3}(a^2-\rho^2)^{1/2}, \quad b \leqslant \rho \leqslant a \\ \tau_c &= -\frac{3fN}{\pi a^3}(a^2-\rho^2)^{1/2}\left\{1+\frac{2}{\pi}\left[k_1^2\boldsymbol{D}(k_1)F(k'_1,\varphi_1)\right.\right. \\ &\qquad \left.\left.-\boldsymbol{K}(k_1)E(k'_1,\varphi_1)\right]\right\}, \quad \rho \leqslant b\end{aligned}\right\} \quad [19]$$

TABLE 2 COMPARISON OF VALUES OF $\mu a^2\beta/fN$

$k' = c/a$	$k^2 = 1-k'^2$	$\mu a^2\beta/fN$ Exact	Three-term approx	Per cent error	Two-term approx	Per cent error
1	0	0	0	0	0	0
0.95	0.0975	0.0190	0.01899	0	0.01895	0.3
0.9	0.19	0.0385	0.03847	0.1	0.03817	1.0
0.85	0.2775	0.0586	0.05838	0.4	0.05744	2.0
0.8	0.36	0.0794	0.07866	0.9	0.07661	3.5
0.7	0.51	0.1234	0.11975	2.9	0.11392	7.7
0.6	0.64	0.1716	0.16527	3.7	0.15375	10.4

In view of the great complications arising from employing three or more terms in the expansions, Equations [12] and [13], we confine ourselves to two-term approximations. A short computation yields the following relations

$$\frac{M}{fNa} = \frac{2}{3}\left[1-\left(\frac{1+3c^2/a^2}{4}\right)^2\right] \quad [14]$$

$$\frac{c}{a} = \frac{1}{\sqrt{3}}\sqrt{4\left(1-\frac{3}{2}\frac{M}{fNa}\right)^{1/2}-1} \quad [15]$$

$$\frac{\mu a^2\beta}{fN} = \frac{3}{128}\left(1-\frac{c^2}{a^2}\right)\left(11-3\frac{c^2}{a^2}\right) \quad [16]$$

$$\frac{\mu a^2\beta}{fN} = \frac{1}{8}\left[1-\left(1-\frac{3}{2}\frac{M}{fNa}\right)^{1/2}\right]\left[3-\left(1-\frac{3}{2}\frac{M}{fNa}\right)^{1/2}\right] \quad [17]$$

Equation [17], which represents the explicit moment-twist relation, leads directly to the torsional compliance

$$c_\tau = \frac{3}{16\mu a^3}\left[2\left(1-\frac{3}{2}\frac{M}{fNa}\right)^{-1/2}-1\right] \quad [18]$$

It is seen that its initial value is the same as in Equation [4].

Decreasing Torsional Moment[6]

Suppose, now, that, after having reached a value M^*, such that $0 < M/fNa < 3\pi/16$, the twisting moment M is reduced. If slip were prevented, the tangential component of traction τ would tend to negative infinity on the boundary $\rho = a$. This conclusion is reached from the solution of the appropriate boundary-value problem in elasticity, as described in the section entitled Summary of Previous Work. Hence slip, opposite in sense to the initial slip, is presumed to start at $\rho = a$ and penetrate to a radius b, assumed, temporarily, to be of magnitude $c \leqslant b \leqslant a$. On the annulus $b \leqslant \rho \leqslant a$, $\tau = -f\sigma$, so that the change of tangential traction is $-2f\sigma$. Since no additional slip occurs on the surface $\rho \leqslant b$, the change of displacement in that region must be that of a rigid-body rotation. Thus the change due to reduction of M presents a boundary-value problem in elasticity identical in form with that solved in reference (2). Hence, by analogy with Equation [5], the change in traction is

[6] The procedure in this and the following sections was first employed in connection with tangential contact of two spheres (6).

where k_1, k'_1, and φ_1 are obtained from k, k', and φ, respectively, by replacing c by b. This distribution is illustrated by curve a-A'-O in Fig. 1.

The resultant traction accompanying a reduction in M is obtained by adding the initial traction, Equation [5], and the change, Equation [19], with the result

$$\left.\begin{aligned}\tau_R &= -\frac{3fN}{2\pi a^3}(a^2-\rho^2)^{1/2}, \quad b \leqslant \rho \leqslant a \\ \tau_R &= -\frac{3fN}{2\pi a^3}(a^2-\rho^2)^{1/2}\left(1+\frac{4}{\pi}A_b\right), \quad c \leqslant \rho \leqslant b \\ \tau_R &= -\frac{3fN}{2\pi a^3}(a^2-\rho^2)^{1/2}\left[1+\frac{2}{\pi}(2A_b-A_c)\right], \\ &\qquad \rho \leqslant c\end{aligned}\right\} \quad [20]$$

where A_b stands for the bracketed expression in Equation [19] and A_c for a similar expression in Equation [5]. The traction profile is illustrated by curve a-D-E-O in Fig. 1.

The condition of equilibrium, Equation [7], yields, upon manipulation described in the section entitled Approximate Formulas

$$M = \frac{2fNa}{3}\left[1-\left(\frac{1+3c^2/a^2}{4}\right)^2\right] - \frac{4fNa}{3}\left[1-\left(\frac{1+3b^2/a^2}{4}\right)^2\right] \quad [21]$$

Noting, from Equation [14], that the first term on the right-hand side of Equation [21] is the initial torsional moment M^*, the inner radius of the annulus of counterslip is

$$b = \frac{a}{\sqrt{3}}\sqrt{4\left(1-\frac{3}{2}\frac{M^*-M}{2fNa}\right)^{1/2}-1} \quad [22]$$

Thus, as long as $-M^* \leqslant M \leqslant M^*$, the assumption $c \leqslant b \leqslant a$ is valid. When $M = -M^*$, i.e., when the twisting moment is fully reversed, $b = c$, i.e., counterslip has penetrated to the depth of initial slip. At the same time, Equations [20] reduce to Equations [5] with signs reversed. The traction is then distributed just as the initial traction at $M = M^*$ was, but with opposite sense. The situation is the same as if no positive M had ever been applied, but only a negative M of magnitude M^*.

The associated rotation of the adhered portion is found by a similar process of superposition. The change in angle of twist is obtained by multiplying Equation [16] by -2 and replacing c by b as given in Equation [22]. The initial twist is given by Equation [16] in which the value of c is found from

Equation [15] wherein M is replaced by M^*. The resultant angle of twist, given by the sum of the two, is given by

$$\frac{\mu a^3 \beta_d}{fN} = \frac{3}{128}\left(1-\frac{c^2}{a^2}\right)\left(11-3\frac{c^2}{a^2}\right)-\frac{3}{64}\left(1-\frac{b^2}{a^2}\right)\left(11-3\frac{b^2}{a^2}\right) = \left(1-\frac{3}{2}\frac{M^*-M}{2fNa}\right)^{1/3}-\frac{1}{2}\left[1+\left(1-\frac{3}{2}\frac{M^*}{fNa}\right)^{1/3}\right] - \frac{3}{16}\frac{M}{fNa} \quad [23]$$

The relation between twisting moment and angle of twist is illustrated by the full lines O-P-R-S in Fig. 2.

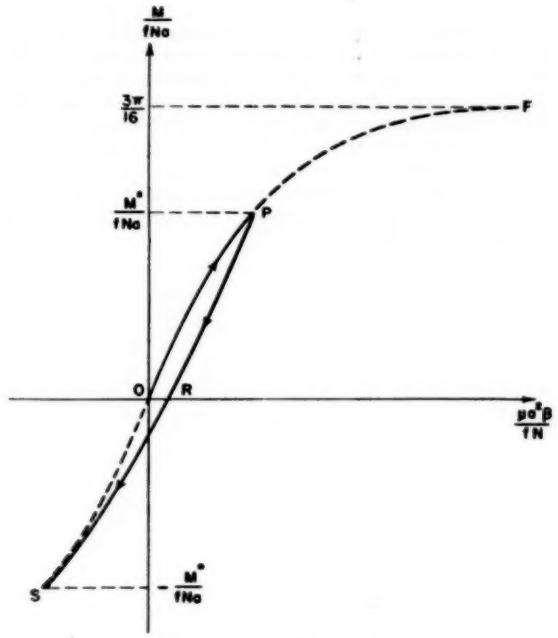

FIG. 2 CURVE ILLUSTRATING RELATION BETWEEN APPLIED TWISTING MOMENT M AND RESULTING ANGLE OF TWIST β DURING INITIAL LOADING AND UNLOADING

The compliance for unloading is

$$c_r = \frac{3}{16\mu a^3}\left[2\left(1-\frac{3}{2}\frac{M^*-M}{2fNa}\right)^{-1/3}-1\right] \quad [24]$$

Thus the initial compliance on unloading ($M = M^*$ in Equation [24]) is the same as the initial compliance on loading ($M = 0$ in Equation [18]); that is, in Fig. 2 the slope of P-R at P is the same as the slope of O-P at O.

When M has been reduced from M^* to zero, there is a permanent set given by O-R in Fig. 2, the magnitude of which is obtained by setting $M = 0$ in Equation [23]. The accompanying traction is not zero, but is a self-equilibrating distribution obtained by setting

$$b = \frac{a}{\sqrt{3}}\sqrt{4\left(1-\frac{3}{4}\frac{M^*}{fNa}\right)^{1/3}-1}$$

in Equations [20].

When M has been reduced to $-M^*$, the twist has reached the negative of the twist at $M = M^*$ (i.e., the abscissa of S in Fig. 2 is the negative of the abscissa of P) and the compliance is identical with that of curve O-P at $M = M^*$. Hence the unloading curve P-R-S is tangent, at S, to the central perversion O-S of the loading curve O-P.

OSCILLATING TORSIONAL MOMENT

In the preceding section, the entire situation at $M = -M^*$ is identical with that at $M = M^*$, except for reversal of sign. Hence a subsequent increase of M from $-M^*$ to M^* will be accompanied by the same events as occurred during the decrease from M^* to $-M^*$, except for reversal of sign. Thus, in starting along S-U, Fig. 3, the compliance at S is the same as the compliance of P-R at P. Slip again starts at $\rho = a$ in the same sense as occurred along path O-P. At an intermediate point of S-U the traction will be like a-D-E-O, Fig. 1, with sign reversed. When the twisting moment once more reaches M^*, b will again have penetrated to c and the traction will be exactly a-A-O, Fig. 1.

The twist along path S-U-P is

$$\beta_i = -\beta_d(-M)$$

so that

$$\frac{\mu a^3 \beta_i}{fN} = -\left(1-\frac{3}{2}\frac{M^*+M}{2fNa}\right)^{1/3} + \frac{1}{2}\left[1+\left(1-\frac{3}{2}\frac{M^*}{fNa}\right)^{1/3}\right]-\frac{3}{16}\frac{M}{fNa} \quad [25]$$

Hence, when $M = M^*$, the terminal points P of S-U-P and P of O-P, Fig. 3, are identical, as may be seen by comparing Equation [25] with Equation [17] for that value of M.

Subsequent diminution of M will then produce a repetition of the events accompanying the first diminution.

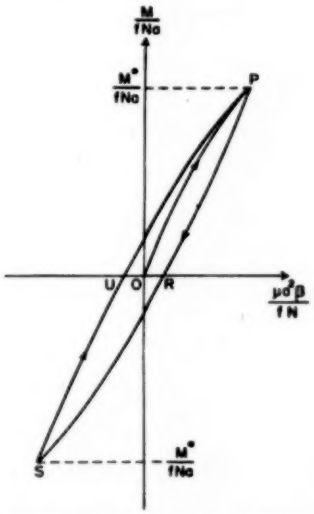

FIG. 3 CURVE ILLUSTRATING TORQUE-TWIST RELATION DURING A COMPLETE CYCLE OF APPLIED COUPLE
(Area enclosed by curve gives frictional energy loss per cycle)

It is now evident that, during oscillation of M between $\pm M^*$, with N maintained constant, the torque-twist curve traverses the loop P-R-S-U-P, Fig. 3.

The area enclosed in the loop gives the frictional energy loss per cycle for each surface

$$F = \int_{-M^*}^{M^*} (\beta_d - \beta_s) dM$$

$$= \frac{2f^2N^2}{\mu a} \left\{ \frac{8}{9} \left[1 - \left(1 - \frac{3}{2} \frac{M^*}{fNa} \right)^{3/2} \right] - \frac{M^*}{fNa} \left[1 + \left(1 - \frac{3}{2} \frac{M^*}{fNa} \right)^{1/2} \right] \right\} \quad [26]$$

For $M^*/fNa \ll 1$, Equation [26] reduces to

$$F = \frac{3M^{*3}}{16\mu a^4 fN} \quad [27]$$

i.e., the energy loss per cycle varies as the cube of the maximum torsional moment. It is interesting to note the close correspondence between oscillating torsional contact and oscillating tangential contact of two spheres. In the latter case, for amplitudes of tangential force small in comparison with fN, the energy loss per cycle is equal to (6)

$$F = \frac{(2 - \nu) T^{*3}}{36\mu a f N} \quad [28]$$

where T^* is the maximum tangential force.

BIBLIOGRAPHY

1 "Compliance of Elastic Bodies in Contact," by R. D. Mindlin, JOURNAL OF APPLIED MECHANICS, Trans. ASME, vol. 71, 1949, pp. 259–268.

2 "The Torsion of Elastic Spheres in Contact," by J. L. Lubkin, JOURNAL OF APPLIED MECHANICS, Trans. ASME, vol. 73, 1951, pp. 183–187.

3 "Theory of Elasticity," by S. Timoshenko and J. N. Goodier, McGraw-Hill Book Company, Inc., New York, N. Y., 1951, p. 372.

4 "Tables of Functions," by E. Jahnke and F. Emde, Dover Publications, New York, N. Y., 1945, pp. 73 and 83.

5 "Formules et Tables Numériques," by L. Potin, Gauthier-Villars, Paris, France, 1925, pp. 712, 713.

6 "Effects of an Oscillating Tangential Force on the Contact Surfaces of Elastic Spheres," by R. D. Mindlin, W. P. Mason, T. F. Osmer, and H. Deresiewicz, Proceedings of the First U. S. National Congress of Applied Mechanics, 1951, pp. 203–208.

7 "Sulla Torsione di Due Sfere Elastiche a Contatto," by C. Cattaneo, *Annali della Scuola Normale Superiore di Pisa*, series 3, vol. 6, 1952, pp. 1–16.

Addendum

Since writing this paper a work by Cattaneo (7) has come to the author's attention in which expressions corresponding to Equations [15] and [16] are derived. Cattaneo's relation between angle of twist and inner radius of slip annulus coincides with Equation [16]; however, he obtains a relation between moment and slip radius which differs from Equation [15], does not check with the numerical values tabulated from the exact solution by Lubkin (2), and yields an initial torsional compliance, corresponding to Equation [4], which does not agree with that obtained by Mindlin (1) and by Lubkin

Stress Concentration Due to a Hemispherical Pit at a Free Surface[1]

By R. A. EUBANKS,[2] CHICAGO, ILL.

This paper contains a solution in series form for the stresses and displacements around a hemispherical pit at a free surface of an elastic body. The problem is idealized by considering a semi-infinite medium which otherwise is bounded by a plane. At infinity the body is assumed to be in a state of plane hydrostatic tension perpendicular to the axis of symmetry of the pit. The present method of solution may be generalized to loadings which are not rotationally symmetric. Numerical results are given for the variation along the axis of symmetry of the normal stress which is parallel to the tractions at infinity; these results are compared with the known corresponding numerical values appropriate to the two-dimensional analog of the present problem.

Introduction, Statement of Problem

In what follows we investigate the stress concentration produced by a hemispherical pit at a free surface of an elastic body. The problem is idealized by considering the medium to occupy a semi-infinite region containing a hemispherical indentation and otherwise bounded by a plane. With reference to Cartesian co-ordinates (x, y, z), the region under consideration, Fig. 1, is defined by $z \geq 0$, $r = (x^2 + y^2 + z^2)^{1/2} \geq 1$ if, for the sake of convenience, we assume the pit to have a radius of unity.

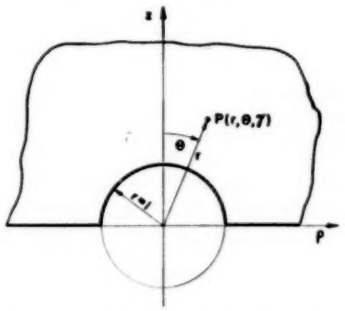

Fig. 1 Meridional Cross Section of the Pitted Region, Spherical Co-Ordinates

The body forces are assumed to vanish. In so far as the loading is concerned, we confine ourselves to the axisymmetric case in which the tractions at infinity constitute a plane hydrostatic field of stress parallel to the plane $z = 0$. It should be emphasized, however, that the method of solution adopted subsequently may be extended to the case in which the plane-stress field at infinity is no longer rotationally symmetric. In the present instance, the boundary conditions at infinity assume the form

$$\sigma_x, \sigma_y \to 1, \quad \sigma_z, \tau_{xy}, \tau_{yz}, \tau_{zx} \to 0 \text{ as } r \to \infty \quad \ldots\ldots [1]$$

where $(\sigma_x, \ldots \tau_{xy}, \ldots)$ are the Cartesian components of stress. With reference to spherical co-ordinates (r, θ, γ), introduced by the mapping

$$\left.\begin{aligned} x &= r \sin\theta \cos\gamma \\ y &= r \sin\theta \sin\gamma \\ z &= r \cos\theta \\ 0 \leq r < \infty, \quad 0 \leq \theta \leq \pi, &\quad 0 \leq \gamma \leq 2\pi \end{aligned}\right\} \quad \ldots [2]$$

the conditions to be met at the stress-free plane boundary appear as

$$\left.\begin{aligned} \sigma_\theta = \tau_{r\theta} = \tau_{\theta\gamma} &= 0 \\ \text{for } 1 \leq r < \infty, \quad \theta = \pi/2, &\quad 0 \leq \gamma \leq 2\pi \end{aligned}\right\} \quad \ldots [3]$$

whereas a traction-free surface of the pit requires

$$\left.\begin{aligned} \sigma_r = \tau_{r\theta} = \tau_{r\gamma} &= 0 \\ \text{for } r = 1, \quad 0 \leq \theta \leq \pi/2, &\quad 0 \leq \gamma \leq 2\pi \end{aligned}\right\} \quad \ldots [4]$$

in which $(\sigma_r, \ldots, \tau_{r\theta}, \ldots)$ are the spherical components of stress.

The two-dimensional analog of this problem, that is, the problem presented by the stress concentration around a semicircular notch in a semi-infinite plate which, at infinity, is in a state of uniaxial tension parallel to its straight edge, has received repeated attention. Maunsell (1)[3] obtained a series solution to this plane problem by first extending the uniform stress field at infinity throughout the half plane and then removing the tractions so arising on the notch with the aid of a doubly infinite sequence of particular solutions of the field equations. This sequence is constructed in such a manner that each of its members is singular at the center of the notch, and leaves the straight boundary, as well as infinity, free from tractions. Subsequently, Weinel (2) and C. B. Ling (3), using bipolar co-ordinates, arrived at more elegant integral representations of the solution to the plane problem. The application to the present space problem of analogous integral approaches, based on the use of toroidal co-ordinates, meets with great analytical difficulties.[4] The method of solution adopted here may be regarded as the three-dimensional counterpart of that employed by Maunsell (1).

Particular Solutions in Spherical Co-Ordinates

The problem characterized by the boundary Conditions [1], [3], and [4], may be attacked by any one of the various available stress-function approaches to axisymmetric problems in elasticity

[1] The results presented in this paper were obtained in the course of an investigation conducted under contract N7onr-32906 with the Office of Naval Research, Department of the Navy, Washington, D. C.

[2] Assistant Professor of Mechanics, Illinois Institute of Technology.

Contributed by the Applied Mechanics Division and presented at the Annual Meeting, New York, N. Y., November 29–December 4, 1953, of The American Society of Mechanical Engineers.

Discussion of this paper should be addressed to the Secretary, ASME, 29 West 39th Street, New York, N. Y., and will be accepted until April 12, 1954, for publication at a later date. Discussion received after the closing date will be returned.

Note: Statements and opinions advanced in papers are to be understood as individual expressions of their authors and not those of the Society. Manuscript received by ASME Applied Mechanics Division, January 23, 1953. Paper No. 53—A-8.

[3] Numbers in parentheses refer to the Bibliography at the end of the paper.

[4] One is led to a system of dual integral equations the kernels of which involve the Legendre functions of the first kind of complex index, $P_{-1/2+it}(q)$, where the index parameter t is the variable of integration. These functions have not been investigated extensively; see (4), p. 451.

theory.[5] We shall utilize the approach originated by Boussinesq (7), according to which the general solution of the displacement equations of equilibrium, in case of torsion-free rotational symmetry, and in the absence of body forces, is representable as the sum of the two displacement fields

$$2G\,(u_x, u_y, u_z) = \text{grad}\ \phi \qquad [5]$$

$$2G\,(u_x, u_y, u_z) = \text{grad}\ (z\,\psi) - 4(1-\nu)\,(0, 0, \psi) \qquad [6]$$

where

$$\nabla^2\phi(r, z) = 0, \qquad \Delta^2\psi(r, z) = 0 \qquad [7]$$

Here u_x, u_y, u_z are Cartesian components of displacement, $r = (x^2 + y^2 + z^2)^{1/2}$, ∇^2 is the Laplace operator, and G and ν are the shear modulus and Poisson's ratio, respectively.

For our present purposes it is expedient to refer to the spherical co-ordinates (r, θ, γ) defined by Equations [2]. The basic displacement fields given in Equations [5], [6], and their associated fields of stress, were transformed into general orthogonal axisymmetric co-ordinates in reference (6). The specific forms assumed by the Boussinesq solutions in spherical co-ordinates appear explicitly in reference (8), which also contains the particular solutions obtained upon introduction of the interior and exterior spherical harmonics of integral order as generating stress functions ϕ and ψ.

In view of the regularity requirements inherent in the current problem, we limit our attention to the two aggregates of harmonic stress functions

$$\left.\begin{aligned} \phi_n(r, \theta) &= r^{-n-1}\,P_n(\cos\theta) \\ \psi_n(r, \theta) &= r^{-n-1}\,P_n(\cos\theta) \\ (n &= 0, 1, 2, \ldots) \end{aligned}\right\} \qquad [8]$$

in which P_n denotes the Legendre polynomial of order n. The stress functions defined in Equations [8] represent exterior spherical harmonics and give rise to displacement and stress fields which are singular at the origin $r = 0$, are otherwise regular, and vanish at infinity. The particular solutions of the field equations generated by ϕ_n and ψ_n will be designated by $[A_n]$ and $[C_n]$, respectively. As explained in reference [8], considerable simplifications arise from a replacement of solution $[C_n]$ with the linear combination

$$[B_n] = (2n+1)\,[C_n] - (n + 4 - 4\nu)\,[A_{n-1}] \qquad [9][6]$$

We now cite[7] the displacement and stress fields appropriate to solutions $[A_n]$ and $[B_n]$. With the auxiliary notations

$$p = \cos\theta, \qquad q = \sin\theta \qquad [10]$$

we obtain for solution $[A_n]$

$$2Gu_r = -\frac{(n+1)\,P_n}{r^{n+2}}, \qquad 2Gu_\theta = -\frac{q\,P_n'}{r^{n+2}} \qquad [11][8]$$

$$\left.\begin{aligned} \sigma_r &= \frac{(n+1)(n+2)}{r^{n+3}}\,P_n \\ \sigma_\theta &= \frac{1}{r^{n+3}}\left[P_{n+1}' - (n+1)(n+2)\,P_n\right] \\ \sigma_\gamma &= -\frac{P_{n+1}'}{r^{n+3}}, \qquad \tau_{r\theta} = \frac{n+2}{r^{n+3}}\,q\,P_n' \end{aligned}\right\} \qquad [12]$$

On the other hand, for $[B_n]$ there results

$$\left.\begin{aligned} 2Gu_r &= -\frac{(n+1)(n+4-4\nu)}{r^{n+1}}\,P_{n+1} \\ 2Gu_\theta &= -q\,\frac{(n-3+4\nu)}{r^{n+1}}\,P_{n+1}' \end{aligned}\right\} \qquad [13]$$

$$\left.\begin{aligned} \sigma_r &= (n+1)\left[(n+1)(n+4) - 2\nu\right]\frac{P_{n+1}}{r^{n+2}} \\ \sigma_\theta &= \frac{-1}{r^{n+2}}\left[(n+1)(n^2 - n + 1 - 2\nu)\,P_{n+1}\right. \\ &\qquad \left. - (n - 3 + 4\nu)\,P_n'\right] \\ \sigma_\gamma &= \frac{-1}{r^{n+2}}\left[(1-2\nu)(n+1)(2n+1)\,P_{n+1}\right. \\ &\qquad \left. + (n - 3 + 4\nu)\,P_n'\right] \\ \tau_{r\theta} &= (n^2 + 2n - 1 + 2\nu)\,q\,\frac{P_{n+1}'}{r^{n+2}} \end{aligned}\right\} \qquad [14]$$

In the preceding equations u_r, u_θ, and σ_r, σ_θ, σ_γ, $\tau_{r\theta}$ denote spherical components of displacement and stress, respectively; the displacement u_γ and the stresses $\tau_{\gamma r}$, $\tau_{\gamma\theta}$, which vanish identically by virtue of rotational symmetry, have been omitted.

The physical significance of the sequences of solutions $[A_n]$, $[B_n]$, $(n = 0, 1, 2, \ldots)$, was examined in reference (8). Solution $[A_0]$ may be identified as that appropriate to a center of compression at the origin, whereas $[B_0]$ is the solution corresponding to a concentrated force acting at $r = 0$ in an infinite body, in the direction of the negative z-axis.[9] Moreover, in Cartesian co-ordinates

$$\left.\begin{aligned} [A_n] &= \frac{(-1)^n}{\lfloor n}\,\frac{\partial^n}{\partial z^n}\,[A_0] \\ [B_n] &= \frac{(-1)^n\,(2n+1)}{\lfloor n}\,\frac{\partial^n}{\partial z^n}\,[B_0] + (n - 3 + 4\nu)\,[A_{n-1}] \\ (n &= 1, 2, 3, \ldots). \end{aligned}\right\} \qquad [15]$$

Hence these two aggregates represent sequences of successively higher singularities which may be obtained by suitable limit processes applied to the basic axisymmetric singularities corresponding to solutions $[A_0]$ and $[B_0]$. In particular, $[B_1]$ represents a force doublet along the z-axis together with a center of compression, both located at the origin. We note that solutions $[A_n]$ $(n = 0, 1, 2, \ldots)$, and $[B_n]$ $(n = 1, 2, 3, \ldots)$, are self-equilibrated in the sense that the associated tractions on any closed surface surrounding the origin are statically equivalent to null.

In the specific problem to be treated presently we need to construct particular solutions which leave the plane $z = 0$ $(p = 0)$ free from surface tractions. To this end, we recall that

$$P_{2n+1}(0) = 0, \qquad P_{2n}'(0) = 0, \qquad (n = 0, 1, 2, \ldots). \qquad [16]$$

Furthermore, Equations [16], by virtue of the Legendre recurrence relations

$$\left.\begin{aligned} (2n+1)p\,P_n &= (n+1)\,P_{n+1} + nP_{n-1} \\ q^2\,P_n' &= nP_{n-1} - npP_n \end{aligned}\right\} \qquad [17]$$

imply

$$\left.\begin{aligned} P_{2n+1}'(0) &= (2n+1)\,P_{2n}(0) \\ P_{2n+2}(0) &= -\frac{2n+1}{2n+2}\,P_{2n}(0) \\ P_{2n}(0) &= (-1)^n\,\frac{\lfloor 2n}{2^{2n}(\lfloor n)^2} \\ (n &= 0, 1, 2, \ldots). \end{aligned}\right\} \qquad [18]$$

[5] Reference (5), chapter viii, and reference (6).

[6] In Equation [9], as in subsequent equations, the letters in brackets denote either the displacement-vector field or the stress-tensor field, and equality, addition, as well as multiplication by a scalar, are to be interpreted accordingly.

[7] See Equations [12], [13], [17], [18] of reference (8).

[8] The argument of P_n is henceforth understood to be p and $P_n' = \frac{dP_n}{dp}$.

[9] Reference (9), pp. 185–187.

Substitution of Equations [16], [18] into [12], [14] thus yields for the normal and shearing stresses of solutions $[A_n]$ and $[B_n]$, on the plane $p = 0$, the following values:

For solution $[A_{2n}]$

$$\sigma_\theta = -\frac{(2n+1)^2}{r^{2n+3}} P_{2n}(0), \quad \tau_{r\theta} = 0 \qquad [19]$$

For solution $[A_{2n+1}]$

$$\sigma_\theta = 0, \quad \tau_{r\theta} = \frac{(2n+1)(2n+3)}{r^{2n+4}} P_{2n}(0) \qquad [20]$$

For solution $[B_{2n+1}]$

$$\sigma_\theta = \frac{(2n+1)(4n^2+4n-1+2\nu)}{r^{2n+3}} P_{2n}(0), \quad \tau_{r\theta} = 0 \qquad [21]$$

For solution $[B_{2n+2}]$

$$\sigma_\theta = 0,$$

$$\tau_{r\theta} = -\frac{(2n+1)(2n+3)(4n^2+12n+7+2\nu)}{(2n+2)\, r^{2n+4}} P_{2n}(0) \qquad [22]$$

In view of Equations [19] to [22], it is clear that the linear combinations

$$\left.\begin{aligned} [D_n] &= \alpha_{2n}[A_{2n}] + (2n+1)[B_{2n+1}] \\ [E_n] &= \alpha_{2n+2}[A_{2n+1}] + (2n+2)[B_{2n+2}] \\ &\quad (n = 0, 1, 2, \ldots) \end{aligned}\right\} \qquad [23]$$

where

$$\alpha_{2n} \equiv (2n+1)^2 - 2 + 2\nu \qquad [24]$$

satisfy Equations [3]; that is, clear the plane $z = 0$ from tractions. From Equations [11], [12], [13], [14], we obtain for $[D_n]$

$$\left.\begin{aligned} 2Gu_r &= -\frac{2n+1}{r^{2n+2}}\left[\alpha_{2n} P_{2n} + (2n+2)(2n+5-4\nu) P_{2n+2}\right] \\ 2Gu_\theta &= -\frac{p}{r^{2n+2}}\left[\alpha_{2n} P_{2n}' + (2n-2+4\nu)(2n+1) P_{2n+2}'\right] \end{aligned}\right\} \qquad [25]$$

$$\left.\begin{aligned} \sigma_r &= \frac{(2n+1)(2n+2)}{r^{2n+3}}(\alpha_{2n} P_{2n} + \beta_{2n} P_{2n+2}) \\ \sigma_\theta &= \frac{1}{r^{2n+3}}\left\{[\alpha_{2n} + (2n+1)(2n-2+4\nu)] P_{2n+1}' - (2n+1)(2n+2)[\alpha_{2n} P_{2n} + (\alpha_{2n} - 2n + 2 - 4\nu) P_{2n+2}]\right\} \\ \sigma_\gamma &= -\frac{4n+3}{r^{2n+3}}\left[(2n+1)(2n+2)(1-2\nu) P_{2n+2} + (2n-1+2\nu) P_{2n+1}'\right] \\ \tau_{r\theta} &= \frac{p}{r^{2n+3}}\left[(2n+2)\alpha_{2n} P_{2n}' + (2n+1)\alpha_{2n+1} P_{2n+2}'\right] \end{aligned}\right\} \qquad [26]$$

and for $[E_n]$

$$\left.\begin{aligned} 2Gu_r &= -\frac{2n+2}{r^{2n+3}}\left[\alpha_{2n+2} P_{2n+1} + (2n+3)(2n+6-4\nu) P_{2n+3}\right] \\ 2Gu_\theta &= -\frac{p}{r^{2n+3}}\left[\alpha_{2n+2} P_{2n+1}' + (2n+2)(2n-1+4\nu) P_{2n+3}'\right] \end{aligned}\right\} \qquad [27]$$

$$\left.\begin{aligned} \sigma_r &= \frac{(2n+2)(2n+3)}{r^{2n+4}}(\alpha_{2n+2} P_{2n+1} + \beta_{2n+1} P_{2n+3}) \\ \sigma_\theta &= \frac{1}{r^{2n+4}}\left\{[\alpha_{2n+2} + (2n+2)(2n-1+4\nu)] P_{2n+2}' - (2n+2)(2n+3)[\alpha_{2n+2} P_{2n+1} + (\alpha_{2n+1} - 2n + 1 - 4\nu) P_{2n+3}]\right\} \\ \sigma_\gamma &= -\frac{4n+5}{r^{2n+4}}\left[(2n+1+2\nu) P_{2n+2}' + (1-2\nu)(2n+2)(2n+3) P_{2n+1}\right] \\ \tau_{r\theta} &= \frac{p}{r^{2n+4}}\alpha_{2n+2}\left[(2n+2) P_{2n+2}' + (2n+3) P_{2n+1}'\right] \end{aligned}\right\} \qquad [28]$$

where

$$\beta_n \equiv (n+2)(n+5) - 2\nu \qquad [29]$$

Solutions $[D_n]$ and $[E_n]$ are self-equilibrated in the upper half space, in the sense that the resultant of the corresponding tractions vanishes on a hemisphere centered at $r = 0$ and lying in the region $z \geq 0$. To show this, we observe that for any axisymmetric stress field this resultant is a single force coincident with the z-axis, the magnitude of which is given by

$$Z(r) = -2\pi r^2 \int_0^1 (p\sigma_r - p\,\tau_{r\theta})\, dp \qquad [30]$$

where $Z(r)$ is positive if its sense is that of the positive z-axis Equation [30], after a trivial computation, yields for the first Boussinesq solution, defined by Equation [5]

$$Z(r) = 2\pi r \left.\frac{\partial \phi}{\partial r}\right|_{p=0} \qquad [31]$$

whereas for the second Boussinesq solution, defined by Equation [6], we reach

$$Z(r) = 4\pi(1-\nu) r^2 \int_0^1 \frac{\partial \psi}{\partial r}\, dp \qquad [32]$$

Equations [31], [32], together with [8], [9], [23], [24], confirm the self-equilibrance in the upper half space of $[D_n]$, $[E_n]$. We note that self-equilibrance, in the present sense, is not a necessary consequence of the requirement that the tractions of a solution be zero on the plane $p = 0$, with the exception of the origin. The well-known solution of Boussinesq corresponding to a concentrated normal load on the half space[10] conforms to this requirement but, evidently, is not self-equilibrated.

The physical significance of the singular solutions $[D_n]$, $[E_n]$ can be exhibited readily. For example, $[D_0]$ corresponds[11] to two mutually perpendicular tangential force doublets, acting at the origin, on the plane $p = 0$. The physical significance of the other members of these two aggregates, similarly, can be established through suitable limit processes applied to the solutions corresponding to various configurations of normal and tangential forces acting on the plane boundary of the half space.

Solution of Problem

We assume the solution [S] to the problem characterized by the boundary Conditions [1], [3], [4] in the form

$$[S] = [U] + [R] \qquad [33]$$

Solution [U] corresponds to the uniform stress field

$$\sigma_x = \sigma_y = 1, \qquad \sigma_z = \tau_{xy} = \tau_{yz} = \tau_{zx} = 0 \qquad [34]$$

[10] Reference (9), p. 191.
[11] Reference (10).

or, with reference to spherical co-ordinates, to

$$\left.\begin{aligned} \sigma_r &= \bar{p}^2, \quad & \sigma_\theta &= p^2 \\ \sigma_\gamma &= 1, & \tau_{r\theta} &= \bar{p}p \end{aligned}\right\} \quad \ldots\ldots\ldots\ldots [35]^{12}$$

where p, $\bar{p}$ are defined in Equations [10], while [R] is the solution to the "residual" problem, the definition of which is implicit in Equation [33]. Thus [R] is characterized by the boundary Conditions [3], in addition to the requirement

$$\sigma_r, \sigma_\theta, \sigma_\gamma, \tau_{r\theta} \to 0 \text{ as } r \to \infty \ldots\ldots\ldots\ldots [36]^{12}$$

and must satisfy

$$\left.\begin{aligned} &\sigma_r = -\bar{p}^2, \tau_{r\theta} = -\bar{p}p \\ &\text{for } r = 1, 0 \leq p \leq 1, 0 \leq \gamma \leq 2\pi \end{aligned}\right\} \quad \ldots\ldots\ldots [37]$$

The tractions of [R] on the surface of the pit have zero resultant. Since, furthermore, [R] must leave the surface $1 \leq r < \infty$, $p = 0$ free from tractions, we are led to expand [R] in terms of the two aggregates of solutions $[D_n]$, $[E_n]$, Equations [23] to [29], which possess both of these properties. Thus we assume

$$[R] = \sum_{n=0}^{\infty} \{a_n [D_n] + b_n [E_n]\} \ldots\ldots\ldots [38]$$

where a_n, b_n ($n = 0, 1, 2, \ldots$) are, as yet, arbitrary.

In view of the fact that each $[D_n]$, $[E_n]$ ($n = 0, 1, 2, \ldots$) satisfies the boundary Conditions [3], [36], the same is true of [R] provided the series in Equation [38] converges suitably. With a view toward meeting the boundary Conditions [37], we observe that they may be written as

$$\left.\begin{aligned} &\sigma_r = -\frac{2}{3} P_0 + \frac{2}{3} P_2, \quad \tau_{r\theta} = -\frac{1}{3} \bar{p} P_2' \\ &\text{for } r = 1, 0 \leq p \leq 1, 0 \leq \gamma \leq 2\pi \end{aligned}\right\} \quad \ldots [39]$$

Furthermore, the expansions,[13]

$$\left.\begin{aligned} P_{2k+1}(p) &= (2k+1) P_{2k}(0) \sum_{n=0}^{\infty} \omega_k^{(n)} P_{2n}(p) \\ P_{2k+1}'(p) &= (2k+1) P_{2k}(0) \sum_{n=0}^{\infty} \omega_k^{(n)} P_{2n}'(p) \\ \omega_k^{(n)} &= \frac{(4n+1) P_{2n}(0)}{(2k+1-2n)(2k+2+2n)} \\ & \qquad 0 < p \leq 1 \end{aligned}\right\} \quad \ldots [40]$$

with the aid of Equations [28], lead to the following Legendre series representation of σ_r, $\tau_{r\theta}$ of $[E_k]$ on $r = 1, 0 \leq p \leq 1$

$$\left.\begin{aligned} \sigma_r &= (2k+1)(2k+3) P_{2k}(0) \sum_{n=0}^{\infty} [(2k+2)\alpha_{2k+2} \omega_k^{(n)} \\ &\qquad - (2k+3) \beta_{2k+1} \omega_{k+1}^{(n)}] P_{2n}(p) \\ \tau_{r\theta} &= (2k+1)(2k+3) P_{2k}(0) \alpha_{2k+2} \bar{p} \sum_{n=1}^{\infty} \\ &\qquad [\omega_k^{(n)} - \omega_{k+1}^{(n)}] P_{2n}'(p) \\ &\text{for } r = 1, \quad 0 \leq p \leq 1, \quad 0 \leq \gamma \leq 2\pi \end{aligned}\right\} \quad . [41]^{14}$$

Application of the boundary Conditions [37] to [R] in Equation [38], by aid of Equations [26] and [41], yields a doubly infinite system of equations for the coefficients of superposition a_n, b_n ($n = 0, 1, 2, \ldots$). These equations are equivalent to the following set

$$\left.\begin{aligned} a_{n-1} &= \\ &\frac{(2n+2)\alpha_{2n}}{\Delta_n} \left[\frac{5}{3} \delta_1^{(n)} + \sum_{k=0}^{\infty} \left\{ (2n-2k-1) \alpha_{2k+2} \omega_k^{(n)} \right.\right. \\ &\qquad \left.\left. + [(2k+3)\beta_{2k+1} - (2n+1)\alpha_{2k+2}] \omega_{k+1}^{(n)} \right\} c_k \right] \\ &\qquad (n = 1, 2, 3, \ldots), \\ a_n &= \frac{(2n-1)}{\Delta_n} \left[\frac{2}{3} \delta_0^{(n)} - 8\delta_1^{(n)} + \sum_{k=0}^{\infty} \{ [(2k+2)\alpha_{2n-1} \right. \\ &\qquad - 2n\beta_{2n-2}] \alpha_{2k+2} \omega_k^{(n)} \\ &\qquad \left. + [2n\beta_{2n-2}\alpha_{2k+2} - (2k+3)\alpha_{2n-1}\beta_{2k+1}] \omega_{k+1}^{(n)} \} c_k \right] \\ &\qquad (n = 0, 1, 2, \ldots) \end{aligned}\right\} \quad \ldots [42]$$

where $\delta_m^{(n)}$ is the Kronecker delta and

$$\left.\begin{aligned} c_k &= (2k+1)(2k+3) P_{2k}(0) b_k, \ \alpha_{-1} = 1 \\ \Delta_n &= (2n-1)(2n+2)\alpha_{2n}[2n\beta_{2n-2} - (2n+1)\alpha_{2n-1}] \end{aligned}\right\} \quad . [43]$$

The elimination of a_n between the two systems of equations given in Equations [42] yields an infinite system of equations for the unknowns c_k ($k = 0, 1, 2, \ldots$). Since these equations are at once obtainable from Equations [42], they may be omitted here. Once the c_k have been determined, the coefficients of superposition a_n, b_n follow from Equations [42], [43]. The values of these coefficients, together with Equations [24] to [29], [33], [35], [38], constitute the complete solution of the problem.

Stress Evaluations, Acceleration of Convergence, Numerical Results

The infinite system of equations for the c_k, which is immediate from Equations [42], was dealt with by the usual segmentation process, for $\nu = 1/4$. Thus systems of n-equations in n-unknowns, which correspond to principal submatrices of rank n, were solved for values of n ranging from 10 to 26. The systems of equations for $n = 25$ and $n = 26$ yield coefficients c_k which agree to the number of figures shown in Table 1. These values were used in the subsequent stress computations.

TABLE 1 NUMERICAL VALUES OF c_n FOR $\nu = 1/4$

n	c_n
0	−0.1581991
1	0.0467453
2	0.0060369
3	0.0015518
4	0.0004917
5	0.0001635
6	0.0000473

The series, Equations [42], for a_n, converge slowly and, consequently, the same applies to the series for the individual stress components. For the purpose of accelerating the convergence, the following method of stress computation was adopted: Let $s_n(r, \theta)$ be a representative stress component of $[D_n]$. If the first of Equations [42] is written in the form

$$a_{n-1} = f_n + \sum_{k=0}^{\infty} g_n^{(k)} c_k, \ (n = 1, 2, 3, \ldots) \ldots\ldots [44]$$

the corresponding representative stress component $s(r, \theta)$ of

$$\sum_{n=1}^{\infty} a_{n-1} [D_{n-1}]$$

[12] The stresses $\tau_{\gamma r}$ and $\tau_{\gamma\theta}$ are zero by virtue of rotational symmetry and have been omitted.

[13] See, for example, reference (4), pp. 38, 39.

[14] Note that although Equations [40] hold only for the open interval $0 < p \leq 1$, Equations [41] are valid for the closed interval since $\tau_{r\theta}$ of $[E_k]$ vanishes for $p = 0$.

becomes

$$\left.\begin{aligned} s &= \sum_{n=1}^{\infty} a_{n-1}\, s_{n-1} \\ &= \sum_{n=1}^{\infty} \left[f_n + \sum_{k=0}^{\infty} g_n^{(k)}\, c_k \right] s_{n-1} \\ &= \sum_{n=1}^{\infty} f_n\, s_{n-1} + \sum_{k=0}^{\infty} \left[\sum_{n=1}^{\infty} g_n^{(k)}\, s_{n-1} \right] c_k \end{aligned}\right\} \quad \ldots\ldots [45]$$

The slow convergence of the double series in Equations [45] is readily traced to the slow convergence of the series

$$q^{(k)} = \sum_{n=1}^{\infty} g_n^{(k)}\, s_{n-1} \quad \ldots\ldots [46]$$

Since the general term in the series for $q^{(k)}$ is available from Equations [26], [42], [44], Kummer's transformation[15] can be used to accelerate the convergence. Thus a sequence of functions $h_n^{(k)}(r, \theta)$ is determined such that

$$\lim_{n \to \infty} \frac{g_n^{(k)}\, s_{n-1}}{h_n^{(k)}} = 1, \quad (k = 0, 1, 2, \ldots) \quad \ldots\ldots [47]$$

and

$$H^{(k)} = \sum_{n=1}^{\infty} h_n^{(k)} \quad \ldots\ldots [48]$$

admits a closed representation. One then has

$$q^{(k)} = H^{(k)} + \sum_{n=1}^{\infty} [g_n^{(k)}\, s_{n-1} - h_n^{(k)}] \quad \ldots\ldots [49]$$

The series in Equation [49] converges faster than that in Equation [46].

We illustrate the foregoing procedure with the stress component σ_θ, on the axis of symmetry, which is of primary interest in the present investigation. Thus let s in the preceding discussion be σ_θ for $p = 1$. Since

$$P_n(1) = 1, \quad P_n'(1) = \frac{n(n+1)}{2}, \quad (n = 0, 1, 2, \ldots) \quad [50][16]$$

we have from Equations [26], [42], [43], and [50], with $\nu = 1/4$

$$\left.\begin{aligned} g_n^{(k)}\, s_{n-1} &= \frac{n(4n-3)(16n^2-1)(2n\,\xi_k + \zeta_k)\, P_{2n}(0)}{(16n^2+4n+3)(2n+2k+2)(2n-2k-3)(2n+2k+4) r^{2n+2}} \\ \xi_k &= (2k+3)\,\beta_{2k+1} - (2k+2)\,\alpha_{2k+2} \\ \zeta_k &= (2k+3)(2k+2)\,\beta_{2k+1} - 2(2k^2+8k+7)\,\alpha_{2k+2} \\ & (n = 1, 2, 3, \ldots), (k = 0, 1, 2, \ldots) \end{aligned}\right\} \quad \ldots [51]$$

for the general term in Equation [46]. We now choose $h_n^{(k)}$ in Equation [47] in the form

$$\left.\begin{aligned} h_n^{(k)} &= \frac{(4n^2\,\xi_k + 2nL_k + M_k)\, P_{2n}(0)}{(2n+1)(2n+2)\, r^{2n+2}} \\ & (n = 1, 2, 3, \ldots), (k = 0, 1, 2, \ldots), \end{aligned}\right\} \quad \ldots\ldots [52]$$

where L_k, M_k are independent of n. Equation [52] evidently conforms to the limit Condition [47] for arbitrary choice of the sequences L_k, M_k and, as will be seen later, the corresponding $H^{(k)}$ in Equations [48] admits a closed representation. It is apparent from Equation [47] that the best possible convergence, within the present choice of $h_n^{(k)}$, of the series in Equation [46], is secured by determining L_k, M_k in such a way that the coefficients of the highest power of n in the numerator of

$$\frac{g_n^{(k)}\, s_{n-1} - h_n^{(k)}}{h_n^{(k)}} \quad \ldots\ldots [53]$$

vanish. This requirement leads to

$$\left.\begin{aligned} L_k &= \zeta_k - (2k+2)\,\xi_k \\ M_k &= (16k^2 + 44k + 24)\,\xi_k - (2k+2)\,\zeta_k \\ & (k = 0, 1, 2, \ldots) \end{aligned}\right\} \quad \ldots [54]$$

We now proceed to establish $H^{(k)}$ in closed form. To this end we recall[17] that

$$\sum_{n=1}^{\infty} \mu^{2n} P_{2n}(0) = \frac{1}{\sqrt{1+\mu^2}} - 1, \quad 0 \le \mu \le 1 \quad \ldots [55]$$

Two successive integrations with respect to μ of Equation [55], and subsequent division by μ^2, yield

$$\sum_{n=1}^{\infty} \frac{\mu^{2n} P_{2n}(0)}{(2n+1)(2n+2)} = \frac{\sinh^{-1}\mu}{\mu} - \frac{\sqrt{1+\mu^2}}{\mu^2} + \frac{1}{\mu^2} - \frac{1}{2} \quad \ldots [56]$$

Similarly, we obtain by successive differentiation with respect to μ of Equation [56]

$$\left.\begin{aligned} \sum_{n=1}^{\infty} \frac{2n\,\mu^{2n} P_{2n}(0)}{(2n+1)(2n+2)} &= -\frac{\sinh^{-1}\mu}{\mu} + \frac{2\sqrt{1+\mu^2}}{\mu^2} - \frac{2}{\mu^2} \\ \sum_{n=1}^{\infty} \frac{(2n)^2 \mu^{2n} P_{2n}(0)}{(2n+1)(2n+2)} &= \frac{\sinh^{-1}\mu}{\mu} - \frac{(4+3\mu^2)}{\mu^2\sqrt{1+\mu^2}} + \frac{4}{\mu^2} \end{aligned}\right\} \quad \ldots [57]$$

In view of Equations [48], [52], $H^{(k)}$ in the present instance is obtained by replacing μ in Equations [56], [57] with r^{-1}, subsequently dividing these equations by r^2, and forming the linear combination apparent from Equation [52]. This computation results in

$$\left.\begin{aligned} H^{(k)} &= (\xi_k - L_k + M_k) \frac{\sinh^{-1}\left(\frac{1}{r}\right)}{r^2} + \frac{\xi_k}{r^2\sqrt{r^2+1}} \\ &\quad + (4\xi_k - 2L_k + M_k)\left(\frac{1}{r} - \frac{\sqrt{r^2+1}}{r^2}\right) - \frac{M_k}{2r^2} \\ & (k = 0, 1, 2, \ldots) \end{aligned}\right\} \quad \ldots [58]$$

[15] See, for example, reference (11), p. 247.

[16] Reference (12), p. 553.

[17] Reference (4), p. 15.

To demonstrate the improvement in the convergence of the original series for $q^{(k)}$, Equations [46], in the present instance, we observe that the general term in this series is of the order $(r^{2n+3}\, n^{3/2})^{-1}$ as $n \to \infty$, whereas $g_n^{(k)}\, s_{n-1} - h_n^{(k)}$ in Equations [49] here is of the order $(r^{2n+3}\, n^{3/2})^{-1}$.

An analogous procedure was used in the determination of σ_r for $r = 1$, $p = 1$, which was computed merely as a check on the satisfaction of the boundary conditions. Within the number of terms considered in the numerical evaluations of the series solution established earlier, this value of σ_r, which should be zero, was found to be -4×10^{-3} for $\nu = 1/4$. This indicates satisfaction of the boundary conditions to at least four significant figures. The variation of the maximum stress σ_θ along the axis of symmetry is shown in Table 2. These results are compared

TABLE 2 STRESS σ_θ FOR $p = 1$, $\nu = 1/4$

r	σ_θ
1	2.23
1.15	1.63
1.35	1.29
1.55	1.15
2	1.04
3	1.00

in Fig. 2 with the corresponding stress values given by Maunsell

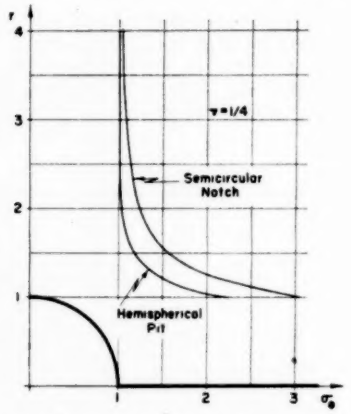

FIG. 2 DECAY OF MAXIMUM STRESS σ_θ, ALONG AXIS OF SYMMETRY $\sigma_x = \sigma_y = 1$ AT INFINITY

(1) for the plane analog of the present space problem. As usual, the stress concentration in the space problem is found to be less severe in intensity and more localized in character than it is in its two-dimensional counterpart.

It is interesting to note that the maximum value 2.23 of σ_θ at the bottom of the pit is 7 per cent larger than the maximum stress concentration induced by a spherical cavity in an infinite medium under the same loading conditions,[18] and for $\nu = 1/4$. In contrast, the maximum stress concentration at the bottom of a semicircular notch in a plate under unit tension at infinity is only 2 per cent larger than the corresponding value appropriate to the infinite plate with a circular hole.[19]

ACKNOWLEDGMENT

The author is greatly indebted to Dr. E. Sternberg for invaluable advice and guidance in this investigation. Thanks are also due to Dr. M. A. Sadowsky for helpful suggestions. The assistance of Messrs. S. Parter, K. Fukuda, and W. F. Darsow in voluminous numerical computations is gratefully acknowledged.

BIBLIOGRAPHY

1 "Stresses in a Notched Plate Under Tension," by F. G. Maunsell, *London, Edinburgh and Dublin Philosophical Magazine*, series 7, vol. 21, 1936, p. 765.

2 "Die Spannungserhohung durch Kreisbogenkerben," by E. Weinel, *Zeitschrift für angewandte Mathematik und Mechanik*, vol. 21, 1941, p. 228.

3 "On the Stresses in a Notched Plate Under Tension," by Chih-Bing Ling, *Journal of Mathematics and Physics*, vol. 26, 1947, p. 284.

4 "The Theory of Spherical and Ellipsoidal Harmonics," by E. W. Hobson, Cambridge University Press, Cambridge, England, 1931.

5 "Tratado de Elasticidad," by E. Butty, Centro Estudiantes de Ingenieria, Buenos Aires, Argentine, 1946.

6 "On the Stress-Function Approaches of Boussinesq and Timpe to the Axisymmetric Problem of Elasticity Theory," by E. Sternberg, R. A. Eubanks, and M. A. Sadowsky, *Journal of Applied Physics*, vol. 22, 1951, pp. 1121–1124.

7 "Application des Potentiels," by J. Boussinesq, Gauthier Villars, Paris, France, 1885.

8 "On the Axisymmetric Problem of Elasticity Theory for a Region Bounded by Two Concentric Spheres," by E. Sternberg, R. A. Eubanks, and M. A. Sadowsky, Proceedings of the First National Congress of Applied Mechanics, June, 1951 . . . THE AMERICAN SOCIETY OF MECHANICAL ENGINEERS, New York, N. Y., 1952, pp. 209–215.

9 "A Treatise on the Mathematical Theory of Elasticity," by A. E. H. Love, fourth edition, Dover Publications, New York, N. Y., 1944.

10 "The Elastic Sphere Under Concentrated Loads," by E. Sternberg and F. Rosenthal, JOURNAL OF APPLIED MECHANICS, Trans. ASME, vol. 74, 1952, pp. 413–421.

11 "Theory and Application of Infinite Series," by K. Knopp, Hafner Publishing Company, New York, N. Y., 1947.

12 "On a Simple Property of the Derivatives of Legendre's Polynomials," by E. Grosswald, Proceedings of the American Mathematical Society, vol. 1, 1950, pp. 553, 554.

13 "Theory of Elasticity," by S. Timoshenko and J. N. Goodier, McGraw-Hill Book Company, New York, N. Y., 1951.

[18] Reference (13), pp. 359–362.

[19] References (1, 2, 3).

Analysis of Plastic Deformation in a Steel Cylinder Striking a Rigid Target

By E. H. LEE[1] and S. J. TUPPER[2]

The G. I. Taylor dynamic compression test consists of firing a cylinder of the material to be tested at a target of hardened armor plate, and deducing the dynamic yield stress from the resulting deformation. In the interpretation of the results, interest is concentrated on the wave front of initial plastic straining. The present paper attempts the theoretical determination of the entire strain distribution in such a test cylinder of nickel-chrome steel, this material being chosen since the dynamic influence on the stress-strain relation is likely to be small, thus permitting the static relation to be used in the theory. Strain distributions deduced by two theoretical approaches compare satisfactorily with the distribution of strain obtained in such a dynamic compression test, thus justifying the assumption for this material at the speed considered. The treatment of this problem requires a theory of the propagation of plastic waves, which is developed in this paper, for the particular type of stress-strain curve pertaining to the high-strength alloy steel tested.

Introduction

It was considered that a theoretical analysis of the entire deformation in a G. I. Taylor dynamic compression test (1)[3] would be of interest. This requires the calculation of the strain distribution produced in a cylinder fired normally with given velocity at a rigid target plate. The analysis was made possible by the development of the theory of the propagation of plastic waves originated by G. I. Taylor (2) and independently by Th. von Kármán (3). Their theory covers stress waves in a material in which the nominal stress-strain curve is convex to the direction of increasing stress and a problem of this type of impact in such a material has been treated by Lee (4). The theory requires modification for analysis of the present material for which the increasing cross section with increasing plastic strain in compression leads to a nominal stress-strain curve which is concave to the direction of increasing stress.

The present work is based on the static stress-strain curve. It is known (see, for example, reference 5) that the increase in yield stress resulting from dynamic loading tends to be small for high-strength alloy steels, and it therefore seems likely that the static stress-strain curve will be least modified by the conditions in the dynamic compression test for materials of this type. Hence the present work is based on a high-strength alloy steel.

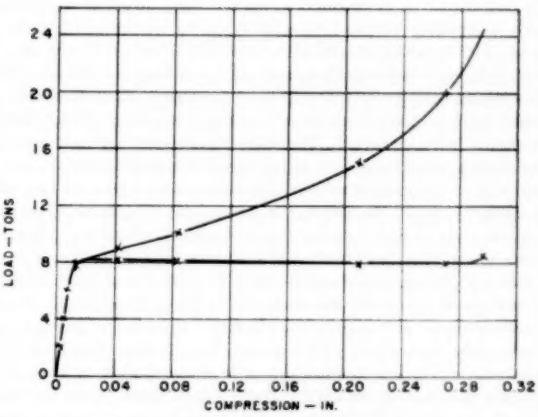

Fig. 1 Load-Compression Curve for Cylinders, 0.3 In. Diam, 0.45 In. Long, of Ni-Cr Steel

(Lower curve corrected for increase in cross section of specimen.)

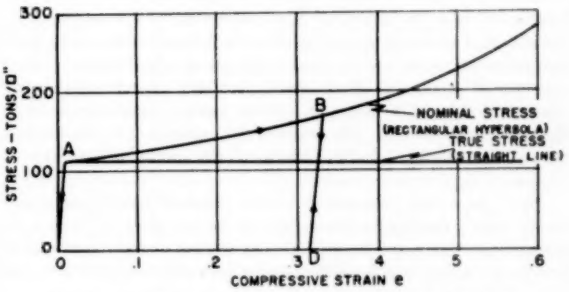

Fig. 2 Assumed Stress-Strain Curve in Compression

(Lower curve, true stress; upper curve, nominal stress.)

Fig. 1 shows a load-compression curve, taken at the National Physical Laboratory, for the steel under consideration. It is evident that the true stress-strain curve, based on the varying cross-sectional area of the specimen as the test proceeds, can be represented adequately by an elastic line, followed by plastic flow at constant stress. Fig. 2 shows both the true stress, and nominal stress (stress based on the original cross-sectional area)—strain curves using this assumption. The latter takes the form of a rectangular hyperbola in the region of plastic flow. The plastic-wave theory is carried out on the basis of these curves.

Firings were carried out by A. C. Whiffin and H. L. D. Pugh of the Road Research Laboratory, Department of Scientific and Industrial Research, for comparison with the theoretical strain distribution, and as detailed later, satisfactory agreement was obtained.

Initial Stress Wave Resulting From Impact

When the cylinder first strikes the rigid target plate, a compressive stress wave emanates from the surface of contact. It is

[1] Professor of Applied Mathematics, Brown University, Providence, R. I. Mem. ASME.

[2] Scientific Officer, Armaments Research Establishment, Fort Halstead, Sevenoaks, Kent, England.

[3] Numbers in parentheses refer to the Bibliography at the end of the paper.

Contributed by the Applied Mechanics Division and presented at the Annual Meeting, New York, N. Y., November 29–December 4, 1953, of The American Society of Mechanical Engineers.

Discussion of this paper should be addressed to the Secretary, ASME, 29 West 39th Street, New York, N. Y., and will be accepted until April 12, 1954, for publication at a later date. Discussion received after the closing date will be returned.

Note: Statements and opinions advanced in papers are to be understood as individual expressions of their authors and not those of the Society. Manuscript received by ASME Applied Mechanics Division, January 22, 1953. Paper No. 53—A-28.

the plastic deformation caused by this wave front as modified by reflections from the free end of the cylinder which is to be calculated.

We consider first the initial stress wave emanating from the surface of impact before any reflections have taken place at the rear of the cylinder. It is perhaps simpler to consider the motion relative to the initial steady motion of the cylinder, and this course has been adopted. Therefore we consider the cylinder and target at rest in contact, when the rigid target is suddenly given a forward constant velocity equal to the velocity of impact. The resulting stress waves are not affected by the constant velocity thus superimposed on the actual conditions. If the striking velocity is only sufficient to cause a stress below the elastic limit, a stress wave front travels down the cylinder with the elastic wave velocity. The material through which the wave front has passed is subject to uniform compressive stress proportional to the impact velocity, and moves with the velocity of the target. When the striking velocity exceeds that required to produce a stress equal to the elastic limit, the theory of plastic waves mentioned previously (2, 3) shows that each increment of stress is propagated along the cylinder with the velocity based on the gradient of the stress-strain curve at that stress. For a stress-strain curve convex toward the direction of increasing stress, this leads to a continuously broadening plastic wave front since each increment of stress is propagated with a monotonically decreasing velocity. For a stress-strain curve of the form shown in Fig. 2, however, such a plastic wave front would tend to close up, and the conditions of the problem of the initial wave emanating from the surface of contact can be satisfied only by the assumption of a plastic shock wave front across which a stress discontinuity occurs as was pointed out by White and Griffis (6) and by Lee (7). The relationship between impact velocity and resulting maximum stress is obtained from the Hugoniot relations across a wave front which are developed later. The concept of a plastic shock wave involving discontinuities in stress and velocity is based on certain assumptions discussed at the end of this section. In practice the existence of discontinuities will be inhibited by the effects of the inertia of lateral expansion.

Fig. 3 shows the progress of a wave of stress discontinuity (or shock wave) moving to the right. It is convenient to use Lagrange co-ordinates; i.e., a particular section of the rod is specified by its distance x from the impact end while the rod is in its initially unstrained condition. Though the strain due to impact produces relative displacements of the various sections, conditions at a section are always expressed as functions of the time t, and this original abscissa x.

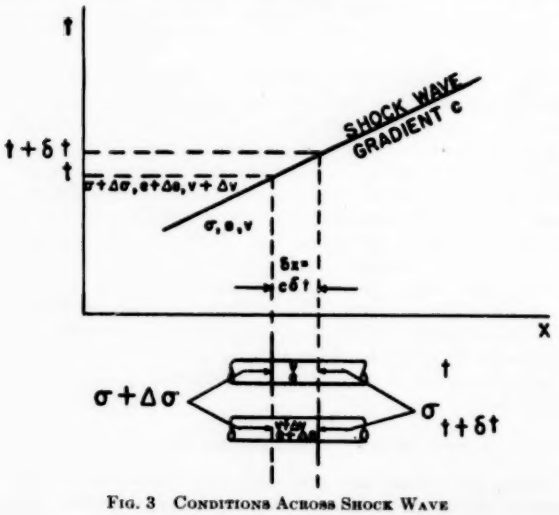

FIG. 3 CONDITIONS ACROSS SHOCK WAVE

The principal symbols used are as follows:

- σ = nominal compressive stress, equal to total compressive force across a section divided by the original cross-sectional area A_0
- ρ = original density of material
- v = particle velocity of any section of cylinder, positive to right
- e = compressive strain measured by decrease in length of an element divided by its unstrained length
- c = wave velocity in terms of Lagrange co-ordinates, i.e., rate of progress of a wave measured along unstrained cylinder
- c_0 = corresponding elastic wave velocity
- Δ = discontinuous increase in stress, strain, or velocity due to passage of a shock wave across a section

Let us consider the motion of the element of length δx shown in Fig. 3 during the time δt while the wave front is traversing it. The stress difference across the element during the time δt leads to the momentum equation

$$\left.\begin{aligned} \Delta\sigma\,\delta t &= \rho\,\delta x\,\Delta v \\ \text{or} \qquad \Delta\sigma &= \rho\,c\,\Delta v \end{aligned}\right\} \qquad [1]$$

The velocity difference Δv between the ends of the element produces the increase in strain Δe

$$\left.\begin{aligned} \Delta v\,\delta t &= \Delta e\,\delta x \\ \text{or} \qquad \Delta v &= c\,\Delta e \end{aligned}\right\} \qquad [2]$$

Elimination of Δv between Equations [1] and [2] determines the wave velocity c

$$c^2 = \frac{1}{\rho}\frac{\Delta\sigma}{\Delta e} \qquad [3]$$

These relations determine the initial stress wave emanating from the surface of impact. For impact stresses in the elastic region, O-A in Fig. 2, the gradient of the stress-strain curve is E_0, the elastic Young's modulus, and the corresponding wave velocity is c_0. The impact velocity corresponding to each stress is given by Equations [1], c having the constant value c_0, which is a well-known relationship for elastic waves.

For an impact stress $\sigma_B > \sigma_A$ represented by B in Fig. 2, an elastic wave is propagated from the impact surface of magnitude σ_A with velocity c_0, followed by a plastic wave front. We are assuming that the stress-strain relationship shown in Fig. 2 applies under dynamic conditions, so that Equations [1], [2], and [3] are satisfied for a plastic shock wave front of stress amplitude $\sigma_B - \sigma_A$ propagated with velocity corresponding to the chord A-B in Fig. 2. The corresponding impact velocity is then given by the application of Equations [1] in two stages, namely

$$v_B = \frac{\sigma_A}{\rho c_0} + \frac{\sigma_B - \sigma_A}{\rho c_{AB}}$$

in which c_{AB} is given by Equation [3] on substituting the gradient of the chord A-B for $\Delta\sigma/\Delta e$.

Fig. 4 shows the form of the resulting stress wave fronts corresponding to various values of maximum strain. The associated relationship between the impact velocity and the resulting maximum stress is shown in Fig. 5.

Certain assumptions are involved in the foregoing analysis

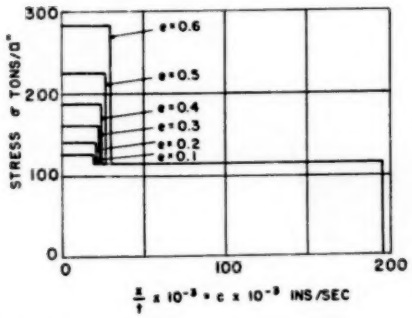

FIG. 4 STRESS WAVE FRONTS DUE TO IMPACTS AT VARYING VELOCITIES

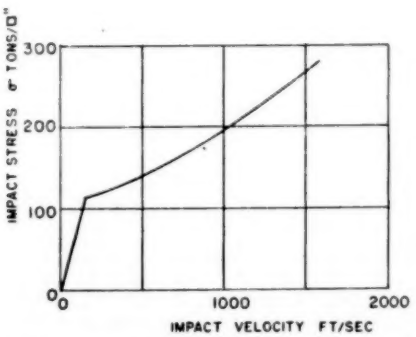

FIG. 5 RELATION BETWEEN IMPACT VELOCITY AND RESULTING MAXIMUM STRESS

which will modify this simple theory but which are expected to have only a small effect at moderate velocities:

1 The static isothermal stress-strain curve in Fig. 2 is assumed to apply for the very high rate of strain in the shock wave front. The rate of strain has an important influence on the stress-strain curves of some materials and will have a corresponding effect on the resulting stress wave propagation. For the high-strength steels considered in this paper, however, as mentioned previously, its effect is small.

2 The Hugoniot relations represent conservation of mass and momentum. Energy considerations indicate a release of heat energy in the shock wave front in excess of the normal heat of straining. This excess corresponds to the work represented by the area between the chord *A-B* and the stress-strain curve. Therefore the temperature of the material will be raised above the adiabatic compression condition which further will modify the stress-strain curve in Fig. 2. For moderate stresses this excess heat is small, as can be seen by reference to Fig. 2.

3 The equation for longitudinal motion only has been used. The associated lateral strain also will introduce inertia forces which will modify the propagation of the stress waves. It is clear that a discontinuity in lateral strain corresponding to a discontinuity in stress is not permissible since it would involve infinite lateral acceleration. However, the total lateral motion is, in general, small compared with the longitudinal motion, and so the application of the present analysis can be expected to produce the correct magnitude of the strain, although the details of the effects of the shock waves will not occur in practice.

4 It is assumed that lateral buckling does not take place. This is expected to obtain in practice, for the inertia of the material prevents lateral buckling during the short duration of the compressive force, although the magnitude of this force is momentarily extremely high. No buckling was observed in the experimental firings.

Without a considerable extension of plasticity theory, the justification of the foregoing assumptions can be made only by comparison with experiment, and satisfactory agreement was obtained.

GENERAL THEORY

The Hugoniot relations developed in the previous section can be used to investigate the interplay of the plastic wave front emanating from the impact surface with the elastic waves reflected from the free end of the specimen.

It has been found convenient to use as one independent variable $\tau = c_0 t$. The associated nondimensional wave velocity is $(dx)/(d\tau) = c/c_0 = c'$, and is therefore unity in the elastic region. The Hugoniot relation Equations [1] is used in the form

$$\Delta(\rho c_0 v) = \frac{1}{c'} \Delta\sigma \quad \ldots\ldots\ldots\ldots\ldots\ldots [4]$$

$\rho c_0 v$ has the dimensions of a stress and is expressed in tons/sq in.

O-A-B in Fig. 2 represents the stress-strain curve for continuously increasing stress. If at *B* the stress decreases, we assume the stress release or unloading conditions to be represented by the straight line *B-D* parallel to the initial elastic line *O-A*. Subsequent increase in stress will produce conditions represented by *B-D* until the stress at *B* is exceeded, when the plastic flow curve—the continuation of *A-B*—will be resumed.

Experiments carried out by J. V. Howard and S. L. Smith (8) show that *B-D* should form one arc of a hysteresis loop, the tangent at the point *B* being parallel to the elastic line when true stress is plotted against true strain. Therefore the unloading lines will not be parallel on the nominal stress diagram. In fact, the stress-wave velocities (in the Lagrange sense) corresponding to the tangents to the hysteresis loops at the initiation of stress release are given by $c_0/(1 - e)$. Introduction of this variable unloading velocity complicates the analysis considerably, and since most of the stress release results from the elastic waves reflected from the free end of the cylinder in the region of no plastic strain, it does not play a major part in the plastic flow process. We assume, therefore, that the unloading line on the nominal stress-strain curve is parallel to the elastic line, indicating a constant wave velocity in the Lagrange sense. The amplitude of the stress waves in the deformed part of the cylinder, behind the plastic wave front, will indicate the error involved.

Fig. 6 shows a typical intersection of stress waves. Repeated application of the type of analysis represented enables the complete plastic flow to be investigated. Fig. 6(*a*) shows the propagation of the wave fronts in the x, τ-plane. *O-D* is the initial advancing plastic shock wave, the material ahead of it having been stressed to σ_A by the elastic wave which preceded it. The particle velocities in these regions v_B and v_A are given by the initial impact wave solution considered in the previous section. The region *D-O-E* is in the condition *B* on the stress-strain curve Fig. 6(*b*). *H-O* represents the elastic wave reflected from the free end of the cylinder. The stress behind it is zero, and the particle velocity double that ahead of it. This is deduced by application of Equation [4], the values of c' for each wave front being indicated in the circles in Fig. 6(*a*). Fig. 6(*c*) shows the stress distribution at $\tau = \tau_1$ before these waves collide.

At $\tau = \tau_2$ when these waves meet, the stress distribution is shown in Fig. 6(*d*). The resulting wave fronts are deduced by a trial-and-error method using the Relation [4]. If σ_B is suffi-

ciently large, an elastic wave O-G, of amplitude σ_A will be propagated from O, leaving the material behind it in the condition A in Fig. 6(b). This is followed by a plastic shock wave O-F, which raises the stress to σ_I represented by the point I on the stress-strain curve. The material to the left of O which has been stressed to the point B in Fig. 6(b) is traversed by a stress-release wave which reduces the stress to σ_I represented by the point I' in Fig. 6(b) on the unloading line through B. Stress σ_I is determined by the condition that the velocity in the region E-O-F must be consistent, whether obtained by applying Equation [4] across O-E or across O-F. This condition is

$$\rho c_0 v_B + (-1)(\sigma_I - \sigma_B) = 3\rho c_0 v_A + \left(\frac{1}{c'_{AI}}\right)(\sigma_I - \sigma_A) \quad [5]$$

Term c_{AI} is given by Equation [3] in terms of the gradient of the chord A-I in Fig. 6(b). Stress σ_I is thus determined by a trial-and-error method which is quite rapid since c' changes only slowly with stress.

Fig. 6(e) shows the resulting stress distribution at $\tau = \tau_3$. The unloading wave O-H has passed through the plastic wave front, though somewhat reduced in magnitude. The amplitude of the plastic shock wave also is reduced.

Repeated application of this type of analysis determines the entire plastic-flow process until plastic flow ceases and the permanently deformed specimen rebounds from the target. The maximum stress to which each section of the projectile has been subjected determines the residual strain, so that the final shape can be obtained.

Particular Solutions

Two particular cases have been worked out in detail for impact velocities of 481 and 935 fps. The first case involves a maximum strain of 0.2, the second 0.4.

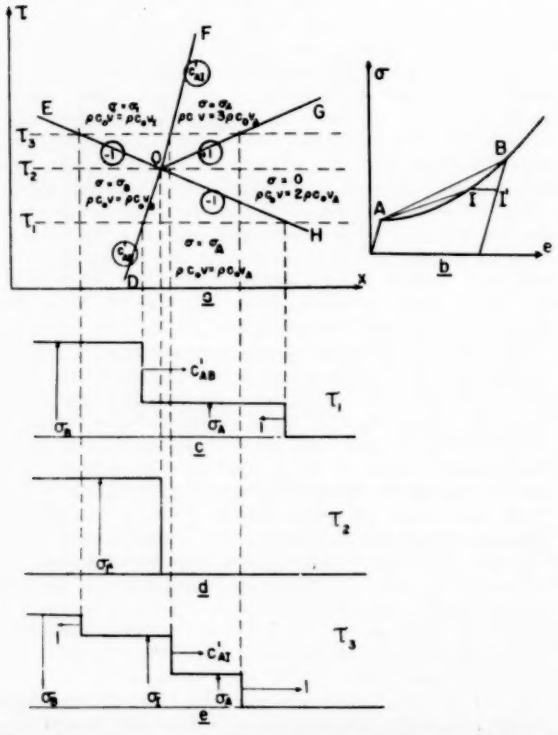

Fig. 6 Intersection of Plastic and Elastic Wave Fronts

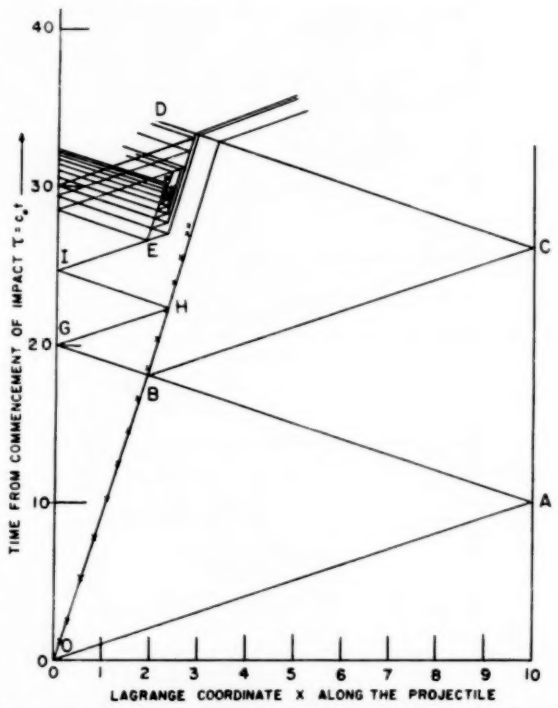

Fig. 7 Elastic and Plastic Fronts for Impact at 481 Fps Until Plasticity Ceases
(Crosses show plastic wave front of plastic-rigid solution.)

Fig. 7 shows the progress of the wave fronts in the x, τ-plane for the lower velocity impact. O-A is the initial elastic wave emanating from the surface of impact and O-B the plastic shock wave front. The nominal stress behind O-B, the maximum stress occurring, is 141 tons/sq in. At B another elastic wave front B-C, is propagated away from the target, as discussed in the previous section.

At E a plastic region forms behind the main plastic wave front. This arises as a result of the detail of the reflections of the unloading wave A-B at the impact surface. B-G is an unloading wave, which on reflection at the impact end (where the velocity is prescribed so that it behaves as a fixed end) gives additional unloading along G-H. However, the intensity is not enough to penetrate the main plastic wave front at H, and it is reflected as a loading wave H-I, and at the same time it produces a reduction in the intensity of the main plastic wave front. This loading wave is enhanced by reflection at the impact surface I, producing the loading wave I-E. The stress after passage of this wave is below that behind the initial plastic wave O-B, but above that behind the plastic wave B-H. Thus at E, which has the same abscissa as B, the wave emerges into a region in which the yield stress as modified by the previous plastic flow is less than the stress wave magnitude, and a plastic wave results. This discontinuous change in yield stress also produces two elastic waves emanating from E. By a similar process many wavelet reflections occur between E and F as shown in Fig. 7.

Plastic flow is entirely absorbed by the reflection of the second elastic wave from the free end and the cylinder is left in elastic vibration. During the remainder of the rebound procedure no additional permanent deformation will occur.

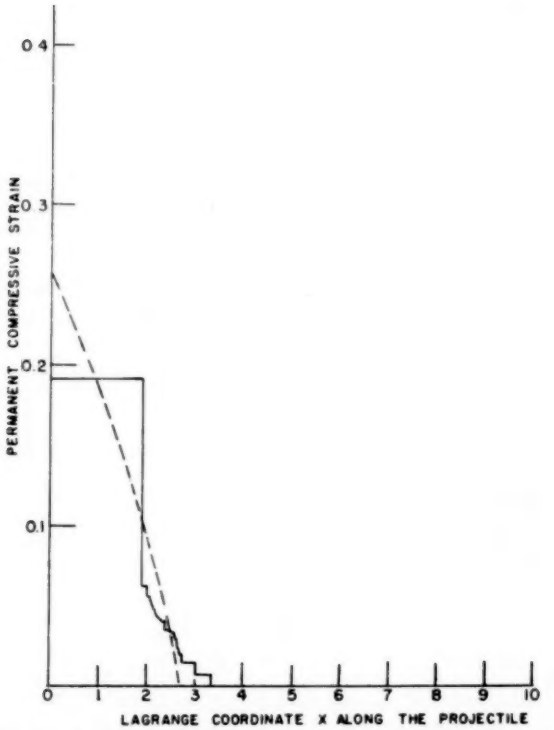

FIG. 8 CALCULATED PERMANENT STRAIN DISTRIBUTION CORRESPONDING TO FIG. 7
(Broken line is for plastic-rigid material.)

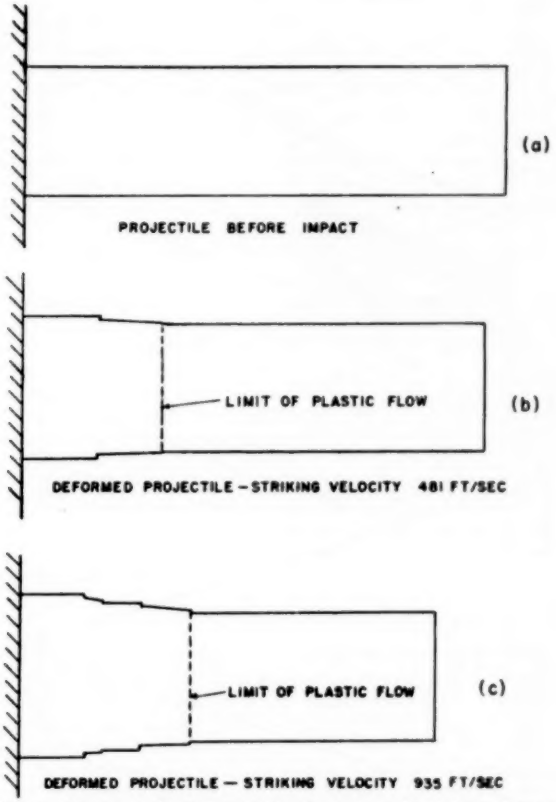

FIG. 9 COMPUTED PERMANENT DEFORMATION OF PROJECTILE AFTER STRIKING RIGID PLATE AT DIFFERENT VELOCITIES

The resulting permanent strain distribution is shown by the full line in Fig. 8. In this case the strain in the initial plastic wave front dominates the distribution. Fig. 9(*b*) shows the resulting shape of the projectile compared with the undeformed state, Fig. 9(*a*).

Figs. 10 and 11 show the corresponding solution for impact at 935 fps. In this case plastic flow is not absorbed until the third elastic reflection has reacted on the plastic wave front. The initial plastic wave does not, in this case, so dominate the permanent strain distribution. Fig. 9(*c*) shows the calculated final shape of the projectile.

SOLUTION NEGLECTING ELASTIC STRAINS

Sir Geoffrey Taylor suggested a simplified solution which will be detailed for comparison with the solutions just given. It is an extension of the theory detailed in (1) to the case when the stress-strain relation is prescribed. As in other problems of plasticity, it may be permissible to neglect elastic strains in comparison with plastic strains. Making this assumption is equivalent to supposing that the hinder part of the cylinder, not reached by the plastic wave front at any instant, behaves as a rigid body. This assumption leads to a considerably simplified solution of the plastic flow resulting from impact.

The conditions are as shown in Fig. 12. The rigid back part of the projectile is approaching the target with velocity u. The plastic wave front is propagated away from the impact surface with velocity v, leaving the material behind it at rest since elastic recovery is neglected. These are absolute velocities, the solution not being carried out explicitly in terms of Lagrange co-ordinates. A and σ are the cross section and nominal stress just behind the plastic wave front, and A_0 and σ_0 just ahead of it; σ_0 is the yield-point stress since the material ahead of the wave front is about to become plastic.

Neglecting compressibility in the plastic flow, the equation of continuity becomes

$$(u + v)A_0 = vA \quad [6]$$

This leads to an expression for the strain behind the plastic wave front

$$e = \frac{A - A_0}{A} = \frac{u}{u + v} \quad [7]$$

Defining x as the undistorted length at any instant, we have

$$-\frac{dx}{dt} = u + v \quad [8]$$

Momentum considerations across the wave front yield the equation

$$\rho(u + v)A_0 u = A_0(\sigma - \sigma_0) \quad [9]$$

The equation of motion of the rigid part of the projectile is

$$\rho x \frac{du}{dt} = -\sigma_0 \quad [10]$$

Eliminating dt from Equations [8] and [10] and using Equation [7] gives

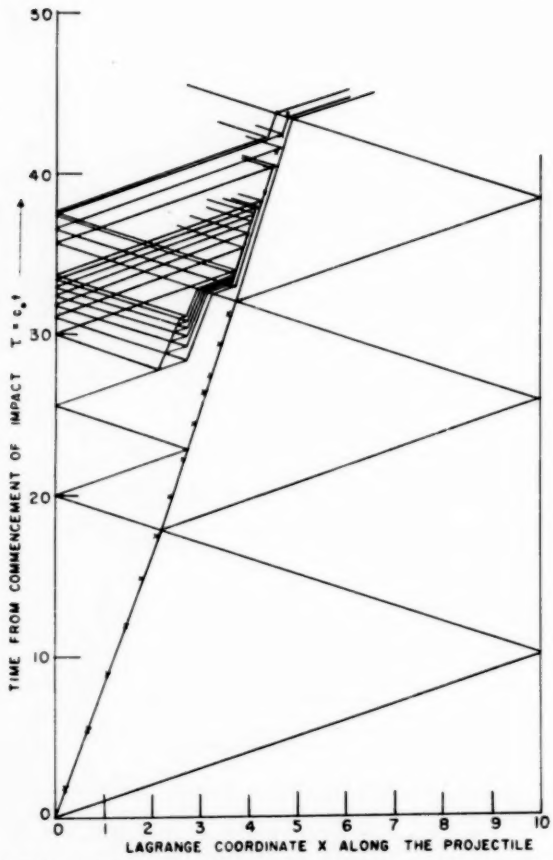

FIG. 10 ELASTIC AND PLASTIC WAVE FRONTS FOR IMPACT AT 935 FPS UNTIL PLASTICITY CEASES
(Crosses show plastic wave front of plastic-rigid solution.)

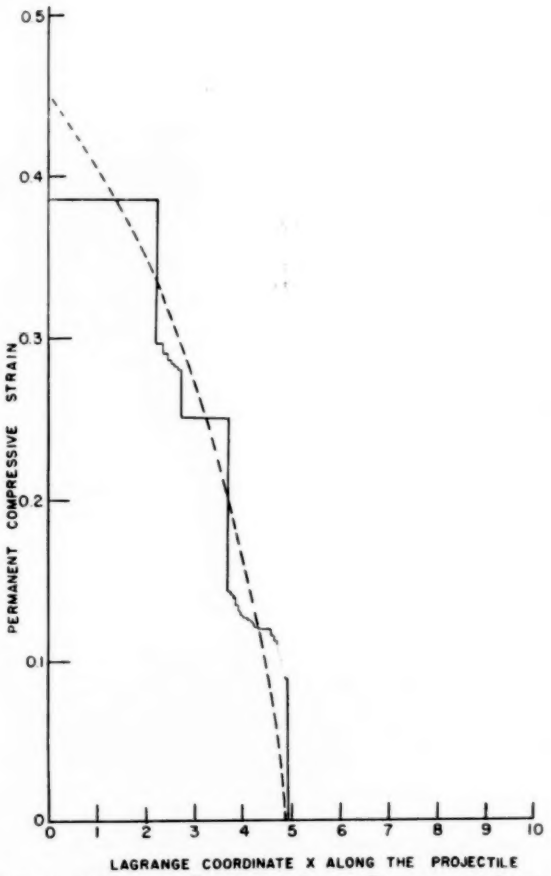

FIG. 11 CALCULATED PERMANENT STRAIN DISTRIBUTION CORRESPONDING TO FIG. 10
(Broken line is for plastic-rigid material.)

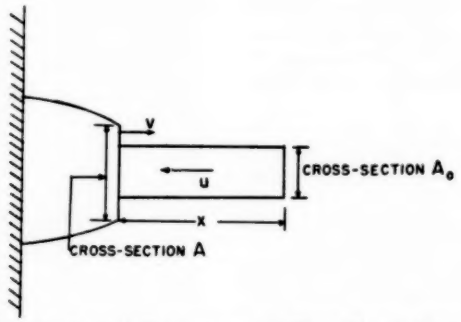

FIG. 12 FORM OF DEFORMATION ON WHICH PLASTIC-RIGID SOLUTION IS BASED

$$d(\rho u^2) = 2\,\frac{\sigma_\theta e}{x}\,dx \qquad [11]$$

Using Equations [7] and [9], this becomes

$$\log x^2 = \int_{\sigma_1}^{\sigma} \frac{d(\sigma - \sigma_\theta e)}{\sigma_\theta e} \qquad [12]$$

Writing

$$F(\sigma) = \frac{1}{\sigma_i}\left[\sigma(1 + \log e) - \int_{\sigma_0}^{\sigma} \log e\, d\sigma\right] - \log e \qquad [13]$$

we have

$$\log x^2 = F(\sigma) - F(\sigma_1) \qquad [14]$$

The initial stress σ_1 is given by Equations [7] and [9]

$$\rho U^2 = e_1(\sigma_1 - \sigma_0) \qquad [15]$$

where U is the impact velocity and e_1 the resulting maximum strain.

The function $F(\sigma)$ can be obtained readily for the stress-strain curve given in Fig. 2 and the permanent strain distribution calculated. The use of the unstrained length x as the dependent variable leads at once to comparison with the Lagrange co-ordinate solution.

The progress of the plastic wave fronts given by this solution are shown by the crosses in Figs. 7 and 10. The resulting permanent strain distributions are shown by the broken lines in Figs. 8 and 11.

As would be expected, this solution averages out the discontinuities in the wave solution. The rigid-body assumption involves an infinite elastic wave velocity and so, an infinite number of elastic wavelet reflections from the free end. Comparison of Figs. 8 and 11 shows that, as the number of elastic wave reflections increases, the two solutions move into closer agreement.

The agreement on the progress of the major plastic wave front is remarkable. Equally close agreement is not to be expected for the time at which all plastic flow ceases, since this is, in general, restricted to occur on one of the elastic wave reflections for the wave solution. In the plastic-rigid solution the absorption of plastic flow changes continuously with impact velocity, whereas for the elastic-plastic body this increases in steps according to the number of elastic wave reflections, the remaining rebound energy varying accordingly.

The close agreement between the two methods of treatment is associated with the magnitude of the plastic strain, which is just under 20 and 40 per cent, respectively, for the two cases. The maximum elastic strain is just under 1 per cent, and thus has a relatively small over-all influence. For lower impact velocities the difference between the two types of solution will become more marked, and it will become essential to consider the material as elastic-plastic. As the impact velocity is decreased toward zero, the plastic-rigid solution always determines plastic flow, whereas there is a definite limit below which only elastic straining occurs. As demonstrated in Fig. 13, the plastic-rigid solution determines larger total compression, since all the energy of impact is transformed into plastic flow, whereas for the elastic-plastic solution some remains as kinetic energy of rebound, and some in residual elastic vibration of the cylinder. If the total energy is large compared with the maximum elastic energy which the cylinder can hold, as in the present cases, then the plastic-rigid solution provides a satisfactory approximation. The order of magnitude of the impact velocity in the present investigation was determined by the dynamic test being studied, and the fact that the cylinders were fired from a revolver which prescribed a limited range of velocities. This range of interest lies in the region of large plastic flow, and so of close agreement between the two theoretical solutions.

Comparison With Experiment

The two types of solution given in the foregoing are both based on certain assumptions enumerated in the section, Initial Stress Wave Resulting From Impact, so that agreement between them has only limited significance. A series of Taylor dynamic compression tests was carried out on the alloy steel by A. C. Whiffin and H. L. D. Pugh of the Road Research Laboratory, Department of Scientific and Industrial Research. Cylinders of the nickel-chrome steel studied, 0.34 in. diam and 0.5 in. long, were fired at a hardened armor plate with a range of impact velocities. Fig. 14 shows the final form of some of the specimens. It was difficult to control the speed exactly owing to the uncertainties of barrel friction, and 916 fps was the nearest velocity which was reached in attempting to reproduce the computed case of 935 fps. The lower velocity studied theoretically was below the threshold of satisfactory firing with a revolver. Fig. 13 shows a comparison

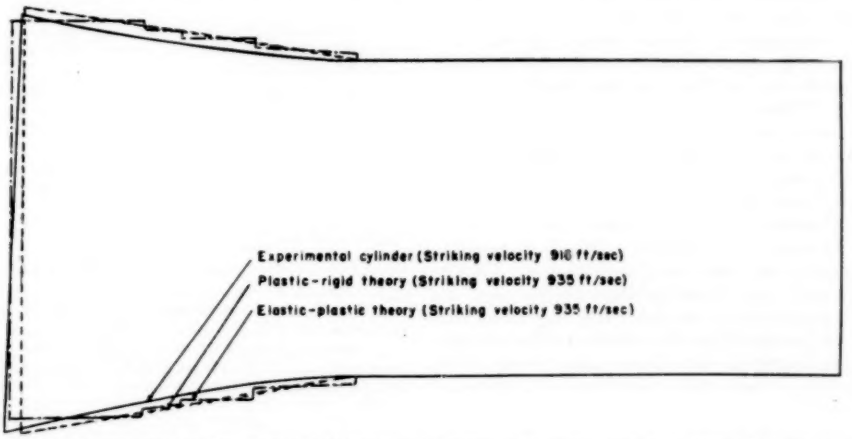
Experimental cylinder (Striking velocity 916 ft/sec)
Plastic-rigid theory (Striking velocity 935 ft/sec)
Elastic-plastic theory (Striking velocity 935 ft/sec)

Fig. 13 Comparison of Final Shape of Cylinder, Striking Velocity 916 Fps, With Calculated Shapes for a Striking Velocity of 935 Fps, Obtained From Elastic-Plastic and Plastic-Rigid One-Dimensional Theory

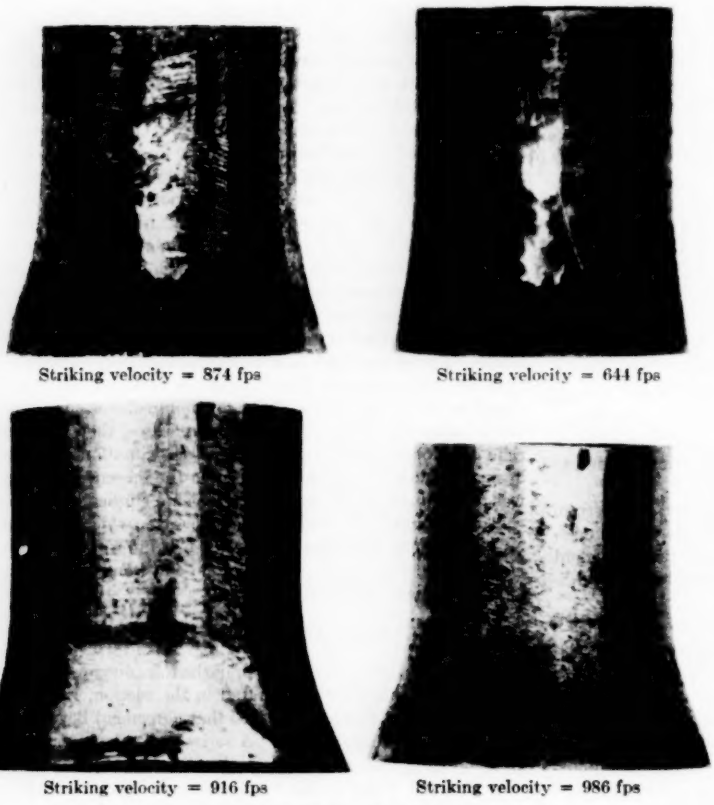

Striking velocity = 874 fps | Striking velocity = 644 fps

Striking velocity = 916 fps | Striking velocity = 986 fps

FIG. 14 SHAPE OF REVOLVER CYLINDERS AFTER TEST
(All cylinders were originally 0.34 in. diam × 0.5 in. long. Due to Whiffin and Pugh. Photographs in Fig. 14, British Crown copyright, reserved.)

of the permanent deformation of the cylinder with the computed values. A convenient scale was chosen for plotting the dimensions, and the cylinder in Fig. 13 is more slender than the actual specimen, but the correct strains are reproduced. In studying the deformation obtained experimentally, an increase of velocity to the value for the calculated cases would produce an additional decrease in length of the cylinder less than one half the difference between the two calculated solutions, so that this represents a very small effect. Fig. 13 shows that the impact was not quite normal but the disturbance resulting from this effect is small.

A study of Fig. 13 shows that the magnitude and extent of the strain predicted by the two theoretical solutions and found experimentally are in good agreement. This indicates that for this steel the static stress-strain relation applies under the conditions of high-speed straining during the impact. The experimental strain distribution is smooth, showing that the shock waves of strain discontinuity predicted by the one-dimensional theory are inhibited by the influence of lateral inertia. Thus in using this theory such steps should be smoothed out, and the theoretical results would then be in satisfactory agreement with experiment. Since the ratio of length to diameter of the cylinders is less than 2, it is remarkable that the one-dimensional theory proves so satisfactory. It cannot be that this and the influence of strain rate have opposing effects since both would tend to constrain the motion.

The conclusion from this study is that for high-strength alloy steel, impacts of the order 1000 fps can be analyzed on the basis of the static stress-strain relation. The one-dimensional theory gives satisfactory results, even for cylinders with a length to diameter ratio of 2:1, if a smooth curve is taken through the predicted stepped strain distribution. For plastic strains large compared with elastic strains, the plastic-rigid type of analysis provides a satisfactory and simple analytical method.

ACKNOWLEDGMENT

The solutions discussed were taken from an official report (9) written while the authors were on the staff of the Armaments Research Department, Ministry of Supply, United Kingdom. Thanks are due to the Chief Scientific Officer, Ministry of Supply, for permission to publish this work. We also wish to thank Messrs. Whiffin and Pugh and the Department of Scientific and Industrial Research for permission to use the experimental work discussed, and to Sir Geoffrey Taylor for stimulating discussions during the development of the work.

BIBLIOGRAPHY

1 "The Use of Flat-Ended Projectiles for Determining Dynamic Yield Stress," by G. I. Taylor, Proceedings of the Royal Society, London, England, series A, vol. 194, 1948, pp. 289–299.

2 "Propagation of Earth Waves From an Explosion," by G. I. Taylor, British Official Report R. C. 70, 1940; "The Plastic Wave in a Wire Extended by an Impact Load," R. C. 329, 1942.

3 "On the Propagation of Plastic Deformation in Solids," by Th. von Kármán, NDRC Report A-29 (OSRD No. 365), 1942. See "The Propagation of Plastic Deformation in Solids," by Th. von Kármán and Pol Duwez, *Journal of Applied Physics*, vol. 21, 1950, pp. 987–994.

4 "A Boundary Value Problem in the Theory of Plastic Wave Propagation," by E. H. Lee, *Quarterly of Applied Mathematics*, vol. X-4, 1953, pp. 335–346.

5 "The Relationship Between Stress and Strain in the Tensile Impact Test," by A. F. C. Brown and N. D. G. Vincent, Proceedings of the Institution of Mechanical Engineers, London, England, vol. 145, 1941, pp. 126–134.

6 "Wave Propagation in a Uniform Bar Whose Stress-Strain Curve Is Concave Upward," by M. P. White and L. Griffis, NDRC Report No. 152, OSRD 1302, 1943; also in JOURNAL OF APPLIED MECHANICS, Trans. ASME, vol. 70, 1948, pp. 256–260.

7 "Plastic Waves in Compression," by E. H. Lee, British Official Report APP. Coord. Sub-Committee No. 57, 1943.

8 "Recent Developments in Tensile Testing," by J. V. Howard and S. L. Smith, Proceedings of the Royal Society, London, England, series A, vol. 107, 1925, p. 113.

9 "The Analysis of the Plastic Deformation in a Cylinder of Shot Steel Striking a Rigid Target," by E. H. Lee and S. J. Tupper, British Official Report TRR 4/44, 1944.

Coulomb Friction, Plasticity, and Limit Loads[1]

By D. C. DRUCKER,[2] PROVIDENCE, R. I.

Additional attention is given to the somewhat subtle but extremely important difference between Coulomb friction and the apparently corresponding resistance to plastic deformation. It is shown that the limit theorems previously proved for assemblages of perfectly plastic bodies do not always apply when there is finite sliding friction. Theorems are developed which relate the limit loads with finite Coulomb friction to the extreme cases of zero friction and of complete attachment, and also to the case where the frictional interfaces are "cemented" together with a cohesionless soil.

Sliding Friction Versus Plastic Resistance

IT WAS pointed out previously (1)[3] that the similarity between the stress-strain relation for a rigid or elastic-perfectly plastic material and the force-displacement relation for the Coulomb friction case, Fig. 1, may be misleading. The essential feature may be stated best in mechanical-thermodynamic terms for an assemblage of elastic-plastic bodies in equilibrium, Fig. 2. If either the attachment is complete or if all coefficients of friction are zero, no work can be extracted from the bodies and any equilibrium system of forces acting upon them. In other words, there is no way in which the bodies plus the forces can act as an engine in this thermodynamic sense. They can, however, if a coefficient of friction is finite (1).

This point of view is made clearer and less abstract by a comparison between Coulomb sliding friction and shearing on a plane through a Coulomb cohesionless soil obeying the generalized plastic-potential laws, Fig. 3. The relation between the normal vertical force N and frictional horizontal force F in each case may be written as $F = \mu N$. The displacement picture, however, is fundamentally different (2). The block in the friction case slides in the direction of the force F. It also moves up in the case of shearing of soil because of the volume expansion which accompanies shear if the generalized plastic-potential relations are followed (2). The displacement or velocity vector makes an angle ϕ with the horizontal where $\phi = \tan^{-1}\mu$ is the angle between the straight-line envelope to the limiting Mohrs circles and the negative σ-axis. Work is done, therefore, against the downward force N. It is this negative work which prevents

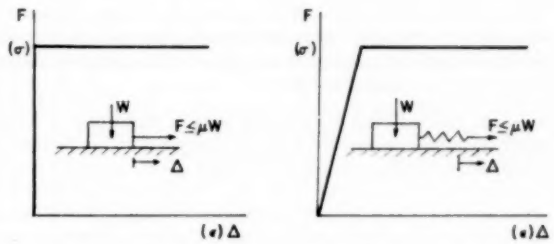

Fig. 1 Apparent Analogy Between Friction and Plasticity

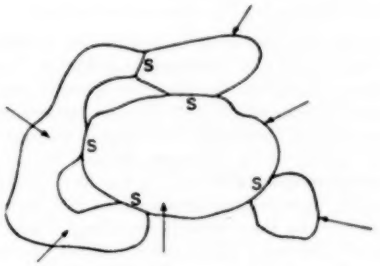

Fig. 2 An Assemblage of Bodies in Equilibrium

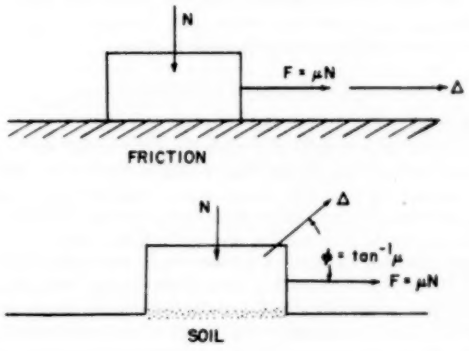

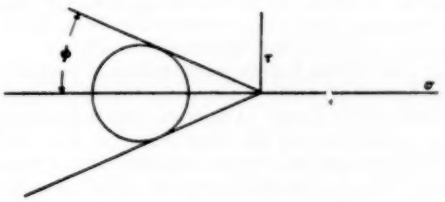

Fig. 3 Difference Between Coulomb Sliding and Coulomb Shear

---

[1] Results presented in this paper were obtained in the course of research sponsored by the Office of Naval Research under Contract N7onr-35801 with Brown University.

[2] Chairman, Division of Engineering, Brown University, Mem. ASME.

[3] Numbers in parentheses refer to the Bibliography at the end of the paper.

Contributed by the Applied Mechanics Division and presented at the Annual Meeting, New York, N. Y., November 29–December 4, 1953, of The American Society of Mechanical Engineers.

Discussion of this paper should be addressed to the Secretary, ASME, 29 West 39th Street, New York, N. Y., and will be accepted until April 12, 1954, for publication at a later date. Discussion received after the closing date will be returned.

Note: Statements and opinions advanced in papers are to be understood as individual expressions of their authors and not those of the Society. Manuscript received by ASME Applied Mechanics Division, March 5, 1953. Paper No. 53—A-57.

elastic-plastic bodies and the system of forces acting on them from acting as an engine while apparently similar frictional systems can.

Limit Theorems

The two major limit theorems (3, 4) in a crude sense state that an assemblage of elastic-perfectly plastic bodies, with zero friction or complete attachment at each interface, will, on the one hand, do the best they can to distribute stress to avoid collapse. On the other hand, they will recognize defeat if any kinematic collapse mode exists. This anthropomorphic approach is refined, when geometry change is negligible, in the actual statement of the theorems proved as follows:

1 Collapse will not occur if any state of stress can be found which satisfies the equations of equilibrium and the boundary conditions on stress, and which is "below yield" at each point.

2 Collapse must occur if for any compatible flow pattern, considered as plastic only, the rate at which the external forces do work on the bodies equals or exceeds the rate of internal dissipation.

3 Collapse takes place at constant stress so that strain rates are purely plastic.

Now suppose that the coefficient of friction is finite and nonzero on at least one of the interfaces S in Fig. 2. Is the system still intelligent enough to distribute the stress to avoid collapse, and are the theorems still valid? Trouble immediately appears in the upper-bound Theorem 2. The rate of internal dissipation cannot be calculated in all cases because frictional dissipation is not determined uniquely by the flow pattern. It depends not only upon relative displacement rates but also on the normal pressure on the frictional interface, a quantity which often will not be known. This type of difficulty does not appear in the lower-bound Theorem 1. It might seem plausible to assume that the theorem is valid with the additional requirement that the state of stress must not violate the friction condition at the interface and must stay below yield. A simple example shows this hopeful intuitive approach to be in error.

Illustrative Examples

Fig. 4(a) represents two rigid blocks; the heavy horizontal one is balanced on a rough ledge while the light small one is on an inclined plane with friction angle ϕ and inclination α. The contact surface between the blocks is at a slightly flatter angle β than the plane and will be considered frictionless. There need be no force between the blocks, and yet a large force N could be carried between the blocks without violating equilibrium, Fig. 4(b). If $\phi > \alpha - \beta$, such a force is stabilizing. Clearly, however, if $\alpha > \phi$, the block will slide down the plane and no stabilizing force will be developed. On the other hand, if the sliding was really plastic shearing as for a soil, then the incipient velocity vector V would point away from the inclined plane at an angle ϕ, as in Fig. 4(c). The large block would have to lift up and the force N would be mobilized to prevent sliding down the plane. A modified Theorem 1 thus is seen to be improper for the friction case but again is verified for the "plasticity" problem.

The problem of Fig. 4 might seem tricky and exceptional because the little block really is not confined by the large one and because the bodies are rigid. A more elaborate example probably is needed to demonstrate the point properly. The punch or, equally well, the uniform-pressure example in Fig. 5 has special dimensions to avoid calculations but otherwise is a good representative plane-strain problem. The interface U-M-N-W between the upper arch-shaped block and the lower support is supposed to have an extremely large but finite friction angle. The

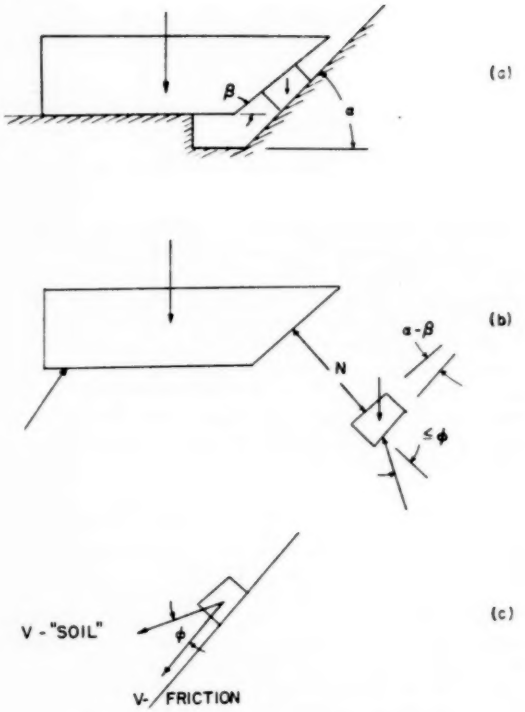

Fig. 4 A Counterexample—Rigid Bodies

yield stress in shear will be called k and either the Mises or Tresca yield condition is employed.

Fig. 5(a) shows a discontinuous stress solution passing through the interface as though the two bodies were one. This is the often-used 30-deg wedge solution slightly modified (5). In the equilateral-triangle region A-B-C, the principal stresses are compressive and of magnitude $3k$ in the vertical direction, and k horizontally. In the sloping region B-C-D-E, the stress is $2k$ parallel to B-E, and zero in the perpendicular direction. Region D-H-E has principal stresses $+k$ and $-k$. The shearing stress, if any, and the normal traction on the planes of discontinuity B-C, D-E, H-E, H-D are continuous across the planes.

Both compressive and shearing tractions σ and τ, in magnitudes which are easily calculated, will act on the interface U-M-N-W. The coefficient of friction μ is assumed large enough so that $\tau < \mu\sigma$. Therefore the stress field in Fig. 5(a), multiplied by a number slightly less than unity will be "below yield" everywhere and does not violate the friction condition. The total force P per unit dimension perpendicular to the paper can be made as close to $3kb$ as desired.

The question of whether or not the bodies are able to adjust themselves in this static manner is answered by the possible discontinuous rigid-block kinematic-collapse pattern, Fig. 5(b). Block A-T-B is taken to move vertically downward at velocity V requiring A-T-M-U and B-T-N-W to move at 45 deg with velocity $V/\sqrt{2}$ so that separation occurs on M-U and N-W. Block M-T-N is stationary. The velocity discontinuity on the surfaces of sliding, B-T-M and A-T-N, each of length $b\sqrt{2}$, is $V/\sqrt{2}$. The rate of energy dissipation per unit perpendicular dimension is just $2(k\, b\sqrt{2}\, V/\sqrt{2}) = 2kbV$, because in this permissible virtual displacement pattern there is separation along the friction surfaces M-U and N-W and they contribute nothing. Equating the

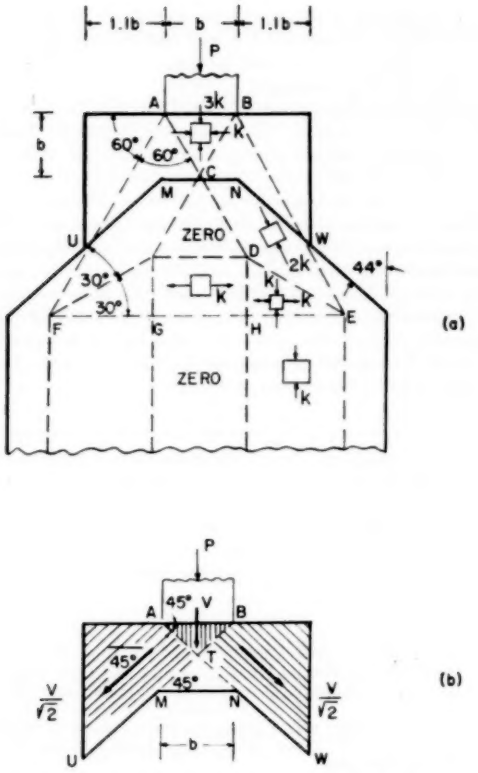

FIG. 5 TWO-DIMENSIONAL PROBLEM WITH ELASTIC-PLASTIC BODIES

(a, An equilibrium solution; b, Velocity, i.e., kinematic, solution involving separation.)

rate of work of the external forces P-V to $2kbV$ gives the upper bound and, in this case, correct result for Fig. 5, $P = 2kb$, and not $3kb$.

The intuitive limit theorem on the inherent intelligence of the material thus is seen to be incorrect for finite and nonzero friction. Again, substitution of an elastic-plastic "soil" for the Coulomb friction interface fixes matters. Surfaces *M-U* and *N-W* do increase the energy dissipation (2) and the value $3kb$ is a proper lower bound if the angle ϕ is large enough.

It might be thought that the separation counterexamples given in this section are unfair. However, in the friction case, it is precisely the freedom to slide with an arbitrary normal stress on the surface of sliding and, therefore, an arbitrary dissipation which prevents the application of the "intuitive theorems." Sliding at zero normal stress and actual separation are essentially the same. An angle of 45 deg instead of 44 deg in Fig. 5 would not change the result.

FRICTION THEOREMS

The question now arises as to what can be said about limit loads for assemblages of bodies with frictional interfaces. Two theorems seem intuitively obvious:

A Any set of loads which produces collapse for the condition of no relative motion at the interfaces will produce collapse for the case of finite friction. No relative motion is a more inclusive term than infinite friction because separation is not permitted.

B Any set of loads which will not cause collapse when all coefficients of friction are zero will not produce collapse with any values of the coefficients.

Although at this stage, intuition may not seem completely reliable, the theorems are, in fact, true. Their proof follows in part the technique employed in developing the limit theorems for plastic bodies (4). The most important tool is the theorem of virtual work

$$\int_A T_i^* \bar{\dot{u}}_i dA + \int_V F_i^* \bar{\dot{u}}_i dv = \int_V \sigma_{ij}^* \bar{\dot{\epsilon}}_{ij} dv + \int_S T_i^* \Delta\bar{\dot{u}}_i dS \quad [1]$$

in which the summation convention is employed.[4] There is no necessary tie between the equilibrium system of surface tractions T_i^*, stresses σ_{ij}^*, and body forces F_i^*, and the compatible system of velocities $\dot{u}_i$, strain rates $\bar{\dot{\epsilon}}_{ij}$, and velocity discontinuities $\Delta\bar{\dot{u}}_i$. The surface area A of the assemblage of bodies of volume V does not include the frictional interfaces S. For convenience of description, the velocity will be assumed continuous except across S. The term $\int_\Sigma T_i^* \Delta\bar{\dot{u}}_i d\Sigma$ for velocity discontinuities in the material is omitted, but this actually does not restrict the generality of the result (3, 4).

Use also will be made of the properties of the yield surface $f(\sigma_{ij}) = k^2$, Fig. 6. The rate of dissipation of energy per unit volume,

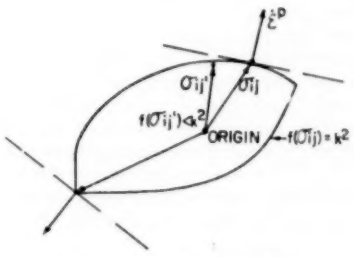

FIG. 6 THE YIELD SURFACE

$D = \sigma_{ij}\dot{\epsilon}_{ij}^p$, is determined uniquely by the plastic-strain rate $\dot{\epsilon}_{ij}^p$. The "vector" $\dot{\epsilon}_{ij}^p$, Fig. 6, is normal to the yield surface at a smooth point or lies between the normals to the surface at adjacent points to a vertex or corner. Furthermore, the surface is convex so that the dot product of the plastic-strain-rate vector with any stress vector to a point σ_{ij}' inside the surface, $f(\sigma_{ij}') < k^2$, cannot be as large as D

$$\sigma_{ij}'\dot{\epsilon}_{ij}^p < D = \sigma_{ij}\dot{\epsilon}_{ij}^p \quad [2]$$

To prove Theorem A, assume that a set of loads T_i^N, F_i^N produces collapse when all relative motion is prevented at the interfaces S (bodies welded together). This type of composite body can be analyzed by the established limit theorems which state

$$\int_A T_i^N \dot{u}_i^N dA + \int_V F_i^N \dot{u}_i^N dv \geq \int_V \sigma_{ij}^N \dot{\epsilon}_{ij}^N dv \quad [3]$$

and $\dot{\epsilon}_{ij}^N$ is purely plastic

$$\dot{\epsilon}_{ij}^N(\text{elastic}) = 0 \quad [4]$$

For Theorem A to be false, there must exist some equilibrium state of stress σ_{ij}^A such that $f(\sigma_{ij}^A) < k^2$. Using the virtual work Equation [1], with $\dot{u}_i^N$, $\dot{\epsilon}_{ij}^N$ as the compatible state

$$\int_A T_i^N \dot{u}_i^N dA + \int_V F_i^N \dot{u}_i^N dv = \int_V \sigma_{ij}^A \dot{\epsilon}_{ij}^N dv + \int_S T_i^A \Delta\dot{u}^N dS \quad [5]$$

[4] Reference (5), chapter 8. As an example:

$$\sigma_{ij}^* \dot{\epsilon}_{ij} \equiv \sigma_x^* \dot{\epsilon}_x + \sigma_y^* \dot{\epsilon}_y + \sigma_z^* \dot{\epsilon}_z + \tau_{xy}^* \bar{\dot{\gamma}}_{xy} + \tau_{yz}^* \bar{\dot{\gamma}}_{yz} + \tau_{zx}^* \bar{\dot{\gamma}}_{zx}$$

However, $\Delta \dot{u}^N \equiv 0$ because the velocity solution represents no relative motion at S and, from Equation [2], $\sigma_{ij}{}^A \dot{\epsilon}_{ij}{}^N < \sigma_{ij}{}^N \dot{\epsilon}_{ij}{}^N$. Equation [5] is, therefore, in contradiction to Inequality [3] and Theorem A cannot be false.

The proof of Theorem B starts from the given set of loads $T_i{}^0$, $F_i{}^0$ and stresses $\sigma_{ij}{}^0$ which do not cause collapse with $\mu = 0$. Next, suppose that collapse can occur for $\mu > 0$ with a collapse field $\dot{u}_i{}^B$, $\dot{\epsilon}_{ij}{}^B$, $\Delta \dot{u}_i{}^B$, and stress field $\sigma_{ij}{}^B$. Virtual work Equation [1] becomes

$$\int_A T_i{}^0 \dot{u}_i{}^B dA + \int_V F_i{}^0 \dot{u}_i{}^B dv = \int_V \sigma_{ij}{}^0 \dot{\epsilon}_{ij}{}^B dv + \int_S T_i{}^0 \Delta \dot{u}_i{}^B dS \quad \ldots\ldots [6]$$

and the collapse condition is

$$\int_A T_i{}^0 \dot{u}_i{}^B dA + \int_V F_i{}^0 \dot{u}_i{}^B dv \geq \int_V \sigma_{ij}{}^B \dot{\epsilon}_{ij}{}^B dv + \int_S T_i{}^B \Delta \dot{u}_i{}^B dS \quad \ldots\ldots [7]$$

Equations [6] and [7] are incompatible and Theorem B cannot be false because $\sigma_{ij}{}^B \dot{\epsilon}_{ij}{}^B > \sigma_{ij}{}^0 \dot{\epsilon}_{ij}{}^B$, $T_i{}^B \Delta \dot{u}_i{}^B$ is a frictional dissipation and, therefore, zero or positive, and $T_i{}^0 \Delta \dot{u}_i{}^B$ is zero or negative. The last statement follows from the fact that $T_i{}^0$ is normal to S at each point and is compressive while $\Delta \dot{u}_i{}^B$ is a relative tangential displacement, and possibly a separation as well, but not an overlap.

The friction Theorems A and B thus have been proved for all stable convex-yield functions. Occasionally they enable the limit load to be computed precisely for finite nonzero friction. The well-known two-dimensional punch problem for a Prandtl-Reuss or a Mises material provides such an example. Two solutions are available for upper-bound computations. One by Prandtl (6), Fig. 7(*a*), contains a rigid region which acts as an extension of the punch; there is no relative motion between the punch and the contact area. The other by Hill (7), Fig. 7(*b*), assumes zero friction, and appreciable slip does take place. Both solutions give the same answer for the average pressure, $p = (2 + \pi)k$, where k is the yield stress in shear. A lower-bound solution of $5k$ has been reported (8) and Shield has recently found $(2 + \pi)k$. Therefore the limit pressure is $(2 + \pi)k$ for all possible values of the coefficient of friction.

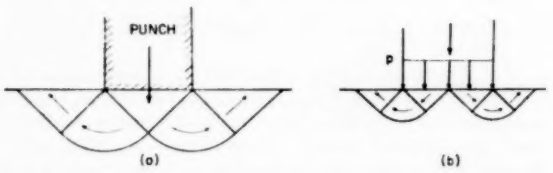

FIG. 7 PRANDTL (*a*) AND HILL (*b*) SOLUTIONS TO PUNCH PROBLEM

It often will be found, however, that Theorems A and B do not provide very close bounds. The concept of the plastic cohesionless-soil interface, already discussed in considerable detail, then may be of further help in the following theorem:

C Any set of loads which will not cause collapse of an assemblage of bodies with frictional interfaces, will not produce collapse when the interfaces are "cemented" together with a cohesionless soil of friction angle $\phi = \arctan \mu$.

The proof of Theorem C follows essentially from the observation that the state of stress in the friction case satisfies the conditions $f(\sigma_{ij}) \leq k^2$ and $|\tau| \leq \mu |\sigma|$ at impending collapse. A safe state of stress exists, therefore, for the soil case when collapse does not occur in the friction problem.

CONCLUSIONS

The limit load for an assemblage of bodies with frictional interfaces is bounded below by the limit load for the same bodies with zero friction on the interfaces. It is bounded above by the limit load for no relative motion at the interfaces and also by the limit load for the same assemblage cemented at the interfaces by a cohesionless soil. Limit theorems applicable to these bounding problems do not apply generally.

BIBLIOGRAPHY

1 "Some Implications of Work-Hardening and Ideal Plasticity," by D. C. Drucker, *Quarterly of Applied Mathematics*, vol. 7, 1950, pp. 411–418.

2 "Soil Mechanics and Plastic Analysis or Limit Design," by D. C. Drucker and W. Prager, *Quarterly of Applied Mathematics*, vol. 10, 1952, pp. 157–165.

3 "The Safety Factor of an Elastic-Plastic Body in Plane Strain," by D. C. Drucker, H. J. Greenberg, and W. Prager, JOURNAL OF APPLIED MECHANICS, Trans. ASME, vol. 73, 1951, pp. 371–378.

4 "Extended Limit Design Theorems for Continuous Media," by D. C. Drucker, H. J. Greenberg and W. Prager, *Quarterly of Applied Mathematics*, vol. 9, 1952, pp. 381–389.

5 "Theory of Perfectly Plastic Solids," by P. G. Hodge and W. Prager, John Wiley & Sons, Inc., New York, N. Y., section 26.

6 "Über die Haerte plastischer Körper," by L. Prandtl, Nachrichten von der Koeniglichen Gesellschaft der Wissenschaften zu Goettingen, *Mathematisch-physikalische Klasse*, 1920, pp. 74–85.

7 "The Plastic Yielding of Notched Bars Under Tension," by R. Hill, *Quarterly Journal of Mechanics and Applied Mathematics*, vol. 2, 1949, pp. 40–52.

8 "The Application of Limit Analysis to Punch-Indentation Problems, by R. T. Shield and D. C. Drucker, JOURNAL OF APPLIED MECHANICS, Trans. ASME, vol. 75, 1953, pp. 453–460.

The Wave Method for Solving Flexural Vibration Problems

By R. P. N. JONES,[1] SHEFFIELD, ENGLAND

In this paper the use of normal mode and wave methods in problems of dynamic loading on beams is discussed, and the methods are applied to simple problems of uniform beams under a suddenly applied load. For these problems, mathematically exact results have been obtained, enabling a comparison to be made between the two types of solution. Experimental results for these problems also have been obtained, using an apparatus which releases the beam from a deflected position, and displays a record of the resultant response on an oscillograph screen, using a time base synchronized with the release of the beam. Good agreement is obtained between the experimental and theoretical results, and it is shown that the wave solution is useful for determining the initial response of the beam, while the subsequent response can be better obtained from the normal-mode solution.

Nomenclature

The following nomenclature is used in the paper:

$C(z)$, $S(z)$ = Fresnel's integrals
EI = flexural rigidity of beam
$F(x, t)$ = distributed lateral load
$H(t)$ = Heaviside unit function
l = length of beam
M = bending moment
P = concentrated lateral load
p = inversion parameter used in Laplace transform
$q = [p^2\mu/4EI]^{1/4}$
t = time
y = deflection of beam
$\bar{y}$ = Laplace transform of y
y_n = deflection corresponding to nth natural mode of vibration
x = distance along beam
$z = \frac{x^2}{4t}\sqrt{\frac{\mu}{EI}}$
μ = mass of beam per unit length
ω_n = natural circular frequency corresponding to nth mode of vibration

Introduction

Many new problems involving dynamic loads on structures have arisen in recent years, particularly in connection with aircraft structures, such as, the stress due to landing loads.

The usual method of treating such problems is to obtain a solution in terms of the normal modes of vibration of the structure and, in most cases, this solution shows a convergence which is adequate for practical computation. Moreover, the method can be applied to structures whose modes of vibration have been determined experimentally.

An alternative method of solution is the so-called "wave method." Whereas the normal-mode solution is merely an extension of the treatment of systems having only a finite number of degrees of freedom, the concept of the wave solution is associated with a continuous system, having an infinite number of degrees of freedom. The solution is, in fact, in the form of a series, the first term of which represents an initial disturbance spreading through the system, while the succeeding terms represent reflections of this disturbance from the boundaries of the system.

This wave method can be applied to diffusive problems, such as the conduction of heat, as well as to problems in which there is a characteristic velocity of propagation, as, for example, in the case of longitudinal impact of bars. In the latter case the wave solution consists of a finite number of terms only, depending on how many reflections have taken place, while in diffusive problems, in which there is no limiting velocity of propagation, reflections occur simultaneously with the initial disturbance, and the wave solution is an infinite series.

While the wave method probably has a narrower field of practical application than the normal-mode method, there are cases in which it is of value, such as the determination of the initial response of a system under a suddenly applied load, or an impulse of short duration. In a problem of this type the normal-mode solution converges very slowly during the initial period of the response (that is, up to about $^1/_{20}$ of the fundamental period of the system) while the wave solution, on the other hand, shows excellent convergence in these circumstances.

A disadvantage of the wave method is the difficulty of applying it to a practical system not directly amenable to mathematical treatment. In such a case a step-by-step numerical solution would be necessary, and the computation would be considerably more laborious than in the normal-mode method in which, once the modes have been determined, nothing more difficult than a few graphical integrations is involved.

In the present paper the author has applied the normal-mode and wave methods to the treatment of simple problems involving the response of uniform beams to a suddenly applied load. For these problems, mathematically exact solutions have been obtained, which have enabled a comparison to be made between the results obtained by the two methods. A comparison also has been made with the results obtained from models, using an apparatus which produces, in effect, a suddenly applied load on the model, and displays a record of the subsequent response on a cathode-ray-oscillograph screen, using a time base synchronized with the application of the load.

Normal-Mode Solutions

The classical method of obtaining a solution of dynamic-loading problems in terms of the natural modes of vibration of the structure is probably sufficiently well known to require no detailed description here. The usual method of solution, as given,

---

[1] Lecturer in Applied Mechanics, University of Sheffield.

Paper presented at the National Conference of the Applied Mechanics Division, State College, Pa., June 16–21, 1952, of The American Society of Mechanical Engineers.

Discussion of this paper should be addressed to the Secretary, ASME, 29 West 39th Street, New York, N. Y., and will be accepted until April 12, 1954, for publication at a later date. Discussion received after the closing date will be returned.

Note: Statements and opinions advanced in papers are to be understood as individual expressions of their authors and not those of the Society. Manuscript received by the ASME Applied Mechanics Division, July 3, 1951.

for example, by Den Hartog (1),[2] makes use of the orthogonal property of the modes, by means of which the applied-load distribution is resolved into a series of "natural loading functions."

The first problem considered in this paper is that of a simply supported uniform beam having a concentrated load $PH(t)$ applied at the mid-point, $H(t)$ being Heaviside's unit function, defined by

$$\left.\begin{aligned} H(t) &= 0, \; t < 0 \\ H(t) &= 1, \; t > 0 \end{aligned}\right\} \quad \ldots\ldots [1]$$

In this case only the symmetrical modes are excited. These are given by

$$y_n = \cos \frac{n\pi x}{l}, \; n = 1, 3, 5 \ldots\ldots [2]$$

l being the length of the beam and origin of x being taken at the mid-point. The natural circular frequencies are

$$\omega_n = \frac{n^2\pi^2}{l^2}\sqrt{\frac{EI}{\mu}}, \; n = 1, 3, 5 \ldots\ldots [3]$$

The normal-mode solution obtained for this problem gives, for the deflection

$$y = \frac{2Pl^3}{EI\,\pi^4}\sum \frac{1}{n^4} \cos \frac{n\pi x}{l}\,(1 - \cos \omega_n t) \ldots\ldots [4]$$

and for the bending moment

$$M = \frac{2Pl}{\pi^2}\sum \frac{1}{n^2} \cos \frac{n\pi x}{l}\,(1 - \cos \omega_n t) \ldots\ldots [5]$$

The second problem considered is that of a cantilever with a load $PH(t)$ applied at the free end.

Taking origin of x at the free end, the natural modes are

$$y_n = (\cosh \alpha_n l + \cos \alpha_n l)(\cosh \alpha_n x + \cos \alpha_n x) - (\sinh \alpha_n l - \sin \alpha_n l)(\sinh \alpha_n x + \sin \alpha_n x) \ldots\ldots [6]$$

and the natural frequencies are given by

$$\omega_n = \frac{1}{l^2}\sqrt{\frac{EI}{\mu}}\,(\alpha_n l)^2, \; n = 1, 2, 3 \ldots\ldots [7]$$

where $\alpha_1 l$, $\alpha_2 l$, and so on, are the roots of the frequency equation

$$1 + \cos \alpha l \cosh \alpha l = 0 \ldots\ldots [8]$$

The deflection and bending moment obtained in this case are

$$y = \frac{2P}{\mu l}\sum \frac{y_n\,(1 - \cos \omega_n t)}{\omega_n^2(\cosh \alpha_n l + \cos \alpha_n l)} \ldots\ldots [9]$$

$$M = -\frac{2P\,EI}{\mu l}\sum \frac{d^2y_n}{dx^2}\,\frac{(1 - \cos \omega_n t)}{\omega_n^2\,(\cosh \alpha_n l + \cos \alpha_n l)} \ldots [10]$$

The Infinite Beam Problem

As a preliminary to the development of wave solutions, the basic problem of the response of an infinite beam will be investigated. Solutions to problems of this type have been obtained by Boussinesq (2) and Rayleigh (3) using definite integrals, and by Carslaw and Jaeger (4) using operational methods. In this paper the latter method is employed.

Considering the problem of an infinite beam, having a concentrated load $PH(t)$ applied at the point $x = 0$, the basic equation of motion is

$$\frac{\partial^4 y}{\partial x^4} + \frac{\mu}{EI}\,\frac{\partial^2 y}{\partial t^2} = 0 \ldots\ldots [11]$$

[2] Numbers in parentheses refer to the Bibliography at the end of the paper.

The boundary conditions for the half of the beam $x > 0$ are

$$\frac{\partial y}{\partial x} = 0, \; \frac{\partial^3 y}{\partial x^3} = \frac{P}{2EI} \quad \text{at} \quad x = 0 \ldots\ldots [12]$$

Multiplying Equation [11] by e^{-pt} and integrating from $t = 0$ to $t = \infty$ gives

$$\frac{d^4\bar{y}}{dx^4} + \frac{p^2\mu}{EI}\,\bar{y} = 0 \ldots\ldots [13]$$

where $\bar{y}$ is the Laplace transform of y with respect to t, defined by

$$\bar{y}(x, p) = \int_0^\infty y(x, t)e^{-pt}\,dt \ldots\ldots [14]$$

The Boundary Conditions [12] are transformed to

$$\frac{d\bar{y}}{dx} = 0, \; \frac{d^3\bar{y}}{dx^3} = \frac{P}{2p\,EI} \quad \text{at} \quad x = 0 \ldots\ldots [15]$$

The general solution of Equation [13] is

$$\bar{y} = e^{-qx}(A \cos qx + B \sin qx) + e^{qx}(C \cos qx + D \sin qx) \ldots\ldots [16]$$

where

$$q^4 = \frac{p^2\mu}{4EI} \ldots\ldots [17]$$

Since y must tend to zero for large values of x the constants C and D in Equation [16] must be taken equal to zero. The remaining constants A and B can be determined from the Boundary Conditions [15] giving the following solution for $\bar{y}$

$$\bar{y} = \frac{P}{8p\,EI\,q^3}\,e^{-qx}(\cos qx + \sin qx) \ldots\ldots [18]$$

The solution of the problem is now obtained by inversion of the Transform [18]. However, the inversion is difficult and it is more convenient to deal with the transform

$$\frac{d^3\bar{y}}{dx^3} = \frac{P}{2p\,EI}\,e^{-qx} \cos qx \ldots\ldots [19]$$

This transform is evaluated by Carslaw and Jaeger (4) who obtain a solution in terms of definite integrals, which, after rearrangement, may be written in the form

$$\frac{\partial^3 y}{\partial x^3} = \frac{P}{2EI}\,\{1 - C(z) - S(z)\} \ldots\ldots [20]$$

where

$$z = \frac{x^2}{4t}\sqrt{\frac{\mu}{EI}} \ldots\ldots [21]$$

and $C(z)$, $S(z)$, are Fresnel's integrals defined by

$$\left.\begin{aligned} C(z) &= \int_0^z \frac{\cos \psi\,d\psi}{\sqrt{(2\pi\psi)}} \\ S(z) &= \int_0^z \frac{\sin \psi\,d\psi}{\sqrt{(2\pi\psi)}} \end{aligned}\right\} \ldots\ldots [22]$$

Short tables of $C(z)$ and $S(z)$ are given by Jahnke and Emde (5). In some cases approximations by series can be used, details of which are given by Watson (6).

The bending moment in the beam may be obtained from Equation [20] by integrating with respect to x, using the relations

$$\left.\begin{aligned}\int C(z)\,dx &= x\left\{C(z) - \frac{\sin z}{\sqrt{2\pi z}}\right\}\\ \int S(z)\,dx &= x\left\{S(z) + \frac{\cos z}{\sqrt{2\pi z}}\right\}\end{aligned}\right\} \quad \ldots\ldots [23]$$

This gives

$$M = -EI\frac{\partial^2 y}{\partial x^2} = -\frac{Px}{2}\left[1 - C(z) - S(z) + \frac{\sin z - \cos z}{\sqrt{2\pi z}}\right] \ldots [24]$$

By integrating twice more, the deflection may be obtained

$$y = \frac{Px^3}{12EI}\left\{1 - C(z) - S(z) + \frac{3}{2z}[S(z) - C(z)] + \frac{1}{z\sqrt{(2\pi z)}}[z(\sin z - \cos z) + (\cos z + \sin z)]\right\} \ldots [25]$$

It may be verified by substitution that the solution satisfies the differential Equation [11] and the Boundary Conditions [12].

The solution to the problem of a beam extending to infinity in one direction only, with a load $PH(t)$ applied at the free end $x = 0$, may be obtained by a similar analysis. The result is

$$M = -Px\left[1 - 2C(z) + \sqrt{\frac{2}{\pi z}}\sin z\right] \ldots\ldots [26]$$

$$y = \frac{Px^3}{6EI}\left[1 - 2C(z) + \frac{3}{2z}(2S(z) - 1) + \frac{1}{z}\sqrt{\frac{2}{\pi z}}(\cos z + z\sin z)\right] \ldots\ldots [27]$$

The Wave Method

Wave methods were so-called by Heaviside (7) who was one of the first investigators to use this type of solution. In some cases a wave solution can be obtained very simply by the use of an image system, on an infinite beam, suitably chosen to obtain the correct boundary conditions for the section of the beam under consideration. An example of this is the problem of the simply supported beam, in which the image system, shown in Fig. 1, consists of loads of magnitude $PH(t)$ and alternating sign spaced at distances l along an infinite beam.

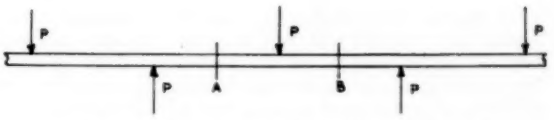

FIG. 1 IMAGE SYSTEM FOR SIMPLY SUPPORTED BEAM

It is seen that this load system is antisymmetrical about the points A and B and, therefore, at these points

$$y = 0, \quad \frac{\partial^2 y}{\partial x^2} = 0 \ldots\ldots\ldots\ldots\ldots [28]$$

The section AB, considered separately, thus has boundary conditions identical with those of the simply supported beam, and the solution of the problem can be obtained from the infinite beam solution, using the principle of superposition. The deflection is therefore given by

$$\left.\begin{aligned}y = \; & y_0(x)\\ & - y_0(l - x) + y_0(2l - x) - \ldots\\ & - y_0(l + x) + y_0(2l + x) - \ldots\end{aligned}\right\} \quad \ldots\ldots [29]$$

where $y_0(x)$ is the solution given by Equation [25] for the infinite-beam problem.

A similar solution can be written for the bending moment.

In the case of beams with other conditions of support, such as free or clamped ends, it is not possible to find an image system on an infinite or semi-infinite beam which will produce the correct boundary conditions. An obvious, but difficult, alternative method involves determining the reflections from the ends of the beam due to the given end conditions. A third method, used here by the author, is by means of the Laplace transform, and as an example the method will be applied to the problem of the cantilever considered earlier.

Taking origin of x at the free end of the cantilever, the boundary conditions are

$$\left.\begin{aligned}&\text{At } x = 0, \quad \frac{\partial^2 y}{\partial x^2} = 0, \quad \frac{\partial^3 y}{\partial x^3} = \frac{P}{EI}\\ &\text{At } x = l, \quad y = 0, \quad \frac{\partial y}{\partial x} = 0\end{aligned}\right\} \quad \ldots\ldots\ldots [30]$$

Applying the Laplace transformation to these conditions gives

$$\left.\begin{aligned}&\text{At } x = 0, \quad \frac{d^2\bar{y}}{dx^2} = 0, \quad \frac{d^3\bar{y}}{dx^3} = \frac{P}{pEI}\\ &\text{At } x = l, \quad \bar{y} = 0, \quad \frac{d\bar{y}}{dx} = 0\end{aligned}\right\} \quad \ldots\ldots\ldots [31]$$

Using these conditions to determine the constants A, B, C, and D in Equation [16] the following solution is obtained for $\bar{y}$

$$\bar{y} = \frac{P}{2pEIq^3\Delta}\left\{\begin{aligned}&e^{-q(2l+x)}[\sin qx + \cos qx - \sin q(2l - x)]\\ &+ e^{-q(2l-x)}[\sin qx - \cos qx - \sin q(2l - x)]\\ &+ e^{-qx}\cos qx - e^{-q(4l-x)}\cos qx\end{aligned}\right\} \quad \ldots\ldots\ldots [32]$$

where

$$\Delta = 1 + 4e^{-2ql} + 2e^{-2ql}\cos 2ql + e^{-4ql} \ldots\ldots [33]$$

The term $1/\Delta$ may be expanded by the binomial theorem, giving

$$1/\Delta = 1 - 4e^{-2ql} - 2e^{-2ql}\cos 2ql - e^{-4ql} + \ldots\ldots [34]$$

By substituting this expansion in Equation [32], after multiplying and arranging the terms in order of ascending negative powers of e, the following series expansion is obtained

$$\bar{y} = \frac{P}{2pEIq^3}\left\{\begin{aligned}&e^{-qx}\cos qx\\ &+ e^{-q(2l-x)}[\sin qx - \cos qx - \sin q(2l - x)]\\ &+ e^{-q(2l+x)}[\sin qx - 3\cos qx - \sin q(2l - x)\\ &- \cos q(2l - x) - \cos q(2l + x)] + \ldots\end{aligned}\right\} \quad \ldots\ldots\ldots [35]$$

The required wave solution for y can now be obtained by inverting the foregoing series term by term. The first term corresponds to the solution for the semi-infinite-beam problem. The succeeding terms, representing the reflections from the ends of the beam, contain transforms of a more general type than those encountered previously. In general, these transforms cannot be evaluated in terms of tabulated functions, but integral and series evaluations are possible.

Both the wave solutions obtained here may be shown to have good convergence, for numerical computation, provided that the time t is small compared with the fundamental natural period of the beam. A good approximation is obtained by taking only the first term of the series, which is equivalent to treating the beam as infinite, or semi-infinite, as the case may be.

Experimental Work

In the development of the apparatus the immediate aim was to obtain results for comparison with the foregoing theoretical work, although the apparatus of course would be equally suitable for the independent investigation of models not amenable to mathematical analysis. The particular function required of the apparatus was that it should produce a suitable dynamic load on a structural model and display a record of the resultant response (e.g., strain or velocity at some chosen measuring point) on a time base synchronized with the application of the load.

For the present investigation, a dynamic load of the "suddenly-applied-force" type was chosen as most suitable for the comparison of theoretical and experimental results, and a convenient way of achieving this type of loading is to release the structure suddenly from a deflected position.

For this purpose a moving-coil loud-speaker element was used, consisting of a coil wound on a stiff paper tube operating in conjunction with a magnet with an annular gap. The coil was cemented to the beam, while the magnet was mounted independently on the test-rig structure, and adjusted in position to allow the coil to move freely in the gap. Thus the only disturbing factors introduced were the mass of the coil and the slight damping resulting from the piston action of the center pole piece within the coil tube.

In both the model beams investigated the initial deflections before release were controlled by means of stops, close to the loading coil, the current through the coil being adjusted to bring the beam lightly against the stop. The force applied by the coil was deduced from a static loading test on the beam. The coil was connected in the anode circuit of a power pentode, the current through the coil being adjusted by means of the grid bias. The beam was released by applying a large negative grid bias from a dry battery, thus cutting off the anode current. The initiating voltage for the single-sweep time base of the cathode-ray oscillograph also was obtained from this battery, thus synchronizing the start of the time base with the release of the beam.

In the first experiment, a steel cantilever of length 3 ft and cross section 1 in. wide $\times$ $^1/_4$ in. deep was used. The loading coil was mounted at the free end of the cantilever, and the load applied before release was 0.080 lb.

Velocity measurements were made at the free end of the cantilever using a coil-and-magnet assembly similar to that used for loading the cantilever. An indirect calibration of the velocity-measuring coil was obtained by determining the effective flux turns of the winding. This was done by measuring the force exerted by the coil when a known current was passed through it. As the velocity measurements were confined to the first $^1/_{10}$ sec of the motion of the beam, an a-c amplifier with a long time-constant (about 2 sec) was used. The amplifier gain was approximately 1000.

In the second experiment, strain measurements were made on a beam with simply supported end conditions. In order to obtain measurable strains, a slender beam was used, consisting of a 6-ft length of steel bar of cross section $^3/_8$ in. wide $\times$ $^1/_8$ in. deep. "Pin-jointed" conditions at the ends of the beam were obtained by using small magneto-type ball races, and the mounting bracket at one end was hinged to allow longitudinal movement.

The loading coil was attached at the mid-point of the beam and strain measurements were made, using wire-resistance strain gages, at three measuring positions (a), (b), and (c), distant 6.6, 18, and 30 in., respectively, from the mid-point. The strain gages used were Baldwin Southwark type C.14, having a resistance of 2000 ohms and a gage factor of 3.4. In order to obtain as high a sensitivity as possible, four operative gages were used, applied on the upper and lower surfaces at two symmetrical positions on the beam, the gages being connected to give additive electrical output from the bridge. The amplifier gain used in these measurements was approximately 10,000 and the load applied by the coil, before release, was 0.82 lb.

Results and Discussion

Fig. 2 shows the experimental record of the velocity at the free end of the cantilever over the first half of the fundamental period, together with the velocity calculated by the normal-mode method using (a) two terms and (b) four terms. The latter curve shows good agreement with the experimental result, apart from a slight progressive phase error in the higher harmonics. In this case the normal-mode method is clearly adequate for determining the response when the time interval is of the same order of magnitude as the fundamental natural period of the beam.

The bending moments in the simply supported beam at the three measuring points (a), (b), and (c) were calculated theoretically using the first four terms of the normal-mode solution, and also using the wave solution with up to five terms. These results are presented in Figs. 3, 4, and 5, together with the experimental records.

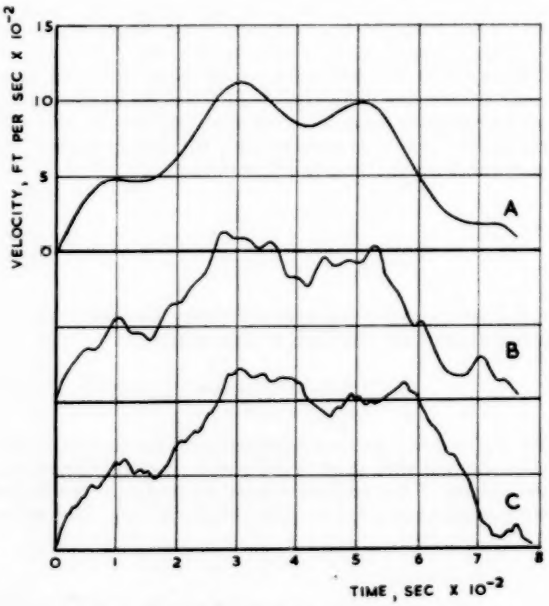

Fig. 2 Velocity at Free End of Cantilever
(*A*, Normal-mode solution, 2 terms. *B*, Normal-mode solution, 4 terms. *C*, Experimental result.)

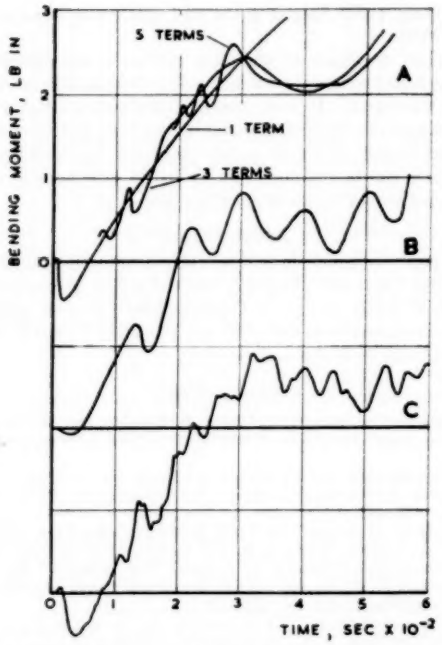

FIG. 3 BENDING MOMENT IN SIMPLY SUPPORTED BEAM, POSITION *a*
(*A*, Wave solution with 1, 3, and 5 terms. *B*, Normal-mode solution, 4 terms. *C*, Experimental result.)

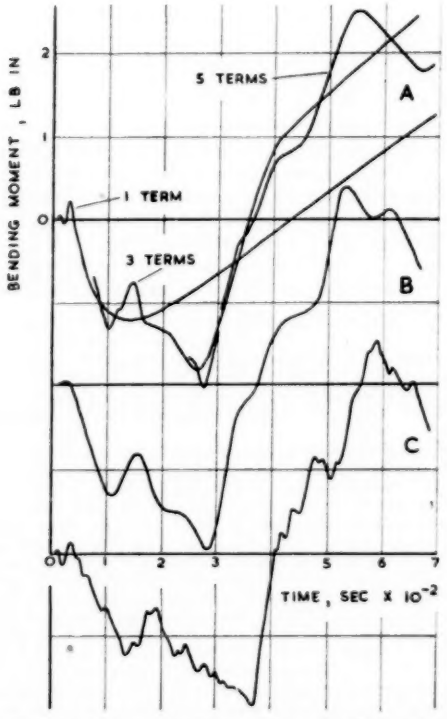

FIG. 4 BENDING MOMENT, IN SIMPLY SUPPORTED BEAM, POSITION *b*
(*A*, Wave solution with 1, 3, and 5 terms. *B*, Normal-mode solution, 4 terms. *C*, Experimental result.)

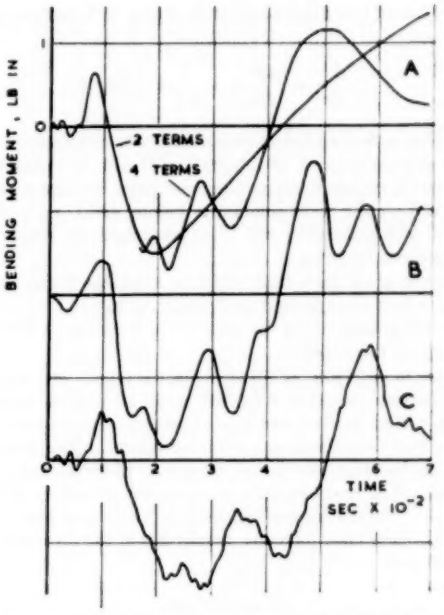

FIG. 5 BENDING MOMENT IN SIMPLY SUPPORTED BEAM, POSITION *c*
(*A*, Wave solution with 2 and 4 terms. *B*, Normal-mode solution, 4 terms. *C*, Experimental result.)

The figures clearly show the superiority of the wave solution for small values of t. The normal-mode solution, using four terms, is evidently unsatisfactory at times less than about 0.01 sec, that is, approximately $^1/_{50}$ of the fundamental period of the beam. The convergence of the wave solution, on the other hand, is excellent at times up to 0.005 sec, a very good approximation being obtained when only the first term is used (except in the neighborhood of the ends of the beam, where the terms tend to regroup themselves in pairs). Even at times up to 0.05 sec, i.e., approximately $^1/_{10}$ of the fundamental period, the convergence is adequate for numerical computation. There is thus a useful overlap in the field of application of the two solutions.

In so far as the values of the bending moment are concerned, there is good agreement between the experimental and theoretical values. There is, however, a discrepancy in the time scales, the measured sequence of events being slower than the calculated sequence. This error may be due to the mass of the loading coil—about 1 per cent of the mass of the beam—and to the effects of internal damping and shear deflection.

APPLICATION TO OTHER LOADING CONDITIONS

As the main object of the paper is to compare the convergence of the normal-mode and wave solutions, the only type of loading considered so far has been a concentrated load in the form of a Heaviside unit function. Many practical problems, however, will involve a distributed load having a more complex time variation, and a brief consideration therefore will be given to the use of the wave method in such problems.

The most general case will lead to an equation of motion for the beam

$$\frac{\partial^4 y}{\partial x^4} + \frac{\mu}{EI}\frac{\partial^2 y}{\partial t^2} = \frac{1}{EI}F(x, t) \quad \ldots\ldots\ldots\ldots [36]$$

where $F(x, t)$ is the distributed load on the beam. The opera-

tional form of this equation, corresponding to Equation [13], is now

$$\frac{d^4\bar{y}}{dx^4} + \frac{\mu p^2}{EI}\bar{y} = \frac{1}{EI}\bar{F}(x, p) \quad [37]$$

where $\bar{F}(x, p)$ is the Laplace transform of $F(x, t)$ with respect to t.

The general solution of Equation [37] will now contain two parts, (*a*) a complementary function, given by Equation [16], which will yield a wave solution as before, and (*b*) a particular integral, which normally will be of comparatively simple form, allowing direct inversion.

An alternative procedure, which is available if the function $F(x, t)$ cannot be expressed analytically, is to build up the solution by integration, using the solution for the simple loading case considered in this paper.

In certain problems, as, for example, the impact of a mass on a beam, the time variation of the load on the beam is not known explicitly, and an auxiliary equation of motion takes the place of the simpler boundary conditions so far considered. The application of the Laplace transform to this equation will yield a simple algebraic equation, enabling an operational solution to be obtained, which, by suitable expansion, may be developed into a wave solution. The chief difficulty usually lies in the inversion of the transforms.

Conclusions

A comparison of the results obtained by the normal-mode and wave methods shows the superiority of the wave method for determining the initial response of an elastic system under a sudden application of load. The results obtained by both methods, within their useful ranges, agree well with those obtained experimentally.

The chief drawback of the wave method is the difficulty of applying it to a practical system not directly amenable to mathematical treatment. In such a case, a step-by-step integration of the equations of equilibrium would be required, and the solution would be considerably more tedious than the normal-mode solution, which can be obtained quickly by an experimental determination of the normal modes of vibration.

Acknowledgment

This paper is based on a thesis submitted by the author to Cambridge University, England, and the author wishes to thank Profs. J. F. Baker and D. G. Christopherson for their guidance, also the Department of Scientific and Industrial Research, whose financial grant made the work possible.

BIBLIOGRAPHY

1 "Mechanical Vibrations," by J. P. Den Hartog, McGraw-Hill Book Company, Inc., New York, N. Y., third edition, 1947, pp. 188-189.

2 "Applications des Potentials à l'Étude de l'Équilibre et du Mouvement des Solides Élastiques," by J. Boussinesq, Paris, France, 1885, pp. 435–463.

3 "Theory of Sound," by Lord Rayleigh, Macmillan and Company, Ltd., London, England, second edition, 1894, pp. 302–304.

4 "Operational Methods in Applied Mathematics," by H. S. Carslaw and J. C. Jaeger, Oxford University Press, London, England, first edition, 1941, pp. 152–154.

5 "Functionentafeln," by E. Jahnke and F. Emde, Dover Publications, New York, N. Y., fourth edition, 1945, pp. 35-36.

6 "Theory of Bessel Functions," by G. N. Watson, Cambridge University Press, London, England, first edition, 1922, p. 545.

7 "Electromagnetic Theory," by O. Heaviside, Ernest Benn, London, England, first edition, vol. 2, 1899, pp. 69, 72, 83.

On the Strain Energy of Shells

By H. L. LANGHAAR[1] and D. R. CARVER[2]

In a previous paper,[3] the strain energy of a shell was derived with the aid of the assumption that only the linear terms in the thickness co-ordinate z need be retained in the expressions for the strains. Recently, Bleich and DiMaggio[4] derived a strain-energy expression for circular cylindrical shells without using power series in z. The present paper shows that power series in z may be eliminated, in general, and that the errors caused by linearizing approximations are frequently significant.

IN the present paper, let (x, y) be co-ordinates on the middle surface of a shell, such that the co-ordinate lines coincide with the lines of principal curvature. Then the square of the line element is

$$ds^2 = A^2\,dx^2 + B^2\,dy^2 \quad \ldots\ldots [1]$$

where $A(x, y)$ and $B(x, y)$ are positive functions.

Let z be the normal distance from the middle surface. The positive sense of z determines the positive side of the shell. Let (R_x, R_y) be the radii of curvature of normal sections of the middle surface in the x and y-directions. These are defined to be positive if their corresponding centers of curvature lie on the negative side of the tangent plane.

The variables (x, y, z) are orthogonal space co-ordinates. The square of the line element is

$$ds^2 = \alpha^2\,dx^2 + \beta^2\,dy^2 + dz^2 \quad \ldots\ldots [2]$$

where

$$\alpha = A\left(1 + \frac{z}{R_x}\right), \quad \beta = B\left(1 + \frac{z}{R_y}\right) \quad \ldots\ldots [3]$$

Let (u, v, w) be the projections of the displacement vector of the middle surface on the tangents to the x, y, and z-co-ordinate lines, respectively. These components are functions of x and y. They are positive if they have the positive senses of the corresponding co-ordinate lines. Since the co-ordinates (x, y, z) are orthogonal, the strain notations $(\epsilon_x, \epsilon_y, \epsilon_z, \gamma_{yz}, \gamma_{zx}, \gamma_{xy})$ may be retained with their conventional meanings.

E. Reissner[5] derived expressions for the strains $(\epsilon_x, \epsilon_y, \gamma_{xy})$ in terms of the displacements (u, v, w), on the basis of the following assumptions:

(a) $\gamma_{xz} = \gamma_{yz} = 0$

(b) Quadratic terms in (u, v, w) and their derivatives need not be retained in the strain tensor.

(c) The variation of the normal displacement with z has a negligible effect on the tangential displacements.

Reissner's formulas may be expressed in the following form

$$\left.\begin{aligned}
\epsilon_x &= \frac{1}{\alpha}\frac{\partial}{\partial x}\left(\frac{u\alpha - zw_x}{A}\right) + \frac{\alpha_y}{\alpha}\left(\frac{v\beta - zw_y}{\beta B}\right) + \frac{\alpha_z}{\alpha}w \\
\epsilon_y &= \frac{1}{\beta}\frac{\partial}{\partial y}\left(\frac{v\beta - zw_y}{B}\right) + \frac{\beta_z}{\beta}\left(\frac{u\alpha - zw_x}{\alpha A}\right) + \frac{\beta_z}{\beta}w \\
\gamma_{xy} &= \frac{\beta}{\alpha}\frac{\partial}{\partial x}\left(\frac{v\beta - zw_y}{\beta B}\right) + \frac{\alpha}{\beta}\frac{\partial}{\partial y}\left(\frac{u\alpha - zw_x}{\alpha A}\right)
\end{aligned}\right\} \quad \ldots [4]$$

where subscripts (x, y, z) denote partial derivatives.

These equations are geometrical; they are not contingent on elastic behavior of the shell.

If plane stress is assumed to exist in any lamina that is bounded by surfaces of the family $z = \text{const}$, the stresses $(\sigma_x, \sigma_y, \tau_{xy})$ are expressed in terms of the strains $(\epsilon_x, \epsilon_y, \gamma_{xy})$ by the usual formulas of plane-stress theory. The membrane forces and the bending and twisting moments in the shell are then obtained by simple integrations of the stresses with respect to[6] z.

The strain-energy density is

$$V = \frac{E}{2(1-\nu^2)}\left[\epsilon_x^2 + \epsilon_y^2 + 2\nu\,\epsilon_x\epsilon_y + \frac{1}{2}(1-\nu)\,\gamma_{xy}^2\right] \quad \ldots [5]$$

The element of volume of the shell is $\alpha\beta\,dx\,dy\,dz$. Consequently, the strain energy of the shell is

$$U = \int\int\int V\,\alpha\,\beta\,dx\,dy\,dz \quad \ldots\ldots [6]$$

In view of Equations [3], [4], and [5], the integrand in Equation [6] is a rational function of z. Consequently, integration with respect to z is not inherently difficult.

For example, for a circular cylindrical shell with axial co-ordinate x and angular co-ordinate $y = \theta$, $A = 1$, and $B = a$, where a is the radius of the middle surface. The formula of Bleich and DiMaggio is obtained by substituting these values into Equations [3], [4], [5], and [6].

The linearizing of Equation [4] with respect to z is a questionable approximation, for the membrane strains and the bending strains often have quite different orders of magnitude. Relatively small inaccuracies in one of these strain components consequently may obliterate the other one entirely. A simple example illustrates these conditions. Fig. 1 represents a cantilever curved beam with a rectangular cross section of depth h

---

[1] Professor of Theoretical and Applied Mechanics, University of Illinois, Urbana, Ill. Mem. ASME.

[2] Associate Professor of Applied Mechanics, Kansas State College, Manhattan, Kans.

[3] "A Strain-Energy Expression for Thin Elastic Shells," by H. L. Langhaar, JOURNAL OF APPLIED MECHANICS, Trans. ASME, vol. 71, 1949, p. 183.

[4] "A Strain-Energy Expression for Thin Cylindrical Shells," by H. H. Bleich and F. DiMaggio, ONR Project NR-360-002, Technical Report No. 6, CU-6-52-ONR-266(08)-CE, September, 1952.

[5] "A New Derivation of the Equations for the Deflections of Elastic Shells," by E. Reissner, *American Journal of Mathematics*, vol. 63, 1941, pp. 177–184.

[6] "Statik und Dynamik der Schalen," by W. Flügge, Edwards Brothers, Inc., Ann Arbor, Mich., 1943.

Contributed by the Applied Mechanics Division and presented at the Annual Meeting, New York, N. Y., November 29–December 4, 1953, of THE AMERICAN SOCIETY OF MECHANICAL ENGINEERS.

Discussion of this paper should be addressed to the Secretary, ASME, 29 West 39th Street, New York, N. Y., and will be accepted until April 12, 1954, for publication at a later date. Discussion received after the closing date will be returned.

NOTE: Statements and opinions advanced in papers are to be understood as individual expressions of their authors and not those of the Society. Manuscript received by ASME Applied Mechanics Division, December 12, 1952. Paper No. 53—A-10.

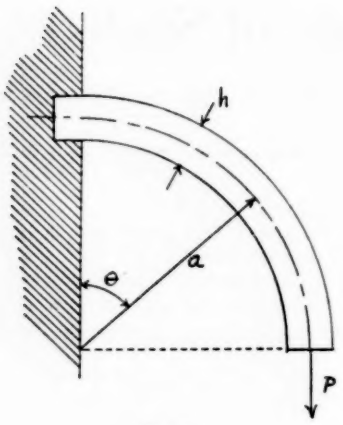

FIG. 1

and width b. The load P is applied at the center of the end section. The radius of the centroidal axis of the beam is a. For the case of plane strain ($u = 0$), the following formulas for the normal displacement w and the circumferential displacement v may be derived by the principle of virtual work and Euler's equations of the calculus of variations, in conjunction with Equations [3], [4], [5], and [6]

$$w = \frac{K}{2\left(\frac{aC}{h} - 1\right)} [\sin\theta - \theta\cos\theta + 2\cos\theta - 2] \quad \ldots [7]$$

$$v = \frac{K}{2\left(\frac{aC}{h} - 1\right)} [2\cos\theta + \theta\sin\theta - 2\sin\theta + 2\theta - 2] + K\theta$$

where

$$K = \frac{P\,a\,(1-\nu^2)}{E\,h\,b}, \quad C = \log\frac{2\,a+h}{2\,a-h}$$

With the relation

$$\sigma_\theta = \frac{E\epsilon_\theta}{1-\nu^2}$$

Equations [4] and [7] yield

$$\sigma_\theta = \frac{P}{b\,h} + \frac{P\,z\,(1-\sin\theta)}{b\,(aC-h)\,(a+z)} \quad \ldots [8]$$

The net tension and the bending moment are

$$F = b\int_{-h/2}^{h/2} \sigma_\theta\,dz, \quad M = b\int_{-h/2}^{h/2} z\,\sigma_\theta\,dz \quad \ldots [9]$$

By Equations [8] and [9], $F = P\sin\theta$, $M = P\,a\,(1-\sin\theta)$. These equations agree with statics.

If Equation [4] is linearized in z (as in Langhaar's paper[3]), Equation [7] is altered merely by replacing C by the first two terms in its power series; i.e.

$$C = \frac{h}{a} + \frac{h^3}{12a^3}$$

However, the stress equation is more sensitive. The linearized form of Equation [4] leads to

$$\sigma_\theta = \frac{P}{b\,h} + \frac{P\,a\,(1-\sin\theta)\,z}{I} \quad \ldots [10]$$

where I is the moment of inertia of the cross section. Equations [9] and [10] yield $M = P\,a\,(1-\sin\theta)$, which is consistent with statics. Accordingly, Equation [10] is equivalent to the formula

$$\sigma_\theta = \frac{P}{A} + \frac{M\,z}{I} \quad \ldots [11]$$

The net tension, calculated by Equations [9] and [11], is $F = P$. This relation disagrees grossly with statics.

This example indicates that the linearized form of Equation [4] may be satisfactory for calculating the displacements (u, v, w), but that the more accurate equations then should be used for determining the strains—particularly if the strains are to be used to calculate the membrane forces and the bending moments. The linearizing of the theory ordinarily causes only a small percentage of error in the stresses, if the shell is thin. Consequently, complete linearization with respect to z may be acceptable if the stresses are desired only for prediction of failure of the material.

Stress Concentrations Around a Small Spherical or Spheroidal Inclusion on the Axis of a Circular Cylinder in Torsion

By SISIR CHANDRA DAS,[1] WEST BENGAL, INDIA

Stresses are calculated for the case of a small elastic inclusion bonded (i.e., continuous displacements and tractions across the surface of the inclusion) to a large circular cylindrical shaft. The inclusions considered are of spherical and spheroidal shapes. The results are discussed for several particular cases.

Nomenclature

The following nomenclature is used in the paper:

u_r, u_θ, u_ϕ = components of displacement in spherical co-ordinates
u_ξ, u_η, u_ϕ = components of displacement in spheroidal co-ordinates
T = twist about the axis of the cylinder
ξ, η, ϕ = spheroidal co-ordinates
r, θ, ϕ = spherical polar co-ordinates
a = radius of the spherical inclusion
c = distance of center of spheroid to either focus of generating ellipse
μ_1 = rigidity of material of inclusion
μ_2 = rigidity of material of cylinder
Δ = cubical dilatation
w_r, w_θ, w_ϕ = components of rotation in spherical polar co-ordinates
w_ξ, w_η, w_ϕ = components of rotation in spheroidal co-ordinates
σ_ξ, σ_η, σ_ϕ = normal components of stress parallel to directions of ξ, η, ϕ
σ_r, σ_θ, σ_ϕ = normal components of stress parallel to directions of r, θ, ϕ
$\tau_{\xi\eta}$, $\tau_{\xi\phi}$, $\tau_{\eta\phi}$ = shear-stress components in spheroidal co-ordinates
$\tau_{r\theta}$, $\tau_{r\phi}$, $\tau_{\theta\phi}$ = shear-stress components in spherical polar co-ordinates

Introduction

The concentration of stresses in the neighborhood of a small spherical flaw has been obtained by Southwell and Gough (1)[2] for the case where the material remote from the flaw is in a state of uniform tension. The result in the case of an inclusion instead of a flaw under the same conditions has been discussed by Goodier (2). Solutions for the problem of spheroidal cavities under uniaxial tension perpendicular to the axis of the cavity have been obtained by Sadowsky and Sternberg (3) and parallel to the axis by Neuber (4). The distribution of stress around spherical and spheroidal inclusions in the case of a uniform state of stress infinitely far from the inclusion has been investigated by Edwards (5). The elastic energy of an ellipsoidal inclusion in an infinite solid has been discussed by Robinson (6) and Donnell (7) has obtained the stress concentrations due to elliptical discontinuities in plates under edge forces.

A Small Spherical Inclusion on Axis

When a circular cylinder is twisted by terminal couples about its axis the radial component u_r and the colatitudinal component u_θ vanish while the azimuthal component is given by

$$u_\phi = -Tr^2 \sin\theta \cos\theta \quad \ldots\ldots [1]$$

in spherical polar co-ordinates, the axis of the sphere coinciding with that of the cylinder.

Assuming u_r and u_θ to be zero and u_ϕ independent of ϕ, two equations of equilibrium (8) are identically satisfied and the third takes the form

$$r^2 \frac{\partial^2 u_\phi}{\partial r^2} + 2r \frac{\partial u_\phi}{\partial r} + \frac{\partial}{\partial \theta}\left(\frac{\partial u_\phi}{\partial \theta} + u_\phi \cot\theta\right) \quad \ldots\ldots [2]$$

The general solution of this equation is given by

$$u_\phi = \sum \left(A_n r^n + \frac{B_n}{r^{n+1}}\right) \frac{d}{d\theta} [P_n(\cos\theta)] \quad \ldots\ldots [3]$$

when A_n and B_n are constants and $P_n(\cos\theta)$ is the Legendre's function of the first kind and the nth degree.

We assume here, when $r < a$, i.e., within the sphere

$$u_{\phi 1} = A_2' r^2 \frac{d}{d\theta} [P_2(\cos\theta)] \quad \ldots\ldots [4]$$

and for $r > a$, i.e., outside the inclusion

$$u_{\phi 2} = \left(A_2 r^2 + \frac{B_2}{r^3}\right) \frac{d}{d\theta} [P_2(\cos\theta)] \quad \ldots\ldots [5]$$

where A_2', A_2, and B_2 are constants.

Then the stresses

$$\sigma_r = \sigma_\theta = \sigma_\phi = \tau_{r\theta} = 0$$

and

$$\left.\begin{aligned} (\tau_{r\phi})_1 &= \mu_1 (A_2' r) \frac{d}{d\theta} [P_2(\cos\theta)], \text{ when } r \leq a \\ (\tau_{r\phi})_2 &= \mu_2 \left(A_2 r - \frac{4B_2}{r^4}\right) \frac{d}{d\theta} [P_2(\cos\theta)], \text{ when } r \geq a \end{aligned}\right\} \quad \ldots\ldots [6]$$

where a is the radius of the spherical inclusion and μ_1 and μ_2 are the rigidities for the inclusion and the cylinder, respectively. The inclusion being assumed to be very small compared to the

[1] Department of Mathematics, Chandernagore College.

[2] Numbers in parentheses refer to the Bibliography at the end of the paper.

Contributed by the Applied Mechanics Division and presented at the Annual Meeting, New York, N. Y., November 29–December 4, 1953, of The American Society of Mechanical Engineers.

Discussion of this paper should be addressed to the Secretary, ASME, 29 West 39th Street, New York, N. Y., and will be accepted until April 12, 1954, for publication at a later date. Discussion received after the closing date will be returned.

Note: Statements and opinions advanced in papers are to be understood as individual expressions of their authors, and not those of the Society. Manuscript received by ASME Applied Mechanics Division, February 5, 1953. Paper No. 53—A-2.

dimensions of the cylinder, the conditions to be satisfied are as follows:

1 $u_{\phi 2} \to (-Tr^2 \sin\theta \cos\theta)$, where r is very large

2 $(\tau_{r\phi})_1 = (\tau_{r\phi})_2$, when $r = a$

3 $u_{\phi 1} = u_{\phi 2}$, when $r = a$

These conditions will be satisfied if

$$\left.\begin{aligned} A_2 &= \frac{T}{3},\ B_2 = -\frac{(\mu_1 - \mu_2)\, a^5 T}{3\,(\mu_1 + 4\mu_2)} \\ \text{and} \\ A_2' &= \frac{5\,\mu_2 T}{3\,(\mu_1 + 4\mu_2)} \end{aligned}\right\} \quad \ldots\ldots [7]$$

The stress $\tau_{r\phi}$ on the surface of the inclusion is given by

$$\tau_{r\phi} = -\frac{5a\mu_1\mu_2 T}{\mu_1 + 4\mu_2} \sin\theta \cos\theta \quad \ldots\ldots [8]$$

This vanishes when $\theta = 0, \pi, \pm \pi/2$.

Also, the numerically greatest value of this stress is

$$\frac{5a\mu_1\mu_2 T}{2(\mu_1 + 4\mu_2)}, \text{ when } \theta = \pm\pi/4 \quad \ldots\ldots [9]$$

If $\mu_1 = 0$ (i.e., a cavity) this stress vanishes and the solution is in agreement with Neuber (4).

If $\mu_1 = \mu_2$ (i.e., no inclusion) the stress is

$$-Ta\mu_2 \sin\theta \cos\theta \quad \ldots\ldots [10]$$

in agreement with the stress computed from Equation [1]. The numerically greatest value of this stress is

$$\frac{T\mu_2 a}{2} \quad \ldots\ldots [11]$$

Because of the inclusion this stress is increased or decreased according to

$$\mu_1 > \text{or} < \mu_2$$

(see Table 1).

A Spheroidal Inclusion on Axis: Prolate Spheroid

We now consider the case when the inclusion is of the form of a prolate spheroid, the axis of revolution of which coincides with that of the cylinder.

The transformation

$$\left.\begin{aligned} x &= c \sinh\xi \sin\eta \cos\phi \\ y &= c \sinh\xi \sin\eta \sin\phi \\ z &= c \cosh\xi \cos\eta \end{aligned}\right\} \quad \ldots\ldots [12]$$

gives a prolate spheroid

$$\frac{z^2}{c^2 \cosh^2\xi} + \frac{x^2 + y^2}{c^2 \sinh^2\xi} = 1 \quad \ldots\ldots [13]$$

when

$$\xi = \text{const}$$

The displacement $(-Tyz, Txz, 0)$ in Cartesian co-ordinates when transformed to spheroidal co-ordinates gives

$$u_\xi = u_\eta = 0,\ u_\phi = -Tc^2 \sinh\xi \cosh\xi \sin\eta \cos\eta \quad \ldots\ldots [14]$$

the displacement being in the directions of the normals to the surfaces indicated by the suffixes.

Assuming $u_\xi = u_\eta = 0$ and u_ϕ, which is denoted by ω, independent of ϕ we have

$$\left.\begin{aligned} \Delta &= 0 \\ 2w_\xi &= h_2 h_3 \frac{\partial}{\partial\eta}\left(\frac{\omega}{h_3}\right) \\ 2w_\eta &= -h_3 h_1 \frac{\partial}{\partial\xi}\left(\frac{\omega}{h_3}\right) \\ 2w_\phi &= 0 \end{aligned}\right\} \quad \ldots\ldots [15]$$

where

$$\left.\begin{aligned} \frac{1}{h_1^2} &= \frac{1}{h_2^2} = c^2(\cosh^2\xi - \cos^2\eta) \\ \text{and} \\ \frac{1}{h_3^2} &= c^2 \sinh^2\xi \sin^2\eta \end{aligned}\right\} \quad \ldots\ldots [16]$$

Two equations of equilibrium are identically satisfied and the third reduces to

$$\frac{\partial}{\partial\xi}\left(\frac{\partial\omega}{\partial\xi} + \omega \coth\xi\right) + \frac{\partial}{\partial\eta}\left(\frac{\partial\omega}{\partial\eta} + \omega \cot\eta\right) = 0 \quad \ldots\ldots [17]$$

We take as a solution

$$\omega_1 = \left\{A_1 \frac{d}{d\xi}[P_2(\cosh\xi)]\right\} \frac{d}{d\eta}[P_2(\cos\eta)] \quad \ldots\ldots [18]$$

within the material of the inclusion and

$$\omega_2 = \left\{A_2 \frac{d}{d\xi}[P_2(\cosh\xi)] + B_2 \frac{d}{d\xi}[Q_2(\cosh\xi)]\right\} \frac{d}{d\eta}[P_2(\cos\eta)] \quad \ldots\ldots [19]$$

outside it, where A_1, A_2, and B_2 are constants and P_2 and Q_2 are the Legendre's function of the second degree and of the first and second kind, respectively, i.e.

$$P_2(x) = \frac{1}{2}(3x^2 - 1)$$

and

$$Q_2(x) = \frac{1}{4}(3x^2 - 1) \ln\frac{(x+1)}{(x-1)} - \frac{3x}{2}$$

Then the stresses are $\sigma_\xi = \sigma_\eta = \sigma_\phi = \tau_{\xi\eta} = 0$

$$\left.\begin{aligned} &\tau_{\xi\phi} = \\ &\frac{\mu}{c(\cosh^2\xi - \cos^2\eta)^{1/2}}\left\{A_2\left[\frac{d^2[P_2(\cosh\xi)]}{d\xi^2} - \coth\xi \frac{d[P_2(\cosh\xi)]}{d\xi}\right] + B_2\left[\frac{d^2[Q_2(\cosh\xi)]}{d\xi^2} - \coth\xi \frac{d[Q_2(\cosh\xi)]}{d\xi}\right]\right\}\frac{d}{d\eta}[P_2(\cos\eta)] \\ &\text{and} \\ &\tau_{\eta\phi} = \frac{3\mu \sin^2\eta}{c(\cosh^2\xi - \cos^2\eta)^{1/2}}\left[A_2 \frac{d[P_2(\cosh\xi)]}{d\xi} + B_2 \frac{d[Q_2(\cosh\xi)]}{d\xi}\right] \end{aligned}\right\}$$

$$\ldots\ldots [20]$$

The conditions to be satisfied are as follows

$$\left.\begin{array}{ll} 1 & \omega_1 = \omega_2, \text{ when } \xi = \alpha \\ 2 & \omega_2 \to -Tc^2 \sinh\xi\cosh\xi\sin\eta\cos\eta, \text{ when } \xi \to \infty \end{array}\right\} \quad [21]$$

$$\left.\begin{array}{ll} 3 & (\tau_{\xi\eta})_1 = (\tau_{\xi\eta})_2 = 0 \\ 4 & (\sigma_\xi)_1 = (\sigma_\xi)_2 = 0 \end{array}\right\} \text{ identically for other components of traction on } \xi = \alpha$$

$$5 \quad (\tau_{\xi\phi})_1 = (\tau_{\xi\phi})_2$$

These are satisfied if

$$\left.\begin{array}{l} A_2 = \dfrac{Tc^2}{9},\ B_2 = -\dfrac{3A_2(\mu_2 - \mu_1)\sinh^2\alpha\cosh^2\alpha}{\mu_1\sinh^2\alpha\,(Q_2'' - 6Q_2) + \mu_2\cosh^2\alpha\,(2Q_2'' - 6Q_2)} \\ \text{and} \\ A_1 = A_2\mu_2\dfrac{\sinh^2\alpha\,(Q_2'' - 6Q_2) + \cosh^2\alpha\,(2Q_2'' - 6Q_2)}{\mu_1\sinh^2\alpha\,(Q_2'' - 6Q_2) + \mu_2\cosh^2\alpha\,(2Q_2'' - 6Q_2)} \end{array}\right\} \quad [22]$$

where Q_2 stands for $Q_2(\cosh\alpha)$ and primes denote derivatives with respect to ξ evaluated at $\xi = \alpha$ and μ_1 and μ_2 are the rigidities of the inclusion and the surrounding material, respectively.

The stress $\tau_{\xi\phi}$ on the surface of the inclusion is given by

$$(\tau_{\xi\phi})_{\xi=\alpha} = -\frac{\mu_1\mu_2 Tc\sinh^2\alpha\,[\sinh^2\alpha(Q_2'' - 6Q_2) + \cosh^2\alpha(2Q_2'' - 6Q_2)]\sin\eta\cos\eta}{(\cosh^2\alpha - \cos^2\eta)^{1/2}\,[\mu_1\sinh^2\alpha(Q_2'' - 6Q_2) + \mu_2\cosh^2\alpha\,(2Q_2'' - 6Q_2)]} \quad [23]$$

which evidently vanishes when $\eta = 0, -\pi, \pm\dfrac{\pi}{2}$. This stress will have the numerically greatest value when

$$\cos^2\eta = \cosh\alpha\,(\cosh\alpha - \sinh\alpha)$$

and in that case the stress is given by

$$-\frac{\mu_1\mu_2 Tc\sinh^2\alpha\,(\cosh\alpha - \sinh\alpha)\,[\sinh^2\alpha(Q_2'' - 6Q_2) + \cosh^2\alpha\,(2Q_2'' - 6Q_2)]}{\mu_1\sinh^2\alpha\,(Q_2'' - 6Q_2) + \mu_2\cosh^2\alpha\,(2Q_2'' - 6Q_2)} \quad [24]$$

If the eccentricity of the spheroid is $1/2$, i.e., $\cosh\alpha = 2$, then Equation [23] takes the form

$$-\frac{3\mu_1\mu_2 Tc}{\sqrt{4 - \cos^2\eta}}\,\frac{7\cos\eta\sin\eta}{\mu_1 + 6\mu_2} \quad [25]$$

the numerically greatest value of which is

$$\frac{3\left(2 - \sqrt{3}\right)\mu_1\mu_2 Tc \times 7}{\mu_1 + 6\mu_2} \quad [26]$$

(see Table 1).

Oblate Spheroid

When the form of the inclusion is an oblate spheroid we can write

$$\left.\begin{array}{l} x = c\cosh\xi\sin\eta\cos\phi \\ y = c\cosh\xi\sin\eta\sin\phi \\ z = c\sinh\xi\cos\eta \end{array}\right\} \quad [27]$$

Here we find that $\xi = \text{const}$ gives an oblate spheroid

$$\frac{x^2 + y^2}{c^2\cosh^2\xi} + \frac{z^2}{c^2\sinh^2\xi} = 1 \quad [28]$$

In this case, assuming $u_\xi = u_\eta = 0$ and $u_\phi = \omega$ (independent of ϕ), we find that two of the equations of equilibrium are satisfied and the third is of the form

$$\frac{\partial}{\partial\xi}\left(\frac{\partial\omega}{\partial\xi} + \omega\tanh\xi\right) + \frac{\partial}{\partial\eta}\left(\frac{\partial\omega}{\partial\eta} + \omega\cot\eta\right) = 0 \quad [29]$$

As a solution to this equation we assume

$$\omega_1 = \left\{A_1\frac{d}{d\xi}\,[P_2(i\sinh\xi)]\right\}\frac{d}{d\eta}\,[P_2(\cos\eta)] \quad [30]$$

within the material of the inclusion and

$$\omega_2 = \left\{ A_2 \frac{d}{d\xi} [P_2(i \sinh \xi)]^{-} + B_2 \frac{d}{d\xi} [Q_2(i \sinh \xi)] \right\} \frac{d}{d\eta} [P_2(\cos \eta)] \quad \ldots\ldots [31]$$

outside it, P_2 and Q_2 denoting Legendre's function of the first and second kind, respectively.

All other stress components except $\tau_{\xi\phi}$ and $\tau_{\eta\phi}$ will vanish. The conditions to be satisfied are

$$\left.\begin{array}{ll} 1 & \omega_1 = \omega_2, \text{ when } \xi = \alpha \\ 2 & \omega_2 \to -Tc^2 \sinh \xi \cosh \xi \sin \eta \cos \eta, \text{ when } \xi \to \infty \\ 3 & (\tau_{\xi\phi})_1 = (\tau_{\xi\phi})_2, \text{ when } \xi = \alpha \end{array}\right\} \quad \ldots\ldots [32]$$

These are satisfied if

$$\left.\begin{aligned} A_2 &= -\frac{Tc^2}{9}, \quad B_2 = \frac{3A_2(\mu_2 - \mu_1) \sinh^2 \alpha \cosh^2 \alpha}{\mu_1 \cosh^2 \alpha\ (Q_2'' - 6Q_2) + \mu_2 \sinh^2 \alpha\ (2Q_2'' - 6Q_2)} \\ \text{and} \\ A_1 &= A_2 \mu_2 \frac{\cosh^2 \alpha(Q_2'' - 6Q_2) + \sinh^2 \alpha\ (2Q_2'' - 6Q_2)}{\mu_1 \cosh^2 \alpha(Q_2'' - 6Q_2) + \mu_2 \sinh^2 \alpha\ (2Q_2'' - 6Q_2)} \end{aligned}\right\} \quad \ldots\ldots [33]$$

The stress on the surface of the inclusion is given by

$$(\tau_{\xi\phi})_{\xi=\alpha} = -\frac{\mu_1\mu_2 Tc \cosh^2 \alpha[\cosh^2 \alpha(Q_2'' - 6Q_2) + \sinh^2 \alpha(2Q_2'' - 6Q_2)] \sin \eta \cos \eta}{(\cosh^2 \alpha - \sin^2 \eta)^{1/2} [\mu_1 \cosh^2 \alpha(Q_2'' - 6Q_2) + \mu_2 \sinh^2 \alpha\ (2Q_2'' - 6Q_2)]} \quad \ldots\ldots [34]$$

This will vanish when $\eta = 0, \pi, \pm\pi/2$.

The numerically greatest value of this stress is obtained when

$$\sin^2 \eta = \cosh \alpha\ (\cosh \alpha - \sinh \alpha)$$

and then this stress is

$$\frac{\mu_1\mu_2\ Tc \cosh^2 \alpha\ (\cosh \alpha - \sinh \alpha)\ [\cosh^2 \alpha(Q_2'' - 6Q_2) + \sinh^2 \alpha(2Q_2'' - 6Q_2)]}{[\mu_1 \cosh^2 \alpha\ (Q_2'' - 6Q_2) + \mu_2 \sinh^2 \alpha\ (2Q_2'' - 6Q_2)]} \quad \ldots\ldots [35]$$

If the eccentricity of the spheroid is $^1/_2$, i.e., $\cosh \alpha = 2$, Equation [34] reduces to

$$-\frac{4\mu_1\mu_2 Tc\ 48 \sin \eta \cos \eta}{\sqrt{4 - \sin^2 \eta}\ (19\mu_1 + 29\mu_2)} \quad \ldots\ldots [36]$$

The numerically greatest value of which is

$$\frac{4(2 - \sqrt{3})\mu_1\mu_2 Tc \times 48}{19\mu_1 + 29\mu_2} \quad \ldots\ldots [37]$$

Conclusion

The results of the three special cases discussed in this paper can be readily obtained from Table 1.

TABLE 1

$$k = \frac{\text{Tangential traction at a point on the surface of inclusion}}{\text{Tangential traction at corresponding point without inclusion}}$$

	$\mu_1 = 4\mu_2$	$\mu_1 = 0.25\ \mu_2$	$\mu_1 \to \infty$
Spherical inclusion $k =$	2.5	0.3	5.0
Prolate spheroid ($e = 1/2$) $k =$	2.8	0.28	7.0
Oblate spheroid ($e = 1/2$) $k =$	1.8	0.36	2.5

Acknowledgment

In conclusion the author offers his sincere thanks to Dr. B. Sen for his kind help in the preparation of this paper

BIBLIOGRAPHY

1 "On the Concentration of Stress in the Neighborhood of a Small Spherical Flaw; and on the Propagation of Fatigue Fractures in 'Statistically Isotropic' Materials," by R. V. Southwell and H. J. Gough, *Philosophical Magazine*, series 7, vol. 1, 1926, pp. 71–97.

2 "Concentration of Stress Around Spherical and Cylindrical Inclusions and Flaws," by J. N. Goodier, JOURNAL OF APPLIED MECHANICS, Trans. ASME, vol. 55, 1933, p. A-39.

3 "Stress Concentration Around an Ellipsoidal Cavity in an Infinite Body Under Arbitrary Plane Stress Perpendicular to the Axis of Revolution of Cavity," by M. A. Sadowsky and E. Sternberg, JOURNAL OF APPLIED MECHANICS, Trans. ASME, vol. 69, 1947, p. A-191.

4 "Kerbspannungslehre," by H. Neuber, J. Springer, Berlin, Germany, 1937; reprint by Edwards Brothers, Ann Arbor, Mich., 1944.

5 "Stress Concentrations Around Spheroidal Inclusions and Cavities," by R. H. Edwards, JOURNAL OF APPLIED MECHANICS, Trans. ASME, vol. 73, 1951, p. 19.

6 "Elastic Energy of an Ellipsoidal Inclusion in an Infinite Solid," by Kenneth Robinson, *Journal of Applied Physics*, vol. 22, 1951, pp. 1045–1054.

7 "Stress Concentrations Due to Elliptical Discontinuities in Plates Under Edge Forces," by L. J. Donnell, Th. von Kármán Anniversary Volume, 1941, pp. 293–309.

8 "A Treatise on the Mathematical Theory of Elasticity," by A. E. H. Love, Cambridge University Press, Cambridge, England, fourth edition, 1927; first American printing by Dover Publications, New York, N. Y., 1944.

Brief Notes*

On the recommendations of the Executive Committee of the ASME Applied Mechanics Division, it has been decided to initiate a section devoted to brief notes on technical matters in mechanics. These notes must not be longer than 750 words (about 2½ double-spaced typewritten pages, including figures) and will be subject to the usual review procedure prior to publication. After approval such notes will be published in the next issue of the Journal. The notes should be submitted to the Secretary of the ASME Applied Mechanics Division.

Note on Thermal Stresses

By J. L. BOGDANOFF,[1] WEST LAFAYETTE, IND.

The purpose of this brief note is to emphasize the utility of complex potentials in solving two-dimensional thermal-stress problems.

Let $T\ (x, y)$ denote the steady temperature, in excess of a uniform temperature, in some region R of the xy-plane. Then, T satisfies Laplace's equation

$$\nabla^2 T = 0 \quad \ldots\ldots [1]$$

in R.

Let $W\ (x, y)$ denote the harmonic conjugate of $T\ (x, y)$ so that

$$T + iW = f(z) \quad \ldots\ldots [2]$$

where $i = \sqrt{-1}$ and $f(z)$ is an analytic function of $z = x + iy$.

Define the function of $g(z)$ by means of the equation

$$g(z) = \int f(z)\, dz \quad \ldots\ldots [3]$$

Assuming a state of plane strain in R, it is easy to show that the stress components, traction, displacement, and rotation ω are given by the formulas

$$\left.\begin{aligned} \sigma_x + \sigma_y &= 2[\varphi'(z) + \bar{\varphi}'(\bar{z})] \\ \sigma_x - \sigma_y + 2i\tau_{xy} &= -2[z\bar{\varphi}''(\bar{z}) + \bar{\chi}''(\bar{z})] \end{aligned}\right\} \quad \ldots [4a]$$

$$X_\nu + iY_\nu = -i\frac{d}{ds}\,[\varphi(z) + z\bar{\varphi}'(\bar{z}) + \bar{\chi}'(\bar{z})] \quad \ldots [4b]$$

$$2\mu(u + iv) = K\varphi(z) - z\bar{\varphi}'(\bar{z}) - \bar{\chi}'(\bar{z}) + 2\mu\beta g(z) \quad \ldots [4c]$$

$$2\mu\omega = \text{imaginary part of } [K\varphi'(z) - \bar{\varphi}'(\bar{z}) + 2\mu\beta f(z)] \quad \ldots [4d]$$

where the notation is that of Timoshenko and Goodier,[2] and

$$\beta = \frac{3\lambda + 2\mu}{2(\lambda + \mu)}\,\alpha = (1 + \nu)\alpha$$

α = coefficient of linear thermal expansion

$$K = \frac{\lambda + 3\mu}{\lambda + \mu}$$

The derivation of Equations [4] can be modified also to yield analog equations when $\nabla^2 T \neq 0$; of course, $f(z)$ and $g(z)$ must be replaced then by functions[3] of z and $\bar{z}$.

The theorem developed by Biot[4] follows directly from a study of Equations [4].

Clearly, the method of Muschelišvili[5] can be used to determine $\varphi(z)$ and $\chi'(z)$.

As a simple example, let us determine the stress distribution when R is the region bounded by two concentric circles of radii a and $b (a < b)$ and the temperature is such that

$$g(z) = -H \log z,\ H = \text{real const} \quad \ldots\ldots [5]$$

Equation [5] implies (with $z = re^{i\theta}$)

$$T_{r=a} = -\frac{H\cos\theta}{a},\ T_{r=b} = -\frac{H\cos\theta}{b} \quad \ldots\ldots [6]$$

Now assume

$$\left.\begin{aligned} \varphi(z) &= A\log z + \varphi_0(z) \\ \chi'(z) &= B\log z + \chi_0'(z) \end{aligned}\right\} \quad \ldots\ldots [7]$$

where $\varphi_0(z)$ and $\chi'(z)$ are single-valued and analytic in R. For single-valued displacements in R, Equation [4c] shows that we need

$$KA + \bar{B} = 2\mu\beta H \quad \ldots\ldots [8]$$

To secure zero traction on the boundaries, we must have

$$\left.\begin{aligned} \varphi_0(z) &= \bar{A}\,\frac{z^2}{a^2 + b^2},\ A = \bar{B} \\ \chi_0'(z) &= A\,\frac{a^2b^2}{z^2(a^2 + b^2)} \end{aligned}\right\} \quad \ldots\ldots [9]$$

Hence

$$\left.\begin{aligned} \varphi(z) &= \frac{E\alpha H}{4(1-\nu)}\left(\log z - \frac{z^2}{a^2 + b^2}\right) \\ \chi'(z) &= \frac{E\alpha H}{4(1-\nu)}\left(\log z - \frac{a^2b^2}{z^2(a^2 + b^2)}\right) \end{aligned}\right\} \quad \ldots\ldots [10]$$

and, for example, with Equations [4a] and [10], we find

$$\sigma_x)_{r=a} = -\frac{E\,\alpha H}{2(1-\nu)\,(a^2 + b^2)}\left(1 - \frac{a^2}{x^2}\right)\left(1 - \frac{b^2}{x^2}\right)x \quad \ldots [11]$$

---

[1] Professor, Purdue University. Mem. ASME.

[2] "Theory of Elasticity," by S. Timoshenko and J. N. Goodier, McGraw-Hill Book Company, Inc., New York, N. Y., 1951, pp. 187–192.

* Discussion of this paper should be addressed to the Secretary, ASME, 29 West 39th Street, New York, N. Y., and will be accepted until April 12, 1954, for publication at a later date. Discussion received after the closing date will be returned.

NOTE: Statements and opinions advanced in papers are to be understood as individual expressions of their authors and not those of the Society. Manuscript received by ASME Applied Mechanics Division, October 12, 1953.

[3] "Complex Potentials in Two-Dimensional Elasticity," by A. C. Stevenson, Proceedings of the Royal Society, London, England, series A, vol. 184, 1945, p. 129.

[4] "A General Property of Two-Dimensional Thermo Stress Distribution," by M. A. Biot, *Philosophical Magazine*, London, England, Serise 7, vol. 19,1935, pp. 540–549.

[5] "Pratiktische Lösung der fundementalen Randwertaufgaben der Elastizitätstheorie in der Ebene der eingige Berandungsformen," by N. I. Muschelišvili, ZAMM, vol. 13, 1933, pp. 264–282.

Discussion

Skin Friction and Heat Transfer for Laminar Boundary-Layer Flow With Variable Properties and Variable Free-Stream Velocity[1]

W. B. Brown.[2] This paper presents a skillful method of extrapolating from a known region, constant fluid properties, into an unknown region, variable properties combined with variable free-stream velocities. The assumptions are made to give a good fit in the constant-property case. Within the limits stated in the paper, namely, $0.5 < T_w/T_1 < 2$ and for $0 < \beta < 1$, the skin-friction and heat-transfer coefficients are not seriously in error. The boundary-layer thicknesses deviate considerably from the exact values, even within these limits.

The reason for the increasing errors is principally the inadequacy of Assumption [8]

$$\frac{u}{u_1} = 1 - e^{a\eta + \frac{b}{2!}\eta^2 + \frac{c}{3!}\eta^3 + \frac{d}{4!}\eta^4}$$

in the region mentioned, $\beta > 0$ and $T_w/T_1 > 1$. The type of profile required in this region is shown in Fig. 1,[3] herewith, where for

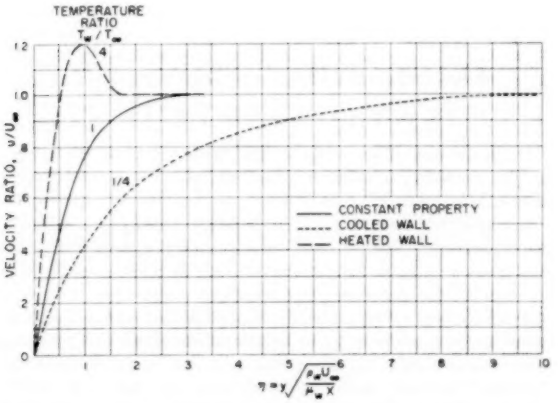

Fig. 1 Velocity Distribution in Boundary Layer for Impermeable Wall and $\beta = 1$

$\beta = 1$, velocity profiles are drawn for the constant-property case, a case where the wall is strongly cooled, and a case where the wall is strongly heated. In the latter case the peak of the velocity profile is 20 per cent above the free-stream value, a fact which cannot be expressed by Equation [8] of the paper. The result is an increasing discrepancy between the exact and approximate values for skin friction, heat transfer, and boundary-layer thickness as β increases above zero and T_w/T_1 increases above 1.

Fig. 2 of this discussion shows this effect. When $T_w/T_1 = 3$, the discrepancy is 28 per cent for skin friction based on free-stream properties, and 8.5 per cent based on wall-temperature properties. Apparently the wall-temperature properties are more accurate in this case. The heat-transfer discrepancy is 7.2 per cent, but the difference from the constant-property value is 12 per cent (not the 6 per cent mentioned in the paper).

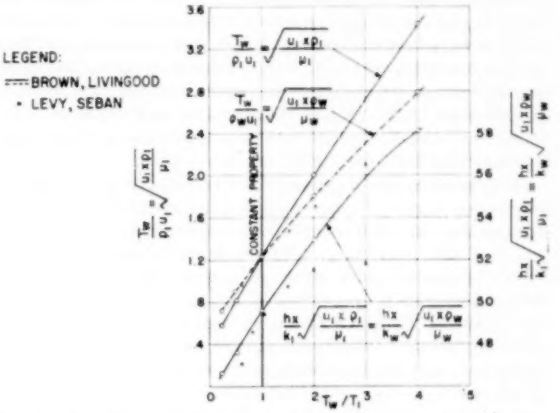

Fig. 2 Skin Friction and Heat Transfer for Variable Property Wedge Flow ($\beta = 1$)

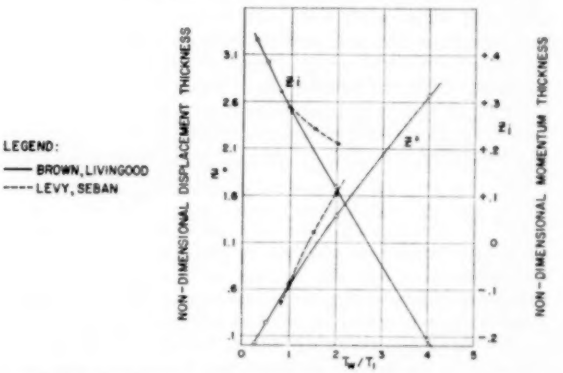

Fig. 3 Nondimensional Displacement and Momentum Thickness for Variable-Property Wedge Flow ($\beta = 1$)

The exact values for $\beta = 1.6$ have not been calculated, in so far as the writer knows, but the discrepancies there may very well be larger than for $\beta = 1$. Fig. 3,[4] herewith, shows the boundary-layer thicknesses when $\beta = 1$. The percentage discrepancies here are larger than in the skin-friction or the heat-transfer coefficients. For a temperature ratio of 2, the discrepancy in the displacement thickness is 18 per cent; in the momentum thickness, 82 per cent.

Finally, the case where the fluid properties, free-stream veloc-

[1] By S. Levy and R. A. Seban, published in the September, 1953, issue of the Journal of Applied Mechanics, Trans. ASME, vol. 75, pp. 415–421.

[2] Address: Santa Monica, Calif.

[3] "Tables of Exact Laminar-Boundary-Layer Solutions When the Wall Is Porous and Fluid Properties Are Variable," by W. B. Brown and P. L. Donoughe, NACA TN 2479, 1951.

[4] "Solutions of Laminar Boundary-Layer Equations Which Result in Specific Weights-Flow Profiles Locally Exceeding Free-Stream Values," by W. B. Brown and H. B. Livingood, NACA TN 2800, 1952.

ity, and wall temperature all vary simultaneously is not quite as difficult as the last sentence of the discussion would imply. It is now in process of numerical solution at the NACA Laboratory in Cleveland.

E. R. G. Eckert.[5] The paper presents an interesting approach to obtain an approximate solution for skin friction and heat transfer in a laminar boundary layer under the condition that the pressure varies along the surface. The flowing fluid is assumed to have its heat conductivity and the viscosity vary proportionally to the absolute temperature and the density to vary inversely proportionally to the temperature; specific heat and Prandtl number are assumed constant. (Unfortunately, in the paper it is in two places stated erroneously that the product of thermal conductivity and viscosity is considered to be constant.) Numerical solutions have been obtained for a wide range of accelerated flow conditions and a ratio of wall temperature to stream temperature varying between 0.6 and 3. These solutions extend the information obtained by Brown and Donoughe through a numerical integration of the differential equations describing flow and heat transfer in laminar boundary layers.[3]

An interesting fact apparent from the results of the present calculations is a significant variation of the skin-friction coefficient for accelerated flow conditions with the ratio wall temperature to stream temperature. This variation cannot be accounted for by the usual procedure to use the friction coefficient as derived for constant-property values and to adapt it to variable properties by introducing the properties at an appropriately defined reference temperature. The Nusselt number describing the heat transfer depends to a much smaller degree on the foregoing temperature ratio.

It is mentioned by the authors that their method of solution breaks down for values of the temperature ratio larger than 3. Brown and Donoughe have observed that for large values of the mentioned temperature ratio, the velocity profile within the boundary layer does not as usual increase monotonously from the value 0 at the wall toward the stream velocity, but reaches a maximum within the boundary layer larger than the stream velocity.[3,4] It may be that a connection exists between this peculiar behavior of the velocity profile and the breakdown of the method as presented in this paper for certain values of the temperature ratio.

J. N. B. Livingood.[6] The paper presents a very interesting and useful method for allowing for property variations in the calculation of laminar skin friction and heat transfer from an isothermal surface for a variable free-stream velocity. Employment of the assumption $\rho\mu$ = const greatly simplifies the solutions of the laminar boundary-layer equations for wedge flows, as compared to the method of Brown and Donoughe,[3] where each property varied as a power of temperature. For the common cases solved by both methods, results are in excellent agreement and it appears that future solutions for isothermal surfaces that may be required might well be obtained by the simpler method of this paper.

Unfortunately, however, the method of this paper is not applicable for accounting for a variable wall temperature. Such effects possibly can be included if the more difficult method of the paper mentioned[3] is applied. Moreover, if wedge-flow solutions are obtained for the variable wall-temperature case, laminar heat transfer around cylinders of arbitrary cross section can be determined by an extension of the method by E. R. G. Eckert and J. N. B. Livingood.[7]

[5] Professor, Mechanical Engineering Department, Institute of Technology, University of Minnesota, Minneapolis, Minn. Mem. ASME.

[6] National Advisory Committee for Aeronautics, Lewis Flight Propulsion Laboratory, Cleveland, Ohio.

Authors' Closure

The authors wish to thank the discussers for their most interesting and welcome comments. As Dr. Brown points out, the assumed velocity profile is inadequate whenever the velocity within the boundary layer exceeds the free-stream velocity. In particular, the displacement and momentum thickness will be in error. However, the simplified calculation method will not exhibit this error exclusively. In the forward integration process used by Brown and Donoughe[3] and Brown and Livingood[4], a very small change (in the third significant figure) in the starting value of the temperature gradient at the wall will produce a large departure in the velocity profile for large values of T_∞/T_1; and the values presented by Brown, even though more accurate, are still uncertain.[8]

The failure of the simplified method to account for a variable wall temperature has been noted. Because the momentum equation is dependent upon the temperature ratio T/T_1, the authors believe still that solutions will have to be computed for each specified wall-temperature variation and that extension of the method of Eckert and Livingood to include surface-temperature variation may be much more complicated than in the incompressible case.

The authors wish to thank Dr. Eckert for calling attention to the fact that the preprint stated erroneously that the product of thermal conductivity and viscosity is assumed constant. His comment enabled the authors to correct the error before publication of the paper.

Determination of Stresses in Cemented Lap Joints[1]

C. D. Coxe.[2] The writer wishes to congratulate the author for this excellent contribution which we believe is of considerable practical importance.

In our rather broad experience with the joining of structural-metal parts by brazing we find among many designers and industrial users a singular lack of appreciation of stress-analysis concepts and of the importance of nonuniform distribution of stresses in brazed joints. The all-too-usual approach in joint design is to calculate the total load, divide by the unit strength of the brazing alloy, and multiply by some empirical factor of safety to obtain the area of joint required. In many cases, of course, this suffices for noncritical applications such as ordinary piping, or where the yield strength of the material being joined is less than the tensile strength (or shear strength) of the brazing alloy. Thus, where copper, brass, or soft steels are joined with a strong silver-brazing alloy, the structural metal will deform before it can transmit any damaging stress to the brazing layer.

On the other hand, where the strength of the metal joined

[7] "Method for Calculation of Heat Transfer in Laminar Region of Air Flow Around Cylinders of Arbitrary Cross Section, Including Large Temperature Differences and Transpiration Cooling," by E. R. G. Eckert and J. N. B. Livingood, NACA TN 2733.

[8] "Effect of Large Temperature Changes (Including Viscous Heating) Upon Laminar Boundary Layers With Variable Free Stream Velocity," by S. Levy, to be published in the *Journal of Aeronautical Sciences*, 1954.

[1] By R. W. Cornell, published in the September, 1953, issue of the Journal of Applied Mechanics, Trans. ASME, vol. 75, pp. 355–364.

[2] Chief Metallurgist, Handy and Harman, Bridgeport, Conn.

greatly exceeds the strength of the brazing alloys, then the concepts set forth by the author may become of controlling importance. A designer, on finding that a simple brazed lap joint in hard steel fails under something less than the desired working load, will often simply lengthen the lap to increase the shear area. The author's graphs dramatically show the futility of such expedients; it is the unit stress "at the tab ending" that determines at what load a lap joint will start to fail; and failure, once started, continues progressively down the entire length of the lap regardless of how long it is. As the author points out, since the thickness of the tab ending determines the magnitude of the stress there, the cure to the problem is to taper the tab ending. This expedient has been used successfully in several designs where it was desired to obtain a more uniform stress distribution and hence greater load-carrying capacity. In many instances a brazed structure may be made stronger by the judicious removal of metal from the right place rather than by the more usual procedure of making the joint bigger and heavier.

The same concepts apply to rod-and-sleeve joints subject to torsional loading.

The author's graphs show that tab-ending stresses also may be reduced by increasing the braze thickness. This is done sometimes in special cases, as in the brazing of tungsten-carbide inserts or tips to steel shanks. More often the same effect is obtained by including a shim of copper or other soft metal in the braze layer. For this purpose a trimetal such as a sandwich sheet of brazing alloy with a copper core is used frequently. If braze-layer thickness is increased very much by simply opening the clearances at the braze interface, practical difficulties are encountered. These include incomplete filling of the joint by the molten brazing alloy because of reduced capillarity, excessive flux inclusions, and shrinkage cavities in the brazing alloys.

The mathematics required for the analytical determination of stress distributions in brazed joints are quite involved and, consequently, may limit the practical quantitative application of this method for a number of industrial users of brazing alloys. Nevertheless, those who must work in a more empirical fashion can deduce from the graphs in what direction and in what order of magnitude a structure should be modified to obtain a better distribution of stress. It would be helpful if the author could explore the effect of tapering the tab ending and show what degree of taper is needed and whether it is desirable for the taper to terminate in a sharp edge.

E. O. Waters.[2] It is the writer's belief that the value of this paper lies not so much in its solution of a specific problem as in its exposition of a method generally applicable to sandwich-type construction, together with the simplifying assumptions that can be made safely. One may assume that the author has tested these assumptions and is prepared to defend them if questioned. Two in particular—neglecting beam stiffness and vertical shear in the braze—might cause some raising of eyebrows since they imply that the braze is nonisotropic and is not in equilibrium.

The following check is suggested for those who are interested in making some private calculations. It involves no differential equations other than those of simple quadrature type: Assume a simple shear and tensile loading for the under side of the tab, Fig. 4 of the paper, say, $\tau_{xy} = c_1 x$ and $\sigma_y = c_2 x$, and compute the tensile force and bending moment at section x. From this the horizontal and vertical displacements of the under side of the tab, at section x can be obtained. Then, having τ_{xy} and σ_y at this point, together with G, E, and h for the braze, the displacement of the corresponding point on the upper surface of the base bar is found. This in turn determines the elastic curve of the neutral axis of the base bar and, from that, the loading (moment and axial tension) necessary to produce this elastic curve.

The difference between this loading and the shear and normal loading on the upper surface of the base bar represents the net external load, and a comparison of the stress pattern in this assumed composite beam with that caused by the same loading on an integral structure of the same over-all dimensions will give a measure of the error introduced by the assumption in question.

Author's Closure

The author wishes to thank Mr. Coxe and Professor Waters for their interesting discussions of his paper. It is gratifying to know that the theoretical and experimental findings help explain certain brazing practices which have been found advantageous and that Mr. Coxe believes the figures in the paper will be useful in the design of brazed joints. Although it would be useful to know the effect of tapering the tab on the significant joint stresses, the analysis of such a case would be difficult and the solution, no doubt, would be rather complex. Also, if the taper makes the tab thickness at the tab ending about the same as the cement thickness, the results would not be very accurate. In general, though, the tab ending stresses are so local that for very gradual tapering of the tab, say, h_0 down to h_1 at the tab ending where $h_1 > h_b$, the maximum stresses at the tab ending would probably be about equal to those which occur for a constant tab thickness of h_1. However, the discontinuity stresses would probably be distributed over a distance somewhat greater than the length of the taper.

The method of checking the error introduced by neglecting the beam stiffness of the cement and the vertical shear stresses in the cement suggested by Professor Waters, is very unique and rather simple. However, the assumed vertical loading σ_y on the under side of the tab must be such that $\int_0^l \sigma_y \, dx = 0$ if there is to be no externally applied shear loading V; for example, $\sigma_y = c_2\left(2\frac{x}{l} - 3\frac{x^2}{l^2}\right)$. Also, the E and G for the braze must be the same as for the tab and base bar, if the final result is to be compared with an integral beam of equivalent dimensions. The comparison of the theoretical and experimental results presented in the paper also gives a good indication of the error introduced by neglecting the cement's beam stiffness and vertical shear stresses.

Effect of Range of Stress on Fatigue of 76S-T61 Aluminum Alloy[1]

R. E. Peterson.[2] It will be noted that the author plots his results (*a*) corrected for yielding (full lines) and (*b*) uncorrected for yielding (dashed lines). Method (*a*) is of interest in giving a more realistic picture of what is happening. Method (*b*) also is of interest, since this gives a "nominal" stress which may be looked upon as a measure of limiting bending moment (or torque for a torsion test). From a design standpoint the nominal stress value is a simple and useful concept. In summary, it can be said that both methods (*a*) and (*b*) are of interest, but for different purposes.

When considering corrections, one would need to consider

[2] Professor, Department of Mechanical Engineering, Mason Laboratory, Yale University, New Haven, Conn. Mem. ASME

[1] By W. N. Findley, published in the September, 1953, issue of the Journal of Applied Mechanics, Trans. ASME, vol. 75, pp. 365–374.

[2] Westinghouse Research Laboratories, East Pittsburgh, Pa.

whether the case at hand represents constant load or constant deflection. Perhaps the author would like to comment on this.

The results which are presented in this paper are of considerable interest, not only from a practical standpoint, but also in trying to derive general relations for the case of combined alternating and steady stress components.

AUTHOR'S CLOSURE

Mr. Peterson's comments are greatly appreciated. A question was raised by Mr. Peterson concerning constant load versus constant deflection. I would like to comment on three points in this connection. First, it is evident that a decision to perform a test at either constant load or constant deflection may be dictated by which method approaches the service condition most closely, if simulated service testing is desired. However, if the testing is part of a scientific investigation it may be that neither method is wholly satisfactory. That is, the constant-deflection test is not necessarily a constant-strain test because of the change in the distribution of strains among parts of the machine and specimen resulting from changes in forces during the test. Also, a constant-load test does not necessarily produce a constant-stress test if changes in stress distribution occur during the test.

Second, when conditions involve repeated stresses at other than zero mean stress, relaxation or creep (depending on whether the stressing is at constant deflection or constant load) may occur. This may change both the distribution and magnitude of stresses and strains during either type of test. At room temperature the effect of creep or relaxation in fatigue tests of metals at high stresses is probably small compared to the effect of yielding.

Third, for some metals and most plastics, increases in temperature resulting from hysteresis damping during the test may cause a decrease in stiffness of the specimen as well as a change in fatigue strength. The decrease in stiffness causes an increase in deflection in a constant-load test and causes a decrease in load in a constant-deflection test. Thus substantial differences in the results obtained from the two tests may occur even at zero mean stress. It has been shown[3] when the temperature is kept more nearly constant during the tests that the results obtained from both types of tests are nearly in agreement.

Effect of Surface Condition on Creep of Some Commercial Metals[1]

L. C. COCKEL, JR.[2] The authors make no mention of the effect of oxidation of the test specimen upon thermal equilibrium. Further, no mention is made of the manner in which the temperature of the specimen was determined. In addition, no mention is made of insulation or other means for thermally isolating the test specimen. These features of the test are important for, according to the following development, the effects noted by the authors might be traced to the change in emissivity of the test specimen, in which case the shown results are a manifestation of the requirements for thermal equilibrium and not a manifestation of any strength property of the metal.

If radiation from the gas is not important, the thermal equilibrium at the surface of the test specimen may, for a given geometry, be stated in an elementary way as

$$h(T_g - T_s) = \frac{1}{\frac{1}{e_s} + \frac{D_s}{D_b}\left(\frac{1}{e_b} - 1\right)} F[(T_s)^4 - (T_b)^4] + f(k_s, T_s, T_b)$$

where

h = convection coefficient at the surface of the specimen
T_s = surface temperature of the test specimen
T_g = temperature of the gas
e_s = emissivity of the surface of the test specimen
e_b = emissivity of the boundary
D_s = diameter of the test specimen
D_b = inside diameter of the boun ling container
F = geometrical factor and constants
T_b = temperature of the boundary
f = a function
k_s = conductivity of the test specimen

The equilibrium expression given may not be exact in that each temperature or property is assumed uniform or constant. Further, details of the flow of gas and the effect of geometry are not included. Perhaps most important to this discussion, it is known that the radiation of unoxidized surfaces can follow a different law than the radiation of oxidized surfaces (see Jacob, *Heat Transfer*, Wiley, 1950).

Nevertheless, the shown relation is very indicative of the possibility involved when data for the normal emissivity, taken according to the given law from the cited source, are considered. The normal emissivity for shaved copper is given as 0.07 while for copper oxide the given value is 0.78, both values being at 25 C. From these data, if the boundary temperature was less than the gas temperature, the shown relation demands that the temperature of the test specimen fall, if the boundary temperature is held constant and the surface of the specimen oxidized. This phenomenon could be an explanation of the shown data.

Angle and Strain Relations in Flat-Plate Lüders' Bands[1]

E. A. DAVIS.[2] The assumption that the displacements in a Lüders' band cannot vary in the direction along the band and, therefore, that the strain in that direction is zero may be valid if the band forms across the full width of the specimen at one instant as it apparently does in 24S-T aluminum and in the necking of comparatively wide strips of cold-rolled steel. This type of flow has been discussed recently by Aronofsky[3] who shows that the localized flow lines[4] at $\theta = 35$ deg are what should be expected from the Mises criterion of yielding and that the deviations from 35 deg are due to anisotropy of the material.

This discussion, however, was prompted by the writer's inability to understand how such an assumption could be used to describe the bands that form in hot-rolled mild steel. For this

[3] "Comparison of Fatigue Tests From Four Different Types of Fatigue Machines for Several Plastics and an Aluminum Alloy," by W. N. Findley and R. L. Sutherland, unpublished report to Monsanto Chemical Company, Plastics Division, August, 1946.

[1] By E. D. Sweetland and E. R. Parker, published in the March, 1953, issue of the JOURNAL OF APPLIED MECHANICS, Trans. ASME, vol. 75, pp. 30–32.

[2] Industrial Engineers, Inc., Los Angeles, Calif. Assoc. Mem. ASME.

[1] By G. R. Irwin, published in the September, 1953, issue of the JOURNAL OF APPLIED MECHANICS, Trans. ASME, vol. 75, pp. 449–450.

[2] Research and Advisory Engineer, Westinghouse Research Laboratories, East Pittsburgh, Pa.

[3] "The Formation of a Necked Region and Fracture Along an Oblique Line in Flat Tensile Bars," by Julius Aronofsky, Proceedings of the First U. S. National Congress of Applied Mechanics, ASME, New York, N. Y., 1952, pp. 521–532.

[4] The same notation is used as in the paper.

material the rolling introduces a slight anisotropy which causes the z-direction to be a principal direction. The traces of the Lüders' bands appear at either 45 or 0 deg to the width direction. To satisfy Equation [5] of the paper, θ can be zero only if the width reduction is zero, but this would constitute a plane strain which should occur only where the intermediate principal stress is the average of the maximum and minimum principal stresses. Also, according to Equation [5], the angle θ can be 45 deg only if the thickness reduction is zero. Such a strain, which also would be a plane strain, would not produce the undesirable "stretcher strains" associated with the yielding of mild steel. In the 45-deg Lüders' bands in mild steel there actually is a strain in the direction along the band. This observation is not in agreement with the explanation given in the paper. The variance probably results from the fact that these bands form by a gradual spreading across and along the specimen. If the maximum shearing-stress criterion of yielding had been used by Aronofsky, slip lines at 45 deg would have been predicted. Thus it seems that the orientation of the Lüders' bands depends upon which criterion of yielding the material chooses to follow.

Author's Closure

The paper by Dr. Aronofsky to which Mr. Davis refers contains a large number of illustrations of flat-plate Lüders' bands which make angles of 59 to 63 deg with the tension direction. All of these appear to be of the kind governed by the simple angle and strain relations discussed by the author. One illustration is shown of markings at 45 deg in a hot-rolled steel which may also be in accordance with the author's Equation [5] if only the extensional plastic strain along the lengthwise direction of any one of these bands is not greater inside the band than it is outside the band. The comment by Mr. Davis states only that there is a lengthwise plastic strain. This latter observation is not, in itself, in disagreement with the explanation given in the author's paper.

On the Use of Singular Yield Conditions and Associated Flow Rules[1]

R. Hill.[2] In the summary of this paper it is suggested that the enlargement of a hole in a sheet is the first nontrivial problem of finite distortion to be solved in closed form when work hardening is present. Actually, such a solution, valid for any potential, was obtained some years ago by the writer in connection with the bulging of a clamped diaphragm.[3] The uniaxial stress-strain relation then used was $\sigma = \sigma_0 \exp \epsilon$, where σ is true stress, σ_0 the initial yield stress, and ϵ the logarithmic strain; this is identical with the relation adopted here when $\alpha = 1$. Such a concave-upward stress-strain curve is, of course, not too realistic, though, when the strain range is small, possibly acceptable as an approximation to the virtually linear hardening of certain cold-worked metals. A linear hardening law, in conjunction with the Mises potential, also was treated in the bulge problem referred to, and an approximate solution in explicit terms was found.

There appears to be no metal whose plastic behavior can be described adequately by the Tresca yield and potential function (certain low-carbon steels are possible exceptions still to be investigated properly). Nevertheless, such a theory may prove useful as an approximation, and a study of the degree of approximation that can be realized in various circumstances is well worth while. The author does not discuss this aspect of the use of singular flow rules. The writer has been considering the matter for some time past, and the following remarks refer to some of the conclusions reached:

In so far as yield-point loads are concerned, the prospects appear to be not unfavorable, and a general theorem is available for assigning limits to the error.[4] As regards strains, however, no such theorem is available or likely. The situation may be illustrated by citing particular cases as follows:

1 Koiter's value of the axial strain in an autofrettaged plastic-elastic tube with open ends, using the Tresca potential, is considerably less than Thomas's value with the Mises potential.[5]

2 When a circular annulus of strip metal is drawn inward by internal radial tension, no thickening occurs according to the Tresca potential, whereas with a regular potential the thickness strain at the outside edge is half the hoop strain and can be as much as 0.25.

3 In finite bending of a thin strip in its plane, the thinning is zero on the tension side of the neutral surface according to the Tresca potential, whereas for any regular potential its value at the edge is equal to half the hoop strain.

4 On the other hand, when a circular annulus of strip metal is drawn outward by external radial tension, the agreement in strains is quite good when the ratio of the external and internal radii is less than about four (the width of the annulus is unaltered according to the Tresca potential).[6]

5 The localized necking modes for any potential are identical in tension strips with sufficiently deep and sharp notches, but not in strips with blunt or shallow notches.[7]

6 An exact solution for any hardening law can be obtained to the problem of a bent plastic-elastic bar on the basis of the Tresca potential.[6] The strain rate in the plastic zone has components whose ratios are $1 : -(1 - \nu) : -\nu$, where ν is Poisson's ratio; in the elastic zone the ratios are, of course, $1 : -\nu : -\nu$. The stress is everywhere uniaxial and the plastic-elastic interface is plane, as assumed in the usual engineering treatment. When the potential is regular this treatment is incorrect, unless the material is incompressible. The correct solution is not known but is believed to agree closely with the Tresca one in regard to the bending moment/curvature relation, but not in regard to transverse strains (for the usual values of ν).

Another aspect of the use of singular potentials, which is also not mentioned by the author, is that in certain problems of finite distortion there is more than one possible solution, even where the solution for a regular potential is unique. Finally, it is to be observed that there are other singular strain rules that can be used profitably as approximations or, indeed, that may represent closely the behavior of some material. There is, for instance, the potential represented by a regular hexagonal prism, the normals to whose faces are parallel to the directions representing pure extension or compression.

---

[1] By W. Prager, published in the September, 1953, issue of the Journal of Applied Mechanics, Trans. ASME, vol. 75, pp. 317–320.

[2] Department of Mathematics, University of Nottingham, England.

[3] "A Theory of the Plastic Bulging of a Metal Diaphragm by Lateral Pressure," by R. Hill, *Philosophical Magazine*, vol. 41, 1950, pp. 1133–1142.

[4] "A Note on Estimating Yield-Point Loads in a Plastic-Rigid Body," by R. Hill, *Philosophical Magazine*, vol. 43, 1952, pp. 353–355.

[5] "The Autofrettage of Thick Tubes With Free Ends," by D. G. B. Thomas, *Journal of Mechanics and Physics of Solids*, vol. 1, 1953, pp. 124–132; vol. 2, 1953, pp. 67–68.

[6] Unpublished work by the writer, 1952–1953.

[7] "Discontinuous Plastic States, With Special Reference to Localized Necking in Thin Sheets," by R. Hill, *Journal of Mechanics and Physics of Solids*, vol. 1, 1952, pp. 18–30.

AUTHOR'S CLOSURE

The author is indebted to Professor Hill for drawing attention to an earlier example in which a closed-form solution to a nontrivial problem of finite plastic deformation had been obtained with the use of an incremental law of work hardening. There is an important difference, however, between the examples given by Professor Hill and the author. Professor Hill assumed a plausible mode of deformation and then determined the stress-strain law that would give this deformation. The resulting law was not too realistic, and when a more realistic law was used, the solution could no longer be given in closed form. In the present paper, on the other hand, a one-parameter family of stress-strain laws is considered, and a closed-form solution is obtained for any one of these laws. While this family contains the unrealistic law of Professor Hill, it also contains more realistic laws of work hardening.

A Strain-Energy Expression for Thin Cylindrical Shells[1]

E. REISSNER.[2] It seems worth pointing out that a strain-energy expression which contains the authors' example as a special case may be found in a paper by Byrne.[3]

The relation of Byrne's work to Flügge's has been indicated by Hildebrand, Reissner, and Thomas.[4]

The authors' statement, "The differential equations for the cylindrical shell given by Flügge. . . . may be presumed to be correct up to terms of the order $(h/a)^2$" is believed to be in error. Reference may be made to the discussion of this point in a number of earlier papers.[4, 5, 6, 7]

An Improved Electrical Analogy for the Analysis of Beams in Bending[1]

WILBUR T. MCKINNEY.[2] In connection with this very stimulating paper it is interesting to note that the same results can be achieved by a somewhat different approach which may seem more simple and direct.

The following derivation uses the nomenclature and basic figures (Figs. 2 and 3) of the original paper, also the same basic assumptions. Therefore

$$V_x = V_a = V_b \quad [1]$$

$$M_x = M_b + (r - x)\,V_b \quad [2]$$

Since $x = 0$ at point a (Fig. 2 of the paper)

$$M_a = M_b + rV_b \quad [3]$$

The incremental slope is given by

$$\Delta\theta = \theta_b - \theta_a = \int_0^r \frac{M_x}{EI}\,dx \quad [4]$$

Substitution of Equation [2] into Equation [4] and expansion of the result gives

$$\Delta\theta = M_b \int_0^r \frac{1}{EI}\,dx + V_b r \int_0^r \frac{1}{EI}\,dx - V_b \int_0^r \frac{x}{EI}\,dx \quad [5]$$

Let

$$\lambda_a = \int_0^r \frac{x}{EI}\,dx \Big/ \int_0^r \frac{1}{EI}\,dx \quad [6]$$

Then

$$\Delta\theta = [M_b + V_b\,(r - \lambda_a)] \int_0^r \frac{1}{EI}\,dx \quad [7]$$

The incremental deflection is derived from

$$\Delta w = w_b - w_a = \int_0^r \theta_x\,dx \quad [8]$$

but

$$\theta_x = \theta_b - \int_x^r \frac{M_x}{EI}\,dx$$

$$= \theta_b - M_b \int_x^r \frac{1}{EI}\,dx - V_b r \int_x^r \frac{1}{EI}\,dx + V_b \int_x^r \frac{x}{EI}\,dx \quad [9]$$

Substitution of Equation [9] into Equation [8] yields

$$\Delta w = \theta_b \int_0^r dx - M_b \int_0^r \int_x^r \frac{1}{EI}\,dx\,dx$$

$$- V_b r \int_0^r \int_x^r \frac{1}{EI}\,dx\,dx + V_b \int_0^r \int_x^r \frac{x}{EI}\,dx\,dx \quad [10]$$

To integrate $\displaystyle\int_0^r \int_x^r \frac{1}{EI}\,dx\,dx$ by parts, let

$$u = \int_x^r \frac{1}{EI}\,dx = -\int_r^x \frac{1}{EI}\,dx \text{ and } dv = dx$$

in the equation

$$\int_0^r u\,dv = [vu]_0^r - \int_0^r v\,du$$

$$= \left[x\left(-\int_r^x \frac{1}{EI}\,dx\right)\right]_0^r - \int_0^r x\left(-\frac{1}{EI}\,dx\right)$$

This yields

---

[1] By H. H. Bleich and F. DiMaggio, published in the September, 1953, issue of the JOURNAL OF APPLIED MECHANICS, Trans. ASME, vol. 75, pp. 448-449.

[2] Massachusetts Institute of Technology, Cambridge, Mass.

[3] "Theory of Small Deformations of a Thin Elastic Shell," by Ralph Byrne, Jr., University of California Publications in Mathematics, N. S., vol. 2, 1944, pp. 103–152.

[4] "Notes on the Foundations of the Theory of Small Displacements of Orthotropic Shells," by F. B. Hildebrand, E. Reissner, and G. B. Thomas, NACA TN 1833, March, 1949, pp. 23–25.

[5] "The Equilibrium of Thin Elastic Shells," by A. E. Green and W. Zerna, *Journal of Mechanics and Applied Mathematics*, vol. 3, 1950, pp. 9–22.

[6] "Note on the Expressions for Strains in Bent Thin Shells," by E. Reissner, *American Journal of Mathematics*, vol. 64, 1942, pp. 768–772.

[7] "Stress Strain Relations in the Theory of Thin Elastic Shells," by E. Reissner, *Jounal of Mathematics and Physics*, vol. 31, July, 1952, pp. 109–119.

[1] By W. T. Russell and R. H. MacNeal, published in the September, 1953, issue of the JOURNAL OF APPLIED MECHANICS, Trans. ASME, vol. 75, pp. 349–354.

[2] Senior Structures Engineer, Consolidated Vultee Aircraft Corp., San Diego, California

$$\int_0^r \int_x^r \frac{1}{EI}\,dx\,dx = \int_0^r \frac{x}{EI}\,dx \quad \ldots\ldots [11]$$

Similarly, if

$$u_1 = \int_x^r \frac{x}{EI}\,dx = -\int_r^x \frac{x}{EI}\,dx \text{ and } dv_1 = dx$$

then

$$\int_0^r u_1\,dv_1 = \left[x\left(-\int_r^x \frac{x}{EI}\,dx\right)\right]_0^r - \int_0^r x\left(\frac{-x}{EI}\,dx\right)$$

and

$$\int_0^r \int_x^r \frac{x}{EI}\,dx\,dx = \int_0^r \frac{x^2}{EI}\,dx \quad \ldots\ldots [12]$$

Equation [10], therefore, becomes

$$\Delta w = \theta_b r - M_b \int_0^r \frac{x}{EI}\,dx - V_b r \int_0^r \frac{x}{EI}\,dx + V_b \int_0^r \frac{x^2}{EI}\,dx \ldots [13]$$

In order that the electrical analog shown in Fig. 3 of the paper shall yield correct values of shear, moment, slope, and deflection at points a and b, it must correctly represent Equations [1], [3], [7], and [13].

From Fig. 3 it is obvious that Equation [1] is satisfied.

If the quantity $r - \lambda_a$ is represented as λ_b, so that $\lambda_b = r - \lambda_a$ then

$$r = \lambda_a + \lambda_b \quad \ldots\ldots [14]$$

Equation [3] may, therefore, be written as

$$M_a = M_b + (\lambda_a + \lambda_b)\,V_b$$
$$= M_b + V_a\lambda_a + V_b\lambda_b \quad \ldots\ldots [15]$$

If λ_a and λ_b are the turns ratios of the transformer coils, this equation is also obviously fulfilled by the circuit since the current at point a is the sum of the current at point b plus the currents $V_a\lambda_a$ and $V_b\lambda_b$ from the transformers.

Inspection of Fig. 3 shows that the potential difference between points a and b of the bending moment circuit (and the analogous increment in beam slope) is given by the product of the resistance R_M times the current flowing through it. The current M_b can be seen to be equal to $M_b + V_b\lambda_b$.

Let
$$R_M = \int_0^r \frac{1}{EI}\,dx \quad \ldots\ldots [16]$$

Then the incremental beam slope $\Delta\theta$ is represented by the equation

$$\Delta\theta = M_b R_M = (M_b + V_b\lambda_b) \int_0^r \frac{1}{EI}\,dx$$

This fulfills the requirement that Equation [7] be satisfied, since $\lambda_b = r - \lambda_a$.

In the case of the shear circuit the potential difference between points a and b (which represents the incremental deflection of the beam between these points) is the sum of three potential differences. One of these is the potential difference across the resistance R_V, which is equal to the current V_b times the resistance R_V.

The other two potential differences are those existing across the shear circuit coils of the transformers shown at d and e in Fig. 3.

If
$$R_V = \int_0^r \frac{(x - \lambda_a)^2}{EI}\,dx \quad \ldots\ldots [17]$$

the potential difference across this resistance is

$$V_b \int_0^r \frac{(x - \lambda_a)^2}{EI}\,dx$$

The potential difference across the shear circuit coil of the transformer shown at point e is equal to the potential difference across the moment circuit coil of that transformer times the turns ratio of the transformer and thus is equal to $\theta_b\lambda_b$. Likewise, the potential difference across the shear circuit coil of the transformer shown at point d is equal to $\theta_a\lambda_a$.

The total potential difference between points a and b in the shear circuit is therefore expressed by the equation

$$\Delta w = \theta_b\lambda_b + \theta_a\lambda_a + V_b \int_0^r \frac{(x - \lambda_a)^2}{EI}\,dx \quad \ldots\ldots [18]$$

Fig. 3 shows that the potential θ_a is equal to the potential θ_b minus the potential difference across the resistance R_M.

$$\theta_a = \theta_b - (M_b + \lambda_b V_b)\,R_M \quad \ldots\ldots [19]$$

Substitution of Equations [19] and [16] into Equation [18] yields

$$\Delta w = \theta_b\lambda_b + \left[\theta_b - (M_b + \lambda_b V_b) \int_0^r \frac{1}{EI}\,dx\right]\lambda_a + V_b \int_0^r \frac{(x - \lambda_a)^2}{EI}\,dx \ldots [20]$$

Use of Equation [14] and expansion gives

$$\Delta w = \theta_b r - (M_b + V_b r - V_b\lambda_a)\,\lambda_a \int_0^r \frac{1}{EI}\,dx + V_b \int_0^r \frac{x^2}{EI}\,dx - 2\,V_b\lambda_a \int_0^r \frac{x}{EI}\,dx + V_b\lambda_a^2 \int_0^r \frac{1}{EI}\,dx$$

Use of Equation [6], and recognition of $\int_0^r \frac{x}{EI}\,dx$ as being equal to $\lambda_a \int_0^r \frac{1}{EI}\,dx$ yields

$$\Delta w = \theta_b r - M_b \int_0^r \frac{x}{EI}\,dx - V_b r \int_0^r \frac{x}{EI}\,dx + V_b\lambda_a^2 \int_0^r \frac{1}{EI}\,dx + V_b \int_0^r \frac{x^2}{EI}\,dx - 2V_b\lambda_a^2 \int_0^r \frac{1}{EI}\,dx + V_b\lambda_a^2 \int_0^r \frac{1}{EI}\,dx$$

So that

$$\Delta w = \theta_b r - M_b \int_0^r \frac{x}{EI}\,dx - V_b r \int_0^r \frac{x}{EI}\,dx + V_b \int_0^r \frac{x^2}{EI}\,dx$$

Since this is the same as Equation [13], and since Equations [1], [3], and [7] have also been correctly represented, the analogy correctly represents the shear, bending moment, slope, and deflection of the beam at points a and b.

Measurement of Acceleration Pulses With Multifrequency Reed Gage[1]

C. E. Crede.[2] The authors should be commended for the logical and straightforward analysis of the reed gage set forth in this paper. Such a reed gage is not new and has received some attention in the technical literature. Its importance apparently has been overlooked to a considerable extent, however, and it does not have the prestige that it deserves.

The writer has been interested in the multifrequency reed gage for several years. As the authors point out, a description of a shock motion is relatively unimportant, but the effect of the shock motion upon structures is of paramount importance. The reed gage evaluates this effect directly and may be used to indicate either the response of various structures in their fundamental modes of vibration or, alternatively, the relative importance of the several modes of vibration of structures having distributed mass. The reed gage thus answers questions that often arise in shock studies. The authors' statement that the reed-gage applications studied in the current paper are of relatively minor importance seems to be a fair appraisal.

The reed gage, as discussed in this paper, is the outgrowth of wartime studies by J. M. Frankland, R. D. Mindlin, and others on the fundamentals of the response of elastic systems to shock motions and forces. The concept of the multifrequency reed gage grew out of these studies. Owing to the nature of the problem, it is practicable in most instances to obtain the response of the multifrequency reed gage only by analog methods, and the technical literature includes information on the response to a few regular pulses. This paper includes interesting extensions of these analog solutions to pulses of less regular shape. For the shapes of pulse assumed by the authors, the solutions set forth in the paper appear quite logical. Practically, however, a pulse usually includes superimposed vibrations at various frequencies. A reed gage is very sensitive to vibration at a frequency near the natural frequency of any reed, and the large response of such reeds may confuse attempts to analyze the reed-gage output in the manner described by the authors.

Commenting specifically on the contents of the paper, it may be stated that the analysis going from the pulse to the reed-gage response is logical and unquestioned. In the reverse direction, there may be some question on the validity of the interpretation of the response in the following respects:

1 In Fig. 7 of the paper, the exact relation between the maximum negative tangent and the time to maximum acceleration is not evident. The authors state that the time to maximum acceleration is determined from the slope and intercepts of the maximum negative tangent but do not give the details of this relation.

2 Fig. 8 is somewhat confusing. The confusion apparently arises from the fact that the ordinates actually are the values of the stated ordinate parameter at which the positive and negative responses reach a maximum.

The foregoing criticisms are very minor and are not intended to detract from the merit of the paper. It would be interesting to see an extension of this investigation, particularly for less regular pulses and for pulses with superimposed vibration of relatively high frequency.

[1] By Henry Shapiro and D. E. Hudson, published in the September, 1953, issue of the Journal of Applied Mechanics, Trans. ASME, vol. 75, pp. 422–426.

[2] Chief Engineer, The Barry Corporation, Watertown, Mass. Mem. ASME.

Stresses Due to Tangential and Normal Loads on an Elastic Solid[1]

N. M. Wickstrand.[2] This paper presents an interesting contribution to the literature of contact stresses. The analysis is certain to be a great help in those problems of plane strain or plane stress where, because of the existence of tangential loads, the older methods of Hertz and later authors are inadequate.

This paper states, "The crack starts either at the surface or underneath the surface . . . . . " This statement sheds considerable light upon some of the theories of failure as applied to gear teeth and rolling bearings which are known to fail by fatigue. Some writers have stated that all fatigue failures are surface failures and others have said that ball and roller bearings fail from a crack which originates at the point of maximum subsurface shear. The present paper, by taking account of stresses due to tangential loads, makes it possible to analyze more carefully fatigue failures under rolling loads. It is hoped that this fine paper will be an aid in clarifying what is at present a confusing issue in some fatigue problems.

Since the present derivation applies only to plane stress or to plane strain it is not exactly applicable to three-dimensional problems such as are encountered in ball bearings. At the present time a complete stress analysis of a ball bearing under normal and tangential loads must be performed by Southwell's relaxation methods. This is such a tedious operation that it is rarely performed. However, it seems very likely that in some ball-bearing problems the method of the authors could very nicely be used as an initial step and then the results could be smoothed out by relaxation. This probably will represent a considerable saving in time and effort from what is at present required.

[1] By J. O. Smith and C. K. Liu, published in the June, 1953, issue of the Journal of Applied Mechanics, Trans. ASME, vol. 75, pp. 157–166.

[2] Mechanical Engineer, Bristol, Conn.

Book Reviews

Dynamics

DYNAMIK. By Wilhelm Müller. Part 1—Dynamik des Einzelkörpers, 128 pp., 48 figs.; Part 2—Systeme von starren Körpern, 102 pp., 41 figs. Paper, 4 × 6¼ in., references, index, Dm 2,40 each. Sammlung Göschen Band 902, 903. Walter de Gruyter & Co., Genthiner Strasse 13, Berlin, Germany, 1952.

REVIEWED BY STEPHEN H. CRANDALL[1]

THE first editions of these two little books (Nos. 902 and 903 in the Sammlung Göschen series) were published in 1925. The second editions have been considerably revised. Brief indexes have been added and many of the mathematical manipulations have been streamlined. The readers of the second editions have been given credit for greater mathematical maturity. The number of diagrams has been curtailed. All of the vector analysis is gathered together in a preliminary section instead of being developed as needed. Some of the examples are now integrated in terms of elliptic functions where previously they had been left in terms of the integrals.

The general scope and approach of the books have not been materially altered, however. They contain a brief but surprisingly complete account of rigid-body dynamics from Newton's laws to Hamilton's principle. A large collection of classical problems including, for instance, Kepler's laws, balancing of reciprocating machines, and gyroscopic ship stabilization are explicitly treated. There are no exercises for the reader.

Undoubtedly, these books were written to be used by continental university students as supplements to their lecture courses. In this country their level is perhaps more appropriate to our graduate schools. They would provide a compact solution for the doctor's candidate who is faced with simultaneously brushing up on dynamics and technical German.

Compressible Air-Flow Calculation Tables

A SELECTION OF TABLES FOR USE IN CALCULATONS OF COMPRESSIBLE AIRFLOW. Prepared on behalf of the Aeronautical Research Council by the Compressible Flow Tables Panel, L. Rosenhead, chairman. Oxford University Press, New York, N. Y., 1953. Cloth 8 × 10¼ in., viii and 143 pp., $8.

REVIEWED BY ASCHER H. SHAPIRO[2]

THIS book is authoritative and definitive; it has obviously been prepared with much thought and with unfailing care; and the typographical style of the tables leaves nothing to be desired in the way of clarity and elegance. In brief, it is a volume essential to all who carry out numerical calculations of gas-dynamics problems.

The tables refer to a perfect gas with a specific-heat ratio (γ) of 1.4. They contain, in those forms most suited for theoretical computations or the reduction of experimental data, tables of compressible flow functions of widest and most lasting use. Each group of tables is accompanied by a brief text giving the corresponding formulas, typical applications, and associated information concerning accuracy, interpolation, and so on.

There are six groups of tables in all, namely: 1 Isentropic Flow Tables; 2 Characteristic Tables; 3 Shock Tables; 4 Tables for the Reduction of Pressure Ratios; 5 Tables of Powers of x and $(1 - x^2)$; 6 Miscellaneous Tables.

Each group contains several tables with different arrangements of the arguments and of the respondents, in order to facilitate calculations for a variety of problems. In all there are 28 tables. The ranges and intervals of the arguments are adequate for almost any problem. In general, tables of first differences are adjoined for purposes of interpolation, and the style of typography indicates where linear interpolation is sufficient. The respondents of the tables, it is noted gratefully, are profuse to the extent of being simply related to each other; the user is therefore virtually assured of finding the particular function he desires, with no need of further calculation.

The scope of the book is indicated by the previously-stated list of groups. The reviewer regrets that group 3 (Shock Tables) refers mainly to normal shocks; the authors concluded that functions relating to the flow past cones and wedges are more suitably presented in the form of graphs, and they promise these in a later companion volume of graphs.

For this service to the large and growing professional area of gas dynamics, the authors deserve a hearty "well done!"

Elasticity

ELASTICITY IN ENGINEERING. By Ernest E. Sechler. Galcit Aeronautical Series. John Wiley & Sons, Inc., New York, N. Y., 1952. Cloth, 6 × 9 in., ix and 419 pp., illus., $8.50.

REVIEWED BY P. S. SYMONDS[3]

THE book consists of three parts entitled as follows: "Fundamental Equations and Analysis Methods," "Engineering Problems in Stable Structures," and "Engineering Problems in Instability." The first part contains derivations of the general equations of theory of elasticity and includes a chapter on stress functions and one on energy principles. In the second part the author presents solutions for a number of familiar problems of elasticity and theory of structures. Some exact solutions are discussed; e.g., two-dimensional problems via Airy's stress function and Saint Venant's theory of bending and torsion of uniform bars; then conventional treatments are given for problems of bending and torsion of thin-walled section, statically indeterminate beams and frames, beams on elastic foundations, and thin plates. The last part deals with buckling of columns, beam-columns, plates, and shells.

The book attempts to give only "basic theory," and hence it has very little discussion of when or why the classical methods fail to give answers, as they often do in the difficult problems of modern engineering. Hence the engineer will find few indications as to what he can do in such cases. There are no references to solutions by numerical methods (relaxation, iteration, finite differences, and so on), nor to dimensional analysis. Virtually all of the bibliographical references are to standard texts or treatises, about one in ten referring to a published paper. Certainly the basic theory must be understood before the intractable cases can be dealt with. However the usefulness of the book to the engineer will be limited by its almost exclusive concern for

[1] Associate Professor of Mechanical Engineering, Massachusetts Institute of Technology, Cambridge, Mass.

[2] Professor of Mechanical Engineering, Massachusetts Institute of Technology, Cambridge, Mass. Mem. ASME.

[3] Associate Professor of Engineering, Brown University, Providence, R. I. Mem. ASME.

the classical methods and standard problems, for most of which, satisfactory presentations are already available in well-known books.

The reviewer feels bound to register a protest at the treatment of "energy principles" in chapter 7. The terms "work," "energy," and "strain energy" seem to be used indiscriminately. There are no definitions of the fundamental quantities "complementary energy" and "potential energy" and hence no clear statements of the two minimum principles concerned, respectively, with these quantities.

Theory of Plasticity

INTRODUCTION TO THE THEORY OF PLASTICITY FOR ENGINEERS. By Oscar Hoffman and George Sachs. McGraw-Hill Book Company, New York, N. Y., 1953. Cloth, 6 × 9 in., xiv and 275 pp., illus., $6.50.

REVIEWED BY MILTON C. SHAW[4]

WHILE there are several excellent classical texts available that treat the elastic behavior of structures in a comprehensive manner, there are relatively few works that attempt a similar coverage in the plastic region. This new book presents a fairly complete picture of the present state of development of plasticity theory.

The subject matter covered is divided into four parts. In the first of these, basic concepts and theories are considered. Stress at a point in a continuum is first defined and the dependence of stress on direction emphasized by developing the general relationships among stress components that arise from considerations of static equilibrium. The Mohr stress diagram is introduced as a convenient means for graphically representing the interrelationship between the several significant stress components. Strain is then considered and the Mohr strain diagram introduced. The special relationships that obtain between stress and strain in the elastic region as well as expressions for elastic strain energy are next presented. A number of strength theories are reviewed and the conclusion reached that the Mohr treatment is the best available for brittle materials while either the distortion-strain energy or maximum shear theories are of value for ductile metals. The types of plastic stress-strain relations experimentally observed are considered in the remaining chapter of the first section and an attempt is made to show that the distortion-energy theory is in better agreement with yield point experiments than is the maximum shear theory. The classical experiments of Taylor and Quinney and Lode that are cited in this connection are not convincing due to the complexity arising from the stress gradient across the section of the specimen that results from the combined loading that is used. Other experiments not mentioned by the authors may be cited in which the maximum shear theory provides at least as good correlation with experimental data, particularly when the plastic strains are carried well beyond the yield point.

In part two, several specific problems are considered in which elastic and plastic regions exist in equilibrium in the same structure. In the treatment of these problems the material is considered incompressible and nonstrain hardening. The cases considered include thick-walled spherical and cylindrical shells under internal pressure, rotating cylinders, and disks and shafts subjected to combined torsion and bending. In all of these examples the symmetry is sufficiently simple to enable solutions in closed form to be obtained and the handling of problems involving compatible boundary conditions at plastic-elastic boundaries are well illustrated. The last chapter of this portion of the text very briefly presents the slip-line field technique and two of the most elementary solutions of Prandtl are given as examples.

In the third part of the book the plastic flow of strain-hardening materials is considered. By treating problems in this section that were previously treated from the ideal plastic point of view, the influence of strain hardening is clearly illustrated. The instability of compression and tension members exhibiting strain-hardening characteristics are next briefly considered.

In the fourth and last section of the book metalworking processes are treated from the ideal plastic point of view. Those processes considered include: drawing and extrusion with and without friction and back-pull using tools having plane and curved surfaces, rolling of sheets, strips, and tubes, forging, metal forming with dies, and the bending of plates. In most cases the treatment is from the standpoint of plane strain and where friction is introduced simple Coulomb friction is assumed. In a few cases three-dimensional processes are approximated by use of the slip-line field technique. However, these results do not agree in detail with experimental observations, probably due to the over simplification involved in ideal plastic flow with its sudden transition from elastic to plastic behavior and the absence of strain hardening that is assumed. While most of the important metal processing techniques are considered, the metal-cutting process is excluded. This is unfortunate for this process provides an excellent example in which metal is deformed far into the plastic region under conditions of plane strain.

The book is concisely written and is of reasonable size. It is well indexed and contains a convenient list of notations. One of the useful features of the book is a selected list of references at the end of each chapter that should prove useful to the student who desires to consult the original literature.

While the tensor notation that is adopted is in part responsible for the compactness of the book, the value in its use is questionable in view of the loss in physical interpretation of the individual steps in the developments that accompany such shorthand techniques. If it were considered permissible to enlarge the book somewhat it would appear desirable to include a chapter on microstraining. While the treatment presented in which the material is considered as a continuum yields many useful results there are problems where this approach is misleading and the ultimate inhomogeneous character of strain that arises from a microstrain approach must be followed.

This book should prove useful as a reference volume for those engaged in research in the field of plasticity and also as a text for a graduate subject covering the classical problems of plastic flow.

[4] Professor of Mechanical Engineering, Massachusetts Institute of Technology, Cambridge, Mass. Mem. ASME.

Low-Temperature Physics

LOW TEMPERATURE PHYSICS. Four Lectures. By F. E. Simon, N. Kurti, J. F. Allen, and K. Mendelssohn. Academic Press Inc., New York, N. Y., 1952. Cloth, 5½ × 8½ in., references, vi and 132 pp., illus., $3.50.

REVIEWED BY MELVIN A. HERLIN[5]

THIS book is the contents of four lectures delivered at the Royal Institution early in 1950, summarizing the physical phenomena occurring at temperatures below 20 K. It is intended as an introduction for those entering the field and as a survey for those wishing a general acquaintance with this active field of research. The four lecturers are all leading contributors in the field. The emphasis is on the experimental and descriptive aspects, although the status of the theory is summarized

[5] Assistant Professor of Physics, Massachusetts Institute of Technology, Cambridge, Mass.

briefly for each area of study. Each chapter closes with a list of the important references to the literature.

The first chapter, by Professor Simon, makes a general survey of low-temperature phenomena with a discussion about means of attaining low temperatures and the relationship to the third law of thermodynamics. The breakdown of classical physics is discussed in relation to zero-point energy, liquid helium, electrons in metals, electrical conductivity and superconductivity, and magnetic phenomena at the electronic and nuclear level. The second chapter, by Dr. Kurti, discusses the properties of paramagnetic salts in relation to the technique of adiabatic demagnetization for obtaining temperatures below 1 K. Establishment of the thermodynamic temperature scale and methods for cooling other substances are covered, including the multistage demagnetization of interest in nuclear alignment experiments. The third chapter, by Professor Allen, concerns the properties of liquid helium, including the thermodynamic properties as well as the more spectacular transport phenomena such as the fountain effect, the mobile film, second sound, thermal conduction, and superflow through fine capillaries and slits. The two-fluid model and the current theories of liquid helium are outlined. Finally, the fourth chapter, by Dr. Mendelssohn, discusses superconductivity and related effects. The grouping of the superconducting elements in the periodic table is noted, with a discussion of superconducting alloys. Magnetic effects and the thermodynamics of the magnetic phase transition are given, along with a discussion of the electrodynamic theory of F. and H. London. The concept of the penetration depth is related to experiments on small-size superconductors. The relation of superconductivity to ordered motion is discussed. The intermediate state, time effects in the transition, and thermal conductivity are followed by an outline of the microscopic theory so far as it has been developed.

The book is short in spite of the wide coverage and may be read with little difficulty in a short time.

Strength of Materials

HISTORY OF STRENGTH OF MATERIALS. By Stephen P. Timoshenko. McGraw-Hill Book Company, Inc., New York, N. Y., 1953. Cloth, 6 × 9 in., x and 452 pp., 245 figs., $10.

REVIEWED BY J. ORMONDROYD[6]

THIS book will be read by graduate students in mechanics and many practicing engineers as long as engineering is a living, growing, and improving art.

The book covers the development of the theory of strength of materials from the work of Leonardo da Vinci in the fifteenth century to the present time—the last paper noted bearing the date of 1952. The story is told chronologically—in fact, three stories are told in parallel. Strength of materials, theory of elasticity and elastic stability (including vibration theories), and theory of structures are given separate treatment even though in reality they developed together.

The first 66 pages of the book cover the work done from the fifteenth century to the end of the eighteenth century. All this work can be classified as strength of materials even though Hooke and Coulomb laid the foundations for the basic assumptions of the theory of elasticity in these centuries. Structures of earth, stone, and wood were characteristic of these centuries—and the developed theories of structures refer to such works in this section.

The work of the nineteenth century has 287 pages devoted to it—fully two thirds of the entire volume. This is natural since the nineteenth century saw the whole field of the theory of elasticity started and completed to such a point that the monumental "History of the Elasticity and Strength of Materials," by Todhunter and Pearson, could appear in its completed form in 1893 and Love's almost definitive "Treatise on the Mathematical Theory of Elasticity" could first appear in the same year. Iron and steel as materials of construction came into extensive use in this century and the theory of structures built of these materials was developed completely in the nineteenth century. The structures discussed in this section are railroad rails, trusses, bridges, and ships. Roads and buildings are strangely absent from this structural roll call—perhaps because the automobile and the structural-steel building were to be products of the twentieth century.

The last 86 pages of the book outline the work done in the twentieth century up to 1952. In a sense, the twentieth century so far has been a "mopping-up" period in which the grand outline traced in the preceding centuries has been filled in with improved detail. From the relatively small number of pages devoted to the past fifty years, it can be seen that the work of this century is not treated in the same detail as the work of previous years. However, the vast amount of work done in this century is attested to by the fact that there are three or four times as many reference footnotes per page in this section as appear in the previous sections.

In reading the book one is struck forcibly with the fact that much of the original work in all the fields, including mathematical elasticity, was done by men with engineering training and interest.

The works of over 530 authors are mentioned. Short biographies of some 76 of these men (all now dead) are included. A valuable feature of the book is the great number of footnote references (over 1000) to about 1200 separate books and papers.

Inevitably this book invites comparison with Todhunter and Pearson's great "History." These two books are not competitors. They differ in aim and in scope. They compliment each other. Timoshenko covers the material they covered, briefly, to be sure; but he also covers material that they ignored (and has, of course, the advantage of publishing 60 years after Pearson's editorial work was completed). Todhunter and Pearson omit biographical references completely. While Todhunter and Pearson (especially) were both sympathetic to the use of theory in practical engineering, their three-volume work is devoted almost exclusively to complete résumés of the mathematical work of a small number of the most outstanding original creators of theory of elasticity. For instance, the writings of Saint Venant are reviewed in detail in 325 pages. Even though Timoshenko may regard Saint Venant as the greatest single man discussed in his history he can only devote a few pages to describe Saint Venant's work. After all, there are five hundred other men whose work must be noticed. Castigliano, whose work in elastic energy is so useful to us today, was dead before Pearson's history appeared—yet his work is completely ignored in that history. Pearson's history is practically inaccessible to engineers—it requires a vast mathematical knowledge and the ability to read the six or seven European languages used in the direct quotations, on top of which it is to be found only on the shelves of the best libraries. Timoshenko's history is completely accessible, in all respects, to all engineers who can read English.

Timoshenko's teachers, Jasinsky in Russia, August Föppl and Ludwig Prandtl in Germany, early imbued him with an almost religious devotion to the application of mathematics to engineering problems. This strong conviction led him to be one of the founders of the Applied Mechanics Division of the ASME in 1927. During his half century of activity in teaching, consulting, and industrial work, Timoshenko has written five books in Rus-

[6] Professor, University of Michigan, Ann Arbor, Mich. Mem. ASME.

sian and twelve books in English on the subjects discussed in his history. More than 60 original papers in the same fields have come from his fertile pen, and they have just recently been published in collected form. Of all the books he has written, this history has been given the longest and most careful development. At least 20 years of thought and work have gone into its writing. It was a labor of love. This book may well prove to be the author's most unique and lasting gift to the future.

The works of many Russian writers, generally unknown to English-speaking engineers, are given copious notice in Timoshenko's history. But one looks in vain for mention of several important recent papers written by American elasticians. The work of the Italian writers is, perhaps, not covered extensively enough. There seems to be no easily discovered reference to an important recent development in the field of elasticity—the invention of the resistance-strain gage. It is true this history deals with the development of theory and not with testing devices; but the development of all theories is closely linked with the efficacy of the devices used to test their validity. Bridgman's extensive work on the properties of materials at very high pressures and his theory of failure might have received some notice in this work. However, if all the subjects that might have been discussed in this history had been noticed, the book would have become too bulky and too expensive.

There is no doubt that workers in the field of mechanics will receive this book with great enthusiasm.

Fatigue of Metals

FATIGUE OF METALS. By R. Cazaud. Translated by A. J. Fenner. Foreword by H. J. Gough. Philosophical Library, New York, N. Y., 1953. Cloth, 6 × 10 in. xiv and 334 pp., 245 figs., bibliography, tables, author and subject indexes, $12.50.

REVIEWED BY JOHN M. LESSELLS[7]

IN view of the dearth of books from France on the subject of fatigue, the publication in 1937 of "La Fatigue des Métaux" by Dr. Cazaud, in collaboration with the late L. Persoz, was welcomed. A new edition followed in 1943, and a third in 1948, under a single authorship. This later edition has now been ably translated by A. J. Fenner and carries an interesting foreword by H. J. Gough.

The book comprises 10 chapters, the first few of which are devoted to a discussion of the knowledge of fatigue phenomena as uncovered by the usual laboratory specimens. This is followed by other chapters which emphasize the steps which must be taken in design and manufacturing to minimize fatigue failures. Excellent photographs of fatigue failures are included as well as a complete description of all known types of testing machines. An important feature is the complete bibliographies of the literature which are included at the end of each chapter. These cover particularly well all continental literature.

Chapter 1 indicates how our knowledge of fatigue has developed by the historical review which is made dating from the early work of Albert to the present time. Fatigue failures, with accompanying photographs, are discussed in chapter 2 together with a complete description of all known methods for the detection of fatigue cracks. Chapter 3 reviews the theories of failure, which is followed in chapter 4 by a survey of all known types of testing machines. In chapters 5 to 8 the fatigue strength of metals and alloys are fully discussed based on the usual laboratory conditions and using conventional types of specimens. Useful tables of endurance limits are given with a detailed discussion of the relation to the microstructure which readers will recall was an important feature of the earlier editions. The effects of the various factors influencing the fatigue strength, such as size, form, surface finish, temperature, and environment are all well covered. Chapter 9 is devoted to the fatigue strength of all types of joints, and the final chapter discusses methods of improving the fatigue strength.

As mentioned by Dr. Gough in his foreword the author presents a broad and clear review of the status of the knowledge which is supplemented by results of his own studies, and if such information is usefully applied in the design and production stages the number of fatigue failures can eventually be reduced.

[7] President, Lessells and Associates, Inc., Boston, Mass. Fellow and Hon. Mem. ASME.

Photoelasticity

DESIGNING BY PHOTOELASTICITY. By R. B. Heywood. Chapman & Hall, Ltd., London, England, 1952. Cloth, 5½ × 8½ in., xvi and 414 pp., figures, tables, 65/-net.

REVIEWED BY ARTHUR M. WAHL[8]

THIS book, which covers a somewhat wider field than its title would indicate, is divided into two main parts. Part 1 deals primarily with the photoelastic technique and covers such subjects as the optical phenomena involved, photoelastic materials, preparation and testing of models, interpretation of test results, and three-dimensional photoelasticity techniques. The treatment in this section, written mainly for the guidance of the experimenter is, of course, not so comprehensive as those in the well-known photoelasticity texts by Frocht or by Coker and Filon. Although this portion of the book is of primary interest to research workers, it should also be useful to designers and others interested in gaining some insight into the photoelastic method.

Part 2 of the book is of more direct interest to designers and covers mainly available data on stress concentration factors together with a discussion of methods for applying such factors in practical design. In particular, data on concentration factors and stress distributions in such important machine elements as fillets, notches, holes, grooves, gear teeth, screw-threads, T-heads, etc., are presented. In many cases, empirical formulas are given for calculating stress concentration factors. Emphasis is also placed on methods of utilizing the results of photoelastic tests where fatigue loading is present. An equivalent internal flaw theory is proposed by means of which an attempt is made to account for lack of sensitivity of materials to stress concentration under fatigue loading.

One feature of the book is the long list of references provided (over 800 in all). Many of these references, however, deal with subjects other than photoelasticity, including methods of experimental stress measurement, fatigue problems, and theory of elasticity. The book also bears the imprint of the author's practical experience gained at the Research Laboratory, Rolls-Royce Ltd., and in the Royal Aircraft Establishment.

In the reviewer's opinion, the author deserves credit for bringing together a large amount of useful data into a form convenient for the engineer and designer.

[8] Advisory Engineer, Westinghouse Research Laboratories, East Pittsburgh, Pa. Fellow ASME.

FLOW DATA AND METHODS

DIGITAL AND ANALOG COMPUTERS AND COMPUTING METHODS

DICTIONARY OF TERMS IN MECHANICAL SCIENCE AND TECHNOLOGY

PROCEEDINGS OF THE FIRST (1951) U. S. NATIONAL CONGRESS OF APPLIED MECHANICS

MANNED LIFE STUDIES OF INTERESTED ENGINEERS

THE AMERICAN SOCIETY OF MECHANICAL ENGINEERS
29 W. 39th St., New York 18, N. Y.